COMPLIANT PART MATING
AND
MINIMUM ENERGY CHAMFER DESIGN

by

Michael P. Hennessey

B.S., Math, University of Minnesota
(Institute of Technology, 1980)

Submitted in Partial Fulfillment
Of the Requirements for the
Degree of

Master of Science
in
Mechanical Engineering

at the

Massachusetts Institute of Technology

June, 1982

Signature of Author ______________________________
Department of Mechanical Engineering, June 4, 1982

Approved by ______________________________
Daniel E. Whitney, Technical Supervisor

Certified by ______________________________
Daniel E. Whitney, Thesis Supervisor

Accepted by ______________________________
Warren M. Rohsenow, Chairman, Department Committee on Graduate Students

COMPLIANT PART MATING
AND
MINIMUM ENERGY CHAMFER DESIGN

by

Michael Peter Hennessey

Submitted to the Department of Mechanical Engineering on June 4, 1982 in partial fulfillment of the requirements for the Degree of Master of Science in Mechanical Engineering

ABSTRACT

Theoretical models of compliantly supported rigid pegs entering compliant holes and minimum energy chamfers were used to further understand the mechanics of assembly. Key features of the "peg-in-hole" model include large angle solutions and rotational hole compliance. The effect of various insertion parameters on the "insertion force versus depth" plot was determined. Minimum energy chamfers have been designed according to either minimum insertion work (energy) or minimum frictional work (energy). Both criteria have been shown to yield the same chamfer shapes. Also, chamfers have been designed where the chamfered part, while being displaced rubs against two surfaces with friction (e.g. a doorlatch tongue).

An experiment was carried out which attempted to verify experimentally the existence of minimum energy chamfers. Three aluminum chamfers were made and their insertion energies determined. One of the chamfers was an optimal slope chamfer (aspect ratio, S = 1.40) and the other two were straight line chamfers (S = 0.60, 3.75). The straight line chamfers in theory had 18% (for S = 0.60) and 22% (for S = 3.75) more insertion energy than did the optimal slope chamfer. The experimental percentages were 29% and 18%, respectively which supports the theoretical predictions; namely that chamfers flatter or steeper than the optimal slope chamfer have larger insertion energies.

Thesis Supervisor: Dr. Daniel Whitney, Lecturer
Department of Mechanical Engineering

ACKNOWLEDGMENTS

This thesis was funded by the National Science Foundation under Grant No. DAR 79-10341 and prepared at The Charles Stark Draper Laboratory, Inc.

I would like to thank my thesis supervisor, Dr. Daniel Whitney for his guidance and advice, which saved me time and improved the quality of this thesis. Also, I would like to thank other members of the Draper Staff (10D) for their frequent participation in part mating discussions (Richard Gustavson in particular) and assistance in conducting experiments as well as those responsible for typing the final draft: Technical Publications, Lucille Legner and Kim Obrion.

Publication of this thesis does not constitute approval by the National Science Foundation or the Charles Stark Draper Laboratory, Inc. of the findings or conclusions contained herein. It is published for the exchange and stimulation of ideas.

TABLE OF CONTENTS

LIST OF FIGURES

LIST OF FIGURES (Cont.)

LIST OF TABLES

List of Symbols

ϕ - chamfer angle

μ - friction coefficient

β - friction angle ($\mathrm{Tan}^{-1}\mu$)

C - clearance ratio

γ_c - angle between line perpendicular to hole wall and line from compliance center of hole to contact point during chamfer crossing

γ - angle between line perpendicular to hole wall and line from compliance center of hole to contact point during one-point and two-point contact

D - diameter of hole

d - diameter of peg

Δ - initial lateral error

a - distance from end of peg to compliance center of peg

a_o - optimized distance from end of peg to compliance center of peg

C_h - distance perpendicular to hole wall to hole's compliance center

C_v - distance parallel to hole wall from corner of chamfer to compliance center of hole

r_c - distance between contact point and compliance center of hole during chamfer crossing

r - distance between contact point and compliance center of hole during one-point and two-point contact

Δz - driving insertion variable during chamfer crossing

ζ - $\left(\Delta - \frac{CD}{2}\right) \tan\phi - \Delta z$

ℓ - driving insertion variable during one-point and two-point contact

K_θ - rotational stiffness of peg support

K_{θ_1} - rotational stiffness of left hole wall

K_{θ_2} - rotational stiffness of right hole wall

K_x - lateral stiffness of peg support

K_{x_1} - lateral stiffness of left hole wall

K_{x_2} - lateral stiffness of right hole wall

$\delta\theta$ - rotational displacement of peg

$\delta\theta_1$ - rotational displacement of left hole wall

$\delta\theta_2$ - rotational displacement of right hole wall

δx - lateral displacement of peg's compliance center

δx_1 - lateral displacement of left hole wall

δx_2 - lateral displacement of right hole wall

δz - vertical displacement of peg's compliance center

V - distance parallel to right hole wall from contact point to compliance center of hole

F_x - horizontal peg support force

F_z - vertical peg support force

F_n - normal contact force during chamfer crossing

F_{n_1} - normal contact force on left hole wall during one-point contact and two-point contact

F_{n_2} - normal contact force on right hole wall during two-point contact

M - external moment about peg support point

SECTION 1

COMPLIANTLY SUPPORTED RIGID PEG ENTERING A COMPLIANT HOLE

1.1 INTRODUCTION

A field of study related to industrial automation is part mating. Part mating is primarily concerned with the mechanics of assembly, studying the forces and displacements of the parts involved so as to recommend ways of making the assembly easier. In many assembly situations (e.g., putting a bearing into a housing) there are two parts involved: one is fixed (the "hole") and another part (the "peg"), while being supported, is assembled to the first part as shown schematically in Figure 1.1.1. The subsequent analysis will presume this type of assembly.

Part mating has been researched by The Charles Stark Draper Laboratory, Inc. since 1973. One major accomplishment so far is the invention of a passive device which when mounted to the wrist of a robot aids assembly by providing proper support for the "peg". This device, called a Remote Center Compliance (RCC), was invented in the mid-seventies and versions of the original design are now being used extensively in industrial automation.

Part mating research has continued following the invention of the RCC and has yielded new and interesting results: (a) improved understanding of mating success criteria, (b) design guidelines for parts to aid their assembly, (c) better appreciation of the relationship of friction, geometry, and compliance to mating characteristics, and (d) models of assembly force versus depth that can be used to monitor the assembly process.

In general, there are two classifications of part mating: Rigid and Compliant. In rigid part mating the parts involved do not store a substantial amount of elastic energy during the mating process, whereas in compliant part mating one or both of the parts store a substantial amount of elastic energy during the mating process. Much work has been done in rigid part mating and some areas of rigid part mating have been recently extended to compliant part mating.[1,2] This thesis concentrates on compliant part mating.

A further subclassification of part mating is depicted in Figure 1.1.2, taking into account where the compliant support is located and, more importantly, whether the parts themselves can be considered rigid with respect to the supports. In the part mating theory developed by The Charles Stark Draper Laboratory, Inc. it is the part that is supported compliantly, not the hole. An interesting alternative to this approach is due to Arai and Kinoshita,[3] where the hole (worktable) is supported compliantly while the part remains fixed during the assembly. They recommend the use of compliance in the worktable (hole) for small batch production, but agree that for mass production, locating the compliance in the part's support is more suitable.

Compliant part mating is primarily concerned with the mechanics of assembly of parts that cannot be considered rigid compared to the support. Recently, the theory has been extended to handle restricted cases that involve compliant hole walls (e.g., no friction, small angles).[4,5] This thesis presents even more general models which take into account (1) lateral hole compliance, (2) rotational hole compliance, and (3) combined lateral and rotational hole compliance.[4,6] These three models have been used to analyze a single "peg-in-hole" assembly. Two types of solutions were used for each model, one based on linearized solutions and one based on exact solutions.

In the analysis that follows, various simplifying assumptions will be made that are based on experience and serve to substantially reduce the complexity of the model used. One simplifying assumption is the use of a two-dimensional model. Also, during compliant part mating, the peg's support and the hole are assumed to deform elastically according to a linear stress-strain law. These deformations characterize the assembly and determine its success or failure. The "peg" is assumed to be rectangular in shape and supported compliantly at its compliance center located along the center axis of the peg. For our purposes a compliance center is a point where a fictitious support acts to provide independent lateral and rotational support. In practice, this can be done with the RCC. The "hole" is assumed to be chamfered with parallel sides in its unstressed state. Figure 1.1.3(a) illustrates the initial configuration of the peg and the hole with peg support

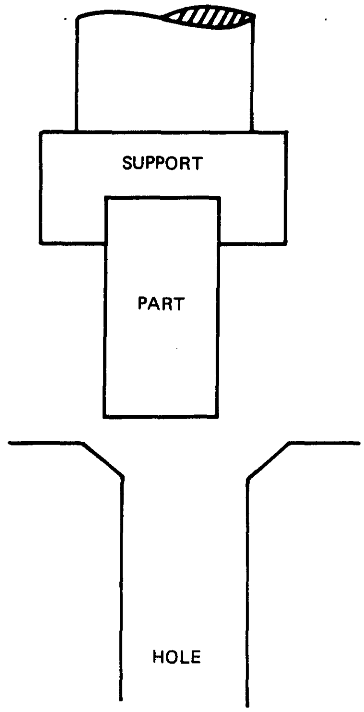

Figure 1.1.1. Initial configuration of peg and hole.

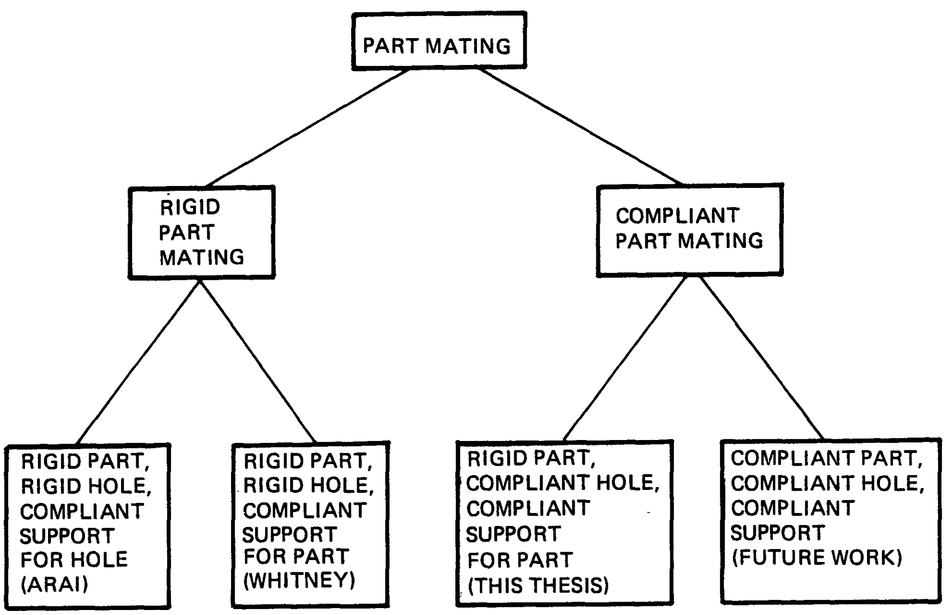

Figure 1.1.2. Classification of part mating.

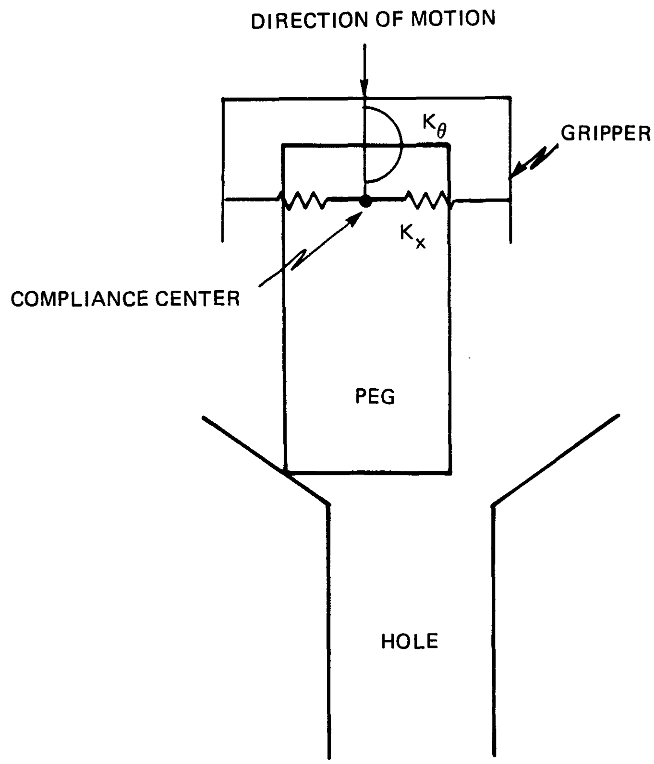

(a) Physical Idealization

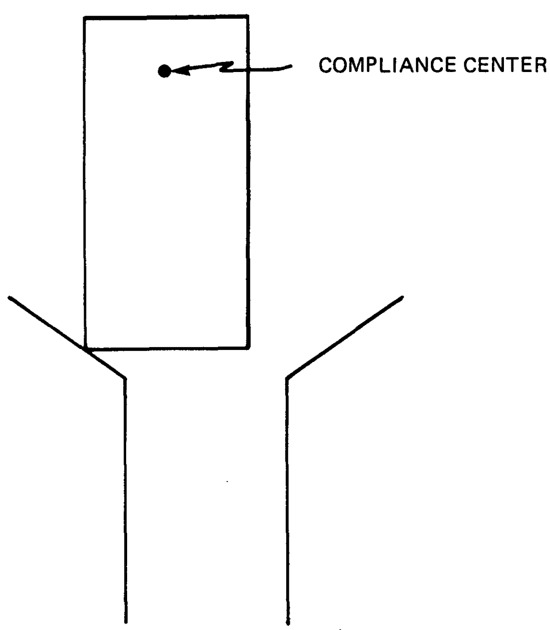

(b) Equivalent Representation

Figure 1.1.3 Initial configuration of peg and hole.

stiffnesses K_x, K_θ (reciprocal compliances) and gripper identified. Physically, the peg may be thought of as being supported by the gripper which moves vertically downward during the assembly process. This situation is equivalent to the one shown in Figure 1.1.3(b) where now the gripper and support springs (compliances) have been replaced with a single solid dot • representing the compliance center of the peg. Note that the initial angular error of the peg's center axis with respect to the hole's center axis is assumed to be negligible. Also, since the parts are typically lightweight and assembly usually proceeds relatively slowly, dynamic effects will be ignored. This justifies the use of quasi-static models where the parts are presumed to be massless.

Regardless of the type of hole compliance, the general quasi-static phases of successful assembly to be considered are (a) chamfer crossing, followed by (b) one-point contact, (c) two-point contact, (d) resumption of one-point contact, and (e) line contact. Figure 1.1.4 illustrates this assembly process. The assembly process is continuous except for the transition from chamfer crossing to one-point contact. This is because the normal force changes direction abruptly when the corner of the peg meets the corner of the chamfer. Physically, the jump in the displacements (horizontal and vertical) of the peg are typically small; however, the jump in the vertical insertion force can be substantial.

The assembly process described above will be formally analyzed in the following sections. Other successful and unsuccessful processes are certainly possible but will not be analyzed in great detail. For example, the location of the compliance center of the peg can greatly affect the assembly process. If it is located too close to the end of the peg a new kind of one-point contact is possible (see Figure 1.1.5). Other locations of the peg's compliance center could be considered too (e.g., not within the boundary of the peg) but are not as practical. Hence this possibility will be ignored. Previous work in compliant part mating has emphasized the assembly phases outlined in Figure 1.1.4 and thus provided the motivation for analyzing this type of assembly. Also, efforts will be made to identify some of the unsuccessful or undesirable modes of assembly; however, finding explicit criteria in terms of the friction, the geometry, or the compliance is often difficult.

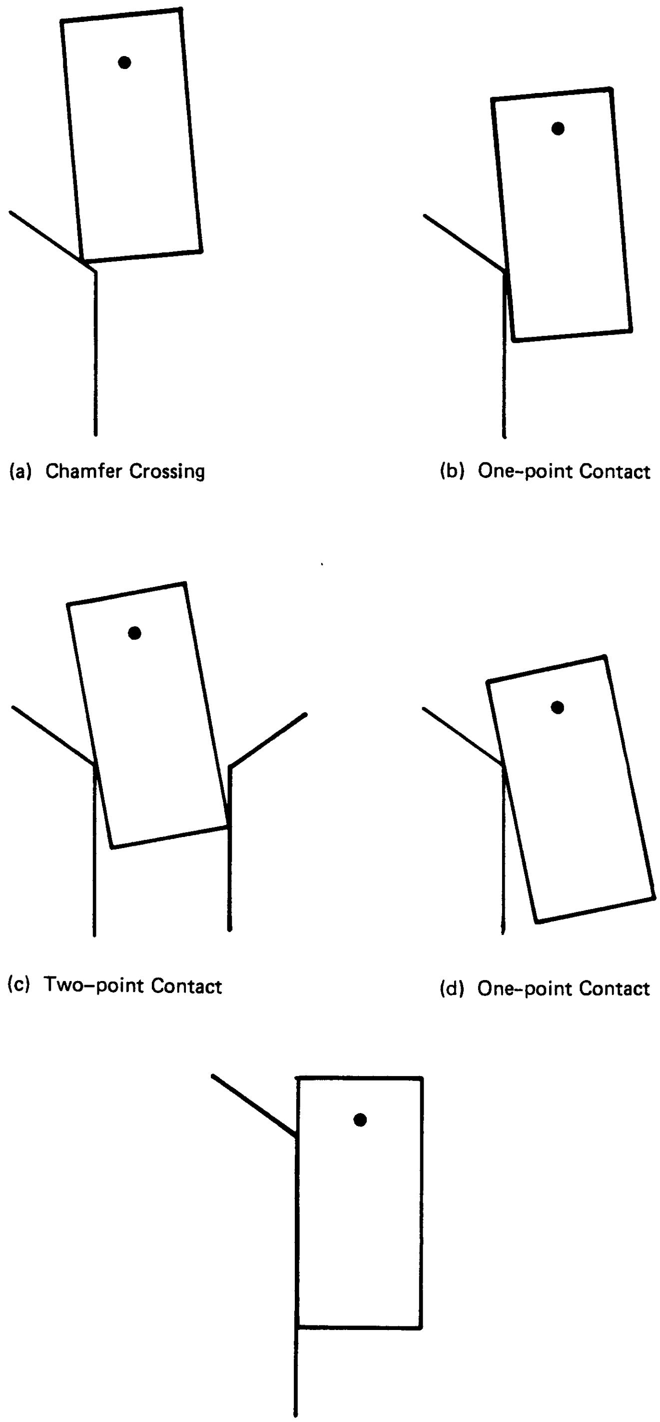

(a) Chamfer Crossing

(b) One-point Contact

(c) Two-point Contact

(d) One-point Contact

(e) Line Contact

Figure 1.1.4. Ideal successful assembly phases.

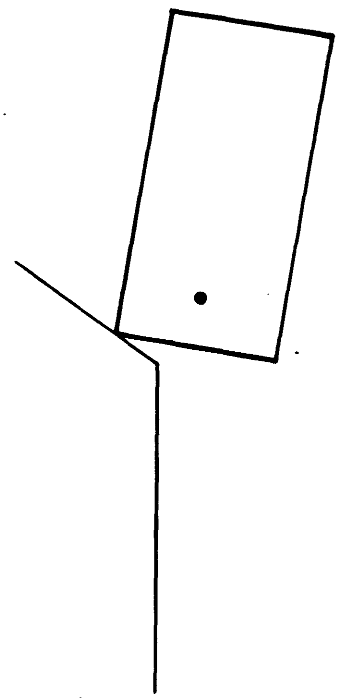

(a) Chamfer Crossing

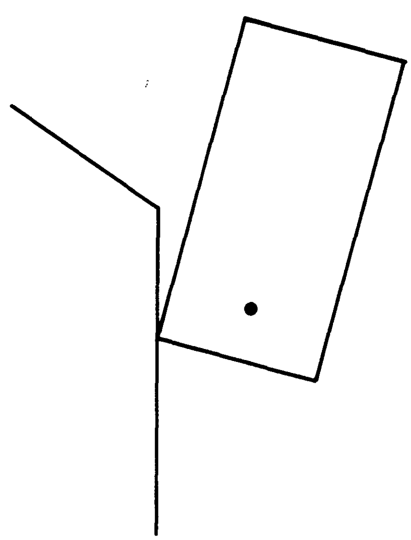

(b) One-point Contact

Figure 1.1.5. Development of new one-point contact.

1.2 LATERAL COMPLIANCE HOLE

1.2.1 Introduction

In many instances it is necessary for the model to incorporate only lateral hole compliance. Figure 1.2.1 illustrates the initial configuration of the peg and the hole with the compliance center of the peg indicated. During the assembly to be considered the hole walls will initially deform outward, enlarging the hole. This deformation will be treated as a uniform lateral translation of the hole walls parallel to their initial position. Both sides (left and right) will then deform away from the center axis of the hole so that the distance between the center axis of the hole and the sides of the hole will always be nonnegative (i.e., $\delta x_1, \delta x_2 \geq 0$). The quasi-static phases of successful assembly to be analyzed are (1) chamfer crossing, followed by (2) one-point contact, (3) two-point contact, (4) resumption of one-point contact, and the final phase, (5) line contact. Line contact occurs when the peg has uprighted itself (vertical) and is in contact with the left side of the hole.

The compliance center's location along the peg's axis can greatly affect the assembly characteristics. If the compliance center of the peg is located too close to the end of the peg the other type of one-point contact will occur. A sufficient criterion for avoiding this type of one-point contact is to require the angle of the peg with respect to the vertical ($\delta\theta$) to be nonnegative ($\circlearrowleft$+) during chamfer crossing.

1.2.2 Chamfer Crossing

Chamfer crossing is depicted in Figure 1.2.2 and will now be analyzed. A free body diagram of the peg is shown with all external forces and moments present. The geometrical parameters and the remaining insertion variables are also indicated.

The positions of the peg and hole during chamfer crossing are completely determined by (1) balancing the external forces and moments on the peg, (2) using the constitutive law for each compliance, and (3) invoking geometric constraints on the peg and hole.[7] The force and moment balance involves a horizontal and vertical force balance along with a moment balance at the peg's compliance center. Constitutive laws for the compliances must be applied to the peg's support (both lateral and rotational compliance) and the left hole wall (lateral compliance). The peg's support and the hole wall's stiffness may be readily identified (e.g. K_{x_1} is the lateral stiffness of the left side of the hole); also see List of Symbols. Two

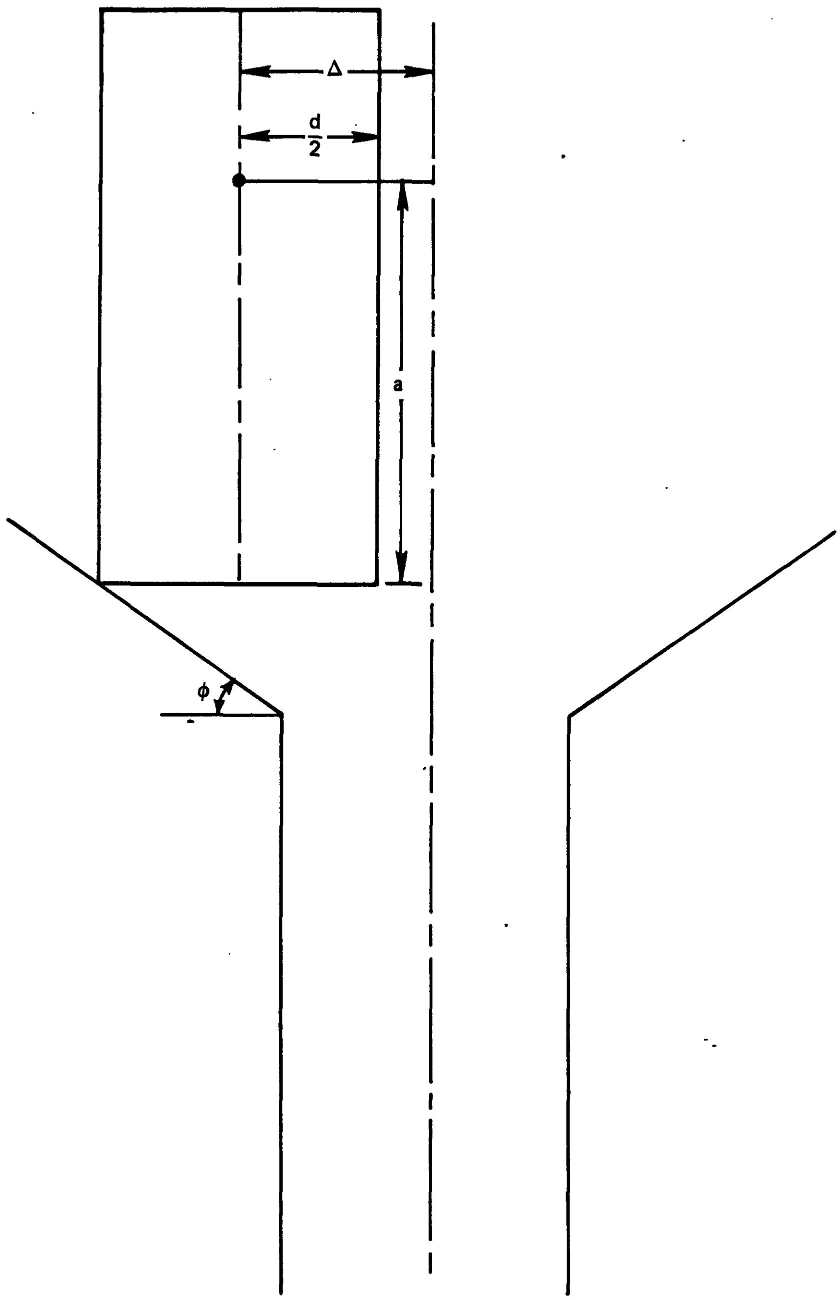

Figure 1.2.1. Initial configuration of peg and hole.

geometric constraints apply, a horizontal geometric constraint and a vertical one. The following equations may then be derived with the aid of Figure 1.2.2.

Equilibrium Requirements

$$F_x = F_n(\sin\phi - \mu\cos\phi)$$

$$F_z = F_n(\cos\phi + \mu\sin\phi)$$

$$M = F_n\{a[\sin(\phi + \delta\theta) - \mu\cos(\phi + \delta\theta)]$$

$$- \frac{d}{2}[\cos(\phi + \delta\theta) + \mu\sin(\phi + \delta\theta)]\} \qquad (1.2.1)$$

Force-Deformation Relations

$$F_x = K_x\delta x$$

$$M = K_\theta\delta\theta$$

$$K_{x_1}\delta x_1 = F_n(\sin\phi - \mu\cos\phi) \qquad (1.2.2)$$

Geometric Compatibility Requirements

$$\frac{\Delta z}{\tan\phi} = \delta x + \delta x_1 + a\sin\delta\theta + d\sin^2\frac{\delta\theta}{2}$$

$$a + \Delta z = \delta z + a\cos\delta\theta + \frac{d}{2}\sin\delta\theta \qquad (1.2.3)$$

The variable Δz is defined as the insertion distance. Chamfer crossing begins when $\Delta z = 0$ and ends when $\Delta z = \left(\Delta - \frac{CD}{2}\right)\tan\phi > 0$. Here C is the clearance ratio, defined by

$$C = \frac{D - d}{D} \qquad (1.2.4)$$

To avoid the other type of one-point contact, the compliance center of the peg must not be located too close to the end of the peg.

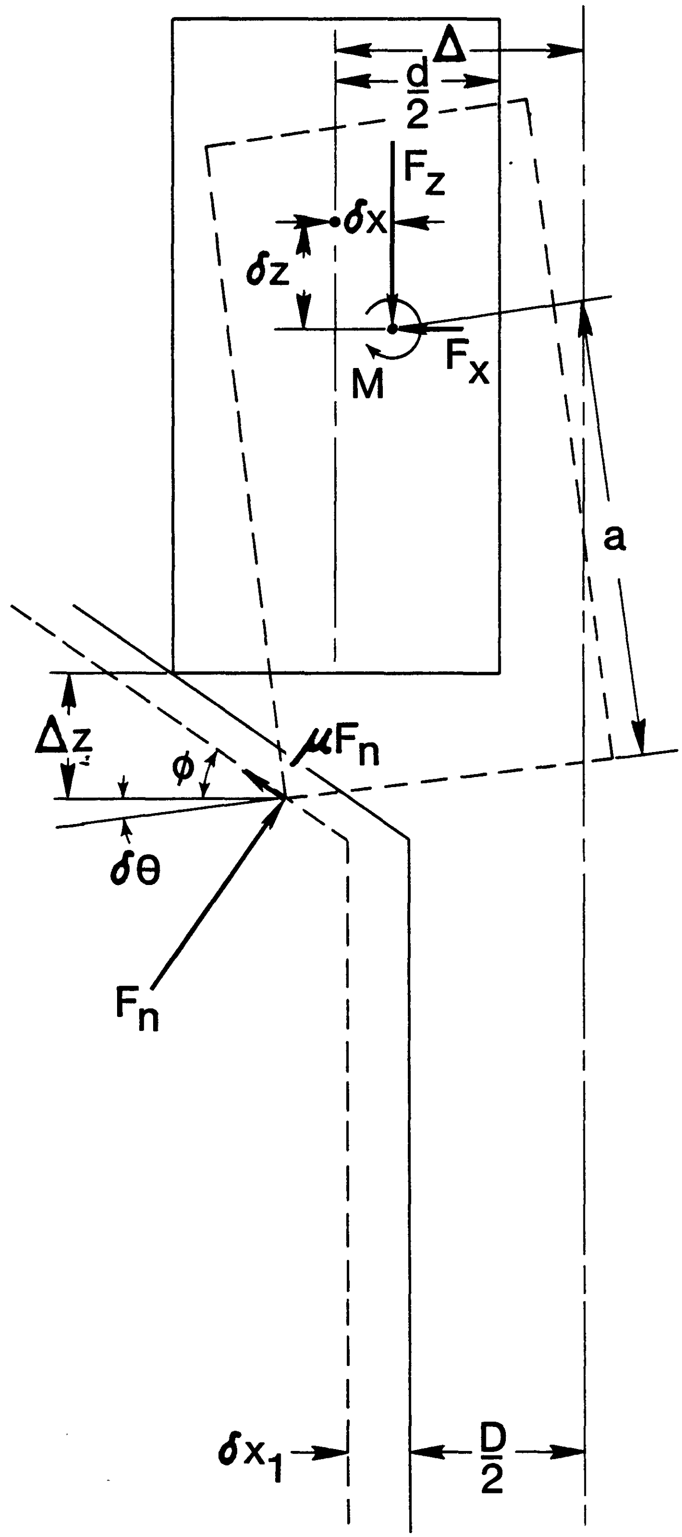

Figure 1.2.2. Chamfer crossing.

In fact, it must be located at a distance of at least $\frac{d}{2\tan(\phi + \delta\theta - \beta)}$ from the end of the peg. Here the friction angle (β) is given by

$$\beta = \tan^{-1}\mu \qquad (1.2.5)$$

This may be derived by requiring the normal force (F_n) and the angle of the peg with respect to the vertical ($\delta\theta$) to be nonnegative in the moment balance equation (Equation 1.2.1). Since $\delta\theta$ is not known beforehand, an estimate of the maximum value of $\delta\theta$ will provide an estimate of the minimum acceptable value of a. Also, to avoid wedging the chamfer angle (ϕ) must be greater than $\beta - \delta\theta$.

1.2.3 <u>One-Point Contact</u>

As mentioned earlier, chamfer crossing is not immediately followed by one-point contact (see Figure 1.2.3). Instead a transient phase occurs while the normal force (F_n) changes direction so as to align itself perpendicularly to the surface of the side of the peg. This phase, although quite brief, is responsible for producing a discontinuity in <u>all</u> of the insertion variables between chamfer crossing and one-point contact. One could, however, construct a quasi-static model to analyze this phase by continuously varying the direction of the normal force while solving for a quasi-static solution. Because computer runs and experience have shown that the "jump" in the geometric variables (e.g., δz) is typically small (less than 5%) this phase will not be analyzed. Therefore the next phase to be analyzed is one-point contact.

The positions of the peg and hole during one-point contact are completely determined by (1) equilibrium requirements, (2) force-deformation relations, and (3) geometric compatibility requirements. The one-point contact phase is shown in Figure 1.2.3 with a free-body diagram of the peg included. Proceeding as before (Section 1.2.2) and with the aid of Figure 1.2.3 it follows that:

<u>Equilibrium Requirements</u>

$$F_x = F_{n_1}(\cos\delta\theta - \mu\sin\delta\theta)$$

$$F_z = F_{n_1}(\sin\delta\theta + \mu\cos\delta\theta)$$

$$M = F_{n_1}\left[(a - \ell) - \frac{\mu d}{2}\right] \qquad (1.2.6)$$

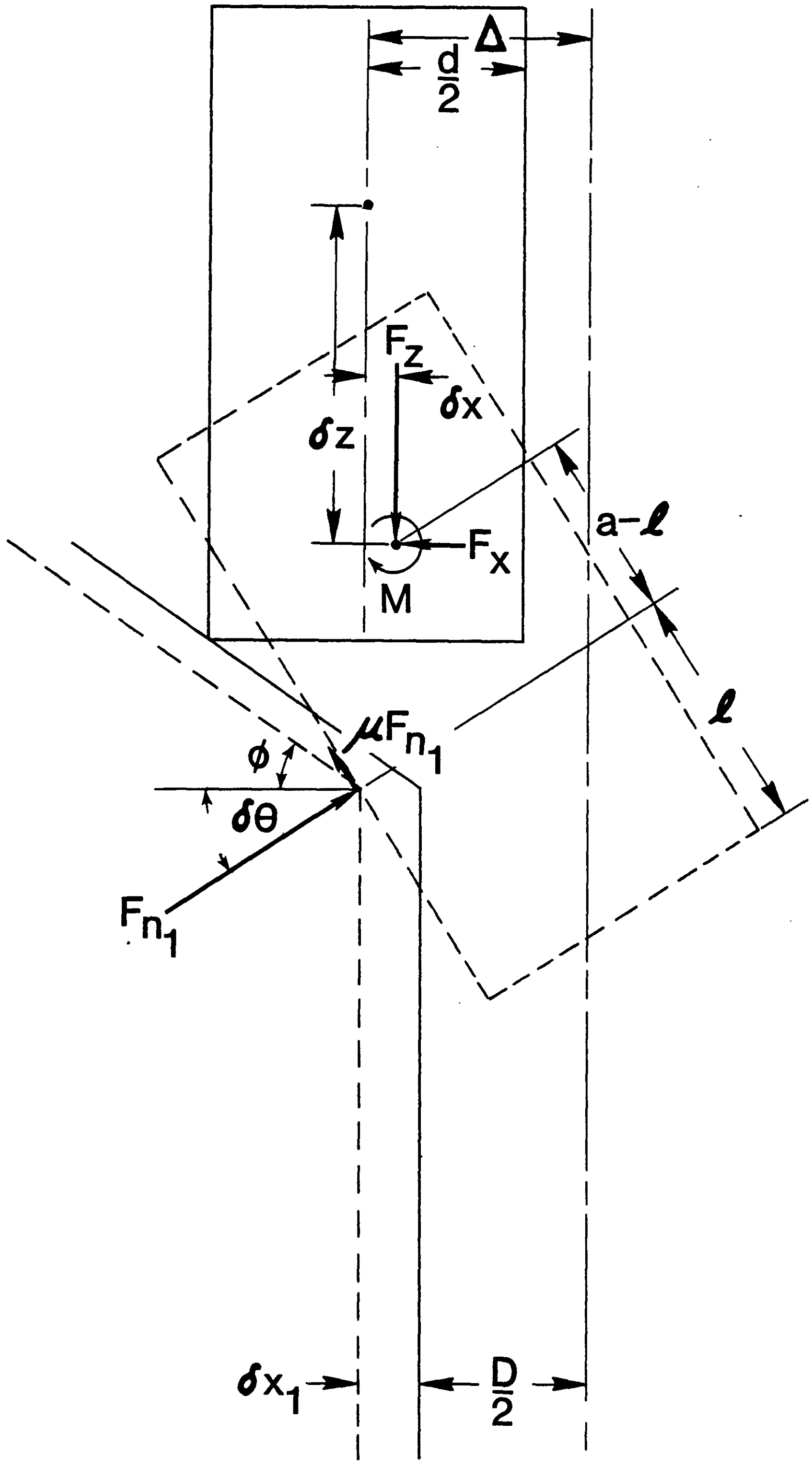

Figure 1.2.3. One-point contact.

Force-Deformation Relations

$$F_x = K_x \delta x$$

$$M = K_\theta \delta\theta$$

$$K_{x_1} \delta x_1 = F_{n_1} (\cos \delta\theta - \mu \sin \delta\theta) \qquad (1.2.7)$$

Geometric Compatibility Requirements

$$\Delta - \frac{CD}{2} = \delta x + \delta x_1 + (a - \ell) \sin \delta\theta + d \sin^2 \frac{\delta\theta}{2}$$

$$a + \left(\Delta - \frac{CD}{2}\right) \tan \phi = \delta z + (a - \ell) \cos \delta\theta + \frac{d}{2} \sin \delta\theta \qquad (1.2.8)$$

Here ℓ is taken to be the insertion distance. One-point contact begins when $\ell = 0$. Also, we must require the angle of the peg with respect to the vertical ($\delta\theta$) to be nonnegative. From Equations 1.2.6 and 1.2.7 it follows that the distance from the tip of the peg to its compliance center (a) must be at least $\frac{\mu d}{2}$, since the equations hold for ℓ arbitrarily small.

One-point contact ends and two-point contact begins when the lower right corner of the peg comes in contact with the right side of the hole. To determine the values of ℓ and other insertion variables for which two-point contact begins, the following additional geometric constraint must be included with the one-point contact equations when solving for these insertion variables

$$\ell \sin \delta\theta + d \cos \delta\theta = D + \delta x_1 \qquad (1.2.9)$$

The above equation is a horizontal relationship which says in effect that the peg's lower right corner has just touched the right wall (no normal force yet).

As mentioned in the Introduction, Section 1.2.1, two-point contact is followed by a resumption of one-point contact. The same equations (Equations 1.2.6, 1.2.7, and 1.2.8), which hold for the first one-point contact, must also hold for the resumption of one-point contact. In addition, Equation 1.2.9 also applies to the boundary between two-point contact and the resumption of one-point contact.

Although the existence of the second one-point contact may not be obvious, it does occur, and a more rigorous justification will now be given. Manipulation of Equations 1.2.6 through 1.2.9 yields the following quadratic in $(a - \ell)$

$$\sin \delta\theta (a - \ell)^2 + B(\delta\theta)(a - \ell) + C(\delta\theta) = 0 \qquad (1.2.10)$$

where $B(\delta\theta)$, $C(\delta\theta)$ are complex expressions. This equation implies that a resumption of one-point contact is possible since its solution yields either two real roots or two complex roots. Two real roots correspond to the case where two-point contact occurs marking the beginning and the end of two-point contact. Two complex roots correspond to the case where two-point contact does not occur. Numerical results have verified this and also suggest that the resumption of one-point contact ends for $\ell < a$. To show that one-point contact is impossible for $\ell > a$ and to establish a lower bound, consider the situation illustrated in Figure 1.2.4. A free-body diagram of the peg is shown for the case $\ell > a$. The moment balance equation

$$M + F_{n_1}(\ell - a) + \mu F_{n_1}\frac{d}{2} = 0 \qquad (1.2.11)$$

is meaningless because each term on the left side is greater than zero. A lower bound for ℓ during one-point contact can be found by requiring M and F_{n_1} in Equation 1.2.11 to be nonnegative, i.e.

$$\ell \leq a - \frac{\mu d}{2} \qquad (1.2.12)$$

The largest value of ℓ for which one-point contact is possible is shown in Figure 1.2.4.

1.2.4 Two-Point Contact

The assembly phase immediately following one-point contact is two-point contact. In Figure 1.2.5 the geometry of two-point contact is illustrated along with a free-body diagram of the peg.

The positions of the peg and hole during two-point contact are completely determined by (1) equilibrium requirements, (2) force-deformation relations, and (3) geometric compatibility requirements. The

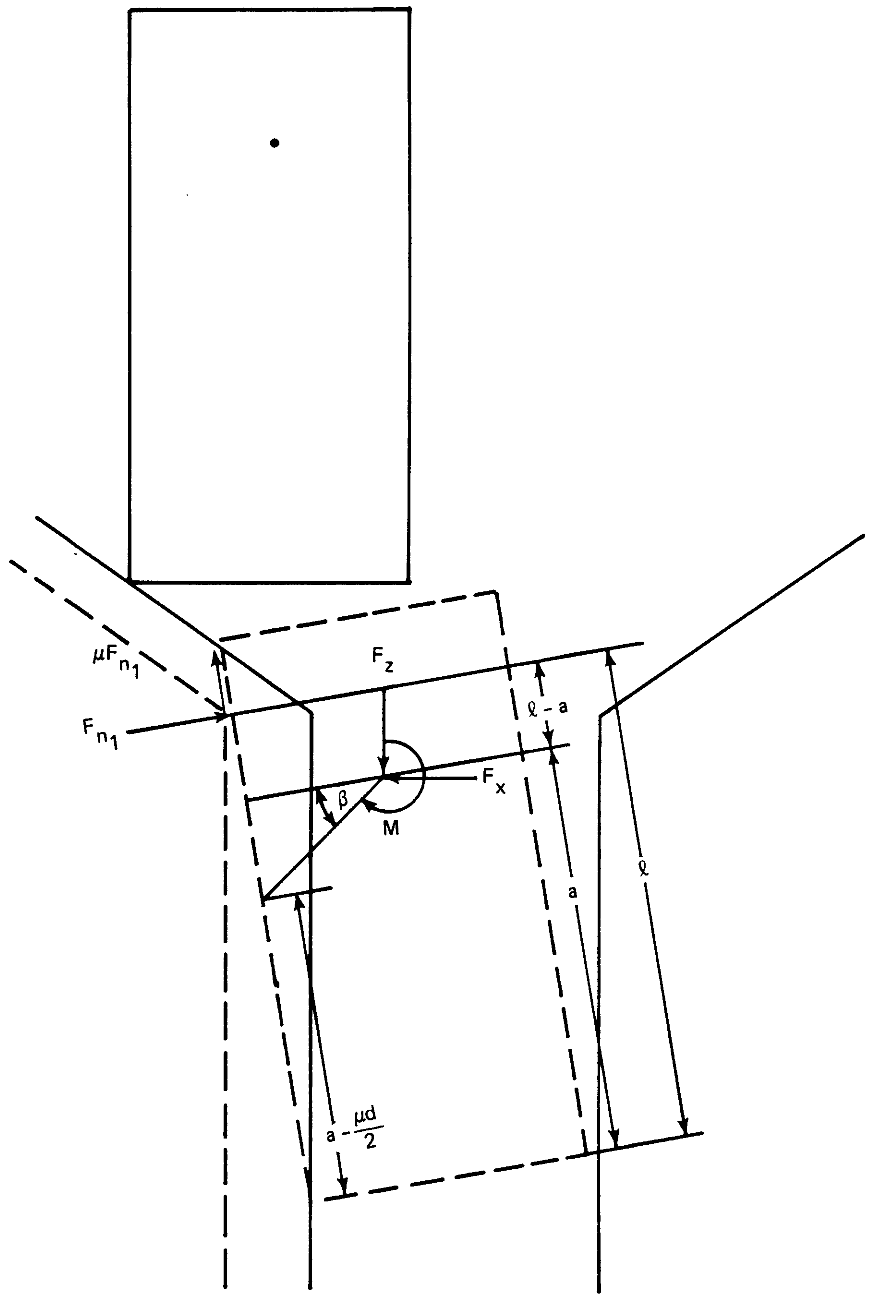

Figure 1.2.4. One-point contact ($\ell > a$).

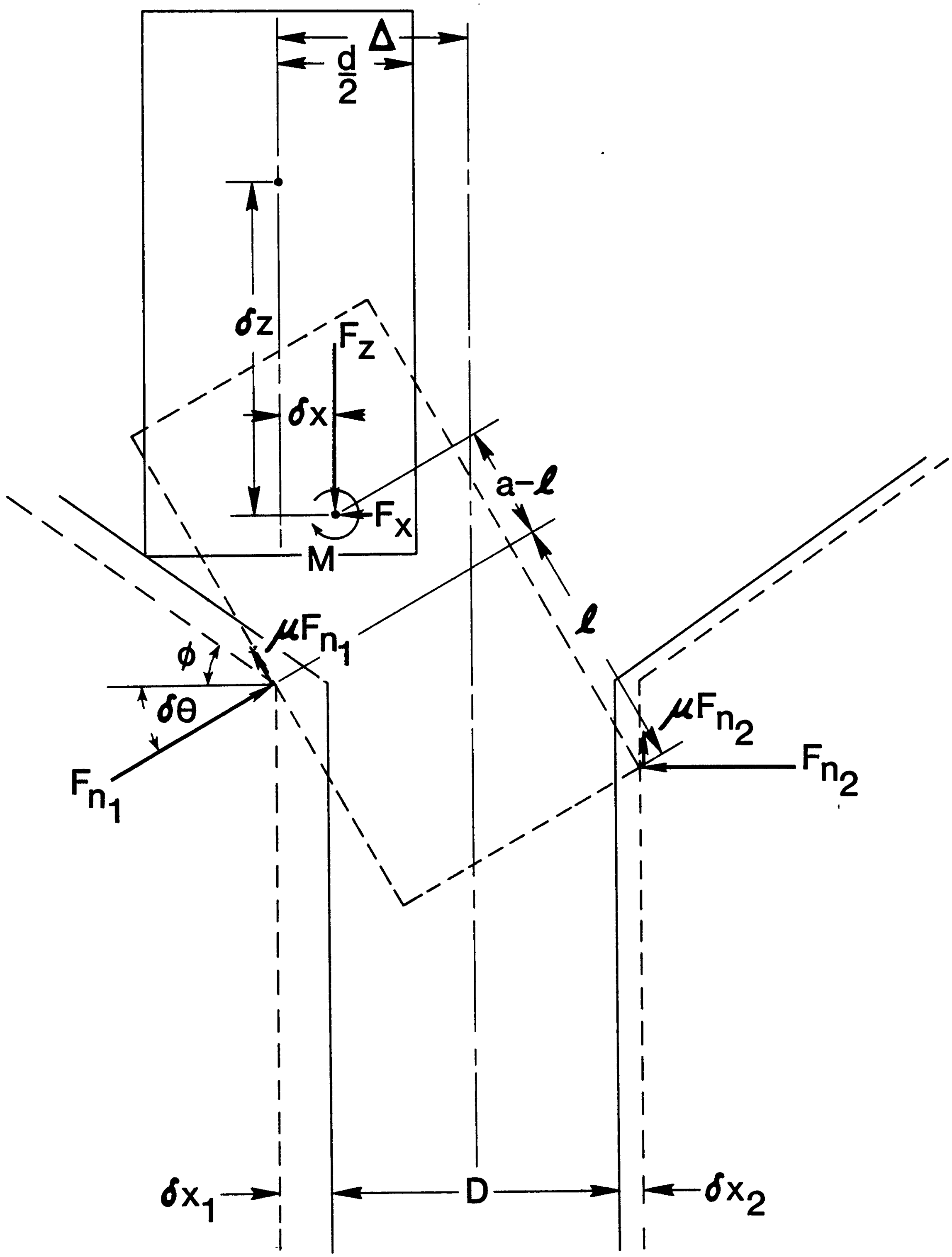

Figure 1.2.5. Two-point contact.

force-deformation relations must of course include the constitutive relations for the right hole wall's lateral compliance as well. An additional geometry constraint must also be present. So, in a similar manner to that shown earlier (see Figure 1.2.5) the following equations may be derived.

Equilibrium Requirements

$$F_x = F_{n_1}(\cos\delta\theta - \mu\sin\delta\theta) - F_{n_2}$$

$$F_z = F_{n_1}(\sin\delta\theta + \mu\cos\delta\theta) + \mu F_{n_2}$$

$$M = F_{n_1}\left[(a - \ell) - \frac{\mu d}{2}\right] - F_{n_2}\left[a(\cos\delta\theta - \mu\sin\delta\theta) - \frac{d}{2}(\sin\delta\theta + \mu\cos\delta\theta)\right] \qquad (1.2.13)$$

Force-Deformation Relations

$$F_x = K_x\delta x$$

$$M = K_\theta\delta\theta$$

$$K_{x_1}\delta x_1 = F_{n_1}(\cos\delta\theta - \mu\sin\delta\theta)$$

$$K_{x_2}\delta x_2 = F_{n_2} \qquad (1.2.14)$$

Geometric Compatibility Requirements

$$\Delta - \frac{CD}{2} = \delta x + \delta x_1 + (a - \ell)\sin\delta\theta + d\sin^2\frac{\delta\theta}{2}$$

$$a + \left(\Delta - \frac{CD}{2}\right)\tan\phi = \delta z + (a - \ell)\cos\delta\theta + \frac{d}{2}\sin\delta\theta$$

$$\ell\sin\delta\theta + d\cos\delta\theta = D + \delta x_1 + \delta x_2 \qquad (1.2.15)$$

The insertion distance is again ℓ and the resumption of one-point contact will occur when $F_{n_2} = \delta x_2 = 0$ is substituted into the two-point contact equations. These new equations, as expected, are the same as the one-point contact equations with the geometric constraint (Equation 1.2.9) imposed.

1.2.5 Solution of Assembly Equations

A. Introduction

Because of the complexity of the assembly equations, it was necessary to use a computer to solve them. Two types of solutions were obtained: (a) exact solutions and (b) linearized solutions. For the exact solutions simple iteration was used, and for the linearized solutions the linearization was carried out with respect to the insertion variables (except $\Delta z, \ell$), leaving the insertion parameters fixed. By definition, insertion variables are quantities which vary during the assembly (insertion) and insertion parameters remain constant during the assembly (insertion). Below, both methods of solution are explained further. In either case, dimensional analysis has been used in computed solutions as outlined in Table 1.2.1.

The dimensional analysis used below is, of course, not the only way to nondimensionalize the variables and parameters. Measuring distances with respect to a offers the advantage that δz for typical cases ranges from 0 to 1.1 ± 0.1 during the assembly process. This allows for easier interpretation of insertion force (F_z) versus depth (δz) plots. Also, because of the popularity of the clearance ratio (C), the diameter of the peg (d) is effectively treated as a dependent parameter.

B. Exact Solutions

Chamfer Crossing

Equations 1.2.1 through 1.2.3 may be manipulated to yield the following transcendental relation in $\delta\theta$ whose solution is shown graphically in Figure 1.2.6

$$\delta\theta = \frac{f_1(\delta\theta)\left\{a\left[\sin(\delta\theta+\phi) - \mu\cos(\delta\theta+\phi)\right] - \frac{d}{2}\left[\cos(\delta\theta+\phi) + \mu\sin(\delta\theta+\phi)\right]\right\}}{K_\theta\left(1/K_x + 1/K_{x_1}\right)\left(\sin\phi - \mu\cos\phi\right)} \tag{1.2.16}$$

Table 1.2.1 Dimensional Analysis

Insertion Parameters	Dimensionless Insertion Parameters
a	1
K_θ	1
μ	μ
ϕ	ϕ
C	C
Δ	Δ/a
D	D/a
d	$(1-C)D/a = \frac{d}{a}$
K_x	$\frac{K_x a^2}{K_\theta}$
K_{x_1}	K_{x_1}/K_x
K_{x_2}	K_{x_2}/K_x

Insertion Variables	Dimensionless Insertion Variables
$\delta\theta$	$\delta\theta$
δx	$\delta x/a$
δx_1	$\delta x_1/a$
δx_2	$\delta x_2/a$
δz	$\delta z/a$
Δz	$\Delta z/a$
ℓ	ℓ/a
F_n	aF_n/K_θ
F_{n_1}	aF_{n_1}/K_θ
F_{n_2}	aF_{n_2}/K_θ
F_x	aF_x/K_θ
F_z	aF_z/K_θ
M	$\frac{M}{K_\theta}$

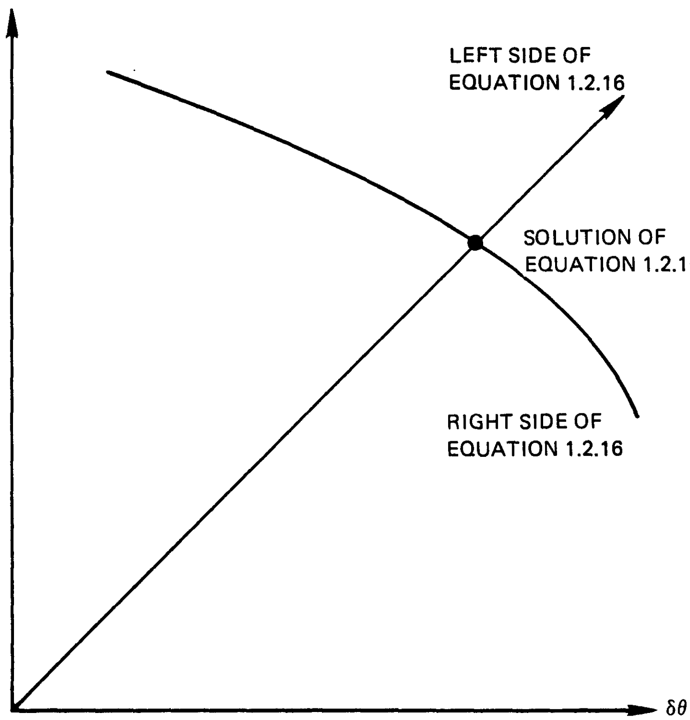

Figure 1.2.6. Graphical solution of equations 1.2.16 and 1.2.17.

where

$$f_1(\delta\theta) = \frac{\Delta z}{\tan\phi} - a\sin\delta\theta - d\sin^2\frac{\delta\theta}{2} \tag{1.2.17}$$

Once $\delta\theta$ has been established by iteration, the remaining variables are obtained easily by direct substitution.

<u>One-Point Contact</u>

Similar manipulation of Equations 1.2.6 through 1.2.8 yields

$$\delta\theta = \frac{\left[\left(\Delta - \frac{CD}{2}\right) - (a - \ell)\sin\delta\theta - d\sin^2\frac{\delta\theta}{2}\right]\left[(a - \ell) - \frac{\mu d}{2}\right]}{K_\theta\left(1/K_x + 1/K_{x_1}\right)\left(\cos\delta\theta - \mu\sin\delta\theta\right)} \tag{1.2.18}$$

which is also solved by iteration as motivated by Figure 1.2.6. Other variables may the be determined by direct substitution.

<u>Two-Point Contact</u>

Again the same iteration scheme works (use Equations 1.2.13 through 1.2.15) when applied to

$$\delta\theta = \frac{f_2(\delta\theta)\left[\left(K_x + K_{x_1}\right)f_3(\delta\theta) + K_{x_1}\left[(a - \ell) - \frac{\mu d}{2}\right]\Big/(\cos\delta\theta - \mu\sin\delta\theta)\right]}{K_\theta\left(K_x + K_{x_1} + K_{x_2}\right)}$$

$$- K_x f_3(\delta\theta)\left[\left(\Delta - \frac{CD}{2}\right) - (a - \ell)\sin\delta\theta - d\sin^2\frac{\delta\theta}{2}\right]\Big/K_\theta \tag{1.2.19}$$

where

$$f_2(\delta\theta) = K_x\left[\left(\Delta - \frac{CD}{2}\right) - (a - \ell)\sin\delta\theta - d\sin^2\frac{\delta\theta}{2}\right]$$

$$+ K_{x_2}(d\cos\delta\theta - D + \ell\sin\delta\theta)$$

$$f_3(\delta\theta) = \frac{d}{2}(\sin\delta\theta + \mu\cos\delta\theta) - a(\cos\delta\theta - \mu\sin\delta\theta) \tag{1.2.20}$$

The other variables may then be solved for directly once $\delta\theta$ is known.

Computer Program

The computer program written to solve the assembly equations is called "LATERAL" (see Appendix A). Given the insertion parameters as inputs it computes F_z, δz, $\delta\theta$, and δx for various insertion distances $(\Delta z, \ell)$ during the entire assembly. Because of the inherent complexity of the equations, care was taken to verify a proposed solution by substituting the insertion solution variables back into all of the equations and displaying an "error matrix" while the program is running. Each entry in the matrix corresponds to the residual error in an equation. The value of ℓ for which one-point contact ended and two-point contact began was not determined exactly since double iteration was required. Instead a modification of Equation 1.2.9 was used. For a given value of ℓ, if the left side is greater than the right side, two-point contact occurs. Otherwise, one-point contact occurs. For the boundary between two-point contact and one-point contact, the sign of the normal force (or δx_2) on the right side of the hole was observed. When its algebraic sign changed (+ to -) the resumption of one-point contact had begun.

C. Linearized Solutions

As mentioned earlier, the linearized solutions were determined by linearizing the assembly equations with respect to all of the insertion variables (except $\Delta z, \ell$) and then solving them. The details of the linearization will not be given, but basically it involves expanding all of the terms that appear in each equation and canceling all of the nonlinear terms, thus arriving at a set of linearized equations.

The program written to solve these linearized equations is called "LINLAT" (see Appendix A). Given the insertion parameters as inputs it computes F_z, δz, $\delta\theta$, and δx for various insertion distances $(\Delta z, \ell)$ during the entire assembly. The linearized equations can also be solved directly and some of these solutions $(\delta x, \delta\theta)$ are given in Table 1.2.2 for each assembly phase. As it turns out δx and $\delta\theta$ are "easier" to solve for than many of the other variables. The variables F_z, δz may be obtained readily once δx and $\delta\theta$ are known. Again the value of ℓ for which one-point contact ended was not solved for exactly. Instead, Equation 1.2.9 was linearized and used as described before. Also, the sign of the normal force on the right side of the hole was used to determine when the resumption of one-point contact begins.

Table 1.2.2. Linearized Solutions for δx and $\delta\theta$.

Chamfer Crossing

$$\delta x = \frac{K_\theta \Delta z}{\tan\phi\left[K_x a^2\left(1 - \frac{d}{2a\tan(\phi - \beta)}\right) + K_\theta + K_x K_\theta / K_{x_1}\right]}$$

$$\delta\theta = \frac{K_x a \Delta z}{\tan\phi\left[K_x a^2 + \frac{K_\theta}{\left(1 - \frac{d}{2a\tan(\phi - \beta)}\right)} + \frac{K_x K_\theta / K_{x_1}}{\left(1 - \frac{d}{2a\tan(\phi - \beta)}\right)}\right]}$$

One-Point Contact

$$\delta x = \frac{K_\theta\left(\Delta - \frac{CD}{2}\right)}{K_x(a - \ell)\left[(a - \ell) - \frac{\mu d}{2}\right] + K_\theta + K_x K_\theta / K_{x_1}}$$

$$\delta\theta = \frac{K_x\left(\Delta - \frac{CD}{2}\right)\left[(a - \ell) - \frac{\mu d}{2}\right]}{K_x(a - \ell)\left[(a - \ell) - \frac{\mu d}{2}\right] + K_\theta + K_x K_\theta / K_{x_1}}$$

Two-Point Contact

$$\delta x = \frac{K_\theta K_{x_1}\left(\Delta - \frac{CD}{2}\right) + K_\theta K_{x_2}\left(\Delta + \frac{CD}{2}\right) + K_{x_1}K_{x_2}\ell\left[\ell\left(\Delta + \frac{CD}{2}\right) - aCD\right]}{K_x K_\theta + K_x K_{x_1}(a - \ell)\left[(a - \ell) - \frac{\mu d}{2}\right] + K_x K_{x_2} a\left(a - \frac{\mu d}{2}\right) + K_\theta K_{x_1} + K_\theta K_{x_2} + K_{x_1}K_{x_2}\ell^2}$$

$$\delta\theta = \frac{K_x K_{x_1}\left(\Delta - \frac{CD}{2}\right)\left[(a - \ell) - \frac{\mu d}{2}\right] + K_x K_{x_2}\left(a - \frac{\mu d}{2}\right)\left(\Delta + \frac{CD}{2}\right) + K_{x_1}K_{x_2}\ell CD}{K_x K_\theta + K_x K_{x_1}(a - \ell)\left[(a - \ell) - \frac{\mu d}{2}\right] + K_x K_{x_2} a\left(a - \frac{\mu d}{2}\right) + K_\theta K_{x_1} + K_\theta K_{x_2} + K_{x_1}K_{x_2}\ell^2}$$

1.2.6 Results and Discussion

Once the assembly equations have been solved for the entire assembly process, the effect of various insertion parameters on the solution can be determined. Of primary interest is the effect of the insertion parameters on the "insertion force versus depth" plot (i.e., F_z versus δz). In the present section the effect of the insertion parameters which are unique to (1) the lateral compliance hole and (2) the lateral and rotational compliance (Section 1.4) hole problems will be analyzed. These parameters are, of course, K_{x_1} and K_{x_2}. Other effects, such as the linearization effect and alternative assembly modes, will also be discussed. In addition, the effect of location of the compliance center of the peg on the assembly will be investigated.

General Features of Force versus Depth Plots

As discussed earlier, the general assembly sequence considered is (1) chamfer crossing, followed by (2) one-point contact, (3) two-point contact, (4) resumption of one-point contact, and (5) line contact. These assembly phases may be identified in the force versus depth plot. In Figure 1.2.7 some typical plots (exact solutions) are shown (use $K_{x_1}/K_x = 10$ curve). The chamfer crossing region is seen to be very linear, followed by a discontinuity where one-point contact begins. The force during one-point contact is also reasonably linear, and in this instance almost constant. After one-point contact the insertion force rises sharply during two-point contact to a maximum and then gradually declines to where one-point contact resumes. This resumption of one-point contact is typically of short duration as the peg snaps back to line contact. The insertion force in this region also tends to be very linear. Finally, line contact occurs and is represented by the end point of the curve.

Effect of the Left Hole Wall Compliance on Insertion Force versus Depth

The effect of the compliance of the left side of the hole (measured by K_{x_1}/K_x) on F_z versus δz is shown in Figure 1.2.7. Decreasing the compliance (increasing the spring rate) of the left side is seen to increase the insertion force during each of the assembly phases and vice versa. If the compliance of the left side is large enough, two-point contact will not occur (e.g., $K_{x_1}/K_x = 0.5$).

Effect of the Right Hole Wall Compliance on Insertion Force versus Depth

In Figure 1.2.8 the effect of the compliance of the right side of the hole (measured by K_{x_2}/K_x) is shown. Chamfer crossing and one-point contact are of course not affected by the right hole wall's compliance. Again decreasing the compliance is seen to increase the insertion force during two-point contact and vice versa.

Effect of Linearization

The linearization, in general, tends to distort the solution and is quite sensitive to insertion parameters which produce large angular misalignments (e.g., $\delta\theta = 10°$). In Figure 1.2.9 two solutions (F_z versus δz) are given, one for a small ratio ($K_{x_1}/K_x = 1$) and one for a large ratio ($K_{x_1}/K_x = 10$). In each case a linearized solution is also given. Note that both the linearized solution and the exact solution agree at the beginning of the assembly and at the end of the assembly (line contact). The linearized solution also exhibits the general features of the exact solution as discussed above but tends to predict larger insertion forces during chamfer crossing and smaller insertion forces during the rest of the assembly.

In Figure 1.2.10 the effect of the linearization on F_z, $\delta\theta$, δx versus δz is shown. The plot of angular misalignment ($\delta\theta$) versus depth (δz) is very linear during chamfer crossing. During one-point contact the angle ($\delta\theta$) increases with a reasonably continuous transition (also in slope) to two-point contact where a maximum occurs. Note that the "jump" in $\delta\theta$ between chamfer crossing and one-point contact is insignificant as mentioned earlier (essentially no jump in <u>geometric</u> variables). The angle then decreases gradually during the remaining portion of two-point contact. During the resumption of one-point contact the angle changes rapidly as the peg snaps back to line contact ($\delta\theta = 0$). The linearization effect is seen to predict slightly smaller angles during two-point contact while predicting the angle very accurately during chamfer crossing, one-point contact, and the resumption of one-point contact. The plot of horizontal displacement (δx) versus depth (δz) (i.e., peg position) is seen to be steadily increasing (almost linearly) and quite insensitive to the different assembly phases (e.g., no discontinuities, sharp rises, etc.). The linearization effect is seen to be insigificant in this example.

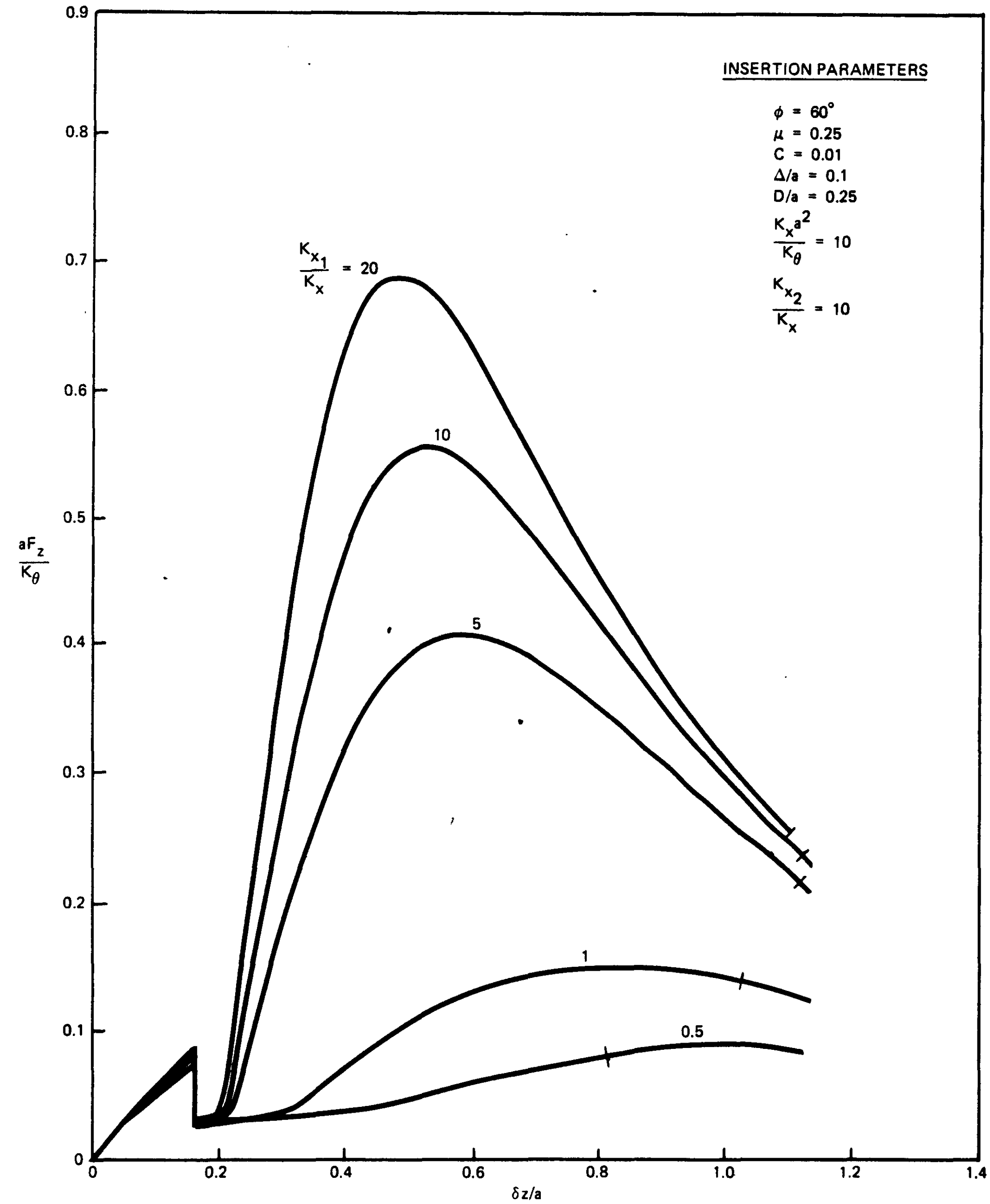

Figure 1.2.7. Effect of K_{x_1}/K_x on F_z versus δz.

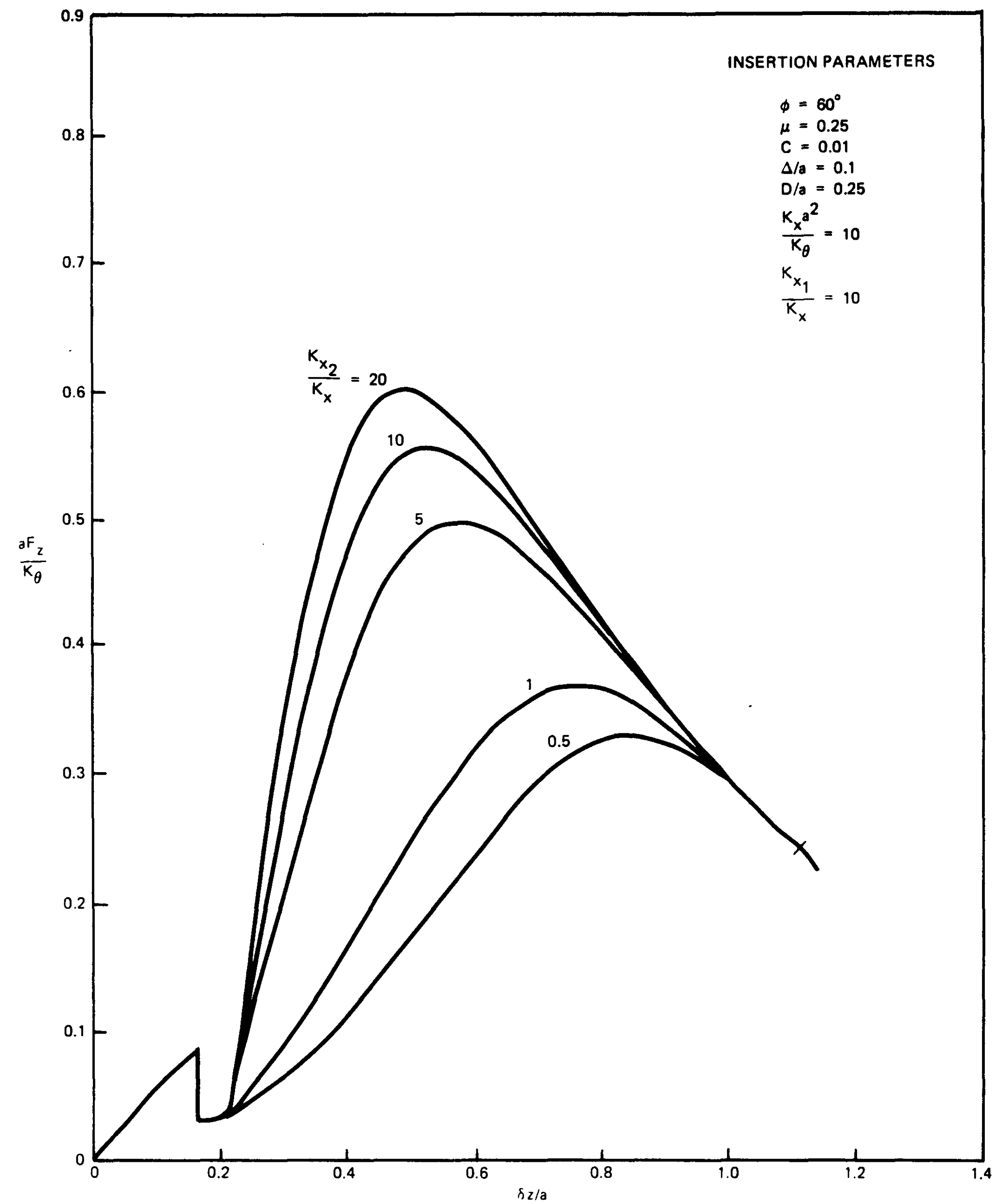

Figure 1.2.8. Effect of K_{x_2}/K_x on F_z versus δz.

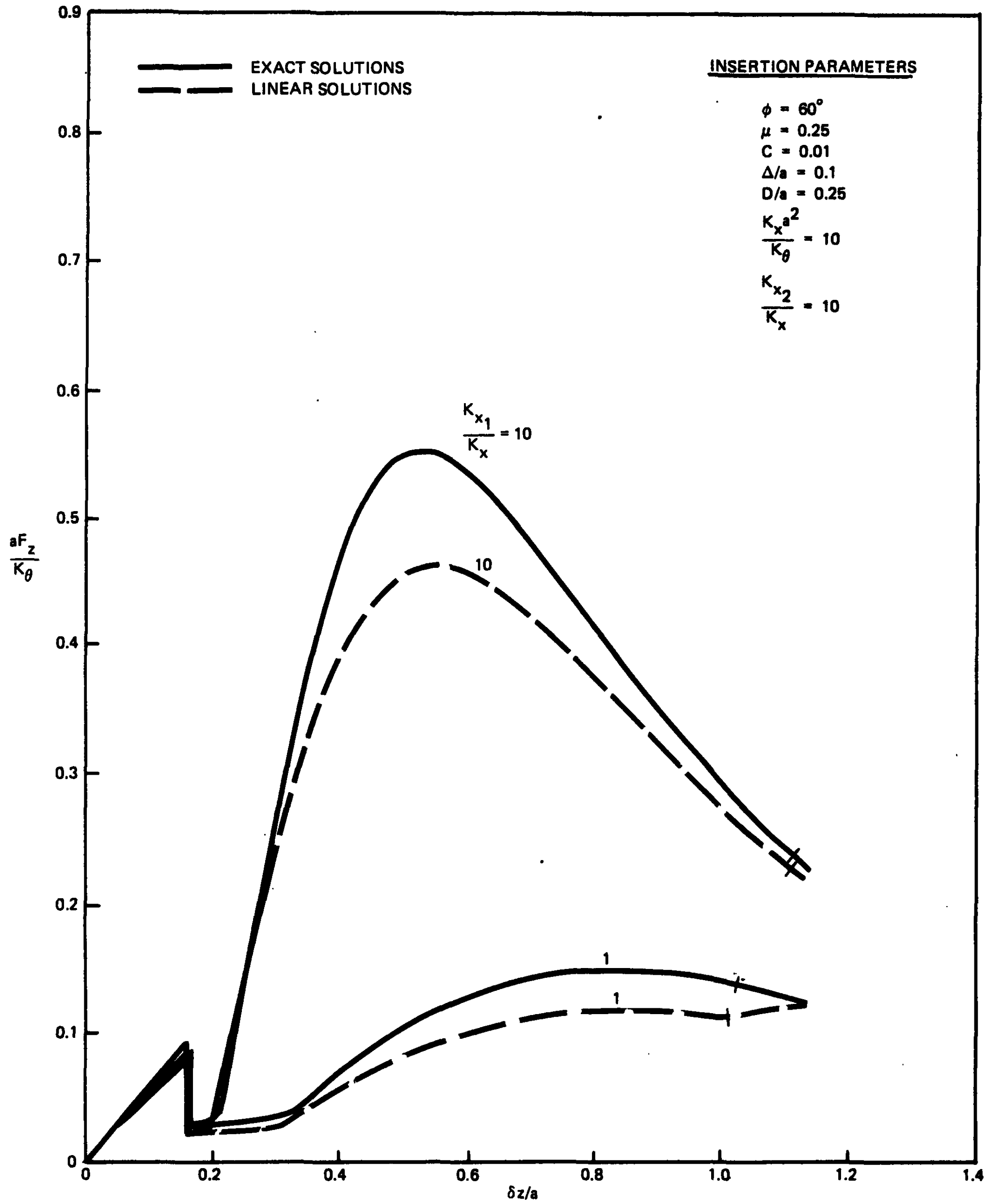

Figure 1.2.9. Comparison of linearized solutions with exact solutions for several K_{x_1}/K_x.

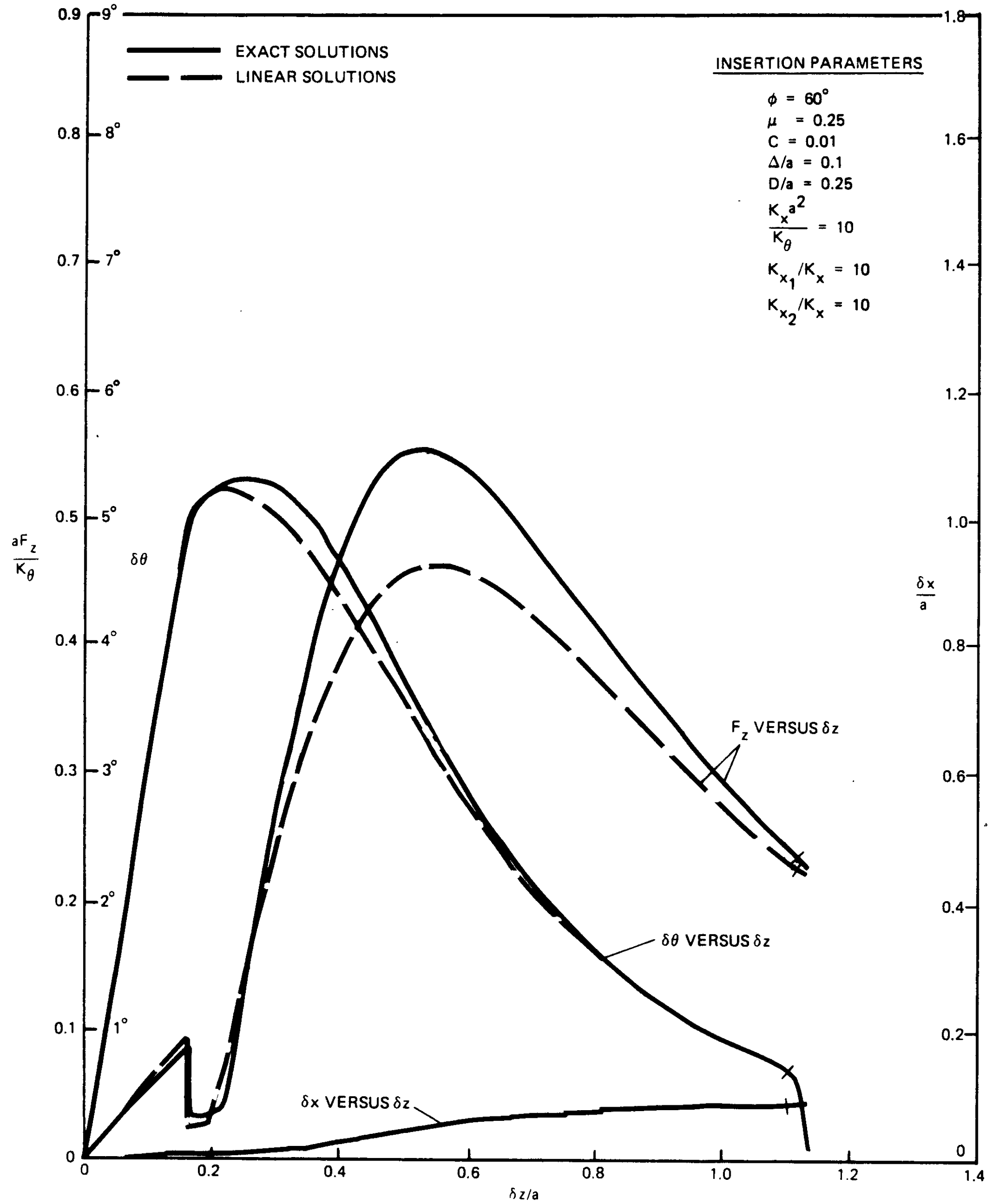

Figure 1.2.10. Effect of linearization on F_z, $\delta\theta$, δx versus δz.

Alternative Assembly Modes

Although successful assembly has been emphasized, one must also consider the alternative, which is also of practical interest. Real parts resembling the peg and hole in the initial configuration, as shown in Figure 1.1.3(b) may be assembled also if additional assembly phases are considered, or they may not be assembled at all. Figure 1.2.11 illustrates two of these undesirable or unsuccessful modes of assembly. These are certainly not the only possibilities.

Even though these and other modes can be identified, finding explicit criteria is often difficult. However, for the undesirable chamfer line contact shown in Figure 1.2.11(a), a simple criterion exists. By using Equations 1.2.1 through 1.2.3 with $\delta\theta$ replaced by $\frac{\pi}{2} - \phi$ (rad) the insertion distance Δz for which line contact will occur may be solved for

$$\Delta z = \tan\phi \left[a\cos\phi + \frac{d}{2}(1 - \sin\phi) + \frac{K_\theta (1/K_x + 1/K_{x_1})\left(\frac{\pi}{2} - \phi\right)(\sin\phi - \mu\cos\phi)}{\left(a - \frac{\mu d}{2}\right)} \right] \quad (1.2.21)$$

To make sense physically the undesirable line contact with the chamfer must occur between the start of the assembly and when the corner of the peg meets the corner of the chamfer so that

$$0 < \Delta z < \left(\Delta - \frac{CD}{2}\right)\tan\phi \quad (1.2.22)$$

Since the stiffnesses K_θ, K_x, and K_{x_1} are positive, Equation 1.2.21 and Inequality 1.2.22 may be reduced to the simple inequality

$$K_\theta (1/K_x + 1/K_{x_1}) < K_{min} \quad (1.2.23)$$

where

$$K_{min} = \frac{\left(a - \frac{\mu d}{2}\right)\left[\left(\Delta - \frac{CD}{2}\right) - a\cos\phi - \frac{d}{2}(1 - \sin\phi)\right]}{\left(\frac{\pi}{2} - \phi\right)(\sin\phi - \mu\cos\phi)} \quad (1.2.24)$$

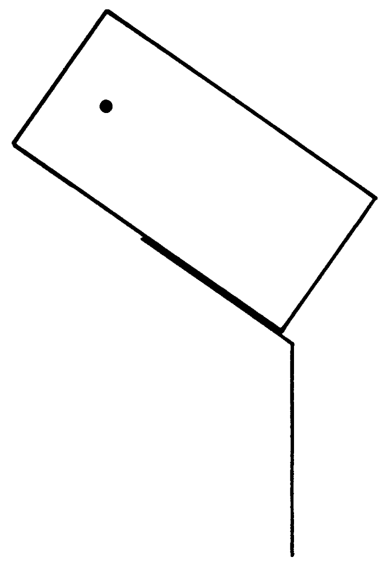

(a) Undesirable Line Contact

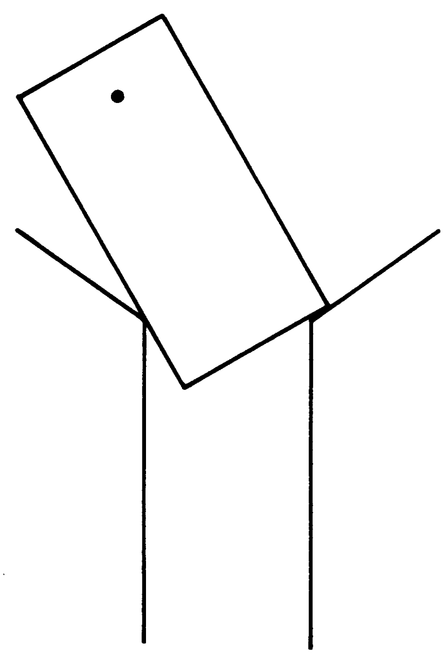

(b) Undesirable Two–Point Contact

Figure 1.2.11. Undesirable assembly phases.

Now to avoid this type of line contact the inequality must be reversed, i.e.,

$$K_\theta (1/K_x + 1/K_{x_1}) > K_{min} \tag{1.2.25}$$

This relation intuitively makes sense. If line contact with the chamfer should occur, then increasing the stiffness K_θ or decreasing either of the stiffnesses K_x, K_{x_1} will prevent line contact from happening. This simple example demonstrates that properly specified compliance can aid assembly.

Location of Compliance Center of Peg

In the analysis so far the location of the compliance center of the peg has been assumed to remain fixed with respect to the peg, and no special considerations have been given to its location other than

$$a \geq \frac{d}{2 \tan(\phi + \delta\theta - \beta)} \tag{1.2.26}$$

during chamfer crossing and

$$a \geq \frac{\mu d}{2} \tag{1.2.27}$$

during one-point contact. If, however, a is taken to be an insertion variable whose value may be independently controlled, a much simpler and shorter assembly sequence is possible.

This simplified assembly sequence consists of only (1) chamfer crossing followed by (2) a vertical motion of the peg (vertical insertion) as illustrated in Figure 1.2.12. Basically, all angular misalignments have been eliminated ($\delta\theta \cong 0$) by carefully selecting the location of the compliance center of the peg during the assembly sequence. Note that since the clearance ratio is taken to be positive, two-point contact does not occur.

As the assembly proceeds angular errors ($\delta\theta$) will be present. These angular errors may be eliminated by locating the compliance center of the peg a distance $a_0(\delta\theta)$ away from the end of the peg

$$a_0(\delta\theta) = \frac{d}{2\tan(\phi - \beta + \delta\theta)} \tag{1.2.28}$$

This may be derived from Equations 1.2.1 and 1.2.2. When $\delta\theta = 0$

$$a_0 = \frac{d}{2\tan(\phi - \beta)} \tag{1.2.29}$$

which may also be obtained from Table 1.2.2. Equation 1.2.28 in some sense represents a feedback scheme; as angular errors arise a is continuously adjusted to eliminate them (see Figure 1.2.13).

Once the corner of the peg reaches the corner of chamfer, chamfer crossing ends and a new assembly phase begins. Exactly which assembly phase begins is not at all clear. Ideally the value of a has been adjusted continuously during chamfer crossing so as to eliminate any angular misalignments which may arise (i.e., $\delta\theta = 0$). The next logical assembly phase would then be line contact. However, by virtue of controlling a, errors will be present so $\delta\theta = 0^{\pm}$ is more realistic. If $\delta\theta = 0^{+}$ the next assembly phase will be one-point contact. By following a similar procedure (see Equations 1.2.6 and 1.2.7 or Table 1.2.2) as in the chamfer crossing case a_0 is given by

$$a_0 = \ell + \frac{\mu d}{2} \tag{1.2.30}$$

where no feedback of $\delta\theta$ is necessary. If $\delta\theta = 0^{-}$ the next assembly phase will be the new type of one-point contact (see Figure 1.1.5(b)). A simple moment balance (not shown here) yields

$$a_0 = \frac{\mu d}{2} \tag{1.2.31}$$

where the feedback relation is given by

$$a(\delta\theta) = \frac{d}{2}\tan(\beta - \delta\theta) \tag{1.2.32}$$

However, this feedback scheme is not stable since $\delta\theta$ must be negative. These results are summarized in Figures 1.2.14 and 1.2.15, where a_0 is plotted against the assembly phase and the sensitivity of the feedback equations is shown for $\phi = 60°$, $\mu = 0.25$.

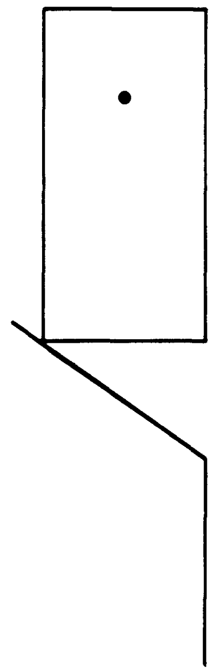

(a) Chamfer Crossing

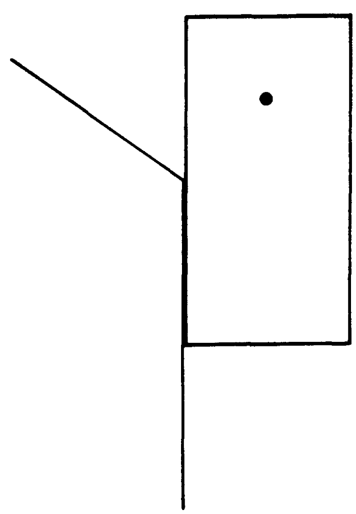

(b) Vertical Insertion

Figure 1.2.12. Simplified assembly sequence.

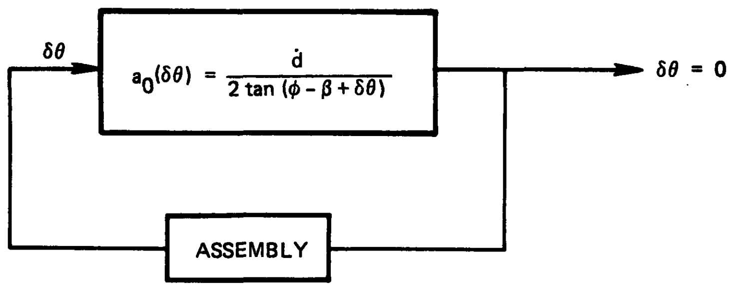

Figure 1.2.13. Feedback scheme.

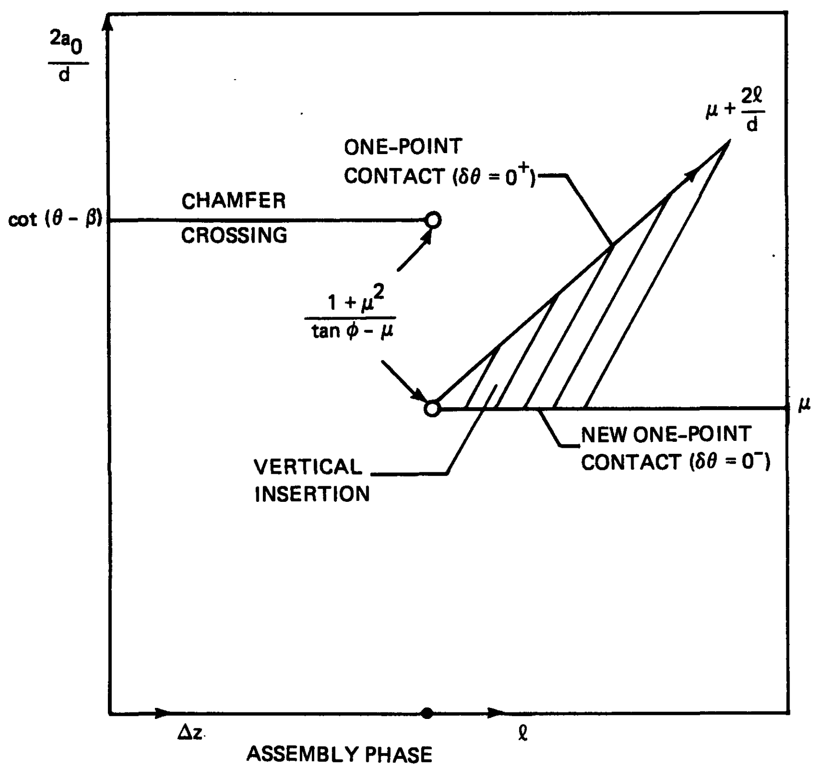

Figure 1.2.14. Optimal compliance location (a_o) versus assembly phase.

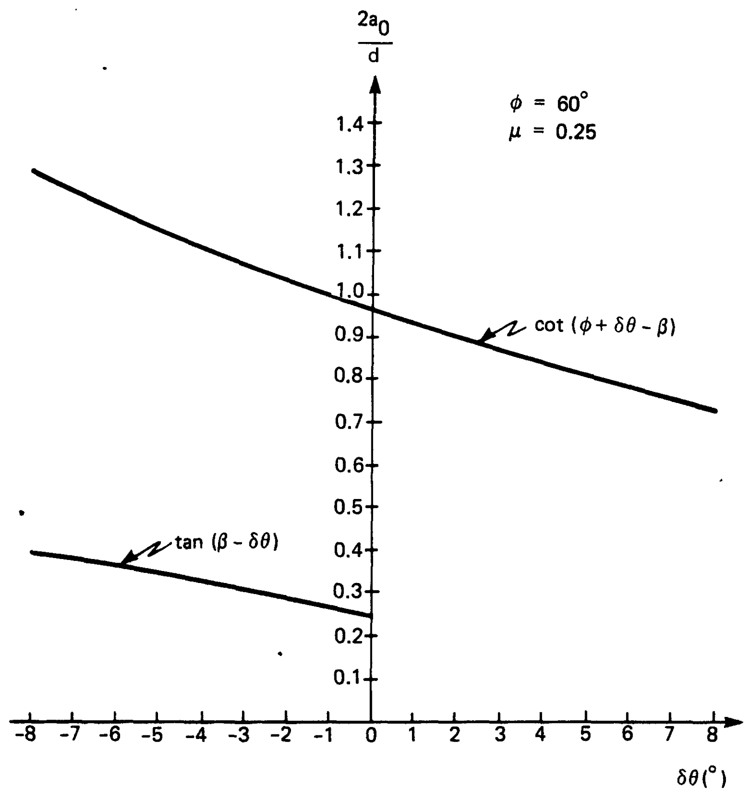

Figure 1.2.15. Sensitivity of feedback equations.

1.3 ROTATIONAL COMPLIANCE HOLE

1.3.1 Introduction

In certain cases it is necessary for the model to incorporate only rotational hole compliance. Figure 1.3.1 illustrates the initial configuration of the peg and hole with the compliance center of the peg indicated. The hole also possesses its own compliance centers as indicated which are assumed to be located symmetrically about the center axis of the hole. During the assembly to be considered the hole walls will initially deform outward, enlarging the hole. This deformation will be treated as a rotation of each hole wall about its compliance center. Both sides of the hole will then rotate away from the center axis of the hole (i.e., $\delta\theta_1, \delta\theta_2 \geq 0$). The quasi-static phases of successful assembly to be analyzed are the same as before: (1) chamfer crossing, followed by (2) one-point contact, (3) two-point contact, (4) resumption of one-point contact, and the final phase, (5) line contact.

The location of the compliance centers can affect the insertion characteristics greatly. If the compliance center of the peg is located too close to the end of the peg, the other type of one-point contact cannot be avoided. If the compliance center of the hole is located in Region 1 (see Figure 1.3.1), it is possible for the left side of the hole to interfere with the assembly by rotating clockwise and decreasing the effective hole diameter. Similarly, in Region II, it is possible for the right side of the hole to complicate the assembly by means of a line contact. This follows in part from the general argument presented in Section 1.2.3 where it was shown that one-point contact must end a distance $\ell = a - \frac{\mu d}{2}$ into the hole. Region III then appears to be the "safest" region since the sides of the hole will not decrease the effective hole diameter. For this reason, the examples analyzed later have the compliance center located in Region III.

Since the derivation of the assembly equations for the rotational compliance hole case is very similar to the derivation of the assembly equations for the lateral compliance hole case, the development will be quite brief with basically only figures and equations used.

1.3.2 Chamfer Crossing

Proceeding as before (Section 1.2.2) with the aid of Figure 1.3.2 the following equations may be derived. Additional insertion parameters may be identified in an obvious manner (e.g., K_{θ_1}—rotational stiffness of left hole wall).

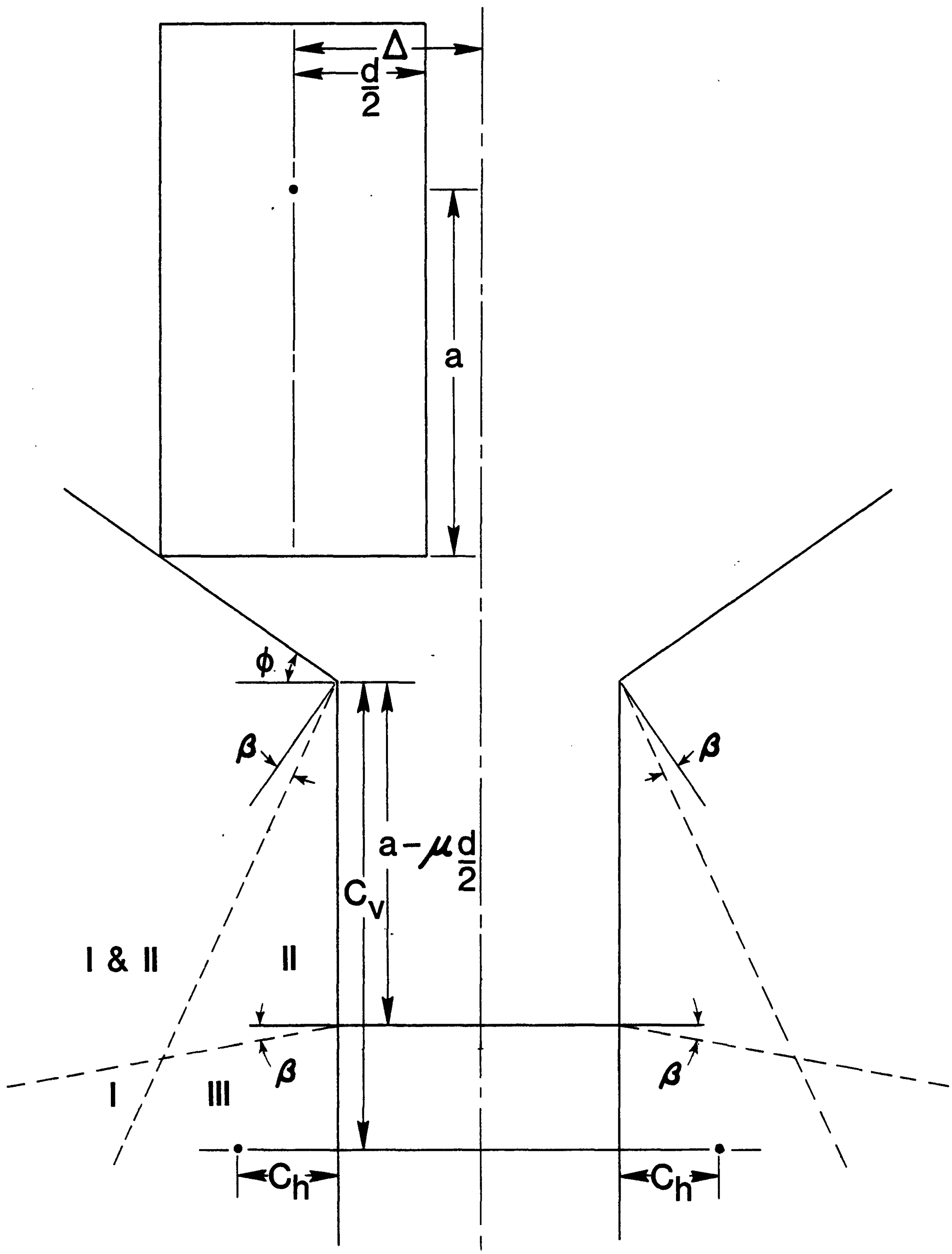

Figure 1.3.1. Initial configuration of peg and hole.

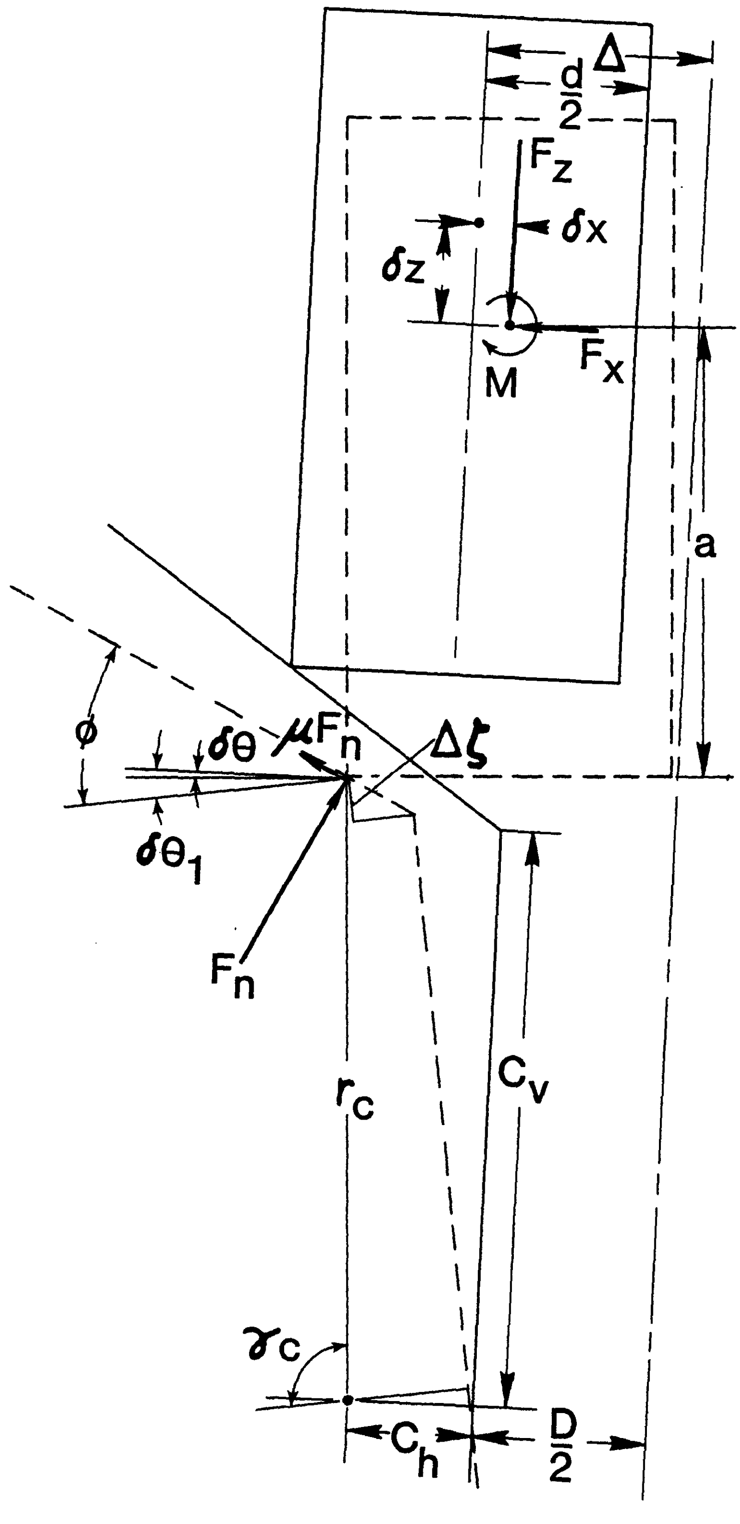

Figure 1.3.2. Chamfer crossing.

Equilibrium Requirements

$$F_x = F_n[\sin(\phi - \delta\theta_1) - \mu\cos(\phi - \delta\theta_1)]$$

$$F_z = F_n[\cos(\phi - \delta\theta_1) + \mu\sin(\phi - \delta\theta_1)]$$

$$M = F_n\{a[\sin(\phi + \delta\theta - \delta\theta_1) - \mu\cos(\phi + \delta\theta - \delta\theta_1)]$$

$$- \frac{d}{2}[\cos(\phi + \delta\theta - \delta\theta_1) + \mu\sin(\phi + \delta\theta - \delta\theta_1)]\} \tag{1.3.1}$$

Force-Deformation Relations

$$F_x = K_x\,\delta x$$

$$M = K_\theta\,\delta\theta$$

$$K_{\theta_1}\delta\theta_1 = F_n\Big[(\Delta\zeta + C_V)(\sin\phi - \mu\cos\phi)$$

$$+\left(\frac{\Delta\zeta}{\tan\phi} - C_h\right)(\cos\phi + \mu\sin\phi)\Big] \tag{1.3.2}$$

Geometric Compatibility Requirements

$$\frac{\Delta z}{\tan\phi} = \delta x + a\sin\delta\theta + r_c[\cos(\gamma_c - \delta\theta_1) - \cos\gamma_c] + d\sin^2\frac{\delta\theta}{2}$$

$$a + \Delta z = \delta z + a\cos\delta\theta + \frac{d}{2}\sin\delta\theta + r_c[\sin(\gamma_c - \delta\theta_1) - \sin\gamma_c] \tag{1.3.3}$$

For convenience the following dependent insertion variables $(\Delta\zeta, r_c, \gamma_c)$ have been introduced by the following relationships

$$\Delta z + \Delta\zeta = \left(\Delta - \frac{CD}{2}\right)\tan\phi$$

$$r_c^2 = (C_V + \Delta\zeta)^2 + \left(\frac{\Delta\zeta}{\tan\phi} - C_h\right)^2$$

$$\cot \gamma_c = \frac{\frac{\Delta\zeta}{\tan \phi} - C_h}{C_V + \Delta\zeta} \qquad (1.3.4)$$

Again chamfer crossing begins when the insertion distance $\Delta z = 0$, and ends when $\Delta z = (\Delta - \frac{CD}{2})\tan \phi$.

To avoid the undesirable type of one-point contact, the compliance center of the peg must be located a distance at least $\frac{d}{2\tan(\phi + \delta\theta - \delta\theta_1 - \beta)}$ from the end of the peg where $\delta\theta > \delta\theta_1 \geq 0$. This may be derived by (1) fixing the compliance center of the hole in Region III so that $\delta\theta_1 \geq 0$, (2) requiring $\delta\theta > \delta\theta_1$ so that the other type of one-point contact won't happen, and (3) using Equation 1.3.1 with (1) and (2) imposed. In Section 1.3.6, however, it will be shown that the other type of one-point contact can be used to simplify the assembly sequence.

1.3.3 One-Point Contact

Immediately following chamfer crossing is the "discontinuity phase" discussed earlier and then one-point contact. In a similar manner (see Section 1.2.3) the following equations may be derived with the aid of Figure 1.3.3.

Equilibrium Requirements

$$F_x = F_{n_1}(\cos \delta\theta - \mu \sin \delta\theta)$$

$$F_z = F_{n_1}(\sin \delta\theta + \mu \cos \delta\theta)$$

$$M = F_{n_1}\left[(a - \ell) - \frac{\mu d}{2}\right] \qquad (1.3.5)$$

Force-Deformation Relations

$$F_x = K_x \, \delta x$$

$$M = K_\theta \delta\theta$$

$$K_{\theta_1}\delta\theta_1 = F_{n_1}\{C_V[\cos(\delta\theta - \delta\theta_1) - \mu \sin(\delta\theta - \delta\theta_1)]$$

$$- C_h[\sin(\delta\theta - \delta\theta_1) + \mu \cos(\delta\theta - \delta\theta_1)]\} \qquad (1.3.6)$$

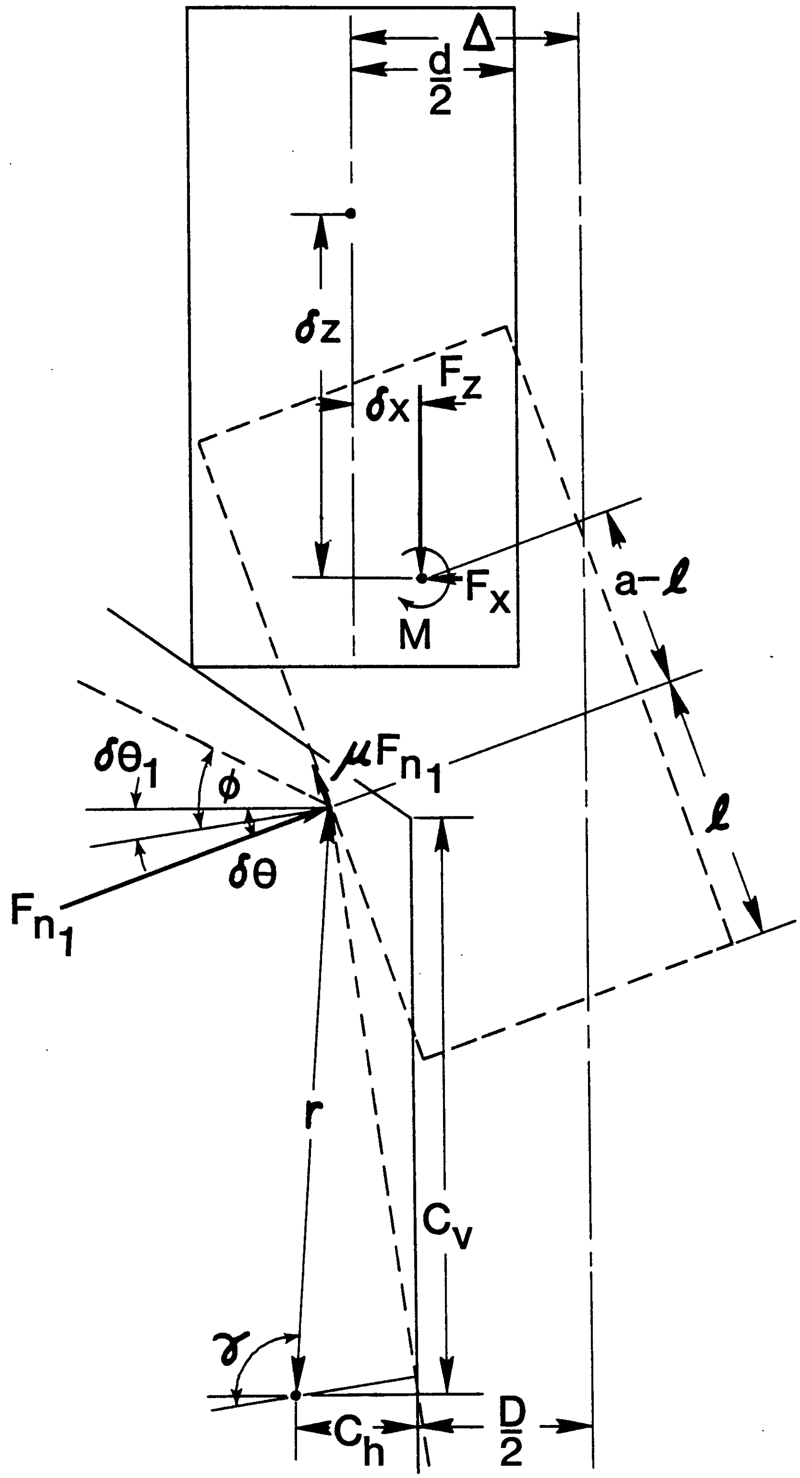

Figure 1.3.3. One-point contact.

Geometric Compatibility Requirements

$$\Delta - \frac{CD}{2} = \delta x + (a - \ell) \sin \delta\theta + r[\cos(\gamma - \delta\theta_1) - \cos \gamma]$$

$$+ d \sin^2 \frac{\delta\theta}{2}$$

$$a + \left(\Delta - \frac{CD}{2}\right)\tan \phi = \delta z + (a - \ell)\cos \delta\theta + \frac{d}{2} \sin \delta\theta$$

$$+ r[\sin (\gamma - \delta\theta_1) - \sin \gamma] \qquad (1.3.7)$$

Again ℓ is the insertion distance and one-point contact begins when $\ell = 0$. Also, the angle of the peg with respect to the left hole wall $(\delta\theta - \delta\theta_1)$ must be nonnegative. From Equations 1.3.5 and 1.3.6 it follows that $a \geq \frac{\mu d}{2}$ as before.

One-point contact (two-point contact) ends and two-point contact (resumption of one-point contact) begins when

$$\ell \sin \delta\theta + d \cos \delta\theta = D + r[\cos(\gamma - \delta\theta_1) - \cos \gamma] \qquad (1.3.8)$$

Manipulation of the above equation with the one-point contact equations yields the following quadratic in $(a - \ell)$

$$\sin \delta\theta(a - \ell)^2 + B(\delta\theta,\delta\theta_1)(a - \ell) + C(\delta\theta,\delta\theta_1) = 0 \qquad (1.3.9)$$

where $B(\delta\theta,\delta\theta_1)$, $C(\delta\theta,\delta\theta_1)$ are complicated expressions. Since Equation 1.3.9 will yield two real roots or two complex roots for $(a - \ell)$, a resumption of one-point contact is possible. This has been verified by computer runs. Also, since the argument presented in Section 1.2.3 regarding the duration of one-point contact is completely general, the largest value of ℓ for which one-point contact is possible is $a - \frac{\mu d}{2}$.

1.3.4 Two-Point Contact

In general, one-point contact is followed by two-point contact (see Figure 1.3.4). Similarly (see Section 1.2.4) the following equations may be derived. Here, K_{θ_2} is the rotational stiffness of the right hole wall.

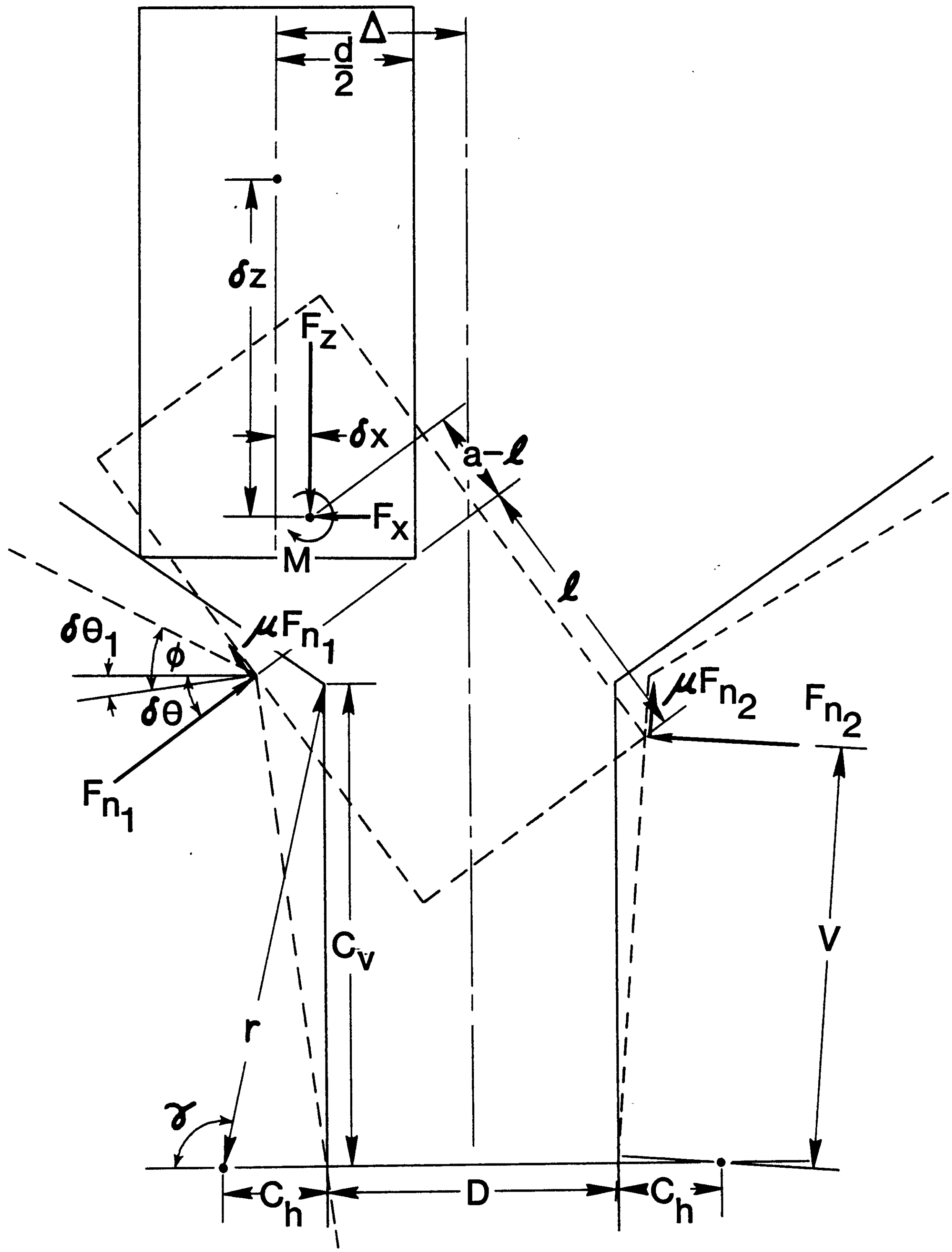

Figure 1.3.4. Two-point contact.

Equilibrium Requirements

$$F_x = F_{n_1}(\cos \delta\theta - \mu \sin \delta\theta) - F_{n_2}(\cos \delta\theta_2 - \mu \sin \delta\theta_2)$$

$$F_z = F_{n_1}(\sin \delta\theta + \mu \cos \delta\theta) + F_{n_2}(\sin \delta\theta_2 + \mu \cos \delta\theta_2)$$

$$M = F_{n_1}\left[(a - \ell) - \frac{\mu d}{2}\right] - F_{n_2}\{a[\cos(\delta\theta + \delta\theta_2) - \mu \sin(\delta\theta + \delta\theta_2)]$$

$$- \frac{d}{2}[\sin(\delta\theta + \delta\theta_2) + \mu \cos(\delta\theta + \delta\theta_2)]\} \tag{1.3.10}$$

Force-Deformation Relations

$$F_x = K_x \delta x$$

$$M = K_\theta \delta\theta$$

$$K_{\theta_1}\delta\theta_1 = F_{n_1}\{C_V[\cos(\delta\theta - \delta\theta_1) - \mu \sin(\delta\theta - \delta\theta_1)]$$

$$- C_h[\sin(\delta\theta - \delta\theta_1) + \mu \cos(\delta\theta - \delta\theta)]\}$$

$$K_{\theta_2}\delta\theta_2 = F_{n_2}(V - \mu C_h) \tag{1.3.11}$$

Geometric Compatibility Requirements

$$\Delta - \frac{CD}{2} = \delta x + (a - \ell)\sin \delta\theta + r[\cos(\gamma - \delta\theta_1) - \cos \gamma]$$

$$+ d \sin^2 \frac{\delta\theta}{2}$$

$$a + \left(\Delta - \frac{CD}{2}\right)\tan \phi = \delta z + (a - \ell)\cos \delta\theta + \frac{d}{2}\sin \delta\theta$$

$$+ r[\sin(\gamma - \delta\theta_1) - \sin \gamma]$$

$$\ell \sin \delta\theta + d \cos \delta\theta = D + r[\cos(\gamma - \delta\theta_1) - \cos \gamma] + 2C_h \sin^2 \frac{\delta\theta_2}{2}$$

$$+ V \sin \delta\theta_2 \tag{1.3.12}$$

For convenience V has been introduced by the relation

$$V \cos \delta\theta_2 = -\ell \cos \delta\theta + d \sin \delta\theta + C_h(\sin \delta\theta_1 - \sin \delta\theta_2)$$

$$+ C_V \cos \delta\theta_1 \qquad (1.3.13)$$

1.3.5 Solution of Assembly Equations

Introduction

Because of the inherent complexity of the assembly equations, it was necessary to use a computer to solve them. Two types of solutions were obtained: (a) exact solutions and (b) linearized solutions. To solve the equations exactly, simple iteration was used for the one-point contact equations and a generalized Newton-Raphson method for the chamfer crossing and two-point contact equations. In both cases the dimensional analysis as described earlier (see Section 1.2.5) was used with the following additions (see Table 1.3.1) to Table 1.2.1 (exclude K_{x_1}, K_{x_2}, δx_1, δx_2). Both types of equations are explained below.

Exact Solutions

To determine the exact solutions, a generalized Newton-Raphson method must be used. This is also true for the lateral and rotational hole compliance case where completely general solutions are derived (Section 1.4.2). The solution scheme for the rotational hole compliance case is very tedious also and may be arrived at by replacing $1/K_{x_1}$, $1/K_{x_2}$ in the general solution scheme by 0. For this reason the solution will not be derived here.

The computer program written to solve the assembly equations is called "ROTATE" (see Appendix A). Given the insertion parameters as inputs it computes F_z, δz, $\delta\theta$, and δx for various insertion distances $(\Delta z, \ell)$ during the entire assembly. The program is very similar to the more general program, "LATROT," and will not be discussed further here.

Linearized Solutions

The program written to solve the linearized equations is called "LINROT" (see Appendix A). Given the insertion parameters as inputs it too computes F_z, δz, $\delta\theta$, and δx for various insertion distances $(\Delta z, \ell)$ during the entire assembly. Some of the linearized solutions on which the program is based are shown in Table 1.3.2. The remaining variables may be obtained readily once δx and $\delta\theta$ are known. Other

Table 1.3.1. Dimensional analysis.

Insertion Parameters	Dimensionless Insertion Parameters
C_v	C_v/a
C_h	C_h/a
K_{θ_1}	K_{θ_1}/K_θ
K_{θ_2}	K_{θ_2}/K_θ

Insertion Variables	Dimensionless Insertion Variables
$\delta\theta_1$	$\delta\theta_1$
$\delta\theta_2$	$\delta\theta_2$
ζ	ζ/a

Table 1.3.2. Linearized solutions for δx and $\delta\theta$.

Chamfer Crossing

$$\delta x = \frac{K_\theta \Delta z}{\tan\phi\left[K_x a^2\left(1 - \frac{d}{2a\tan(\phi-\beta)}\right) + K_\theta + \frac{K_x K_\theta}{K_{\theta_1}}(C_v + \Delta\zeta)\left[(C_v + \Delta\zeta)\tan(\phi-\beta) + \left(\frac{\Delta\zeta}{\tan\phi} - C_h\right)\right]/\tan(\phi-\beta)\right]}$$

$$\delta\theta = \frac{K_x a \Delta z}{\tan\phi\left[K_x a^2 + \frac{K_\theta}{\left(1 - \frac{d}{2a\tan(\phi-\beta)}\right)} + \frac{K_x K_\theta}{K_{\theta_1}}\frac{(C_v + \Delta\zeta)\left[(C_v + \Delta\zeta)\tan(\phi-\beta) + \left(\frac{\Delta\zeta}{\tan\phi} - C_h\right)\right]/\tan(\phi-\beta)}{\left(1 - \frac{d}{2a\tan(\phi-\beta)}\right)}\right]}$$

One-Point Contact

$$\delta x = \frac{K_\theta\left(\Delta - \frac{CD}{2}\right)}{K_x(a-\ell)\left[(a-\ell) - \frac{\mu d}{2}\right] + K_\theta + \frac{K_x K_\theta}{K_{\theta_1}} C_v(C_v - \mu C_h)}$$

$$\delta\theta = \frac{K_x\left(\Delta - \frac{CD}{2}\right)\left[(a-\ell) - \frac{\mu d}{2}\right]}{K_x(a-\ell)\left[(a-\ell) - \frac{\mu d}{2}\right] + K_\theta + \frac{K_x K_\theta}{K_{\theta_1}} C_v(C_v - \mu C_h)}$$

Table 1.3.2. Linearized solutions for δx and $\delta\theta$ (cont.).

Two-Point Contact

$$\delta x = \frac{K_\theta K_{\theta_1}\left(\Delta - \frac{CD}{2}\right)(C_v - \ell)(C_v - \mu C_h - \ell) + K_\theta K_{\theta_2} C_v\left(\Delta + \frac{CD}{2}\right)(C_v - \mu C_h) + K_{\theta_1} K_{\theta_2} \ell\left(\ell\left(\Delta + \frac{CD}{2}\right) - aCD\right)}{\left[\begin{array}{l} K_x K_\theta C_v (C_v - \ell)(C_v - \mu C_h)(C_v - \mu C_h - \ell) + K_x K_{\theta_1}(a - \ell)(C_v - \ell)(C_v - \mu C_h - \ell)\left[(a - \ell) - \frac{\mu d}{2}\right] + \\ K_x K_{\theta_2} a C_v\left(a - \frac{\mu d}{2}\right)(C_v - \mu C_h) + K_\theta K_{\theta_1}(C_v - \ell)(C_v - \mu C_h - \ell) + K_\theta K_{\theta_2} C_v (C_v - \mu C_h) \end{array}\right]}$$

$$\delta\theta = \frac{K_x K_{\theta_1}\left(\Delta - \frac{CD}{2}\right)(C_v - \ell)(C_v - \mu C_h - \ell)\left[(a - \ell) - \frac{\mu d}{2}\right] + K_x K_{\theta_2} C_v\left(a - \frac{\mu d}{2}\right)\left(\Delta + \frac{CD}{2}\right)(C_v - \mu C_h) + K_{\theta_1} K_{\theta_2} \ell CD}{\left[\begin{array}{l} K_x K_\theta C_v (C_v - \ell)(C_v - \mu C_h)(C_v - \mu C_h - \ell) + K_x K_{\theta_1}(a - \ell)(C_v - \ell)(C_v - \mu C_h - \ell)\left[(a - \ell) - \frac{\mu d}{2}\right] + \\ K_x K_{\theta_2} a C_v\left(a - \frac{\mu d}{2}\right)(C_v - \mu C_h) + K_\theta K_{\theta_1}(C_v - \ell)(C_v - \mu C_h - \ell) + K_\theta K_{\theta_2} C_v (C_v - \mu C_h) \end{array}\right]}$$

particulars, such as how the boundary between one-point contact and two-point contact was determined, follow as before (Section 1.2.5).

1.3.6 Results and Discussion

Once the assembly equations have been solved, the effect of the insertion parameters on F_z versus δz can be determined. In this section the effect of the insertion parameters which are unique to (1) the rotational compliance hole and (2) the lateral and rotational compliance hole problems will be analyzed. These parameters are K_{θ_1}, K_{θ_2}, C_h, and C_v. Other effects such as the linearization effect and the location of the compliance center of the peg on the assembly will be investigated. The general features of the force versus depth plot are basically the same as before (Section 1.2.6) except for where line contact begins. This is because a contact force between the peg and the corner of the chamfer exists just before line contact and as a result the angles $(\delta\theta, \delta\theta_1)$ do not vanish.

Effect of the Left Hole Wall Compliance on Insertion Force versus Depth

The effect of the compliance of the left side of the hole (measured by K_{θ_1}/K_θ) on F_z versus δz is shown in Figure 1.3.5. Decreasing the compliance of the left side is seen to increase the insertion force and vice versa during each assembly phase. If the compliance of the left side is large enough, two-point contact will not occur (e.g., $K_{\theta_1}/K_\theta = 5$).

Effect of the Right Hole Wall Compliance on Insertion Force versus Depth

In Figure 1.3.6 the effect of the compliance of the right side of the hole (measured by K_{θ_2}/K_θ) is shown. Chamfer crossing and one-point contact are of course not affected by the right hole wall's compliance. As before, decreasing the compliance is seen to increase the insertion force and vice versa.

Effect of the Horizontal Location of the Compliance Center of the Hole on Insertion Force versus Depth

In Figure 1.3.7 the effect of the horizontal location of the compliance center is shown for several C_h/a within Region III. Chamfer crossing and one-point contact are seen to be quite insensitive to C_h/a whereas two-point contact is. Increasing C_h/a increases the insertion force during two-point contact and vice versa.

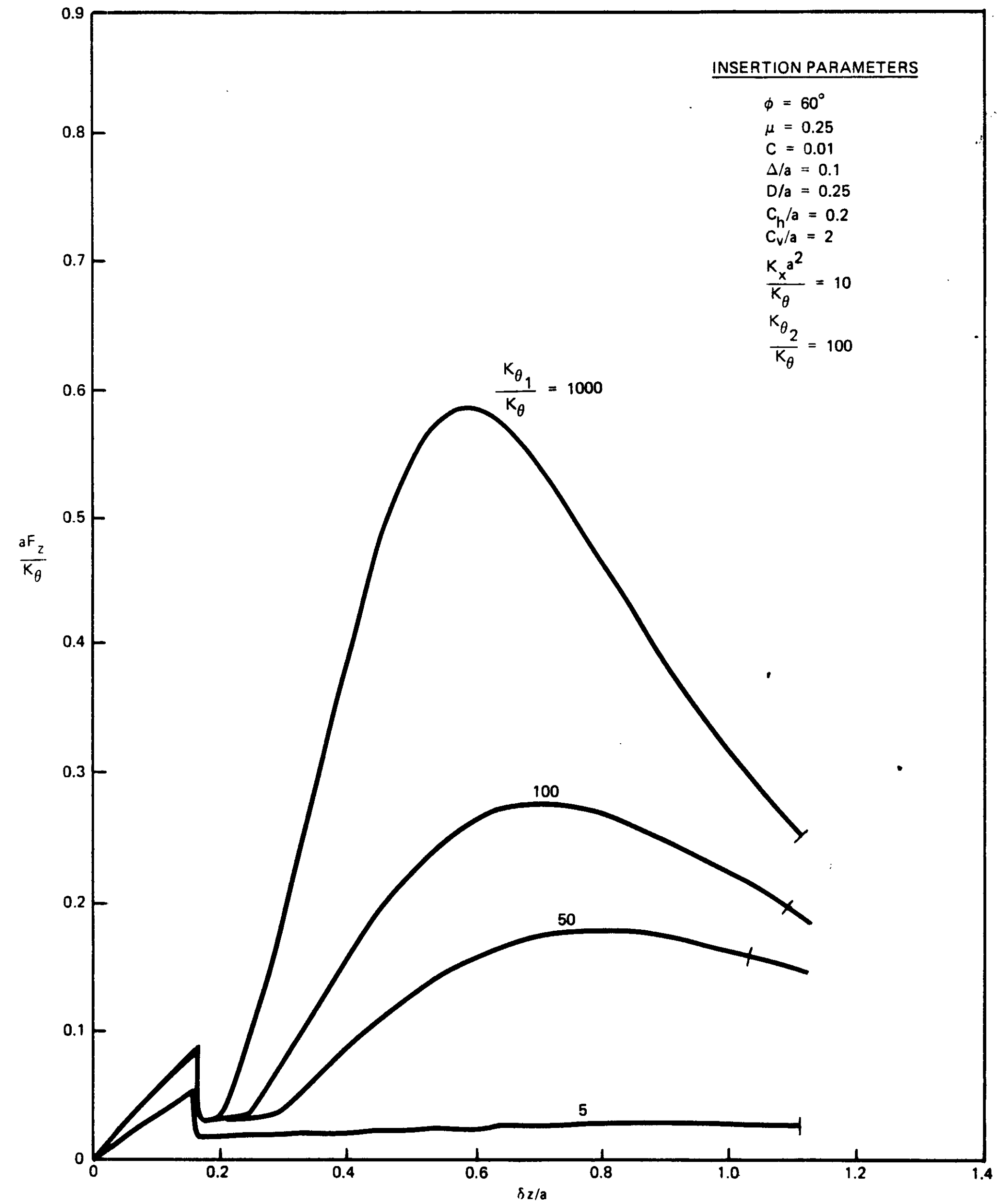

Figure 1.3.5. Effect of K_{θ_1}/K_θ on F_z versus δz.

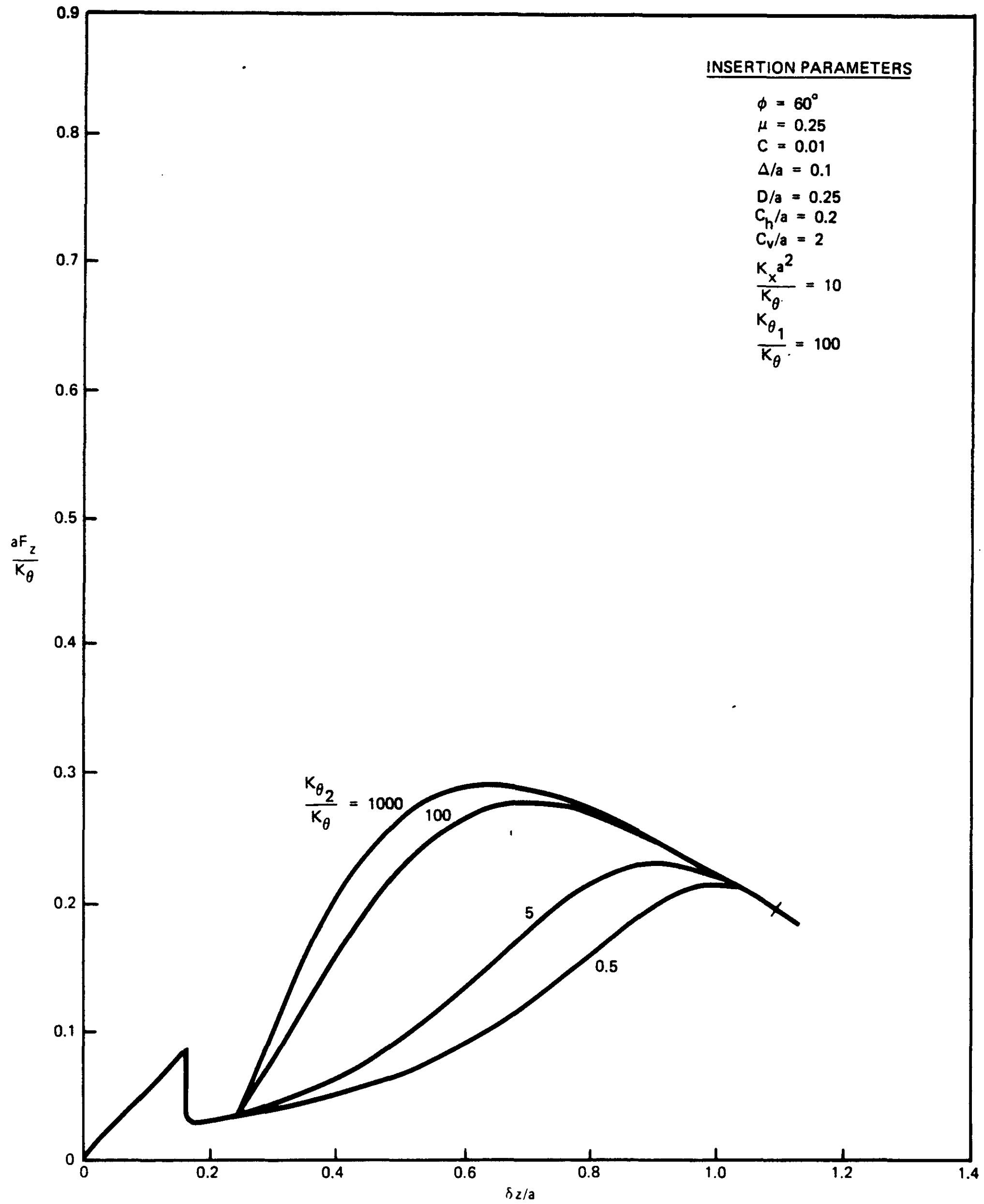

Figure 1.3.6. Effect of K_{θ_2}/K_θ on F_z versus δz.

Effect of the Vertical Location of the Compliance Center of the Hole on Insertion Force versus Depth

The effect of the vertical location of the compliance center is shown in Figure 1.3.8 for several C_V/a within Region III. Again only two-point contact is greatly affected by C_V/a. Increasing C_V/a decreases the insertion force and vice versa.

Effect of Linearization

As mentioned before, the linearization tends to distort the solution and is quite sensitive to insertion parameters which produce large angular misalignments $(\delta\theta, \delta\theta_1)$. In Figure 1.3.9, two solutions (F_z versus δz) are given, one for a small ratio ($C_V/a = 1$) and one for a larger ratio ($C_V/a = 2$). In each case a linearized solution is also given. The linearized solution and the exact solution are seen to agree at both the beginning and at the end of the assembly (line contact). The linearized solution exhibits the general features of the exact solution as discussed above but as before (Section 1.2.6) it tends to predict larger insertion forces during chamfer crossing and smaller insertion forces during the rest of the assembly.

In Figure 1.3.10 the effect of the linearization on F_z, $\delta\theta$, δx versus δz is shown. It is seen to be very similar to the linearization effect for the lateral compliance hole case and will not be discussed further.

Location of Compliance Center of Peg

By optimally choosing the location of the compliance center of the peg during the assembly, a much simpler assembly is possible. This simpler assembly is similar to the one described earlier, but with one important difference. The simplified assembly sequence consists of (1) chamfer crossing, followed by (2) the other (new) type of one-point contact as shown in Figure 1.3.11.

In a similar manner (see Section 1.2.6), an optimal value of a may be found for each assembly phase. For chamfer crossing (use Equations 1.3.1 and 1.3.2) the optimal value of a is given by

$$a_0(\delta\theta_1) = \frac{d}{2\tan(\phi - \delta\theta_1 - \beta)} \qquad (1.3.14)$$

The optimal value a_0 is seen to depend on $\delta\theta_1$ and will not remain constant during chamfer crossing. From Table 1.3.2, the linearized value of a_0 is given by $a_0 = d/(2\tan(\phi - \beta))$. Should $\delta\theta$ deviate from

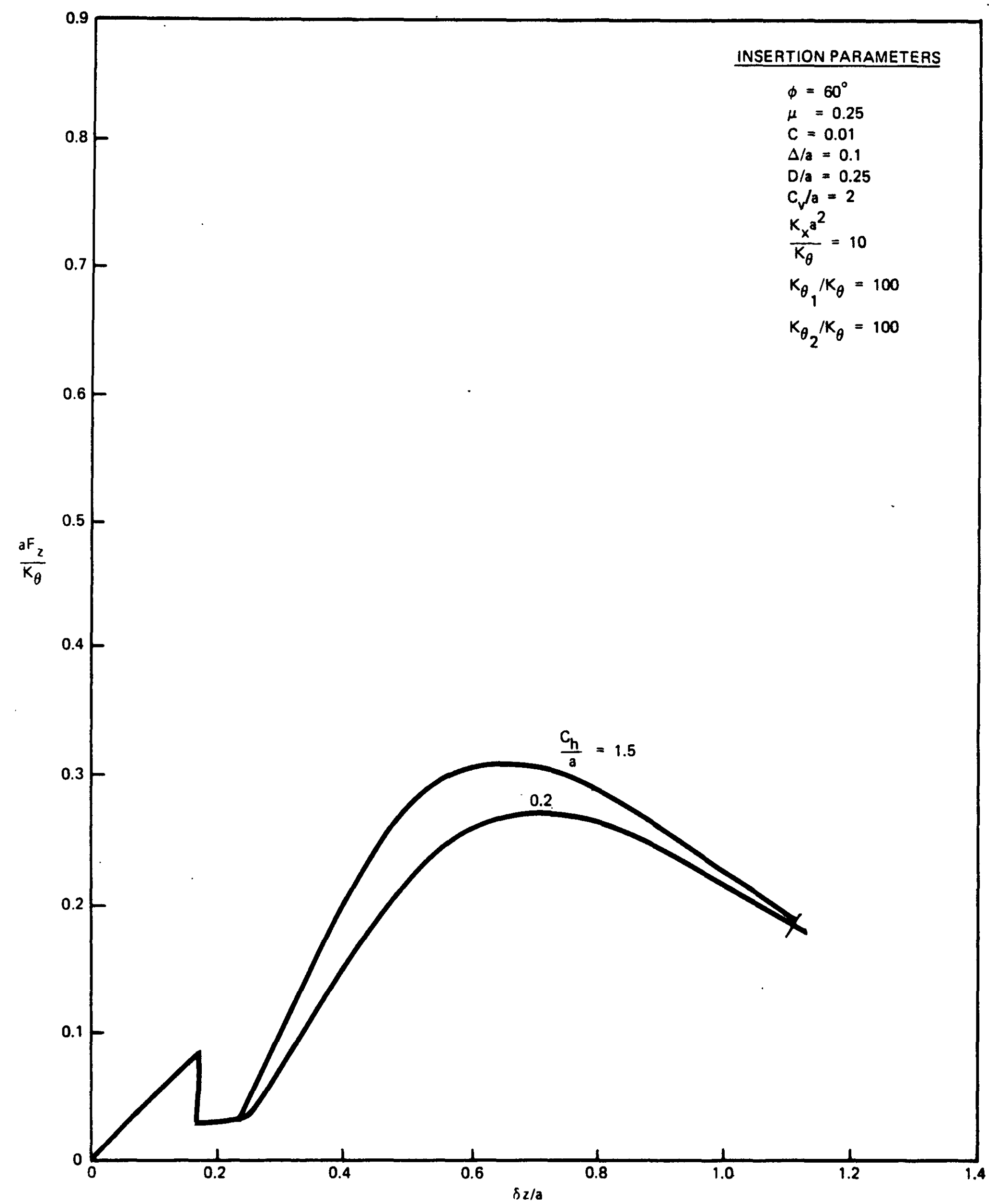

Figure 1.3.7. Effect of C_h/a on F_z versus δz.

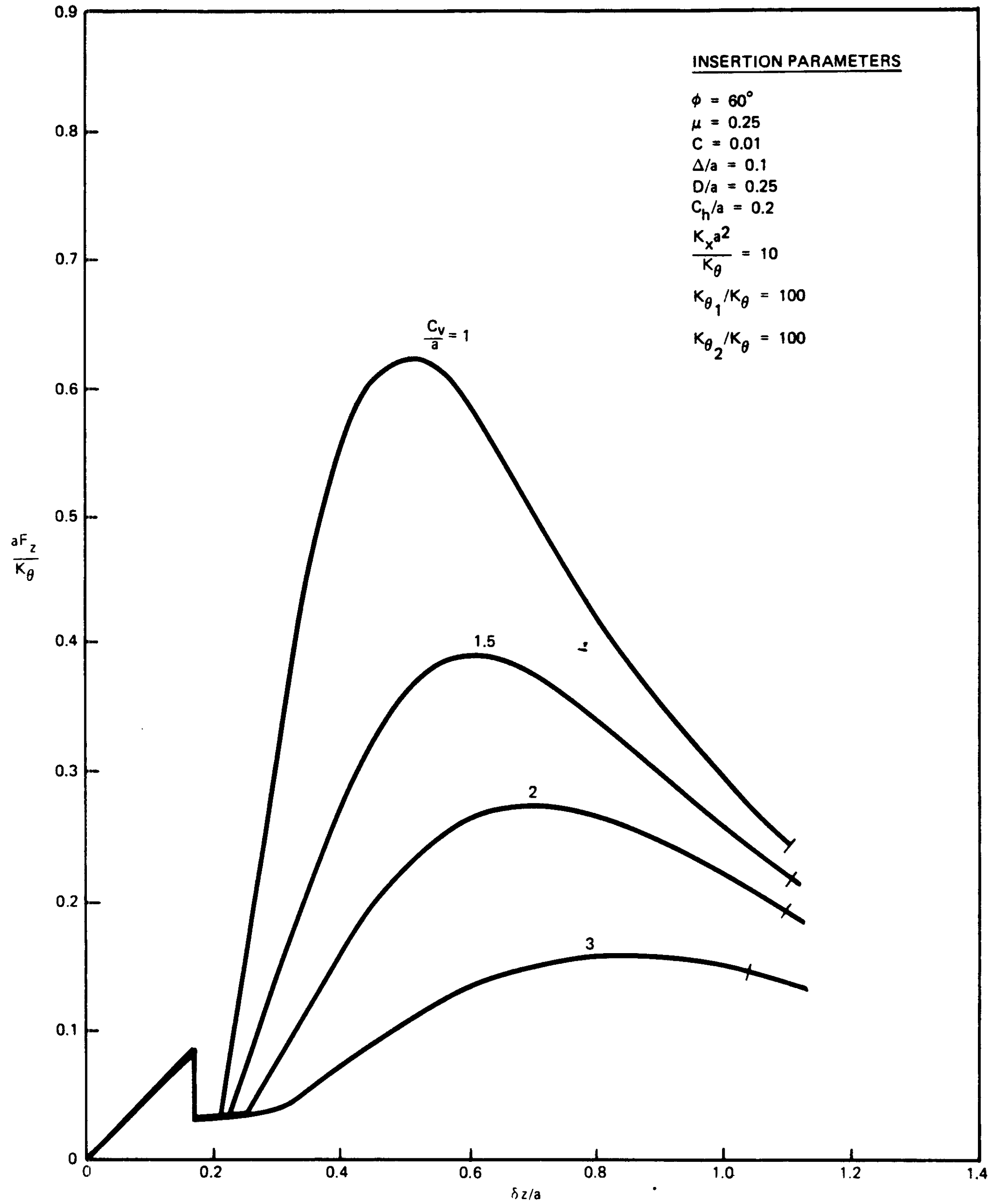

Figure 1.3.8. Effect of C_v/a on F_z versus δz.

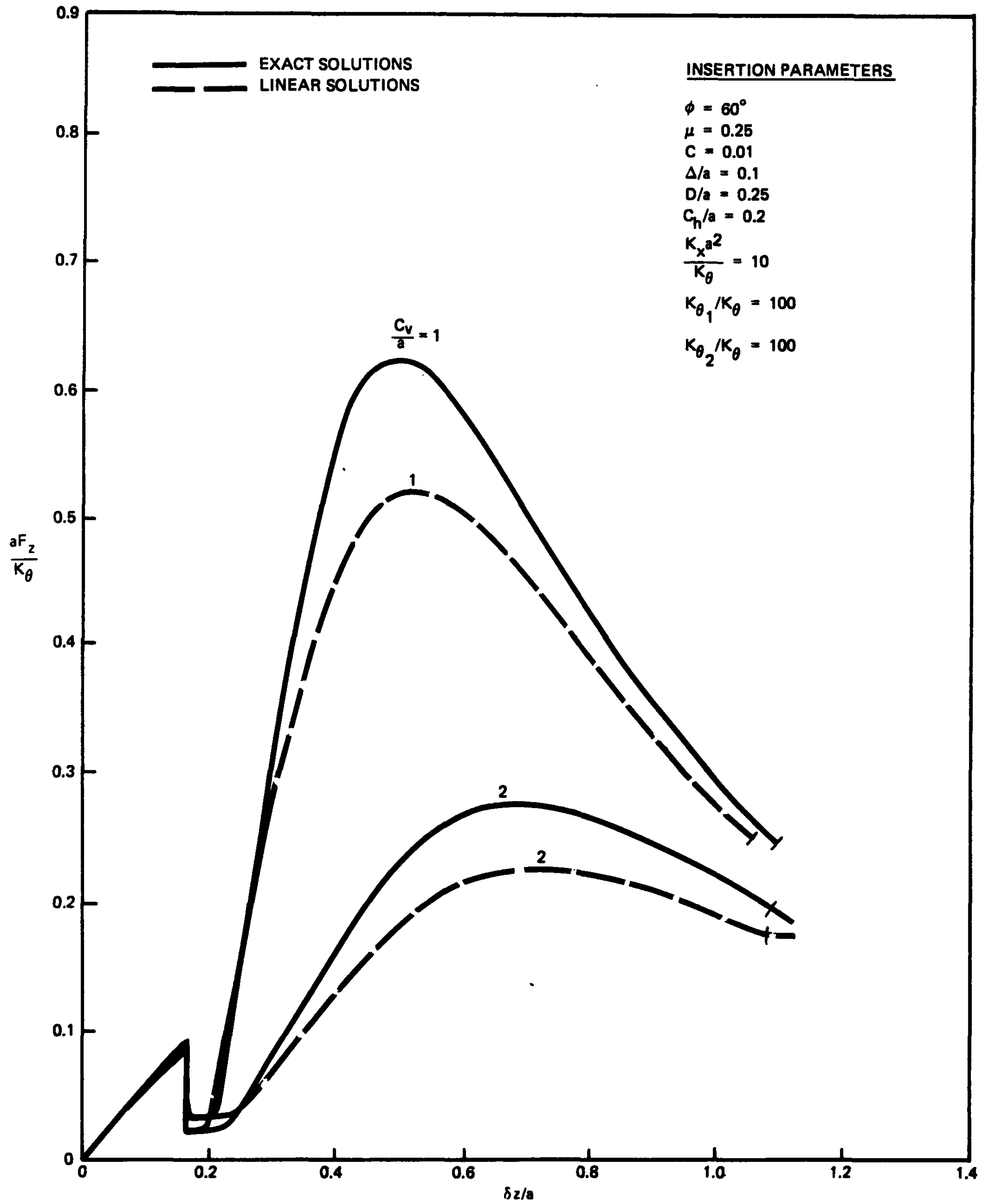

Figure 1.3.9. Comparison of linearized solutions with exact solutions for several C_v/a.

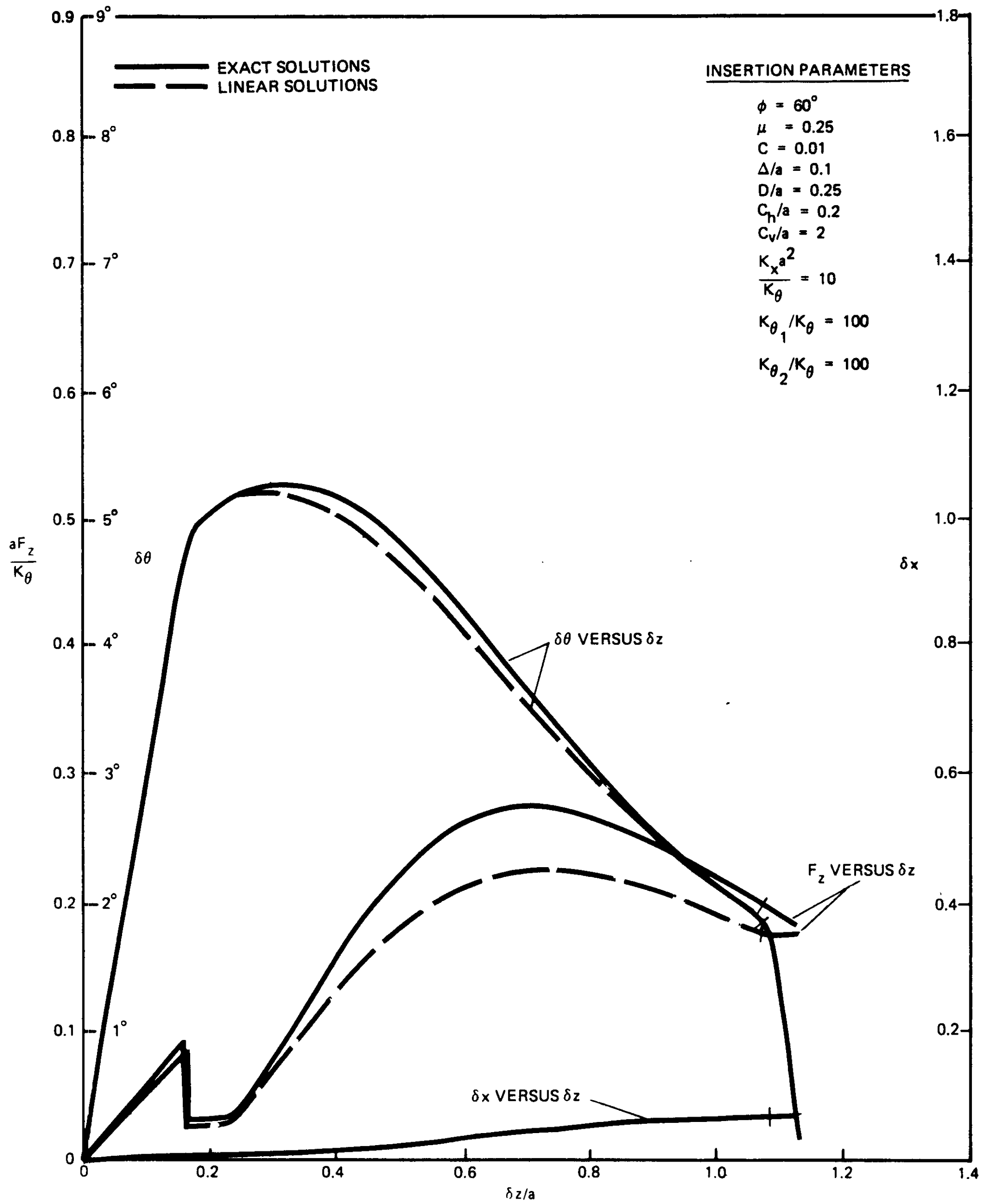

Figure 1.3.10. Effect of linearization on F_z, $\delta\theta$, δx versus δz.

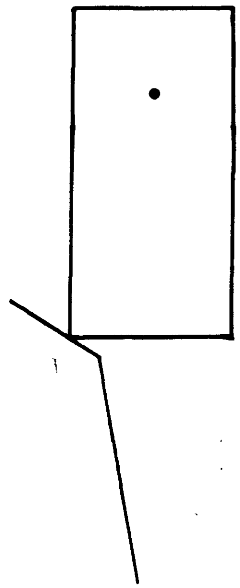

(a) Chamfer Crossing

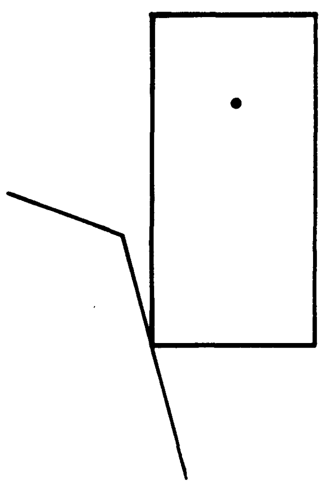

(b) Other Type of One-Point Contact

Figure 1.3.11. Simplified assembly sequence.

zero, a "new" a_0 must be selected based on feedback which forces $\delta\theta$ to be zero again. This value of a is given by

$$a(\delta\theta, \delta\theta_1) = \frac{d}{2\tan(\phi + \delta\theta - \delta\theta_1 - \beta)} \qquad (1.3.15)$$

During the other type of one-point contact the optimal value of a is

$$a_0(\delta\theta_1) = \frac{d}{2}\tan(\beta + \delta\theta_1) \qquad (1.3.16)$$

and the feedback relation is

$$a(\delta\theta, \delta\theta_1) = \frac{d}{2}\tan(\beta - \delta\theta + \delta\theta_1) \qquad (1.3.17)$$

provided $\delta\theta_1 > \delta\theta$. If $\delta\theta_1 \leq \delta\theta$, the assembly phase changes and the above equations no longer apply; so the feedback scheme is not stable. Figures 1.2.13 and 1.2.14 when properly interpreted may be used to plot a_0 in terms of the assembly phase and to plot the feedback equations (e.g., replace β,μ in those figures by $\beta + \delta\theta_1$, $\tan(\beta + \delta\theta_1)$, respectively).

1.4 LATERAL AND ROTATIONAL COMPLIANCE HOLE

1.4.1 Introduction and Derivation of Assembly Equations

In the most general case the model must incorporate both lateral and rotational hole wall compliance. This general model combines the theoretical models presented in Sections 1.2 and 1.3. Because the rotational compliance hole problem is much more difficult than the lateral compliance hole problem, the development of the general problem will follow almost identically to the rotational compliance hole problem (e.g., compliance center location). Initially the peg and hole are positioned as shown in Figure 1.3.1 and during the assembly the hole walls deform outward, enlarging the hole. By Chasle's Theorem, this deformation may be treated as a translation $(\delta x_1, \delta x_2)$ and a rotation $(\delta\theta_1, \delta\theta_2)$ taken in either order. The assembly phases to be considered are the same as before as well as many of the assembly equations. In Figures 1.4.1, 1.4.2, and 1.4.3 the chamfer crossing, one-point contact, and two-point contact phases are shown, respectively. The equilibrium requirements for each assembly phase are the same as the corresponding ones in Section 1.3. The force-deformation relations for each assembly phase are the same as the corresponding ones in both

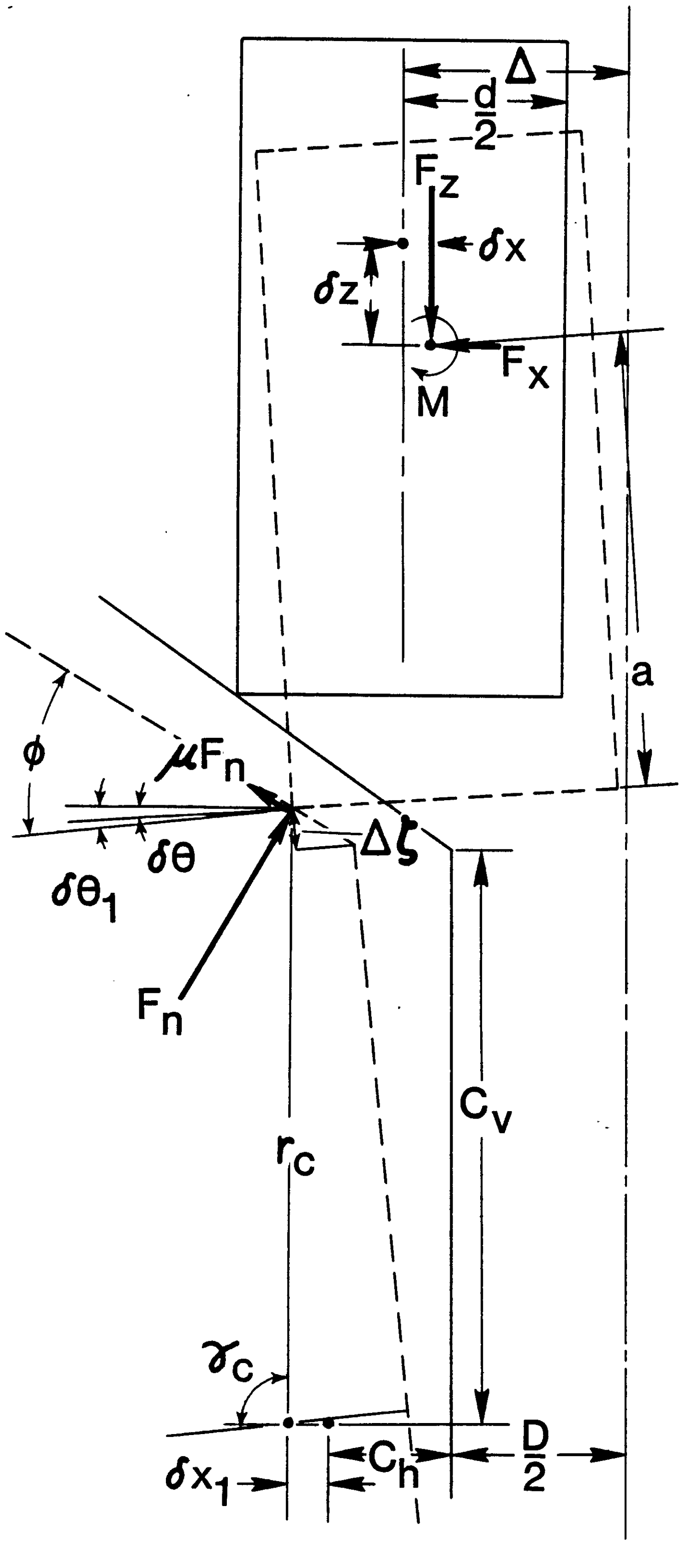

Figure 1.4.1. Chamfer crossing.

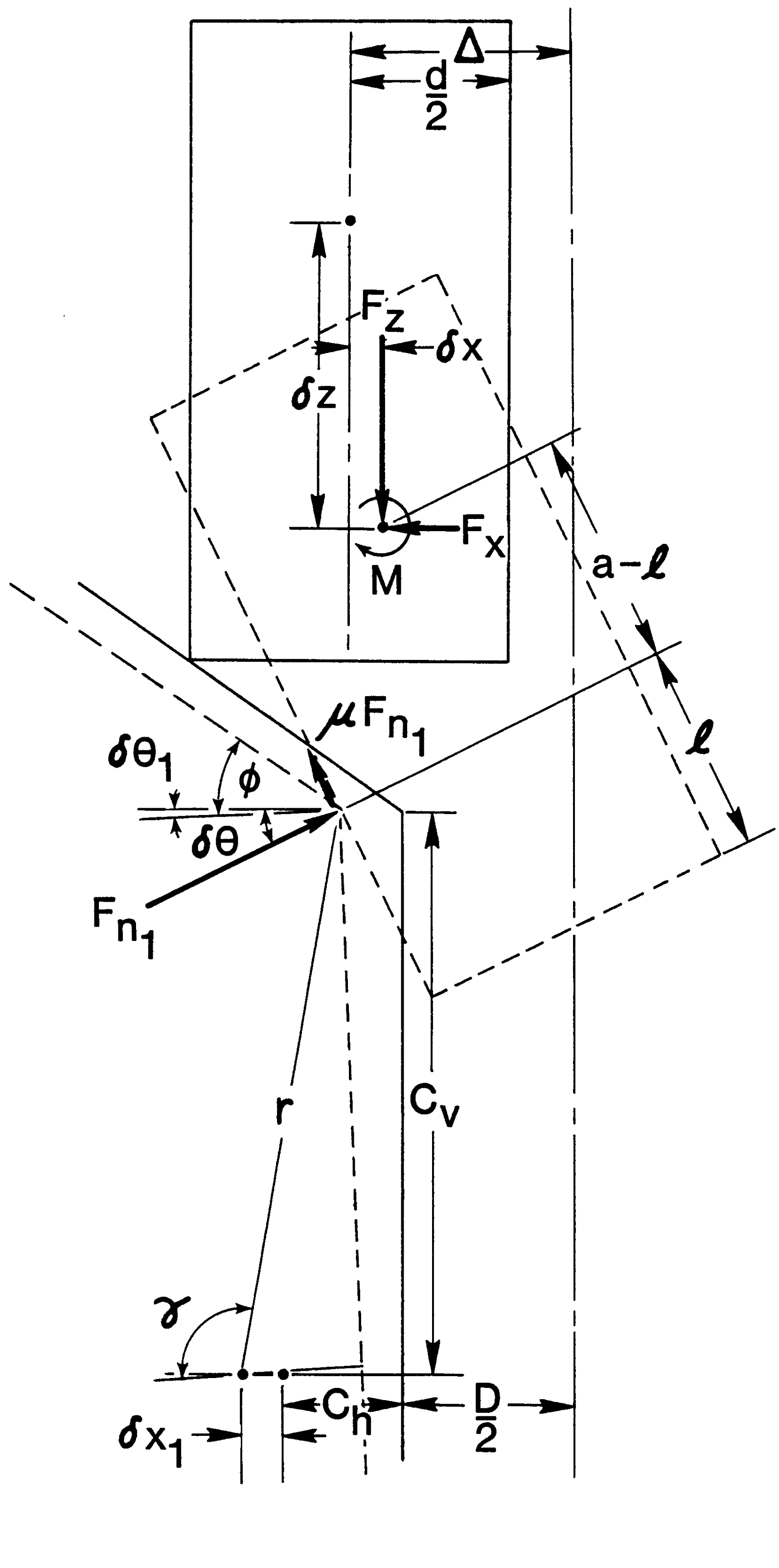

Figure 1.4.2. One-point contact.

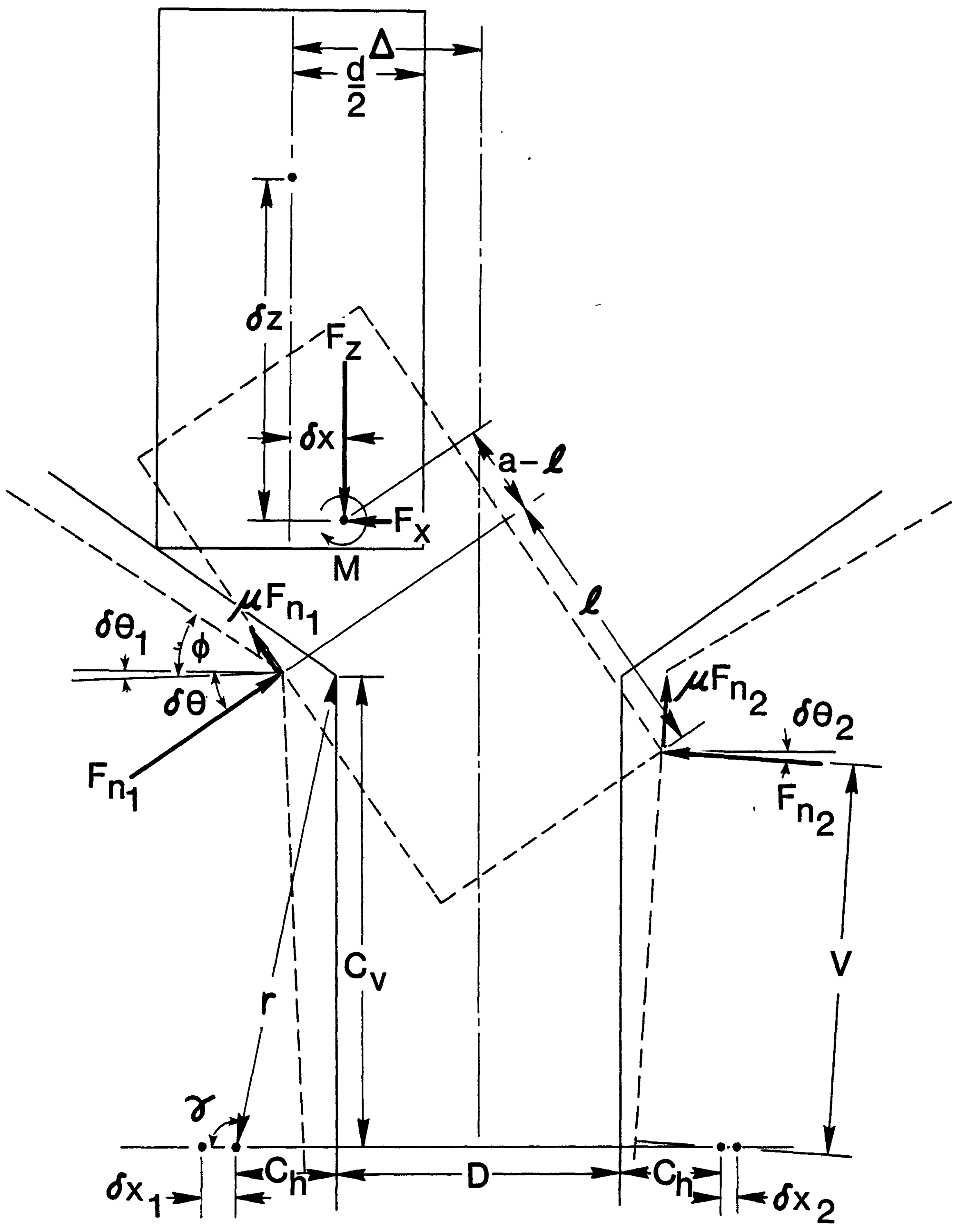

Figure 1.4.3. Two-point contact.

Sections 1.2 and 1.3 (except for Equation 1.2.2—replace ϕ by $\phi - \delta\theta_1$) and will not be relisted. The geometric compatibility requirements are different and will be given for each assembly phase.

Geometric Compatibility Requirements

Chamfer Crossing

$$\frac{\Delta z}{\tan\phi} = \delta x + \delta x_1 + a \sin\delta\theta + r_c[\cos(\gamma_c - \delta\theta_1) - \cos\gamma_c] + d \sin^2\frac{\delta\theta}{2}$$

$$a + \Delta z = \delta z + a\cos\delta\theta + \frac{d}{2}\sin\delta\theta + r_c[\sin(\gamma_c - \delta\theta_1) - \sin\gamma_c] \tag{1.4.1}$$

One-Point Contact

$$\Delta - \frac{CD}{2} = \delta x + \delta x_1 + (a - \ell)\sin\delta\theta + r[\cos(\gamma - \delta\theta_1) - \cos\gamma] + d\sin^2\frac{\delta\theta}{2}$$

$$a + \left(\Delta - \frac{CD}{2}\right)\tan\phi = \delta z + (a - \ell)\cos\delta\theta + \frac{d}{2}\sin\delta\theta + r[\sin(\gamma - \delta\theta_1) - \sin\gamma] \tag{1.4.2}$$

Two-Point Contact

$$\Delta - \frac{CD}{2} = \delta x + \delta x_1 + (a - \ell)\sin\delta\theta + r[\cos(\gamma - \delta\theta_1) - \cos\gamma] + d\sin^2\frac{\delta\theta}{2}$$

$$a + \left(\Delta - \frac{CD}{2}\right)\tan\phi = \delta z + (a - \ell)\cos\delta\theta + \frac{d}{2}\sin\delta\theta + r[\sin(\gamma - \delta\theta_1) - \sin\gamma]$$

$$\ell\sin\delta\theta + d\cos\delta\theta = D + \delta x_1 + \delta x_2 + r[\cos(\gamma - \delta\theta_1) - \cos\gamma] + 2C_h\sin^2\frac{\delta\theta_2}{2} + V\sin\delta\theta_2 \tag{1.4.3}$$

Also, the boundary between one-point contact (two-point contact) and two-point contact (one-point contact) is defined by

$$\ell \sin \delta\theta + d \cos \delta\theta = D + \delta x_1 + r[\cos(\gamma - \delta\theta_1) - \cos \gamma] \tag{1.4.4}$$

1.4.2 Solution of Assembly Equations

A. Introduction

Due to the inherent complexity of the assembly equations, it was necessary to use a computer to solve them. Two types of solutions were obtained: (a) exact solutions and (b) linearized solutions. To solve the equations exactly, simple iteration was used for the one-point contact equations and a generalized Newton-Raphson method for the chamfer crossing and two-point contact equations. Both types of solutions are explained below.

B. Exact Solutions

Chamfer Crossing

Equations 1.3.1, 1.3.2, 1.2.2, and 1.4.1 may be manipulated to arrive at the following two equations in $\delta\theta$, $\delta\theta_1$

$$(1/K_x + 1/K_{x_1}) \frac{K_{\theta_1}\delta\theta_1}{D_1} [\sin(\phi - \delta\theta_1) - \mu \cos(\phi - \delta\theta_1)]$$

$$+ a \sin \delta\theta + d \sin^2 \frac{\delta\theta}{2} + r_c[\cos(\gamma_c - \delta\theta_1) - \cos \gamma_c] = \frac{\Delta z}{\tan \phi}$$

$$K_\theta \delta\theta + \frac{K_{\theta_1}\delta\theta_1}{D_1}\left[\left(a\mu + \frac{d}{2}\right) \cos(\phi + \delta\theta - \delta\theta_1) - \left(a - \frac{\mu d}{2}\right) \sin(\phi + \delta\theta - \delta\theta_1)\right] = 0 \tag{1.4.5}$$

where $D_1 = (\Delta\zeta + C_v)(\sin \phi - \mu\cos \phi) + \left(\frac{\Delta\zeta}{\tan \phi} - C_h\right)(\cos \phi + \mu\sin \phi)$

These equations may be written in the form

$$f_1(\theta) = \frac{\Delta z}{\tan \phi} \quad , \quad f_2(\theta) = 0$$

or

$$f(\theta) = X \qquad (1.4.6)$$

where $\theta = [\delta\theta, \delta\theta_1]^T$, $X = [\Delta z/\tan\phi, 0]^T$. The initial values X_0 and θ_0 are given by $X_0 = \theta_0 = [0,0]^T$. Differentiating Equation 1.4.6 yields

$$\frac{dX}{d\theta} = J(\theta) \qquad (1.4.7)$$

where $J(\theta)$ (see Appendix B for computation) is the Jacobian of f with respect to θ, i.e.,

$$J_{i1} = \frac{\partial f_i}{\partial(\delta\theta)}; \qquad J_{i2} = \frac{\partial f_i}{\partial(\delta\theta_1)}; \qquad i = 1,2 \qquad (1.4.8)$$

An approximation to Equation 1.4.7 may be rewritten as

$$\Delta X \cong J(\theta)\Delta\theta$$

or

$$\Delta\theta \cong J^{-1}(\theta)\Delta X \qquad (1.4.9)$$

provided J^{-1} exists. The following iteration scheme can then be used to solve for $\delta\theta$, $\delta\theta_1$ [8]

$$\begin{aligned}
\Delta X_k &= s(X - X_k) \\
\Delta\theta_k &= J^{-1}(\theta_k)\Delta X_k \\
\theta_{k+1} &= \theta_k + \Delta\theta_k \\
X_{k+1} &= f(\theta_{k+1}) \qquad k = 0,1,2,\ldots
\end{aligned} \qquad (1.4.10)$$

where s is the scalar step size. Although s was not chosen optimally for each iteration, the values 0.7 or 0.3 were found to always work in a reasonable number of iterations for the desired accuracy—typically 30-40. Once $\delta\theta$ and $\delta\theta_1$ have been determined, the remaining variables may then be determined by direct substitution.

One-Point Contact

Manipulation of Equations 1.3.5, 1.3.6, 1.2.7, and 1.4.2 yields the following transcendental relation in $\delta\theta$

$$\delta\theta = \frac{K_{\theta_1}\delta\theta_1(\delta\theta)\left[(a - \ell) - \frac{\mu d}{2}\right]}{K_\theta[C_v - \mu C_h)\cos(\delta\theta - \delta\theta_1(\delta\theta)) + (C_h + \mu C_v)\sin(\delta\theta - \delta\theta_1(\delta\theta))]} \tag{1.4.11}$$

where

$$\delta\theta_1(\delta\theta) = \gamma - \cos^{-1}\left[\frac{f(\delta\theta)}{r} + \cos\gamma\right]$$

and

$$f(\delta\theta) = \Delta - \frac{CD}{2} - \frac{(1/K_x + 1/K_{x_1})K_\theta\delta\theta(\cos\delta\theta - \mu\sin\delta\theta)}{\left[(a - \ell) - \frac{\mu d}{2}\right]}$$
$$- (a - \ell)\sin\delta\theta - d\sin^2\frac{\delta\theta}{2} \tag{1.4.12}$$

Equation 1.4.11 may be solved by simple iteration as described before (Section 1.2.5). The remaining variables are easily determined.

Two-Point Contact

To solve the two-point contact equations, Newton-Raphson's method must be used in much the same manner as it was used to solve the chamfer crossing equations. It is possible to arrive at three equations in three unknowns ($\delta\theta, \delta\theta_1, \delta\theta_2$) using the two-point contact equations; however, implementing the method with these new equations is very difficult because the equations are extremely cumbersome. To alleviate this apparent difficulty, the two-point contact equations were reduced to six equations in six unknowns. Many more partial derivatives must be computed, but they are much easier to evaluate. These six equations are

$$K_x\delta x - F_{n_1}(\cos\delta\theta - \mu\sin\delta\theta) + F_{n_2}(\cos\delta\theta_2 - \mu\sin\delta\theta_2) = 0$$

$$K_\theta \delta\theta - F_{n_1} \left[(a - \ell) - \frac{\mu d}{2}\right]$$

$$+ F_{n_2} \left[\left(a - \frac{\mu d}{2}\right) \cos(\delta\theta + \delta\theta_2) - \left(a\mu + \frac{d}{2}\right) \sin(\delta\theta + \delta\theta_2)\right] = 0$$

$$K_{\theta_1} \delta\theta_1 + F_{n_1} [(C_h + \mu C_v) \sin(\delta\theta - \delta\theta_1) - (C_v - \mu C_h) \cos(\delta\theta - \delta\theta_1)] = 0$$

$$K_{\theta_2} \delta\theta_2 \cos \delta\theta_2 + F_{n_2} [\ell \cos \delta\theta - d \sin \delta\theta - C_h (\sin \delta\theta_1 - \sin \delta\theta_2)$$

$$- C_v \cos \delta\theta_1 + \mu C_h \cos \delta\theta_2] = 0$$

$$\delta x + F_{n_1} (\cos \delta\theta - \mu \sin \delta\theta)/K_{x_1} + (a - \ell) \sin \delta\theta$$

$$+ r \cos(\gamma - \delta\theta_1) + d \sin^2 \frac{\delta\theta}{2} = \Delta - \frac{CD}{2} - C_h$$

$$\ell \sin \delta\theta \cos \delta\theta_2 + d \cos \delta\theta \cos \delta\theta_2$$

$$- r[\cos(\gamma - \delta\theta_1) - \cos \gamma] \cos \delta\theta_2$$

$$- C_h (1 - \cos \delta\theta_2) \cos \delta\theta_2 + [\ell \cos \delta\theta$$

$$- d \sin \delta\theta - C_h (\sin \delta\theta_1 - \sin \delta\theta_2)$$

$$- C_v \cos \delta\theta_1] \sin \delta\theta_2 - D \cos \delta\theta_2$$

$$- F_{n_1} (\cos \delta\theta - \mu \sin \delta\theta) \cos \delta\theta_2 / K_{x_1}$$

$$- F_{n_2} (\cos \delta\theta_2 - \mu \sin \delta\theta_2) \cos \delta\theta_2 / K_{x_2} = 0$$

(1.4.13)

These equations may be written in the form of Equation 1.4.6 and solved similarly where $\theta = [F_{n_1}, F_{n_2}, \delta x, \delta\theta, \delta\theta_1, \delta\theta_2]^T$, etc. (see Appendix B for calculation of J). The initial value θ_0 was evaluated at the boundary between one-point contact and two-point contact. Also, the initial value x_o was chosen to be 0 which allowed the iteration scheme to move away from the original guess.

Computer Program

A computer program called "LATROT" has been written which solves the assembly equations (see Appendix A). Given the insertion parameters as inputs it computes F_z, δz, $\delta\theta$, and δx for various insertion distances $(\Delta z, \ell)$ during the entire assembly.

C. Linearized Solutions

The program written to solve the linearized equations is called "LINLR" (see Appendix A). It computes F_z, δz, $\delta\theta$, and δx during the entire assembly. Some of the solutions $(\delta\theta, \delta x)$ on which the linearized solutions are based are shown in Table 1.4.1.

1.4.3 Results and Discussion

The effect of the insertion parameters which are common to all of the problems discussed in Section 1 on F_z versus δz will now be discussed (see Sections 1.2.6, 1.3.6).

Effect of the Chamfer Angle on Insertion Force versus Depth

In Figure 1.4.4 the effect of ϕ on F_z versus δz is shown for several ϕ. As the chamfer becomes flatter (ϕ small) the insertion force during chamfer crossing rises and vice versa. During one-point contact and two-point contact the solution is primarily shifted as ϕ varies. This is because the duration of chamfer crossing is sensitive to ϕ; the steeper the chamfer, the longer chamfer crossing lasts.

Effect of the Friction Coefficient on Insertion Force versus Depth

Figure 1.4.5 illustrates the effect of μ on F_z versus δz. Of course increasing μ increases the insertion force during each assembly phase and vice versa. Also as μ increases, $a - \frac{\mu d}{2}$ decreases so that line contact occurs earlier. Although not shown here, if μ is large enough, the peg will tip the other way ($\circlearrowleft$) during chamfer crossing.

Effect of the Clearance Ratio on Insertion Force versus Depth

In Figure 1.4.6 the effect of C on F_z versus δz is shown for various $C > 0$. As C decreases the insertion force increases and vice versa. For very small C there is little difference in insertion force versus depth characteristics (e.g., compare $C = 0.01$, 0.0001 curves). If C is large enough (e.g., $C = 0.2$) two-point contact will not occur.

Table 1.4.1. Linearized solutions for δx and $\delta\theta$.

Chamfer Crossing

$$\delta x = \frac{K_\theta \Delta z}{\tan\phi\left[K_x a^2\left(1 - \frac{d}{2a\tan(\phi-\beta)}\right) + K_\theta + \frac{K_x K_\theta}{K_{x_1}} + \frac{K_x K_\theta}{K_{\theta_1}}(C_v + \Delta\zeta)\left[(C_v + \Delta\zeta)\tan(\phi-\beta) + \left(\frac{\Delta\zeta}{\tan\phi} - C_h\right)\right]/\tan(\phi-\beta)\right]}$$

$$\delta\theta = \frac{K_x a \Delta z}{\tan\phi\left[K_x a^2 + \frac{K_\theta}{\left(1 - \frac{d}{2a\tan(\phi-\beta)}\right)} + \frac{K_x K_\theta / K_{x_1}}{\left(1 - \frac{d}{2a\tan(\phi-\beta)}\right)} + \frac{K_x K_\theta}{K_{\theta_1}} \frac{(C_v + \Delta\zeta)\left[(C_v + \Delta\zeta)\tan(\phi-\beta) + \left(\frac{\Delta\zeta}{\tan\phi} - C_h\right)\right]/\tan(\phi-\beta)}{\left(1 - \frac{d}{2a\tan(\phi-\beta)}\right)}\right]}$$

One-Point Contact

$$\delta x = \frac{K_\theta\left(\Delta - \frac{CD}{2}\right)}{K_x(a-\ell)\left[(a-\ell) - \frac{\mu d}{2}\right] + K_\theta + K_x K_\theta / K_{x_1} + \frac{K_x K_\theta}{K_{\theta_1}} C_v (C_v - \mu C_h)}$$

$$\delta\theta = \frac{K_x\left(\Delta - \frac{CD}{2}\right)\left[(a-\ell) - \frac{\mu d}{2}\right]}{K_x(a-\ell)\left[(a-\ell) - \frac{\mu d}{2}\right] + K_\theta + K_x K_\theta / K_{x_1} + \frac{K_x K_\theta}{K_{\theta_1}} C_v (C_v - \mu C_h)}$$

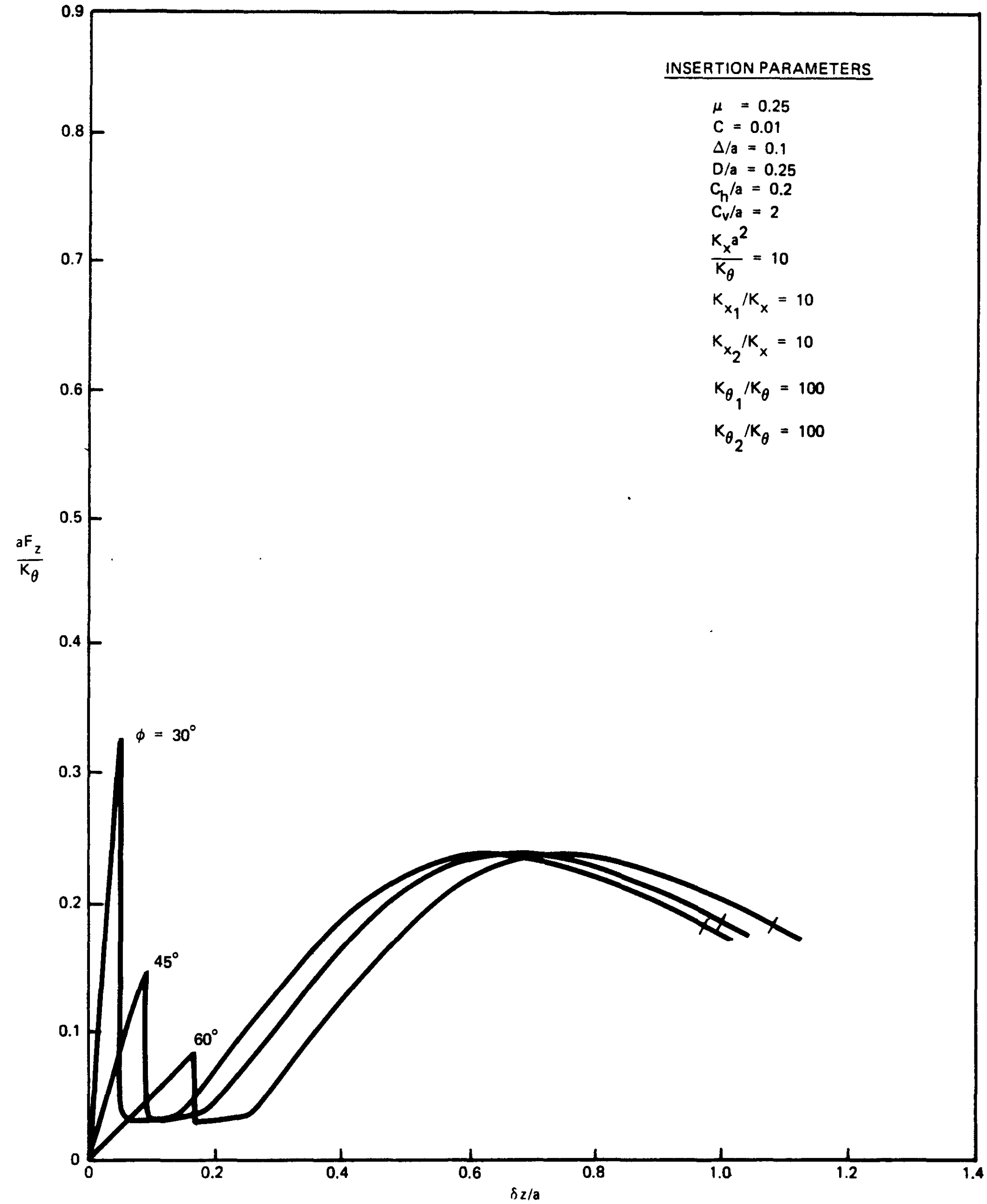

Figure 1.4.4. Effect of ϕ on F_z versus δz.

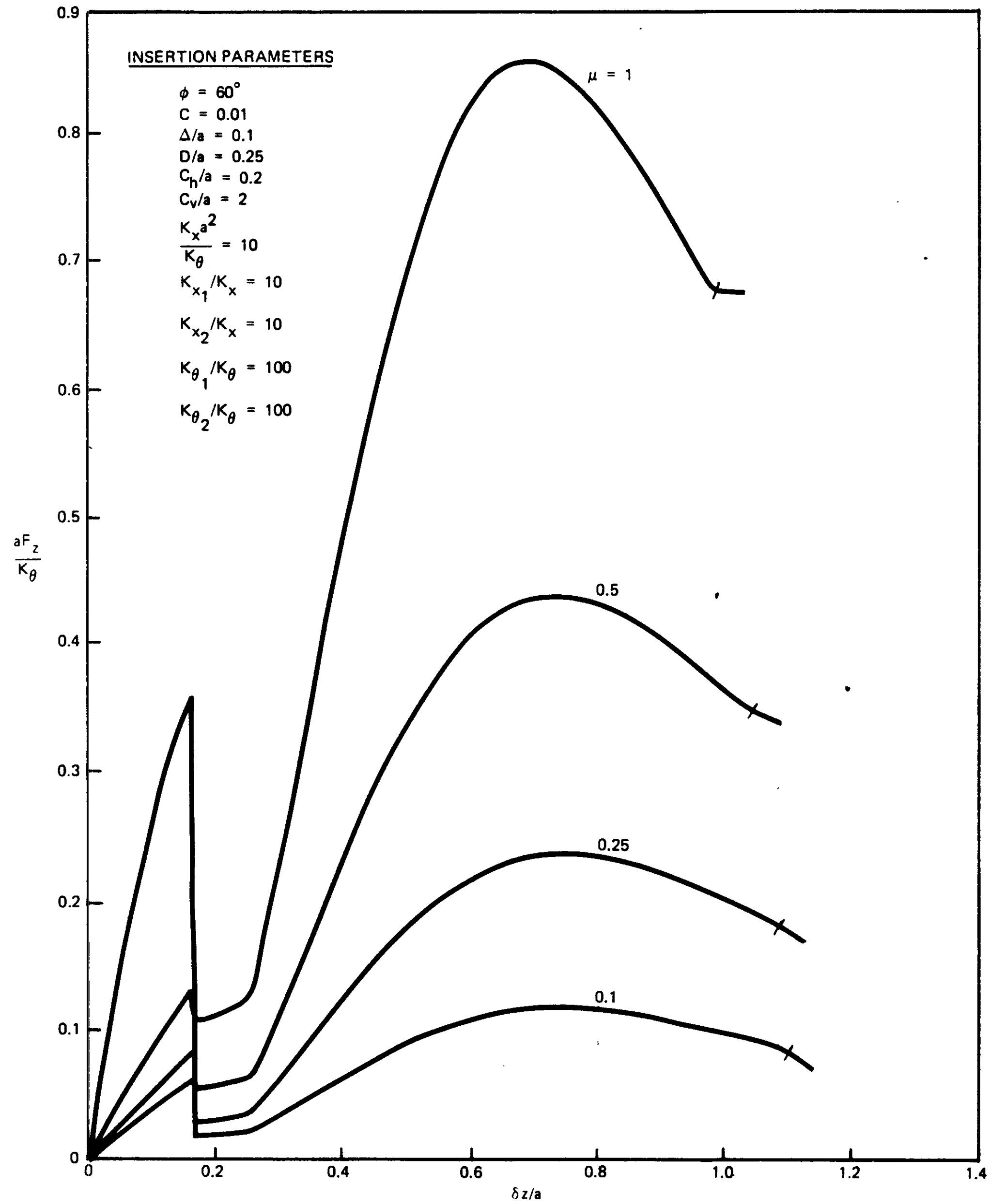

Figure 1.4.5. Effect of μ on F_z versus δz.

Effect of the Initial Lateral Error on Insertion Force versus Depth

Figure 1.4.7 illustrates the effect of Δ/a on F_z versus δz. As the error (Δ/a) increases more insertion force is required and vice versa. If Δ/a is small enough two-point contact will not occur (not shown).

Effect of the Hole Diameter on Insertion Force versus Depth

In Figure 1.4.8 the effect of the hole diameter (D/a) on F_z versus δz is shown. As the diameter of the peg increases, the insertion force increases during chamfer crossing and vice versa. During the remainder of the assembly the effect is not as clear; however, the trend is almost the same during two-point contact and reverses during the one-point contact phase. If the diameter of the peg is large enough, two-point contact does not occur. Also as D/a increases, the resumption of one-point contact occurs earlier because $a - \frac{\mu d}{2}$ is smaller.

Effect of Peg Support Stiffness on Insertion Force versus Depth

The effect of $K_x a^2/K_\theta$ on F_z versus δz is shown in Figure 1.4.9. Increasing $K_x a^2/K_\theta$ increases the insertion force and vice versa during each assembly phase.

Effect of Linearization

The effect of the linearization on F_z versus δz is shown in Figure 1.4.10 for several Δ/a. These results suggest that a small angle assumption is not always valid. As an example, when $\Delta/a = 0.1$, $\delta\theta_{max} = 5.2°$, but $F_{z_{max}}$ is underestimated by about 20%.

Location of Compliance Center of Peg

The optimal location of the compliance center of the peg follows as before (Section 1.3.6) and will not be discussed further here.

1.5 CONCLUSION

In the past, much work has been done at The Charles Stark Draper Laboratory, Inc. in the area of part mating, studying different "peg-in-hole" problems both theoretically and experimentally. The results presented in this section have extended some of the theoretical models used before, including the effect of various hole compliances and non-linearities. It is anticipated that some of the models developed in this section will be the basis of experimental work to be done in the future.

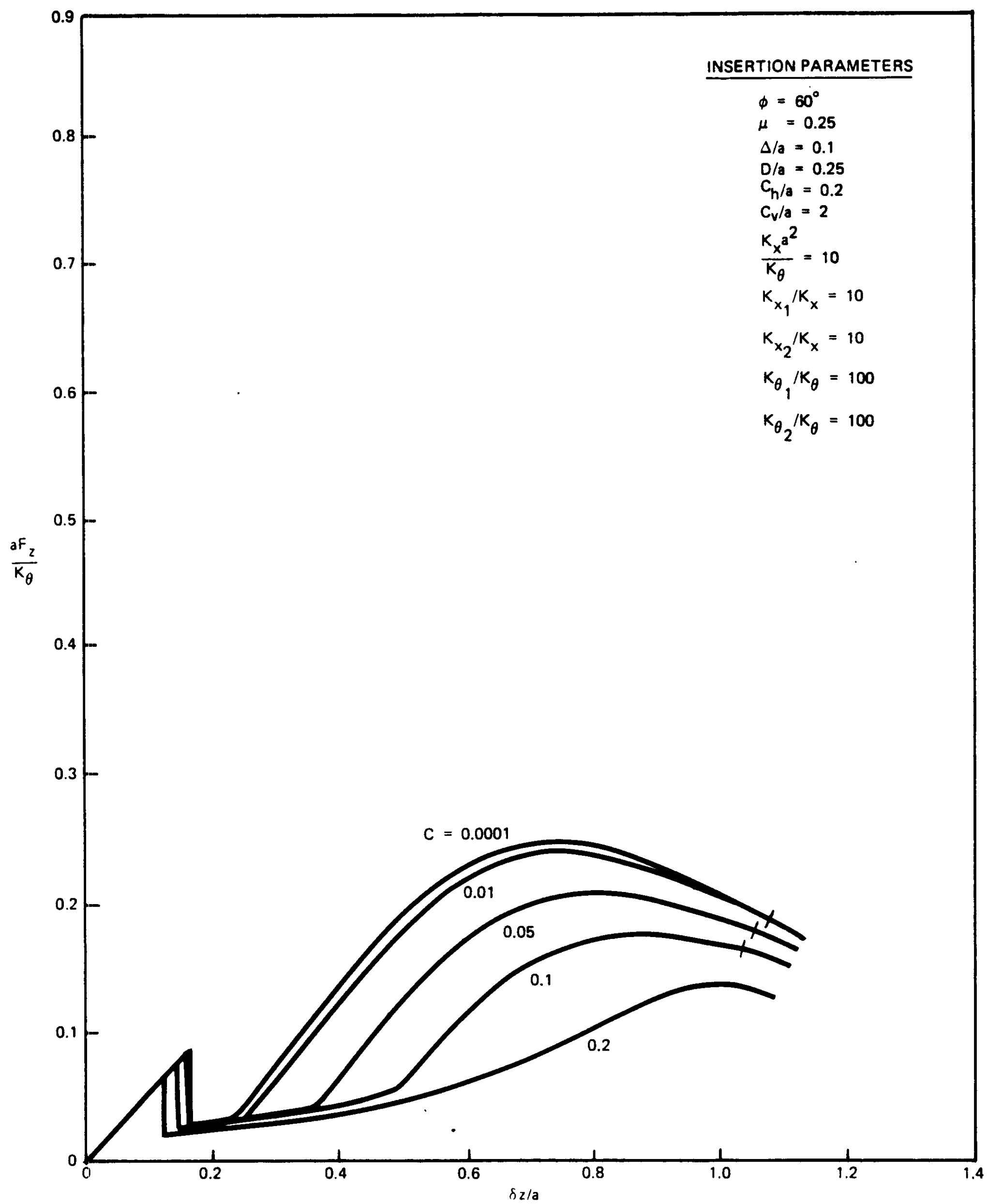

Figure 1.4.6. Effect of C on F_z versus δz.

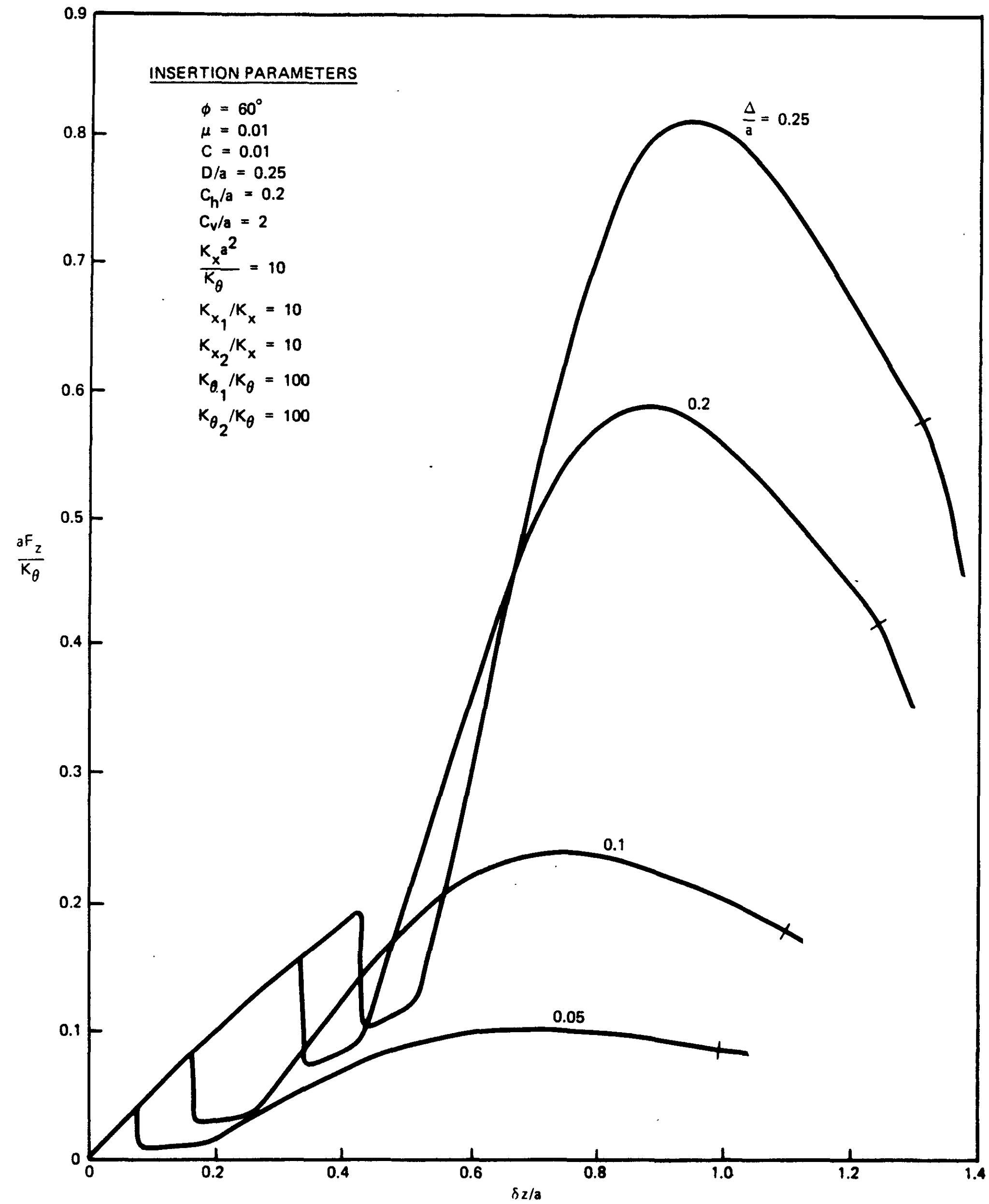

Figure 1.4.7. Effect of Δ/a on F_z versus δz.

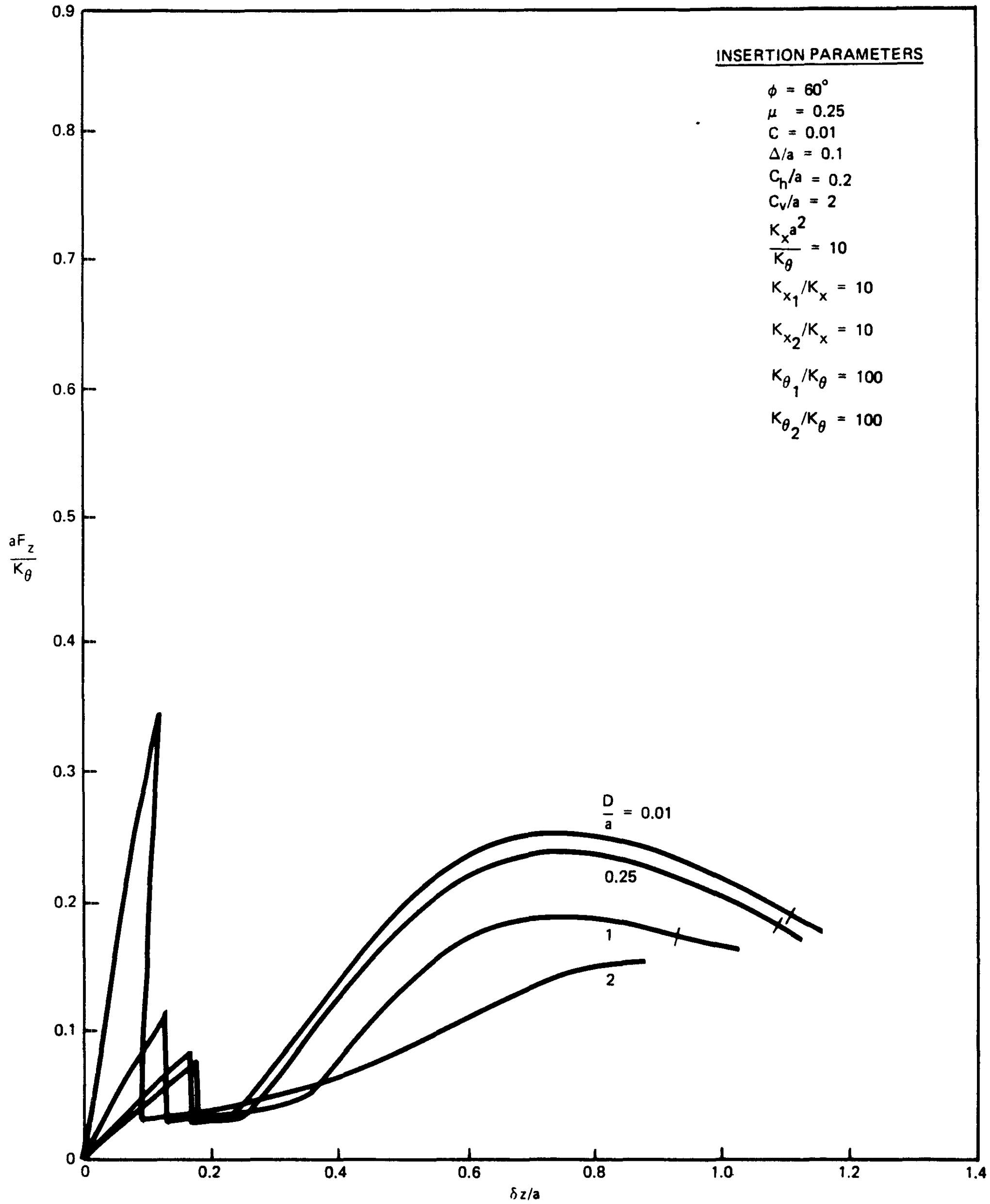

Figure 1.4.8. Effect of D/a on F_z versus δz.

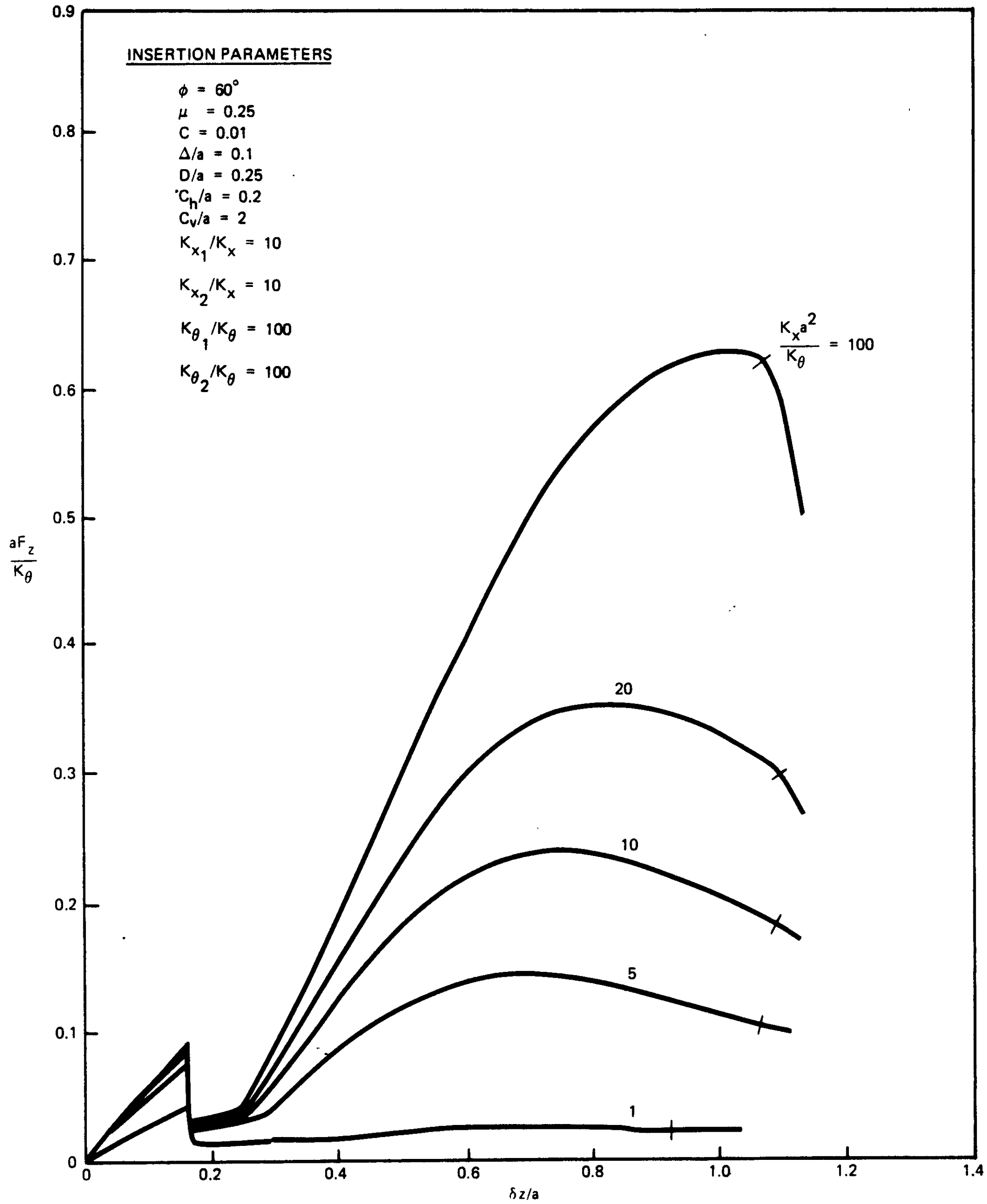

Figure 1.4.9. Effect of $K_x a^2/K_\theta$ on F_z versus δz.

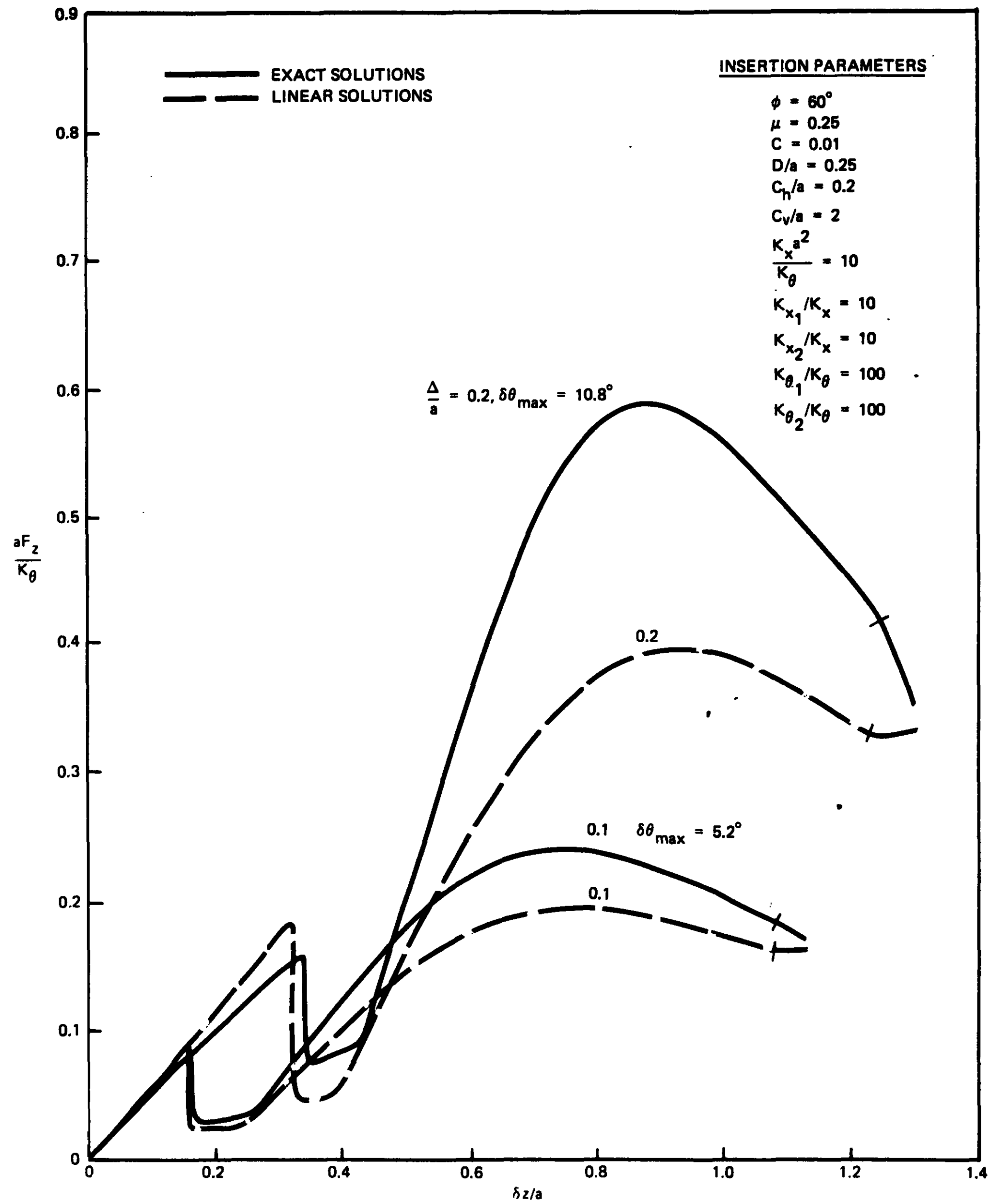

Figure 1.4.10. Comparison of linearized solutions for several Δ/a.

SECTION 2

MINIMUM ENERGY CHAMFER DESIGN

2.1 INTRODUCTION

2.1.1 Chamfer Design in General

From Section 1.4 (Figure 1.4.4) and previous work in Part Mating it is apparent that the slope and shape of the chamfer can greatly affect the insertion forces which arise during chamfer crossing. Knowledge of how these forces depend on the chamfer's slope and shape is essential if better chamfers are to be designed which enable the parts involved to be assembled more easily.

Design criteria have included the following: (1) minimum peak force, (2) constant force, (3) minimum vertical work/energy, and (4) minimum frictional work/energy during chamfer crossing. In general, the chamfers obtained by applying any one of these criteria also depend on the following three factors: friction, geometry (e.g. of peg), and compliance (of peg support and hole). Specification of these factors and one of the design criteria then determines the desired chamfer shape provided it exists.

The various chamfers will now be briefly discussed. Minimum peak force (vertical) chamfers are useful if it is desired to minimize the insertion force. Constant force chamfers are just that; fixing either the vertical insertion force or the normal contact force. If the normal contact force is kept constant, the frictional "wear" on the chamfer will be uniform during the assembly since the frictional force is proportional to the normal force. So far, no theoretical minimum peak force chamfers have been designed, but experimental evidence has suggested that constant force chamfers are in fact minimum peak force chamfers. Minimum "energy" chamfers ((3) and (4)) minimize a type of mechanical work during the assembly - frictional or vertical insertion. The use of the word "energy" is a bit of a misnomer because it is the mechanical work that is minimized, but since an energy source must be present to generate the mechanical work, it is perhaps justified. The words "work" and "energy" will be used interchangeably here. Some minimum energy chamfers have been designed in previous years. In this section the emphasis will be entirely on the design of minimum energy chamfers.

2.1.2 Minimum Energy Chamfer Design

Thus far, minimum energy chamfer design has centered on the original minimum energy chamfer problem proposed a couple of years ago. Much has been learned, with some aspects of the problem revisited in Section 2.3. Briefly, the problem statement is: find the shape of the chamfer (see Figure 2.1.1) which minimizes the vertical insertion work. The peg is assumed to be very long in comparison to its width and is supported compliantly by a rotational support of stiffness K_θ. Small angle assumptions have allowed an explicit solution.

Many problems related to this problem arise naturally. Suppose, for example, that the peg's width is significant or that the small angle assumption is dropped, etc. Ideally, the problem which allows for a lateral and rotational peg support, finite thickness peg, and large angles will eventually admit a solution. In an attempt to solve more general problems such as the one mentioned, two "simpler" problems were addressed with the following unique characteristics: (1) lateral peg support and (2) rotational peg support with large angles. In both of the cases the peg's width will be ignored and chamfers will be designed where the frictional work is minimized. Also, chamfers will be designed where the vertical insertion work is minimized and a very interesting comparison will be made.

2.2 LATERAL PEG SUPPORT

2.2.1 Introduction

In many cases the peg will be supported with only lateral compliance (K_x) as shown in Figure 2.2.1. Here, the chamfer shown in the figure is an arbitrary shape represented by $y(x)$ and the peg is represented by a line segment of length ℓ. Initially the peg is in contact with the top of the chamfer $(0, y_o)$ and coincident with the y axis. During the assembly to be considered, the peg translates laterally (i.e. parallel to y axis) while remaining in contact with the chamfer. Assembly ends when the contact point is at the bottom of the chamfer $(x_o, 0)$.

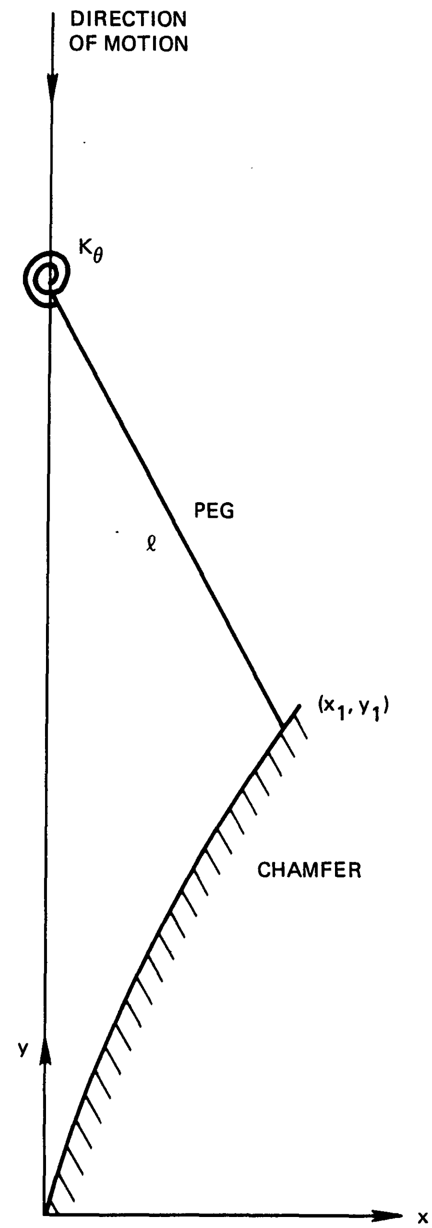

Figure 2.1.1. Original minimum energy chamfer problem.

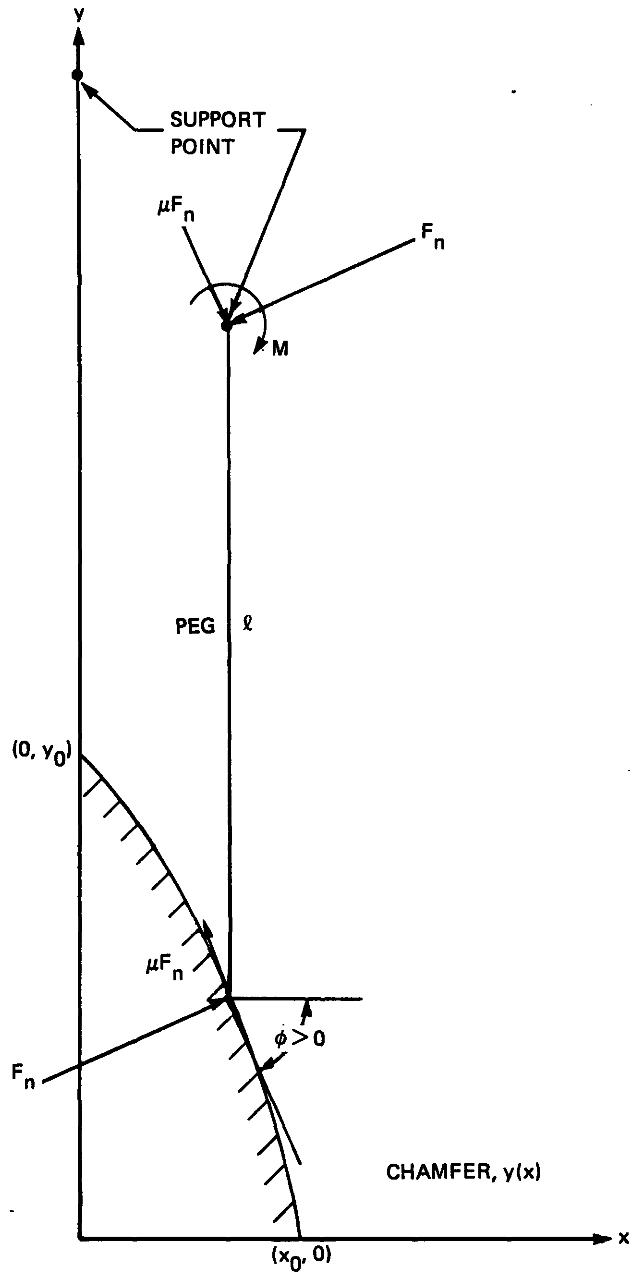

Figure 2.2.1. Chamfer crossing-lateral peg support.

The mechanics of the assembly can be analyzed with the aid of the free-body diagram of the peg provided in Figure 2.2.1. From the definition of a lateral support it follows that the normal contact force (F_n) is given by:

$$F_n = \frac{K_x x}{\sin\phi - \mu\cos\phi} \tag{2.2.1}$$

where

$$\tan\phi = -y' \tag{2.2.2}$$

Simplification yields:

$$F_n = \frac{K_x x\sqrt{1 + y'^2}}{y' + \mu} \tag{2.2.3}$$

Since the normal force is nonnegative, $y' \leq -\mu$. For chamfers that have slopes smaller than μ (in magnitude), wedging will occur. Also of interest are the vertical and horizontal contact forces (F_y, F_x) given by:

$$F_y = \frac{K_x x\ (\mu y' - 1)}{y' + \mu} \tag{2.2.4}$$

$$F_x = K_x x \tag{2.2.5}$$

Now that the mechanics of the assembly have been analyzed for a general chamfer shape, one can impose criteria which determine a desired chamfer shape indirectly. Chamfers will now be designed where either the friction work or the vertical insertion work is minimized. Also, a horizontal work criterion will be investigated.

2.2.2 <u>Frictional Work Criterion</u>

<u>Definition</u>

A natural criterion for designing chamfers involves finding a chamfer which minimizes the frictional work or "wear" on the chamfer. By definition, an increment in the frictional work (dW_μ) is equal to the product of the frictional force (μF_n) and an increment in the distance (ds) through which the end of the peg moves <u>anti-parallel</u> to this frictional force while in contact with chamfer, i.e.

$$dW_\mu = \mu F_n ds \tag{2.2.6}$$

where s is the arc length along the chamfer. The arc length (s) may be related directly to the chamfer slope (y') and x by:

$$ds = \sqrt{1 + y'^2}\,dx \tag{2.2.7}$$

The total frictional work (W_μ) is obtained by summing up all of the incremental contributions along the entire chamfer. This may be expressed as the following integral where appropriate substitutions have been made:

$$W_\mu = -\mu K_x \int_0^{x_0} \frac{x(1 + y'^2)}{y' + \mu}\,dx \equiv \int_0^{x_0} I_\mu(x,y')\,dx \tag{2.2.8}$$

Note that W_μ depends on the chamfer's slope (y') and not its shape (y).

Calculus of Variations Analysis

To find the chamfer shape such that the frictional work is minimized, the Calculus of Variations must be used.[9] Before proceeding with the analysis, one must recall that the Calculus of Variations does not apply when the solution, in this case a chamfer shape, is not expressable in the form y(x) (i.e. not a function) - more about this later.

Legendre's necessary condition for a minimum, $I_{\mu\,y'y'} \geq 0$ is certainly satisfied everywhere along the chamfer since[10],

$$I_{\mu\,y'y'} = -\frac{2\mu K_x x (1 + \mu^2)}{(y' + \mu)^3} \tag{2.2.9}$$

This guarantees that the solution obtained will minimize the frictional work. Euler's equation

$$\frac{d}{dx}\left(\frac{\partial I_\mu}{\partial y'}\right) = 0 \tag{2.2.10}$$

immediately reduces to the following differential equation:

$$\frac{xy'^2 + 2\mu xy' - x}{(y' + \mu)^2} = -c \qquad (2.2.11)$$

where c is an integration constant. The optimal chamfer shape is then independent of the peg support stiffness (K_x). Equation (2.2.11) may be solved for y' by using the quadratic formula to yield:

$$y' = -\mu - \sqrt{1 + \mu^2}\sqrt{\frac{x}{x + c}} \qquad (2.2.12)$$

Here the - sign must be used because $y' \leq -\mu$. Since $x/(x+c)$ must be nonnegative for $0 \leq x \leq x_o$, it follows that $c \geq 0$. This in turn produces a bound on the slope (y') (use $c = 0, \infty$);

$$-\mu - \sqrt{1 + \mu^2} \leq y' \leq -\mu \qquad (2.2.13)$$

By using one of the boundary conditions, it is observed that the $c = 0, \infty$ chamfers serve as an envelope for the rest of the chamfer shapes. This unexpected bound on the slope has to do with the fact that an optimal slope exists (see Section 2.2.5). Chamfers with slopes less than $-\mu - \sqrt{1 + \mu^2}$ certainly exist but will not minimize the frictional work. Using Dwight's Table of Integrals (#'s 195.01 and 195.04) Equation (2.2.11) may be integrated.[11] The dimensionless chamfer equation is then given by:

$$Y = S - \mu X - \sqrt{1+\mu^2}\left[\sqrt{X(X+C)} - C\,\ln(\sqrt{1+X/C} + \sqrt{X/C})\right] \qquad (2.2.14)$$

where

$$Y = y/x_o,\ X = x/x_o,\ C = c/x_o \text{ and}$$

$$\mu < S = y_o/x_o < \mu + \sqrt{1 + \mu^2} \qquad (2.2.15)$$

and the boundary condition $Y(0) = S$ has been used. Here S is defined as the aspect ratio, or baseline slope. To solve for the integration constant C, the boundary condition $Y(1) = 0$ must be used. This boundary condition yields a transcendental relation in C,

$$S = \mu + \sqrt{1+\mu^2}\left[\sqrt{1+C} - C\,\ln(\sqrt{1+1/C} + \sqrt{1/C})\right] \qquad (2.2.16)$$

In summary, given appropriate μ and S, Equation (2.2.14) describes the optimal chamfer shape.

2.2.3 Vertical Insertion Work Criterion

Definition

Chamfers can also be designed where the vertical insertion work is minimized. By definition, an increment in the vertical insertion work (dW_v) is equal to the product of the vertical force (F_y) exerted at the peg's support point and an increment in the distance (-dy) through which the support point moves parallel to this vertical insertion force, i.e.

$$dW_v = - F_y \, dy \tag{2.2.17}$$

By summing up all of the incremental contributions to the vertical insertion work and making appropriate substitutions, the total vertical insertion work (W_v) is given by an integral on x,

$$W_v = K_x \int_o^{x_o} \frac{x(1-\mu y')}{y'+\mu} \, y' dx \equiv \int_o^{x_o} I_v(x,y') dx \tag{2.2.18}$$

Again the work (W_v) depends on the chamfer's slope (y') but not its shape (y).

Calculus of Variations Analysis

The Calculus of Variations can be used to find the chamfer shape which minimizes the vertical insertion work. Legendre's condition $I_{v\,y'y'} \geq 0$ is the same as before (Equation (2.2.9)). In fact, Euler's equation reduces to Equation (2.2.11) so that chamfers designed according to minimum insertion work criteria are the same as chamfers designed according to minimum frictional work criteria! This result is not obvious but certainly not surprising either.

2.2.4 Horizontal Work Criterion

A surprising result happens if a minimum horizontal work criterion is imposed. By definition, an increment in the horizontal work (dW_h) is equal to the product of the horizontal contact force (F_x) on the chamfer and an increment in the distance (dx) through which the end of the peg moves anti-parallel to this horizontal force while in contact with the chamfer, i.e.

$$dW_h = F_x \, dx \tag{2.2.19}$$

By summing up all of the incremental contributions to the horizontal work and making appropriate substitutions, the total horizontal work (W_h) can be expressed as an integral on x which simplifies to

$$W_h = \tfrac{1}{2} K_x x_o^2 \tag{2.2.20}$$

which is independent of the friction involved and the chamfer shape! Since W_h is constant, it is automatically minimized.

2.2.5 Results and Discussion

As mentioned above, minimum vertical work chamfers are the same as minimum frictional work chamfers, which are also minimum horizontal work chamfers. Therefore, when one speaks of a minimum energy chamfer (lateral peg support) the specific criterion used does not have to be mentioned. Based on the Calculus of Variations analysis, the discussion will be broken up into the following areas: (1) Optimal Chamfer Slope and Energies, (2) Computer Program, and (3) Chamfer Shapes.

A. Optimal Chamfer Slope and Energies

By examining Equations (2.2.3) and (2.2.4) it is apparent that if the chamfer slope (y') is too flat (close to $-\mu$) arbitrarily large frictional and vertical insertion forces will be present. As a result, large frictional energies and vertical insertion energies will exist (see Equations (2.2.8) and (2.2.18)). Similarly, if the chamfer slope is too steep ($|y'|$ large), the forces (frictional and vertical insertion) will have to act over a larger distance ($\sim y' \, dx$) which then produce large frictional and vertical insertion energies. Therefore, by selecting a chamfer slope that is not too flat, but yet not too steep, an optimal slope may be arrived at. This optimal slope (m_o) is given by:

$$m_o(\mu) = -\left(\mu + \sqrt{1 + \mu^2}\right) \tag{2.2.21}$$

which incidently, is also equal to the steeper bound on the chamfer slope (see Inequality (2.2.13)). Increasing the friction makes the optimal slope steeper (more negative) and vice-versa. For low friction, the magnitude of the optimal slope is close to 1 (e.g. $|m_o| = 1.22$ when $\mu = 0.2$). When there is no friction ($\mu = 0$), the frictional work vanishes and the vertical insertion work is $\frac{1}{2}K_x x_o^2$ <u>regardless</u> of the chamfer's slope and shape (see Equations (2.2.8 and 2.2.18)). Therefore, there is no optimal slope when $\mu = 0$.

The optimal slope for $\mu > 0$ may be derived by requiring:

$$\frac{\partial W_\mu}{\partial y'} = 0 \tag{2.2.22}$$

or

$$\frac{\partial W_v}{\partial y'} = 0 \tag{2.2.23}$$

and using Leibniz's rule. It follows that the "optimal" optimal chamfer is a straight line chamfer with $S = \mu + \sqrt{1 + \mu^2}$.

The frictional work/energy corresponding to this chamfer is $2\mu\ (\mu + \sqrt{1 + \mu^2})(\frac{1}{2}K_x x_o^2)$ which is proportional to the potential energy stored in the compliant support. It's also dependent on the friction; the larger the friction, the larger the frictional work/energy and vice-versa.

The vertical insertion work/energy corresponding to this chamfer is $(\mu + \sqrt{1 + \mu^2})^2\ (\frac{1}{2}K_x x_o^2)$. It too is proportional to the potential energy stored in the compliant support. Increasing the friction is seen to increase the insertion work and vice-versa.

B. <u>Computer Program "CHAMF"</u>

A computer program called "CHAMF" has been written which determines the dimensionless optimal chamfer shape given appropriate μ and S. The details of the program will not be given here since it is a general program which also solves the "doorlatch" problem discussed later in Section 2.4.

C. <u>Chamfer Shapes</u>

The different types of optimal chamfers can be categorized by their aspect ratios (S) and the friction involved (μ). They will now be discussed with the results summarized in Figures 2.2.2 and 2.2.3.

Case 1 ($S < \mu$)

For $S < \mu$, no optimal chamfers exist since the peg will wedge into the chamfer.

Case 2 ($S = \mu$)

When $S = \mu$, the optimal chamfer is a straight line chamfer of slope $-\mu$. The peg, however, will wedge all of the way down the chamfer. This chamfer shape may be easily derived by using Eq. (2.2.12) and observing that as $c \to \infty$, $y' \to -\mu$.

Case 3 ($\mu < S < \mu + \sqrt{1 + \mu^2}$)

For $\mu < S < \mu + \sqrt{1 + \mu^2}$ the Calculus of Variations yields curved chamfer shapes (Equation (2.2.14)) and several of them are shown in Figure 2.2.3. They are convex because in general $y'' < 0$. The slope is always $-\mu$ at the top of the chamfer and it steadily decreases all of the way to the base of the chamfer.

One quantitative measure of the shape of a chamfer is its curvature, which measures how fast a curve is turning. From elementary calculus, the curvature (κ) of an optimal chamfer shape is:

$$\kappa = \frac{y''}{(1 + y'^2)^{3/2}} \qquad (2.2.24)$$

Recall that the curvature (in absolute value) of a circle of radius R is 1/R. The curvature of an optimal chamfer shape is seen to depend on x and is always negative (as $x \to 0^+$, $\kappa \to -\infty$). The rate of change of the curvature (κ') is:

$$\kappa' = \frac{(1 + y'^2)y''' - 3\,y'y''^2}{(1 + y'^2)^{5/2}} \qquad (2.2.25)$$

The sign (+or-) of κ' then depends on the sign of y' and y'''. By differentiating Equation (2.2.12) it may be easily shown that in general $y''' > 0$. Therefore $\kappa' > 0$ and the curvature (in magnitude) will be the largest (∞) at the top of the chamfer and steadily decrease to its smallest value at the base of the chamfer.

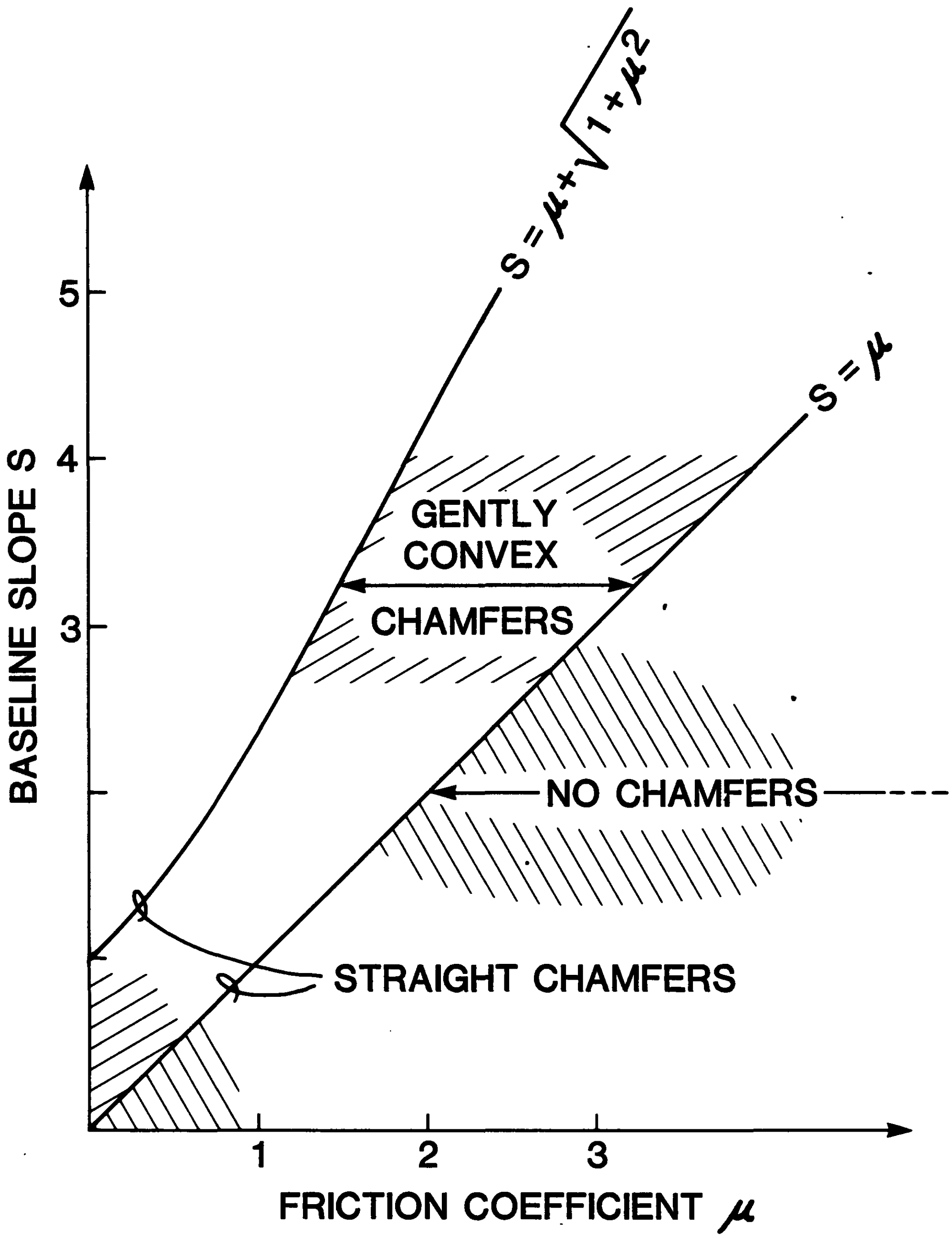

Figure 2.2.2. Regions in the S - μ plane showing allowed minimum insertion energy chamfers and their shapes.

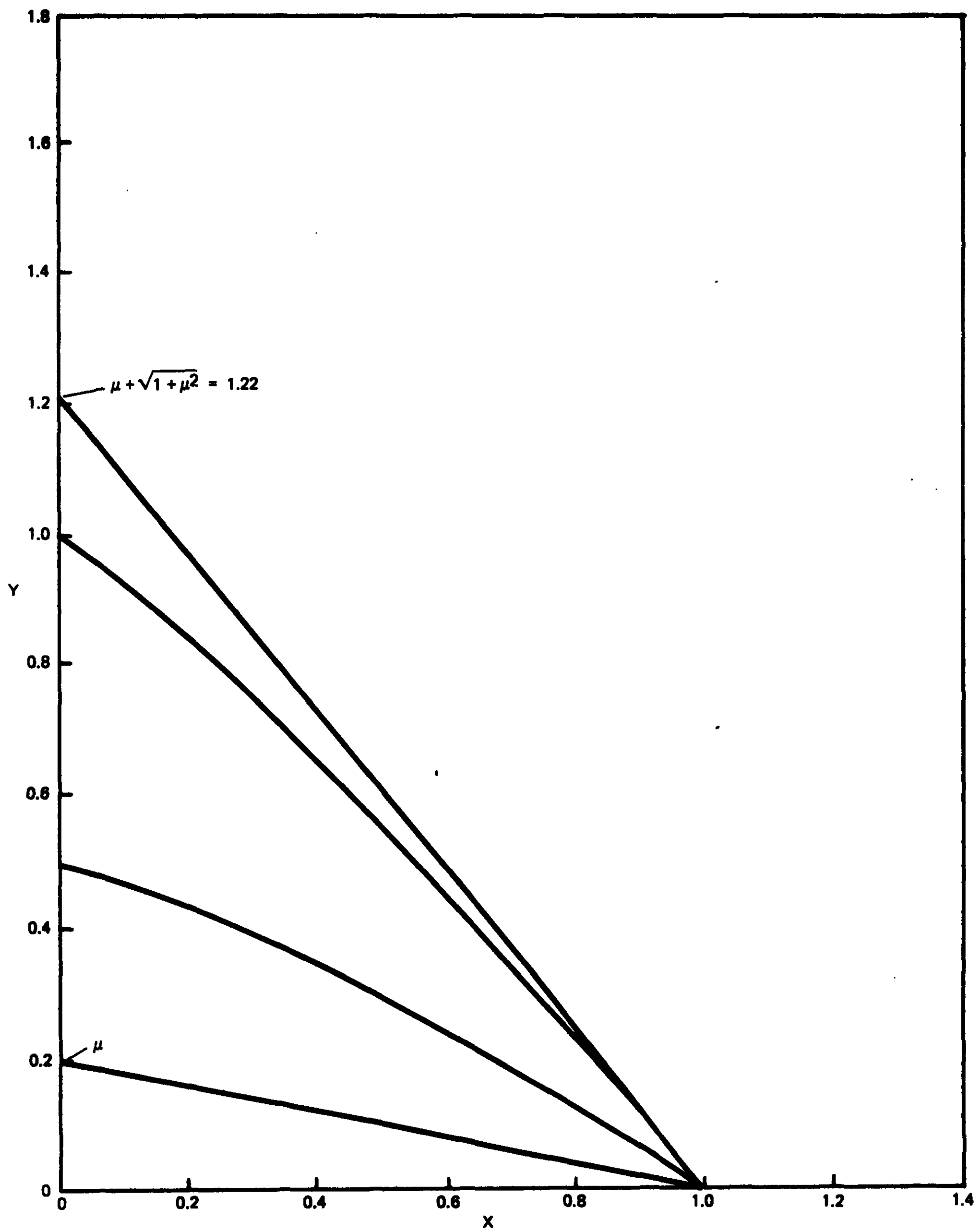

Figure 2.2.3. Minimum energy chamfer shapes for various S, $\mu = 0.2$.

Case 4 ($S = \mu + \sqrt{1 + \mu^2}$)

When $S = \mu + \sqrt{1 + \mu^2}$, the optimal chamfer is a straight line chamfer of slope $-\mu - \sqrt{1 + \mu^2}$. This is easily derived by using Equation (2.2.12) (let c = 0) or by recognizing that $-\mu - \sqrt{1 + \mu^2}$ is the optimal slope. As mentioned earlier, this chamfer is the "optimal" optimal chamfer. All other optimal chamfers give rise to larger frictional and insertion energies.

Case 5 ($S > \mu + \sqrt{1 + \mu^2}$)

For $S > \mu + \sqrt{1 + \mu^2}$ a sort of "concave" chamfer exists, but only in a trivial sense. This minimum energy shape consists of a straight line segment extending from (1,0) to $(0, \mu + \sqrt{1 + \mu^2})$ plus a vertical line segment extending from $(0,\mu + \sqrt{1 + \mu^2})$ to (0, S) (see Figure 2.2.3). The shape cannot be written in the form y(x) and for this reason the Calculus of Variations does not apply. This shape, although a mathematically correct solution, is not a chamfer since there are no contact forces along the vertical portion. Therefore, the minimum energy shape reduces to the optimal straight line chamfer of slope $-\mu-\sqrt{1 + \mu^2}$.

An indirect proof will be used to show that the shape described above is a minimum energy shape. Suppose the shape exists. Is it a minimum energy shape? Well, in going from (0, S) to $(0, \mu + \sqrt{1 + \mu^2})$ no work will be done since there are no contact forces. And in going from $(0, \mu + \sqrt{1 + \mu^2})$ to (1, 0) via a straight line chamfer the minimum possible frictional and insertion work is assured since the slope is optimal. Therefore, it is a minimum energy shape.

2.3 ROTATIONAL PEG SUPPORT

2.3.1 Introduction

The rotational peg support problem is conceptually similar to the lateral peg support problem and so the details of the analysis will be kept to a minimum. This is the original minimum energy chamfer problem proposed by D.E. Whitney and solved for small angles. In the present formulation, the small angle assumption will be dropped. Thus far, the problem has not been solved completely; however, major results such as the derivation of the optimal slope chamfer have been obtained.

In certain instances the peg will be supported with rotational compliance (K_θ) as shown in Figure 2.3.1. Again the chamfer is an arbitrary shape y(x) and the peg is represented by a line segment of

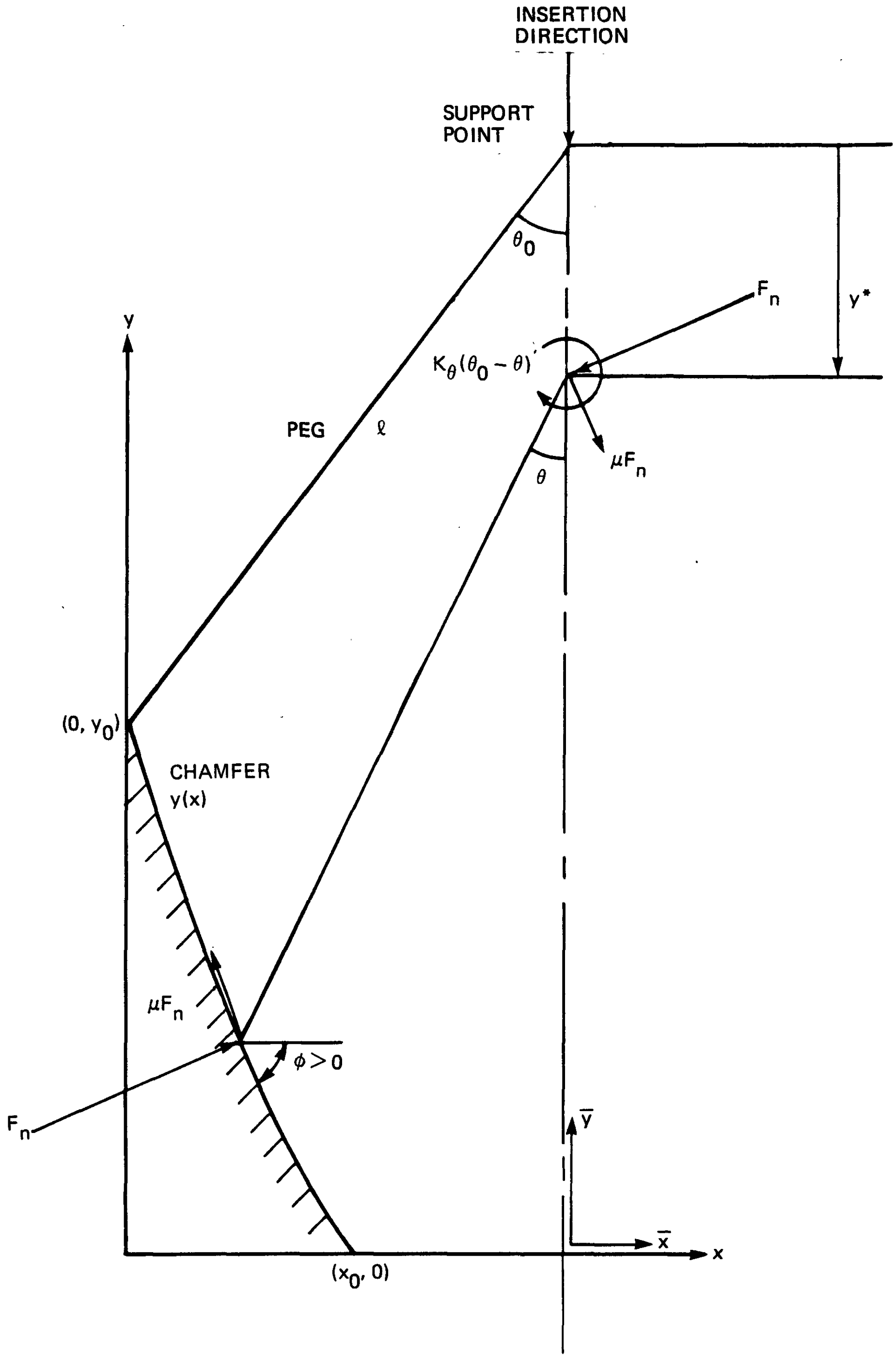

Figure 2.3.1. Chamfer crossing - rotational peg support.

length ℓ. Initially the end of the peg is in contact with the top of the chamfer $(0, y_o)$ and inclined at an angle θ_o to the vertical. During the assembly to be considered, the peg's support point moves vertically downward along the $\bar{y}$-axis, while the end of the peg slides along the chamfer with friction. Chamfer crossing (assembly) ends when the contact point is at the bottom of the chamfer $(x_o, 0)$.

With the aid of the free-body diagram of the peg provided in Figure 2.3.1, the mechanics of the assembly can be analyzed. The normal contact force (F_n) can be solved for by balancing moments at the support point,

$$F_n = \frac{(K_\theta/\ell)(\theta_o - \theta)}{\sin(\phi - \theta) - \mu \cos(\phi - \theta)} \tag{2.3.1}$$

where

$$\ell \sin\theta = \ell \sin\theta_o - x$$

$$\tan\phi = -y' \tag{2.3.2}$$

The normal force may then be expressed in terms of x, y'. However, it is more convenient to do the analysis in the $\bar{x}$, $\bar{y}$ coordinates and then transform back to the x, y coordinates later on. Therefore, F_n is given by:

$$F_n = \frac{K_\theta \left[\theta_o + \mathrm{Sin}^{-1}\left(\frac{\bar{x}}{\ell}\right)\right]\sqrt{1 + \bar{y}'^2}}{(\bar{x} - \mu\sqrt{\ell^2-\bar{x}^2}) - \bar{y}'(\sqrt{\ell^2-\bar{x}^2} + \mu\bar{x})} \tag{2.3.3}$$

where

$$\bar{x} = x - \ell \sin\theta_o$$

$$\bar{y} = y \tag{2.3.4}$$

Since the normal force is nonnegative,

$$\bar{y}' \leq \frac{\bar{x} - \mu\sqrt{\ell^2-\bar{x}^2}}{\sqrt{\ell^2 - \bar{x}^2} + \mu\bar{x}} \tag{2.3.5}$$

provided the initial offset angle (θ_o) is not too large;

$$\cot\theta_o > \mu \tag{2.3.6}$$

For chamfers with larger slopes or pegs inclined at larger initial offset angles, wedging will occur. Also, the vertical contact force (F_y) is given by:

$$F_y = \frac{K_\theta \left[\theta_o + \sin^{-1}\left(\frac{\bar{x}}{\ell}\right)\right](1 - \mu\,\bar{y}')}{(\bar{x} - \mu\sqrt{\ell^2-\bar{x}^2}) - \bar{y}'(\sqrt{\ell^2-\bar{x}^2} + \mu\,\bar{x})} \qquad (2.3.7)$$

Now that the mechanics of the assembly have been analyzed for a general chamfer shape, minimum frictional and vertical insertion work criteria will be used to design chamfers.

2.3.2 Frictional Work Criterion

Chamfers will now be designed where the frictional work is minimized. Proceeding in a similar manner as in Section 2.2.2, the frictional work (W_μ) may be expressed as;

$$W_\mu = \mu K_\theta \int_{\bar{x}} \frac{\left[\theta_o + \sin^{-1}\left(\frac{\bar{x}}{\ell}\right)\right](1 + \bar{y}'^2)\,d\bar{x}}{(\bar{x} - \mu\sqrt{\ell^2-\bar{x}^2}) - \bar{y}'(\sqrt{\ell^2-\bar{x}^2} + \mu\bar{x})} \equiv \int_{\bar{x}} I_\mu(x,y')\,d\bar{x} \qquad (2.3.8)$$

The frictional work is seen to depend on the chamfer's slope ($\bar{y}'$) but not its shape ($\bar{y}$).

Calculus of Variations Analysis

The Calculus of Variations may be used to find the chamfer shape $\bar{y}(\bar{x})$ (or $y'(x)$) such that the frictional work is minimized.

Legendre's necessary condition for a minimum, $I_{\mu_{y'y'}} \geq 0$ is satisfied everywhere along the chamfer since:

$$I_{\mu_{y'y'}} = \frac{\mu K_\theta\, \ell^2(1+\mu^2)\left[\theta_o + \sin^{-1}\left(\frac{\bar{x}}{\ell}\right)\right]}{\left[(\bar{x} - \mu\sqrt{\ell^2-\bar{x}^2}) - \bar{y}'(\sqrt{\ell^2-\bar{x}^2} + \mu\bar{x})\right]^3} \qquad (2.3.9)$$

Euler's equation reduces to the following differential equation:

$$\frac{\left[\theta_o + \sin^{-1}\left(\frac{\bar{x}}{\ell}\right)\right]\left[(\sqrt{\ell^2-\bar{x}^2} + \mu\bar{x})\bar{y}'^2 - 2\left(\bar{x} - \mu\sqrt{\ell^2-\bar{x}^2}\right)\bar{y}' - (\sqrt{\ell^2-\bar{x}^2} + \mu\bar{x})\right]}{\left[(\bar{x} - \mu\sqrt{\ell^2-\bar{x}^2}) - \bar{y}'(\sqrt{\ell^2-\bar{x}^2} + \mu\bar{x})\right]^2} = -c \qquad (2.3.10)$$

where c is an integration constant. This equation may be solved using the quadratic formula to yield:

$$\bar{y}' = \frac{\bar{x} - \mu\sqrt{\ell^2-\bar{x}^2}}{\sqrt{\ell^2-\bar{x}^2} + \mu\bar{x}} - \sqrt{\frac{\left[\theta_o + \sin^{-1}\left(\frac{\bar{x}}{\ell}\right)\right]\left[1 + \left(\frac{\bar{x} - \mu\sqrt{\ell^2-\bar{x}^2}}{\sqrt{\ell^2-\bar{x}^2} + \mu\bar{x}}\right)^2\right]}{\left[\theta_o + \sin^{-1}\left(\frac{\bar{x}}{\ell}\right)\right] + c\left(\sqrt{\ell^2-\bar{x}^2} + \mu\bar{x}\right)}} \tag{2.3.11}$$

Since the argument of the radical must be nonnegative for $-\ell \sin\Theta_o \leq \bar{x} \leq \bar{x}_o = x_o - \ell \sin\Theta_o$, $c \geq 0$. Also, the - sign must be used -- see Inequality 2.3.5. Note that positive slopes are possible (e.g. let c be large, μ small) if $\bar{x}$ is allowed to be positive! This case, however, is not too realistic since the support point will run into the chamfer. For large ℓ, Equation (2.3.11) is seen to reduce to Equation (2.2.12) when $\Theta_o = 0$ (c must be replaced with c/ℓ^2) so that the rotational peg support case reduces to the lateral peg support case. The slope is bounded since (use $c = 0, \infty$);

$$\frac{\bar{x} - \mu\sqrt{\ell^2-\bar{x}^2}}{\sqrt{\ell^2-\bar{x}^2} + \mu\bar{x}} - \sqrt{1 + \left(\frac{\bar{x} - \mu\sqrt{\ell^2-\bar{x}^2}}{\sqrt{\ell^2-\bar{x}^2} + \mu\bar{x}}\right)^2} \leq \bar{y}' \leq \frac{\bar{x} - \mu\sqrt{\ell^2-\bar{x}^2}}{\sqrt{\ell^2-\bar{x}^2} + \mu\bar{x}} \tag{2.3.12}$$

By using one of the boundary conditions, it is observed that the $c = 0, \infty$ chamfers serve as an envelope for the rest of the chamfer shapes. This bound has to do with the fact that an optimal slope exists which depends on $\bar{x}$ and that wedging has been avoided.

It is believed that in general, Equation (2.3.11) cannot be integrated by elementary methods and only a numerical or graphical solution is possible. However, when $c = 0, \infty$ direct integration is possible. For $\ell \sin\Theta_o \geq x_o$ solutions will be obtained. These solutions correspond to the case where the peg's support point does not interfere with the chamfer (see Figure 2.3.1) during assembly. When $c = \infty$, Equation (2.3.11) reduces to:

$$\bar{y}^{\,c=\infty} \equiv \bar{y}^{w} = \int_{\bar{x}} \frac{\bar{x} - \mu\sqrt{\ell^2-\bar{x}^2}}{\sqrt{\ell^2-\bar{x}^2} + \mu\bar{x}}\, d\bar{x} \tag{2.3.13}$$

or expanding,

$$\bar{y}^w = \int_{\bar{x}} \frac{(1+\mu^2)\bar{x}\sqrt{\ell^2-\bar{x}^2}}{\ell^2-(1+\mu^2)\bar{x}^2}\,d\bar{x} - \mu\ell^2 \int_{\bar{x}} \frac{d\bar{x}}{\ell^2-(1+\mu^2)\bar{x}^2} \qquad (2.3.14)$$

The second integral integrates easily to a logarithm term. The first integral may be transformed into the following pseudo-elliptic integral:

$$\ell \int_{x'} \tan x' \sqrt{1-k^2\sin^2 x'}\,dx' \qquad (2.3.15)$$

where

$$k = \frac{1}{\sqrt{1+\mu^2}}$$

$$\sin x' = \frac{\sqrt{1+\mu^2}\,\bar{x}}{\ell} \qquad (2.3.16)$$

which may be integrated using the extensive Rydzik-Gradstein Integral Tables (Section 2.583 #37).[12] By combining the two integrals in Equation (2.3.14) and transforming back to the original chamfer coordinates (x, y), one obtains the dimensionless chamfer equation

$$Y^W = \sqrt{L^2-\bar{X}(1)^2} - \sqrt{L^2-\bar{X}^2} + \frac{\mu L}{\sqrt{1+\mu^2}}\,\ln\left[\frac{(\sqrt{1+\mu^2}\sqrt{L^2-\bar{X}^2}+\mu L)}{(\sqrt{1+\mu^2}\sqrt{L^2-\bar{X}(1)^2}+\mu L)} \cdot \frac{(L+\sqrt{1+\mu^2}\,\bar{X}(1))}{(L+\sqrt{1+\mu^2}\,\bar{X})}\right] \qquad (2.3.17)$$

where

$$Y^W = y^W/x_o,\ X = x/x_o,\ L = \ell/x_o,$$

$$\bar{X}(X) = X - L\sin\theta_o$$

$$\mu>0,\ \cot\theta_o > \mu,\ L\sin\theta_o > 1 \qquad (2.3.18)$$

and the boundary condition $Y^{W}(1) = 0$ has been used. When $c = 0$, Equation (2.3.11) reduces to:

$$y^{c=0} \equiv \bar{y}^{o} = \int_{\bar{x}} \frac{\bar{x}-\mu\sqrt{\ell^2-\bar{x}^2}}{\sqrt{\ell^2-\bar{x}^2}+\mu\bar{x}}\, d\bar{x} - \int_{\bar{x}} \sqrt{1+\left(\frac{\bar{x}-\mu\sqrt{\ell^2-\bar{x}^2}}{\sqrt{\ell^2-\bar{x}^2}+\mu\bar{x}}\right)^2}\, d\bar{x} \qquad (2.3.19)$$

The first integral is the same as Equation (2.3.13) and the second integral may be transformed using Equation (2.3.16) into

$$-\ell\int_{x'} \frac{\sqrt{1-k^2\sin^2 x'}}{\cos x'}\, dx' + \frac{\mu\ell}{\sqrt{1+\mu^2}}\int_{x'} \tan x'\, dx' \qquad (2.3.20)$$

The second integral (Integral 2.3.20) may be integrated easily to a logarithm term and the first integral is another pseudo-elliptic integral which may be integrated using the Rydzik-Gradstein Integral Tables (Section 2.583 #33). By combining the two integrals in Eq. (2.3.19) and transforming back to the original chamfer coordinates (x, y), the dimensionless chamfer equation ($Y^{o} = y^{o}/x_{o}$) is given by:

$$Y^{o} = Y^{W} + \frac{L}{\sqrt{1+\mu^2}}\left[\mathrm{Sin}^{-1}(\bar{X}(1)/L) - \mathrm{Sin}^{-1}(\bar{X}/L)\right]$$

$$+ \frac{\mu L}{\sqrt{1+\mu^2}}\, \ell n\left[\frac{\left(\sqrt{L^2-\bar{X}^2}-\mu\bar{X}\right)\left(L^2-(1+\mu^2)\ \bar{X}(1)^2\right)}{\left(\sqrt{L^2-\bar{X}(1)^2}-\mu\bar{X}(1)\right)\left(L^2-(1+\mu^2)\ \bar{X}^2\right)}\right] \qquad (2.3.21)$$

where the boundary condition $Y^{o}(1) = 0$ has been used.

2.3.3 Vertical Work Criterion

Chamfers can also be designed where the vertical work is minimized. Recall that an increment in the vertical insertion work (dW_{V}) is equal to the product of the vertical force (F_{Y}) exerted at the peg's support point and an increment in the distance (dy*, see Figure 2.3.1) through which the support point moves parallel to this vertical insertion force, i.e.

$$dW_{V} = F_{Y}\, dy^{*} \qquad (2.3.22)$$

The distance y* may be related to x, y indirectly by

$$\ell\cos\theta_o + y_o = y + \ell\cos\theta + y^* \tag{2.3.23}$$

Or, alternatively in differential form:

$$dy^* = \left[\frac{x - \ell\sin\theta_o}{\sqrt{\ell^2 - (x - \ell\sin\theta_o)^2}} - y'\right] dx \tag{2.3.24}$$

By introducing the $\bar{x}$, $\bar{y}$ coordinates and making appropriate substitutions, the total vertical insertion work (W_v) is given by:

$$W_v = K_\theta \int_{\bar{x}} \frac{\left[\theta_o + \sin^{-1}\left(\frac{\bar{x}}{\ell}\right)\right](1-\mu\bar{y}')\,(\bar{x}/\sqrt{\ell^2-\bar{x}^2}-\bar{y}')}{(\bar{x}-\mu\sqrt{\ell^2-\bar{x}^2})-\bar{y}'(\sqrt{\ell^2-\bar{x}^2}+\mu\bar{x})}\, d\bar{x}$$

$$\equiv \int_{\bar{x}} I_v\,(\bar{x},\bar{y}')\,d\bar{x} \tag{2.3.25}$$

Again, the work (W_v) depends on the chamfer's slope ($\bar{y}'$) but not its shape ($\bar{y}$).

Calculus of Variations Analysis

By using the Calculus of Variations, the optimal chamfer shape which minimizes the vertical work can be determined. Legendre's condition $I_{v\bar{y}'\bar{y}'} \geq \hat{0}$ is the same as before (Equation (2.3.9)). Also, Euler's equation reduces to Equation (2.3.10) so that as before (lateral peg support case), chamfers designed according to minimum insertion work criteria are the same as those designed according to minimum frictional work criteria.

2.3.4 Results and Discussion

To date, the rotational peg support problem has not been solved completely and is currently under investigation. Much of the remaining work pertains to solving for the various optimal chamfer shapes. However, most of the theoretical work has been done.

One major result so far is that minimum frictional work chamfers are the same as minimum vertical work chamfers. Another result concerns the derivation of the most important minimum energy chamfer, the optimal slope chamfer. Other results include a computer program written to determine various optimal chamfer shapes and a classification of the different chamfer shapes.

A. Optimal Chamfer Slope

By a similar qualitative argument (see Section 2.2.5) an optimal slope exists. It may be derived by requiring

$$\frac{\partial W_\mu}{\partial \bar{y}'} = 0$$

or

$$\frac{\partial W_v}{\partial \bar{y}'} = 0 \qquad (2.3.26)$$

and using Leibniz's rule. The result is that the optimal slope m_o depends on x and is given by:

$$m_o(x,\mu,\ell) = \frac{\bar{x} - \mu\sqrt{\ell^2-\bar{x}^2}}{\sqrt{\ell^2-\bar{x}^2} + \mu\bar{x}} - \sqrt{1 + \left(\frac{\bar{x} - \mu\sqrt{\ell^2-\bar{x}^2}}{\sqrt{\ell^2-\bar{x}^2} + \mu\bar{x}}\right)^2} \qquad (2.3.27)$$

which is equal to the steeper bound on the slope discussed earlier (Inequality 2.3.12). Equation (2.3.21) then represents the "optimal" optimal chamfer since the slope is optimized at each point on the chamfer. For large ℓ, the optimal slope approaches $-\tan(\theta_o+\beta)-\sec(\theta_o+\beta)$. Of course when $\theta_o = 0$, this slope is $-\mu - \sqrt{1+\mu^2}$, which is the optimal slope when the peg is supported laterally.

B. Computer Program "CHAMFR"

A computer program called "CHAMFR" has been written which computes the dimensionless wedging chamfer (Equation 2.3.17) and more importantly, the dimensionless optimal slope chamfer (Equation 2.3.21) given $\mu>0$, $\theta_o < \mathrm{Cot}^{-1}\mu$, $L > \csc\theta_o$.

C. Chamfer Shapes

By analogy to Section 2.2.5, the different types of optimal chamfers can be categorized by their aspect ratios ($S = y_o/x_o$), the friction involved (μ), the initial offset angle (θ_o), and the length of the peg (L). Given μ, θ_o, and L the shapes Y^w, Y^o are determined. The optimal chamfers can then be categorized in terms of S, Y_o^w, and Y_o^o.

Case 1 ($S < Y_o^w$)

For $S < Y_o^w$, no optimal chamfers exist since the peg will wedge into the chamfer.

Case 2 ($S = Y_o^w$)

When $S = Y_o^w$, the optimal chamfer shape is given by $Y^w(X)$; obtained from Inequality 2.3.5 or Equation (2.3.11) ($C = \infty$). The peg, however; will wedge all of the way down the chamfer. Several of these curved chamfer shapes are shown in Figures 2.3.2 and 2.3.3. Because in general $Y^{w'} > 0$, the shapes are concave, but for large L, the chamfers are very straight ($Y^{w''} \approx 0$). The initial slope is $-\tan(\theta_o+\beta)$ and it steadily increases (less negative) all of the way to the base of the chamfer.

Case 3 ($Y_o^w < S < Y_o^o$)

For $Y_o^w < S < Y_o^o$, Equation (2.3.11) must be integrated numerically and the integration constant solved for to determine the optimal chamfer shape. This has not been done yet, but some insight can be gained into the solution since the optimal chamfers are bounded by the two curves $Y^w(X)$ and $Y^o(X)$ (see Figures 2.3.2 and 2.3.3). For large L ($\theta_o = 0$), the chamfer shapes approach those derived in the lateral peg support case (Equation 2.2.14).

Case 4 ($S = Y_o^o$)

When $S = Y_o^o$, the optimal chamfer shape is given by $Y^o(X)$. This may be established by using Equation (2.3.11)(let $c = 0$) or recognizing that $Y^o(X)$ is the optimal slope chamfer. All other optimal chamfers give rise to larger frictional and insertion energies. Several of these shapes are shown in Figures 2.3.2 and 2.3.3. The chamfer shapes are concave ($Y^{o''} > 0$), but for large L tend to a straight line chamfer of slope $-\tan(\theta_o+\beta)-\sec(\theta_o+\beta)$. The initial slope is always $-\tan(\theta_o+\beta)$ $-\sec(\theta_o+\beta)$ and it steadily increases all of the way to the base of the chamfer.

Case 5 ($S > Y_o^o$)

For $S > Y_o^o$, the solution reduces to the optimal slope chamfer Y^o (X). This result follows by analogy to the corresponding solution

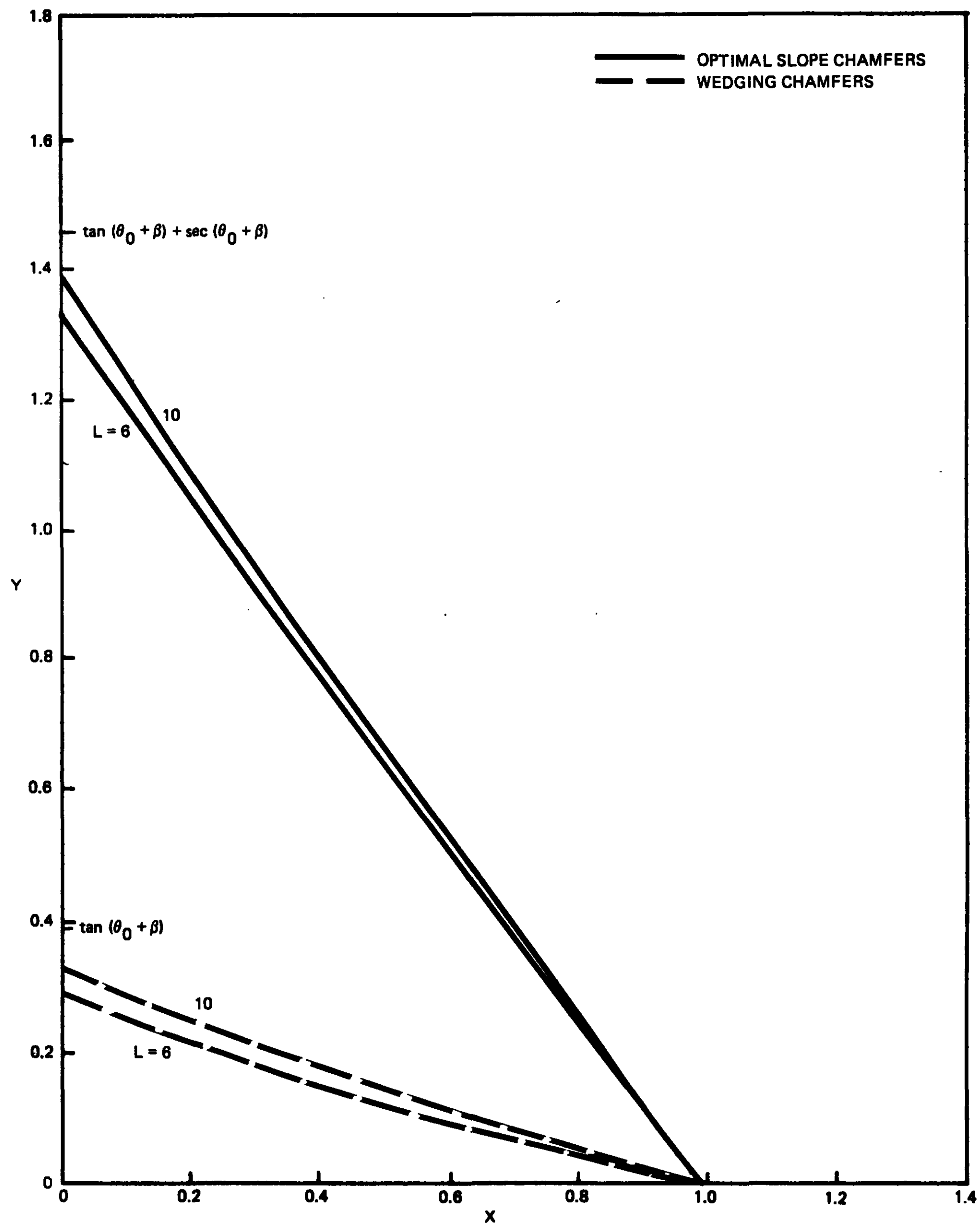

Figure 2.3.2. Optimal and wedging chamfers for various L, $\mu = 0.2$, $\theta_0 = 10°$.

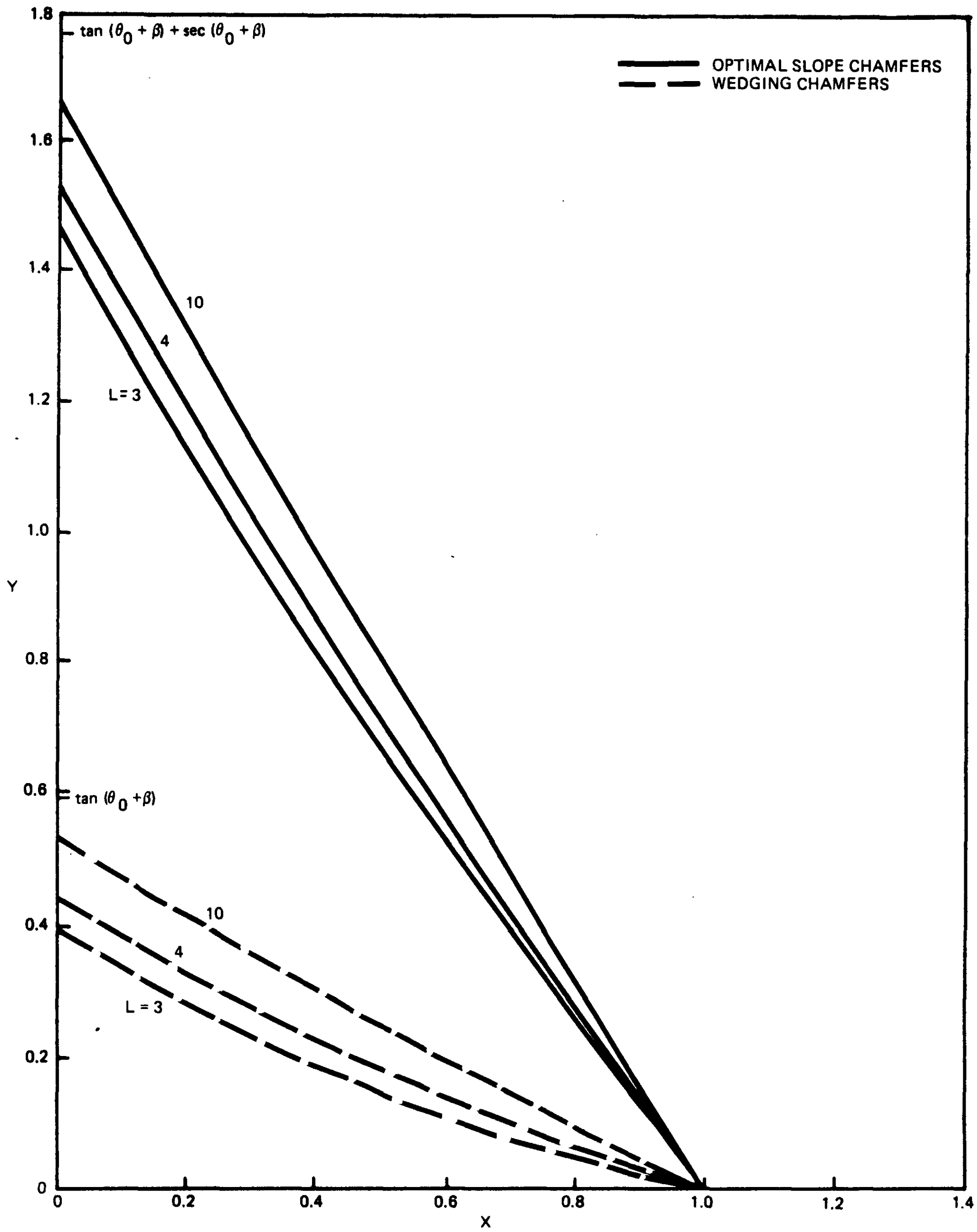

Figure 2.3.3. Optimal and wedging chamfers for various L, $\mu = 0.2$, $\theta_0 = 20°$.

(Case 5) of the lateral peg support problem (Section 2.2.5) and will not be discussed further.

2.4 DOORLATCH PROBLEM

2.4.1 Introduction

So far, minimum energy chamfers have been designed where the chamfered part rubs against another part with friction. An example of a problem where the chamfered part, while being displaced, rubs against a third part with friction is the design of a common household doorlatch illustrated in Figure 2.4.1(a). The problem concerns finding the shape of the chamfer on the doorlatch tongue subject to minimum energy criteria. Although this is a specific problem, it generalizes previous work done in minimum energy chamfer design and it reinforces the dependence of two design criteria which have been used to design chamfers; namely (1) minimum frictional work, and (2) minimum insertion work.

Problem Formulation

The mechanics of the "assembly" will be analyzed for an arbitrary chamfer shape and will be developed in much the same manner as the mechanics were analyzed in Sections 2.2 and 2.3. From this analysis the Calculus of Variations will be used to determine the optimal chamfer shapes.

Before proceeding with the analysis, various simplifying assumptions will be made which serve to reduce the complexity of the mathematical model used to analyze the doorlatch problem. First of all, since the physical dimensions of most doorlatches are small in comparison with the width of the door, the door will essentially move laterally past the door casing so that angular misalignments may be ignored. Secondly, the model will not take into account the effect of a lead-in shape affixed to the door casing. Finally, some "play" (very small) between the tongue and the door will be assumed so that the only frictional contacts will occur between (1) the corner of the door casing and the chamfer and (2) the inside corner of the door and the back of the tongue as shown in Figure 2.4.1(b).

The first step in the analysis is to define the geometry and construct a free-body diagram of the doorlatch tongue (see Figure 2.4.2). From this the mechanics may be analyzed. The chamfer shown

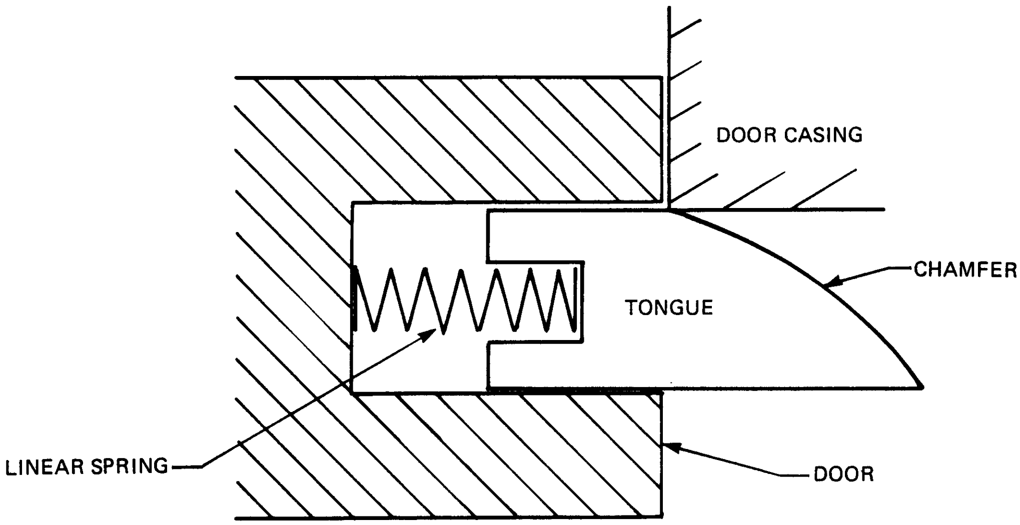

(a) Initial Configuration

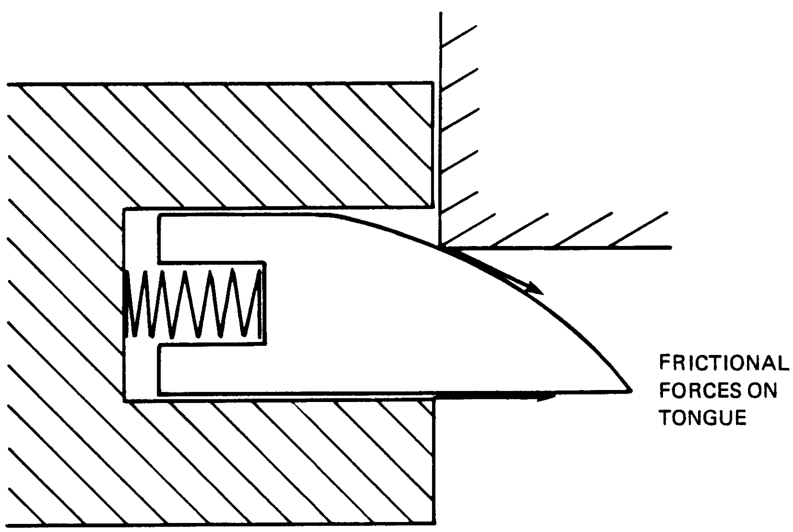

(b) During "Assembly"

Figure 2.4.1. Doorlatch problem.

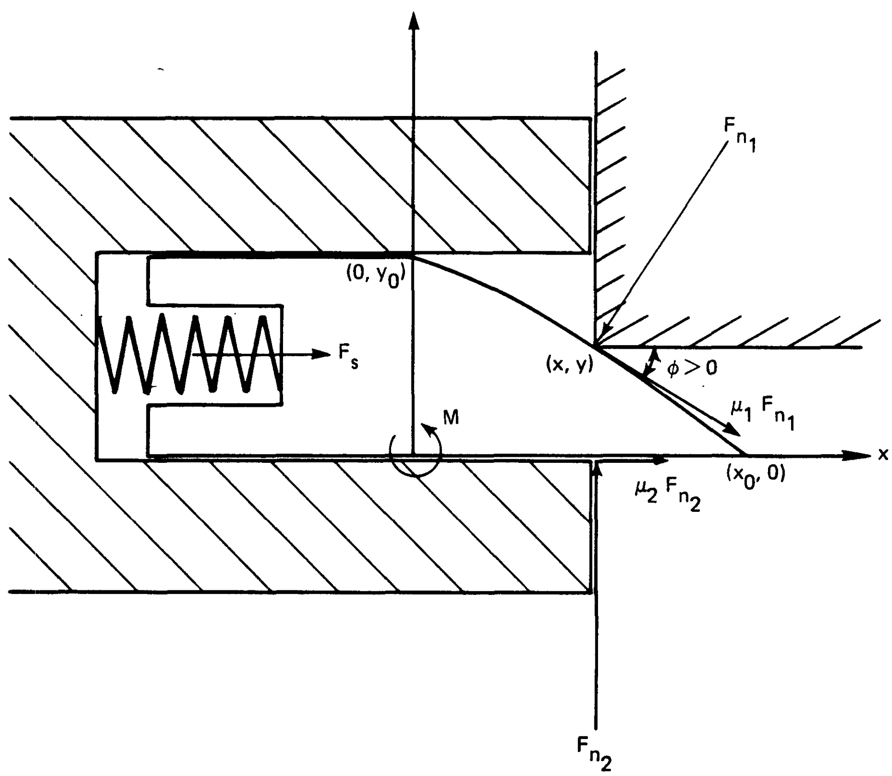

Figure 2.4.2. Free-body diagram of doorlatch tongue.

is a general shape y(x) and initially the top of the chamfer $(0,y_o)$ is in contact with the door casing and the point (0,0) on the back of the tongue is in contact with the inside corner of the door. During the "assembly", the doorlatch tongue translates laterally while remaining in contact with the door casing and the inside corner of the door. Assembly ends when the contact points are at the bottom of the chamfer $(x_o,0)$. The friction coefficients are μ_1, μ_2 and the spring force (F_s) is proportional to the lateral displacement of the doorlatch tongue $(F_s = K_x x)$. Balancing forces in the x and y directions yields:

$$K_x x - F_{n_1}(\sin\phi - \mu_1 \cos\phi) + \mu_2 F_{n_2} = 0$$

$$F_{n_2} - F_{n_1}(\cos\phi + \mu_1 \sin\phi) = 0 \qquad (2.4.1)$$

where F_{n_1}, F_{n_2} are the normal contact forces and $\tan\phi = -y'$. Solving for the normal contact forces gives:

$$F_{n_1} = \frac{-K_x x\sqrt{1+y'^2}}{(1-\mu_1\mu_2)y' + \mu_1 + \mu_2}$$

$$F_{n_2} \equiv F_y = \frac{-K_x x\,(1-\mu_1 y')}{(1-\mu_1\mu_2)y' + \mu_1 + \mu_2} \qquad (2.4.2)$$

Since the normal contact forces are nonnegative, it follows that

$$y' < \frac{-(\mu_1+\mu_2)}{1-\mu_1\mu_2} \qquad \text{for} \quad \mu_1\mu_2 < 1$$

$$y' \geq \frac{-(\mu_1+\mu_2)}{1-\mu_1\mu_2} \qquad \text{for} \quad \mu_1\mu_2 \geq 1 \qquad (2.4.3)$$

Because μ_1, μ_2 are typically small only the first case $(\mu_1\mu_2 < 1)$ is realistic. Also, some obvious difficulties arise if $\mu_1\mu_2 \geq 1$ because the slope must be positive and the boundary conditions cannot be satisfied. For chamfers with flatter slopes, wedging will occur.

2.4.2 Calculus of Variations Analysis

The Calculus of Variations can be used to determine the minimum energy chamfer shape. The derivation follows almost identically to the derivation in Section 2.2 and will be quite brief. As before, minimum "insertion" work ($W_v = F_y dy$) chamfers are the same as minimum frictional work chamfers. Only the later formulation will be presented here.

An increment in the frictional work (dW_μ) is equal to the sum of the frictional work along the chamfer ($\mu_1 F_{n_1} ds$) plus the frictional work along the back of the doorlatch tongue ($\mu_2 F_{n_2} dx$);

$$dW_\mu = \mu_1 F_{n_1} ds + \mu_2 F_{n_2} dx \tag{2.4.4}$$

where s is the arclength along the chamfer. By making appropriate substitutions and integrating, the total frictional work (W_μ) is given by:

$$W_\mu = - K_x \int_0^{x_0} \frac{x(\mu_1 y'^2 - \mu_1\mu_2 y' + \mu_1 + \mu_2)\,dx}{(1-\mu_1\mu_2)y' + \mu_1 + \mu_2} \equiv \int_0^{x_0} I_\mu(x,y')\,dx \tag{2.4.5}$$

Legendre's condition insures that the solution will minimize the frictional work since:

$$I_{\mu_{y'y'}} = \frac{2K_x x\ (\mu_1+\mu_2)(1+\mu_1^2)}{\left[(1-\mu_1\mu_2)y' + \mu_1+\mu_2\right]^3} \tag{2.4.6}$$

Substitution of Equation (2.4.5) into Euler's equation and simplifying yields:

$$\frac{x\left[\mu_1(1-\mu_1\mu_2)y'^2 + 2\mu_1(\mu_1+\mu_2)y' - (\mu_1+\mu_2)\right]}{\left[(1-\mu_1\mu_2)y' + \mu_1+\mu_2\right]^2} = - c \tag{2.4.7}$$

where c is an integration constant. The optimal chamfer shape is seen to be independent of the spring constant. Equation (2.4.7) may be solved using the quadratic formula to give:

$$y' = \frac{-(\mu_1+\mu_2)}{1-\mu_1\mu_2}\left[1 + \sqrt{\frac{1+\mu_1^2}{\mu_1+\mu_2}}\sqrt{\frac{x}{\mu_1 x + c(1-\mu_1\mu_2)}}\right] \qquad (2.4.8)$$

where the + sign has been used (see Inequality 2.4.3). It also follows that $c \geq 0$ and the slope is bounded (use $c = 0,\infty$);

$$\frac{-(\mu_1+\mu_2)}{1-\mu_1\mu_2}\left[1 + \sqrt{\frac{1+\mu_1^2}{\mu_1(\mu_1+\mu_2)}}\right] \leq y' \leq \frac{-(\mu_1+\mu_2)}{1-\mu_1\mu_2} \qquad (2.4.9)$$

so that $c = 0,\infty$ chamfers serve as an envelope for the rest of the chamfer shapes. This bound is due to the fact that an optimal slope exists (see Section 2.4.3). Chamfers with steeper slopes than the lower bound (Inequality 2.4.9) will not be minimum energy chamfers. Equation (2.4.8) may be integrated using Dwight's Table of Integrals (#'s 195.01 and 195.04) to yield the following dimensionless chamfer equation:

$$Y = S - \frac{(\mu_1+\mu_2)}{1-\mu_1\mu_2}\left\{X + \sqrt{\frac{1+\mu_1^2}{\mu_1(\mu_1+\mu_2)}}\left[\sqrt{X(X+C)} - C\ln(\sqrt{1+X/C} + \sqrt{X/C})\right]\right\} \qquad (2.4.10)$$

where

$$Y = y/x_o, \; X = x/x_o, \; C = \frac{c(1-\mu_1\mu_2)}{\mu_1 x_o} \quad \text{and}$$

$$\frac{\mu_1+\mu_2}{1-\mu_1\mu_2} < S = y_o/x_o < \frac{\mu_1+\mu_2}{1-\mu_1\mu_2}\left[1 + \sqrt{\frac{1+\mu_1^2}{\mu_1(\mu_1+\mu_2)}}\right] \text{and}$$

$$\mu_1\mu_2 < 1 \qquad (2.4.11)$$

and the boundary condition $Y(0) = S$ has been used. The integration constant may be defined from $Y(1) = 0$;

$$S = \frac{\mu_1+\mu_2}{1-\mu_1\mu_2}\left\{1 + \sqrt{\frac{1+\mu_1^2}{\mu_1(\mu_1+\mu_2)}}\left[\sqrt{1+C} - C\ln(\sqrt{1+1/C} + \sqrt{1/C})\right]\right\} \qquad (2.4.12)$$

Summarizing, Equation (2.4.10) describes the optimal chamfer shape given appropriate μ_1, μ_2, and S.

2.4.3 Results and Discussion

Based on the above analysis, the discussion will be broken up into (1) Optimal Slope, (2) Computer Program, and (3) Chamfer Shapes.

There is a very strong interrelationship between the doorlatch problem and the lateral peg support problem. In fact when $\mu_2 = 0$, the doorlatch problem reduces to the lateral peg support problem and all of the quations and results of Section 2.2 apply (note that integration constants are different).

Optimal Chamfer Slope

As before (Section 2.2) an optimal chamfer slope exists. The optimal chamfer slope (m_o) is given by:

$$m_o\ (\mu_1,\mu_2) = \frac{-(\mu_1+\mu_2)}{1-\mu_1\mu_2}\left[1 + \sqrt{\frac{1+\mu_1^{\,2}}{\mu_1(\mu_1+\mu_2)}}\right] \tag{2.4.13}$$

A straight line chamfer with this slope is the "optimal" optimal chamfer. All other chamfers give rise to larger frictional and insertion energies. The effect of the second source of friction (μ_2) on the optimal slope can be determined by examining $\frac{\partial m_o}{\partial \mu_2}$. It may be shown in general that $\frac{\partial m_o}{\partial \mu_2} < o$, so that as μ_2 increases, the optimal slope will become steeper. This is also true for the "wedging" slope, $-(\mu_1+\mu_2)/(1-\mu_1\mu_2)$.

Computer Program "CHAMF"

A computer program called "CHAMF" (see Appendix A) has been written which computes the dimensionless optimal chamfer shape (Equation (2.4.10)) given appropriate μ_1, μ_2, and S. When $\mu_2 = 0$, the shape obtained is also the minimum energy chamfer shape for the lateral peg support problem.

A Newton-Raphson method was used to determine the integration constant C numerically. Because of the wide range of C $(0,\infty)$ an initial guess for C is needed. For small aspect ratios (S), a large initial guess is required and vice-versa.

Chamfer Shapes

The various optimal chamfer shapes can be categorized by their aspect ratios (S) and the friction involved (μ_1, μ_2). The discussion of the different cases may be reduced to the case analysis done in Section 2.2.5 by replacing μ by $\frac{\mu_1+\mu_2}{1-\mu_1\mu_2}$; $-\mu-\sqrt{1+\mu^2}$ by $m_o(\mu_1,\mu_2)$ and referring to the corresponding equations in Section 2.4. Some of these chamfer shapes are shown in Figure 2.4.3 for $\mu_1 = 0.5$, $\mu_2 = 0.25$.

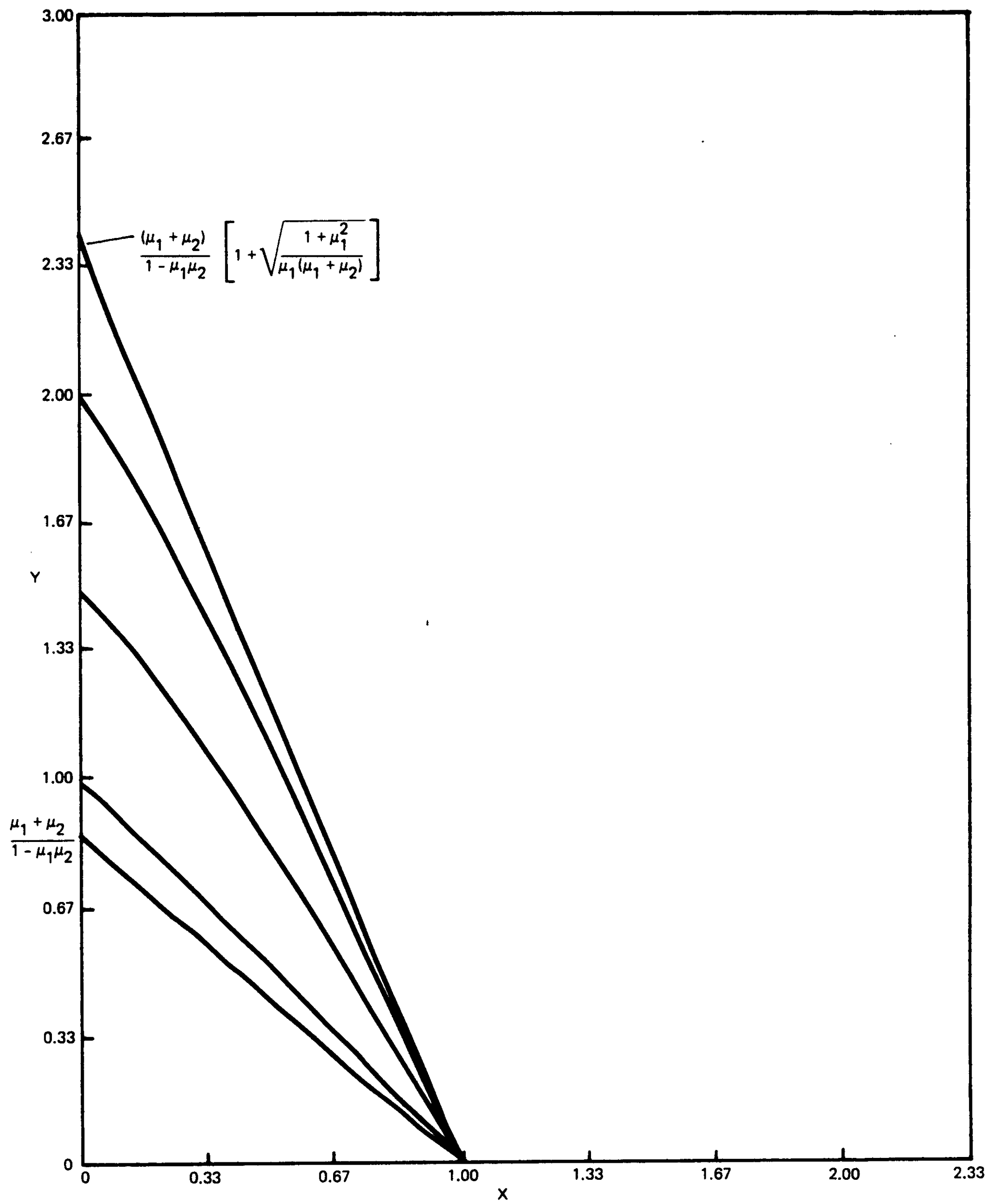

Figure 2.4.3. Minimum energy chamfer shapes for various S, $\mu_1 = 0.5$, $\mu_2 = 0.25$.

2.5 MINIMUM ENERGY CHAMFER EXPERIMENT

2.5.1 Introduction

An experiment was conducted which attempted to support the existence of the minimum energy chamfers developed in Section 2.3. Although it is not possible to verify experimentally that a chamfer is a minimum energy chamfer (since it must be compared to an infinite number of chamfers), some insight can be gained by comparing it to a finite number of chamfers—such as a family of straight line chamfers. In the experiment only three chamfers were used: one optimal slope chamfer and two straight line chamfers. One of the straight line chamfers was flatter than the optimal slope chamfer and the other was steeper than the optimal slope chamfer. According to the theory developed, the flattest chamfer will be nonoptimal primarily because the insertion forces are too large, and the steepest chamfer will be nonoptimal because the insertion forces must act over a very large distance. Also, since minimum vertical work chamfers are the same as minimum frictional work chamfers, either criterion may be implemented experimentally. The vertical work criterion is much simpler because arc lengths and normal forces are more difficult to measure than are vertical displacements and vertical forces. For this reason the experiment was based on the vertical work criterion.

2.5.2 Specifics of the Chamfers Designed

A. Optimal Slope Chamfer

Given μ, L, θ_o an optimal slope chamfer is recommended by Equation 2.3.11. Since the shape is dependent on the friction, the friction coefficient must be predicted accurately beforehand. From previous work using aluminum chamfers made on an N/C (Numerically Controlled) milling machine (200 points/inch and smoothed with emery cloth) and steel tipped pegs, the friction coefficient remained essentially constant at $\mu = 0.15$. This value will be assumed since the chamfers were made out of aluminum as before (however, in some instances the tip of the peg was spring steel) along with L = 5, $\theta_o = 16°$ which are nominal values for the length and offset angle, respectively of a pin to be inserted into a DIP socket.

B. Straight Line Chamfers

The flattest straight line chamfer selected has an aspect ratio between $Y^w(0) = 0.39$, the wedging aspect ratio, and $Y^o(0) = 1.40$, the optimal slope aspect ratio. If the aspect ratio is too close to 1.40

there will be little difference in energy between that chamfer and the optimal one; especially since the friction coefficient is so small. On the other hand, if the aspect ratio is very close to 0.39, very large forces will be present and wedging is even possible since μ can not be known exactly. Buckling and surface galling are also possible if the forces are too large. An aspect ratio of 0.6 was found to satisfy both of these constraints with 22% more energy predicted than optimal.

The steepest straight line chamfer selected has an aspect ratio of 3.75 corresponding to 19% more predicted energy than optimal.

C. Actual Construction

Once the chamfers had been designed, N/C tapes were created to be used as input to a Bridgeport N/C Milling Machine which machined the chamfers. The coordinates on the tapes were not the coordinates of the chamfers (x,y), but instead, the coordinates of the center axis of the cutter $(x - ry'/\sqrt{1 + y'^2},\ y + r/\sqrt{1 + y'^2})$ where r is the cutter radius (1/4"). All three chamfers are shown in Figure 2.5.1 (x_o = 0.600").

2.5.3 Experimental Apparatus and Procedure

A. Experimental Apparatus

The experimental apparatus used consisted of a test bed, force sensor and LVDT, data-acquisition electronics, minicomputer, data-taking software, and hard-copy output units. Much of the apparatus had been used in previous Part Mating experiments as described in Draper Laboratory Report No. R-1218[5].

A Bridgeport Milling Machine served as a test bed supporting the peg and chamfer, as well as the force sensor and LVDT (see Figure 2.5.2). The peg was made out of spring steel and supported by an adjustable fixture (in θ_o) which was held in place by the milling machine directly above the chamfer. A small radius at the end of the peg reduced the effects of surface galling and wedging. This fixture was designed and built by members of the Draper Staff (R. Gustavson and R. Roderick) and had been used in other part mating experiments.

Of primary importance are the sensors which measure insertion force and insertion depth. The vertical force on the chamfer (or support point) was measured using Draper's 6-axis force sensor (Figure 2.5.3) mounted to the test bed directly beneath the chamfer. A preamplifier was used to magnify the sensor's output for further processing. The vertical displacement of the peg's support point was measured

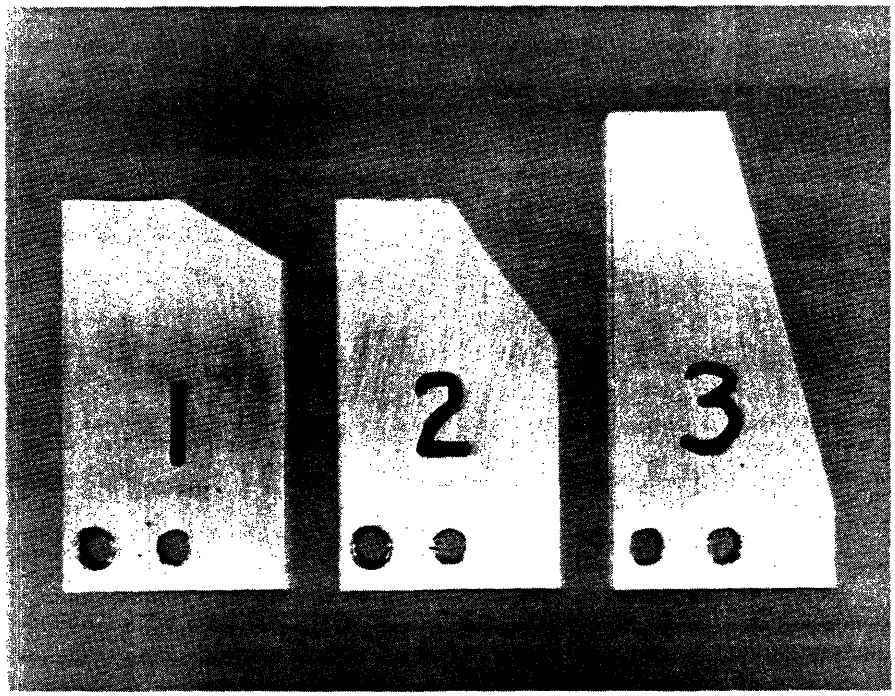

(a) Straight line chamfer (S = 0.60)   (b) Optimal slope chamfer (S = 1.40)   (c) Straight line chamfer (S = 3.75)

Figure 2.5.1. Chamfers used in experiment.

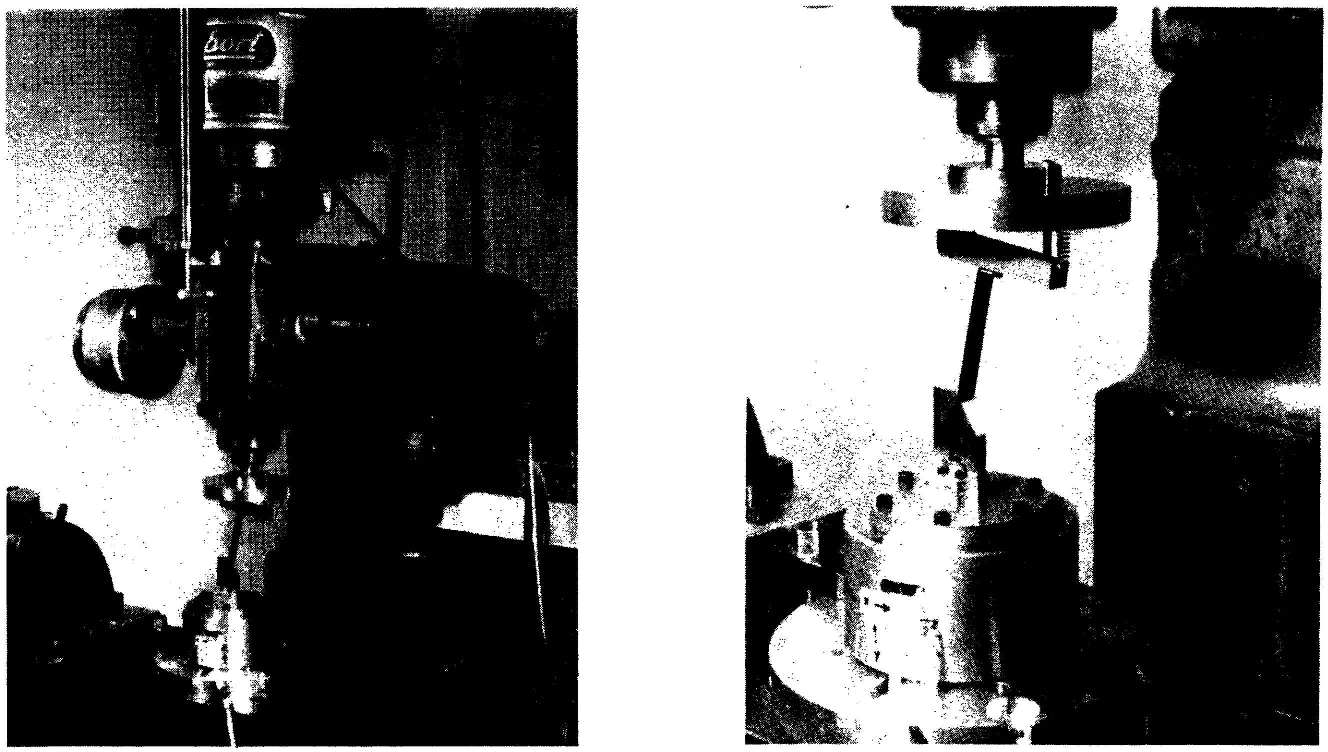

(a) Set-up in Bridgeport Milling Machine

(b) Close-up of peg, chamfer, and force sensor

Figure 2.5.2. Experimental apparatus.

(in mm) using a Schaevitz DC-LVDT (Linear Variable Differential Transformer) with the specifications given in Table 2.5.1. Also, an automatic drive (servo motor) which controlled the vertical displacement permitted efficient data sampling and more accurate data.

Table 2.5.1 Specifications of Schaevitz Engineering DC-LVDT

GENERAL SPECIFICATIONS

Input	24 V dc (nominal), 25ma
Temperature Range	-65°F to +200°F
Null Voltage	0 V dc
Ripple	Less than 1% full scale
Linearity	±0.5% full range
Stability	0.125% full range

TYPE	LINEAR RANGE (INCHES)	SCALE FACTOR (V/INCH)	FREQUENCY RESPONSE (-3db at Hz)	OUTPUT IMPEDANCE (K OHMS)
3000 HR-DC	±3.000	6.5	10	7.0

MIN. LOAD RESISTANCE	WEIGHT (GRAMS) BODY	WEIGHT (GRAMS) CORE
200	270	31

The remaining hardware/software was used to process the data. Signals from the sensors were run through a low-pass filter, multiplexed and digitized by a 12 bit A/D converter before being read by a Nova II minicomputer. In addition, four interactive computer programs written in EXTENDED BASIC were used for (1) sensor biasing, (2) real time data acquisition and storage, (3) printing data on the line printer and (4) plotting data on the plotter.

B. Experimental Procedure

Calibration of Force Sensor

Prior to performing the actual experiment it was necessary to calibrate the force sensor. It was calibrated with weights as described in detail in Draper Laboratory Report No. R-1218[5] but with one important difference. Since only two force components are needed (lateral F_x, vertical F_y) only one leg of the sensor was calibrated (leg #2). The resulting "calibration matrix", W which relates the output voltages of the sensor to the applied loads F_x, F_y was determined experimentally to be:

DRAPER LABORATORY SIX-AXIS FORCE SENSOR
APPROXIMATE CHARACTERISTICS

Weight	6 lb	6 lb
Axial axis force sensitivity	0.026 lb (12 gm)	0.052 lb (24 gm)
Radial axis force sensitivity	0.013 lb (6 gm)	0.026 lb (12 gm)
Radial axis moment sensitivity	0.14 in.-lb	0.28 in.-lb
Maximum axial load	53 lb	106 lb
Buckling load per leg (no springs)	40 lb	320 lb
Diameter	4.5 in.	4.5 in.
Height	2.6 in.	2.6 in.

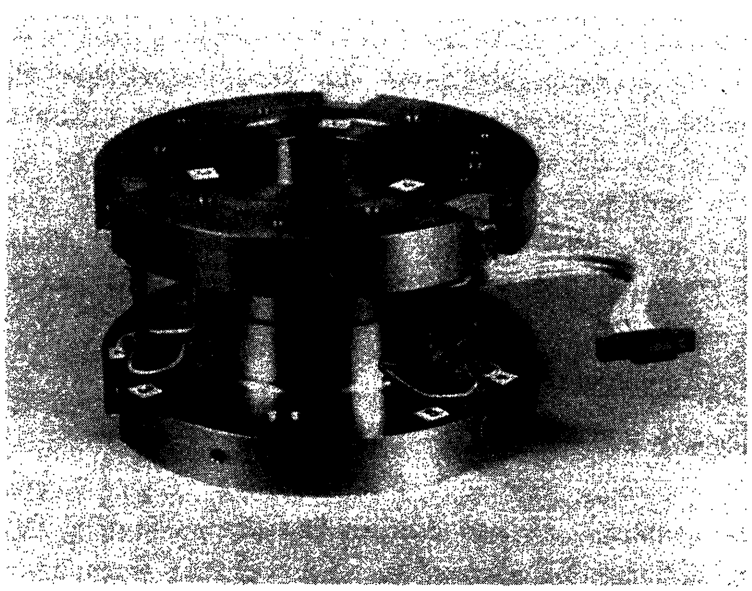

Figure 2.5.3. Draper's 6-axis force sensor.

$$W = \begin{bmatrix} 6.2381 & -0.1080 \\ -3.0468 & 19.3271 \end{bmatrix} \qquad (2.5.1)$$

so that

$$\begin{bmatrix} F_x \\ F_y \end{bmatrix} = W \begin{bmatrix} V_{S3} \\ V_{E3} \end{bmatrix} \qquad (2.5.2)$$

where the forces F_x, F_y are measured in newtons and the voltages V_{S3}, V_{E3} are measured in volts, representing the output of the shear strain gauge and the extensional strain gauge, respectively.

Data Acquisition

Once the force sensor had been calibrated and the apparatus set up as described, experimental data was easily obtained (e.g. see Figure 2.5.4). First the sensor and LVDT were biased, then data taken, printed and plotted. Several data runs were done for each chamfer.

2.5.4 Experimental Results

Many experimental plots, plotting the vertical force, F_y versus depth, y^* for each of the three chamfers were obtained. Unfortunately, not all of the data gathered was "good data". Some of the data demonstrated the sensitivity of the insertion force versus depth plot to localizing effects (e.g. surface galling) yielding many large peaks and valleys. This unpredictable behavior was of course not analyzed in the model since both the peg and the chamfer were treated as rigid objects. Its effect was reduced by adequately preparing the contact surfaces of the peg and chamfer. Only three or four data runs were taken at a time; then the surfaces were sanded with emery cloth before taking more data. The remaining data (~1/2) however was good conclusive data in agreement with the theory predicted. Only data of this quality will be presented here. Typical experimental plots of insertion force versus depth are shown in Figures 2.5.5-2.5.7 for chamfers #1, 2, and 3, respectively. Figure 2.5.8 plots them all on the same axes. There is an obvious trade-off between maximum insertion force and maximum insertion depth.

DATA FROM TESTS ON CHAMFER OPCHE DURING INSERTION #1

TIME	DEPTH	X FORCE	Y FORCE
.06	-.00	.00	-.00
.12	.01	.00	-.00
.18	-.01	.01	.06
.24	-.14	.10	.23
.30	-.47	.33	.40
.36	-.85	.50	.51
.42	-1.30	.70	.97
.48	-1.72	.93	1.12
.54	-2.15	1.12	1.37
.60	-2.60	1.34	1.51
.66	-3.02	1.50	1.61
.72	-3.46	1.66	1.92
.78	-3.94	1.86	2.16
.84	-4.37	2.04	2.23
.90	-4.81	2.22	2.49
.96	-5.30	2.42	2.77
1.02	-5.71	2.56	3.05
1.08	-6.13	2.74	3.24
1.14	-6.55	2.90	3.10
1.20	-7.01	3.03	3.19
1.26	-7.44	3.21	3.48
1.32	-7.90	3.36	3.63
1.38	-8.34	3.51	3.77
1.44	-8.78	3.65	3.92
1.50	-9.22	3.82	4.07
1.56	-9.65	3.96	4.34
1.62	-10.13	4.11	4.55
1.68	-10.57	4.25	4.76
1.74	-11.01	4.40	4.94
1.80	-11.49	4.52	5.13
1.86	-11.90	4.65	5.20
1.92	-12.31	4.77	5.29
1.98	-12.77	4.90	5.45
2.04	-13.21	5.02	5.61
2.10	-13.66	5.14	5.68
2.16	-14.13	5.28	5.80
2.22	-14.56	5.41	5.92
2.28	-15.00	5.51	6.03
2.34	-15.44	5.62	6.20
2.40	-15.87	5.75	6.23
2.46	-16.30	5.85	6.34
2.52	-16.76	5.95	6.44
2.58	-17.19	6.04	6.46
2.64	-17.61	6.15	6.38
2.70	-18.07	6.12	5.67
2.76	-18.34	6.12	3.76
2.82	-18.44	6.13	3.69
2.88	-18.48	6.12	3.54
2.94	-18.53	6.12	3.41
3.00	-18.54	6.14	3.40

Figure 2.5.4. Sample data from experiment - chamfer #2.

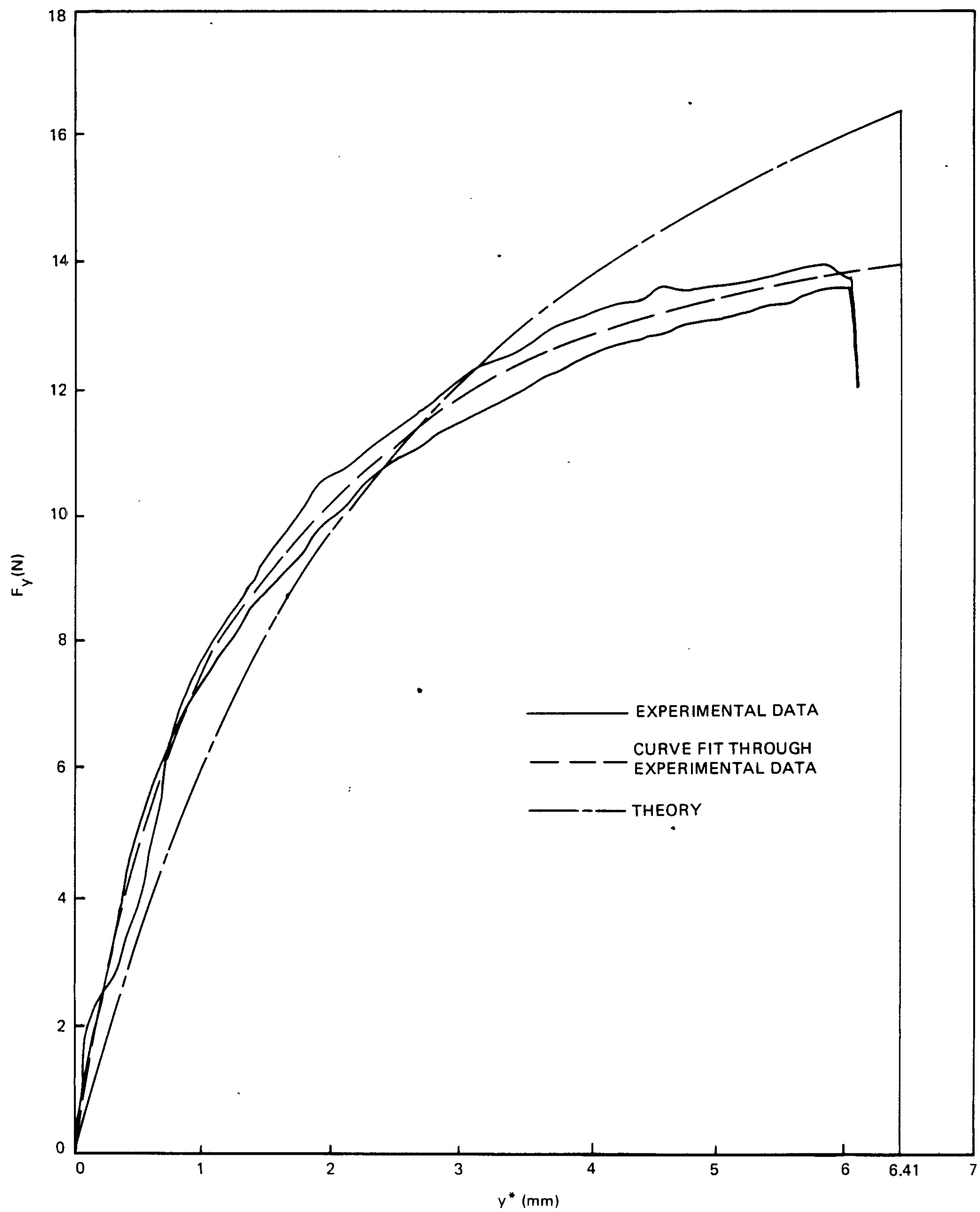

Figure 2.5.5. Insertion force versus depth—chamfer #1.

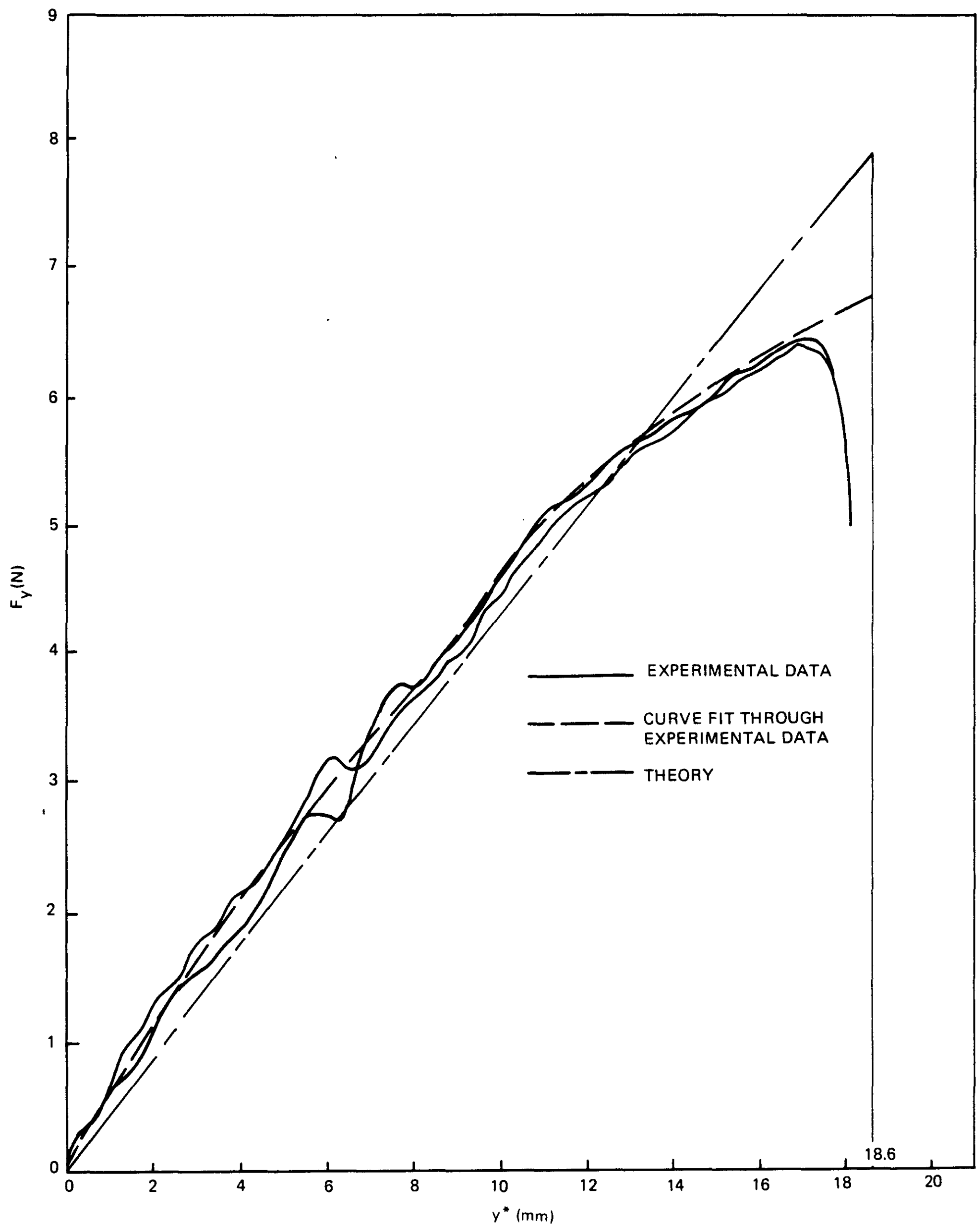

Figure 2.5.6. Insertion force versus depth—chamfer #2.

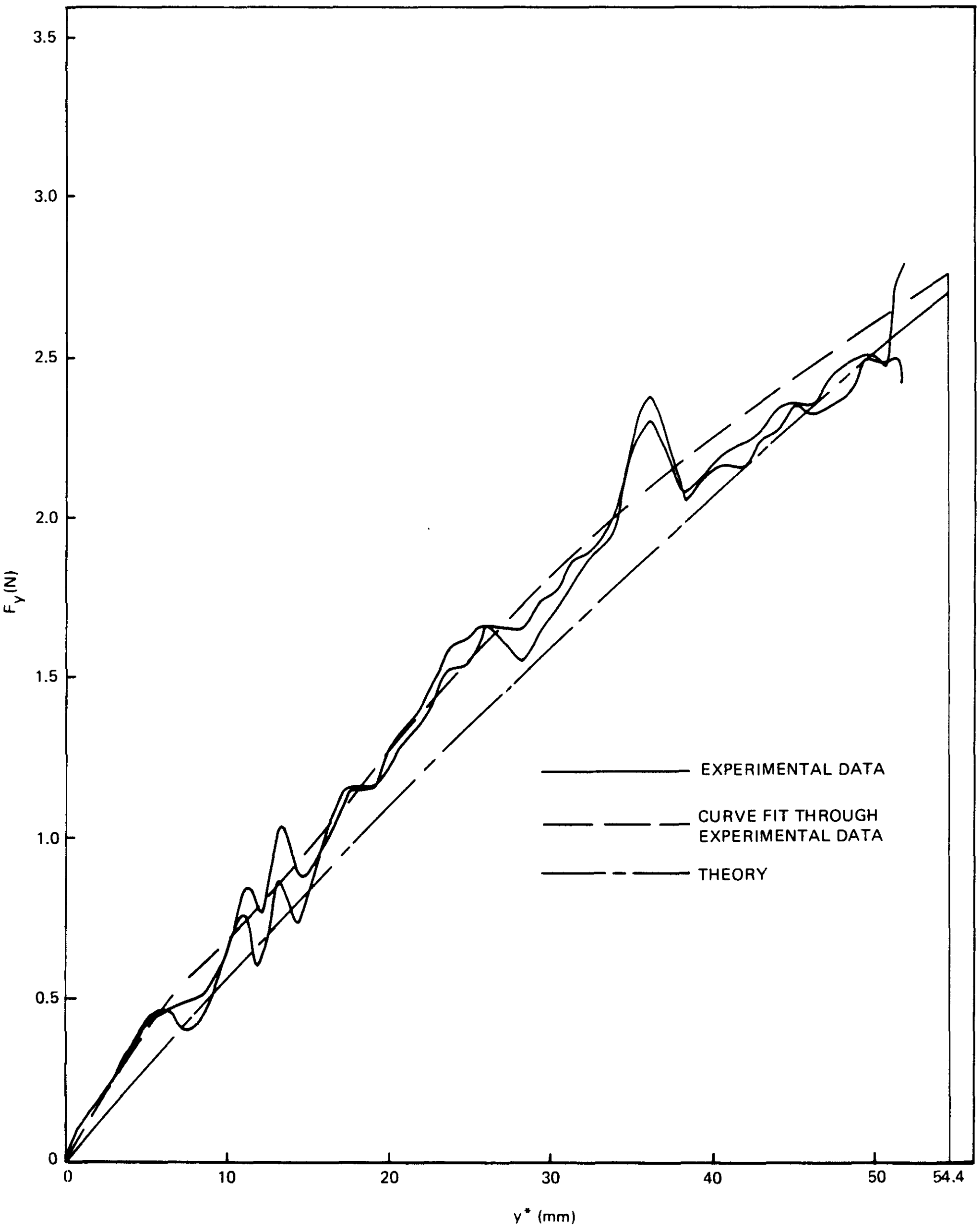

Figure 2.5.7. Insertion force versus depth—chamfer #3.

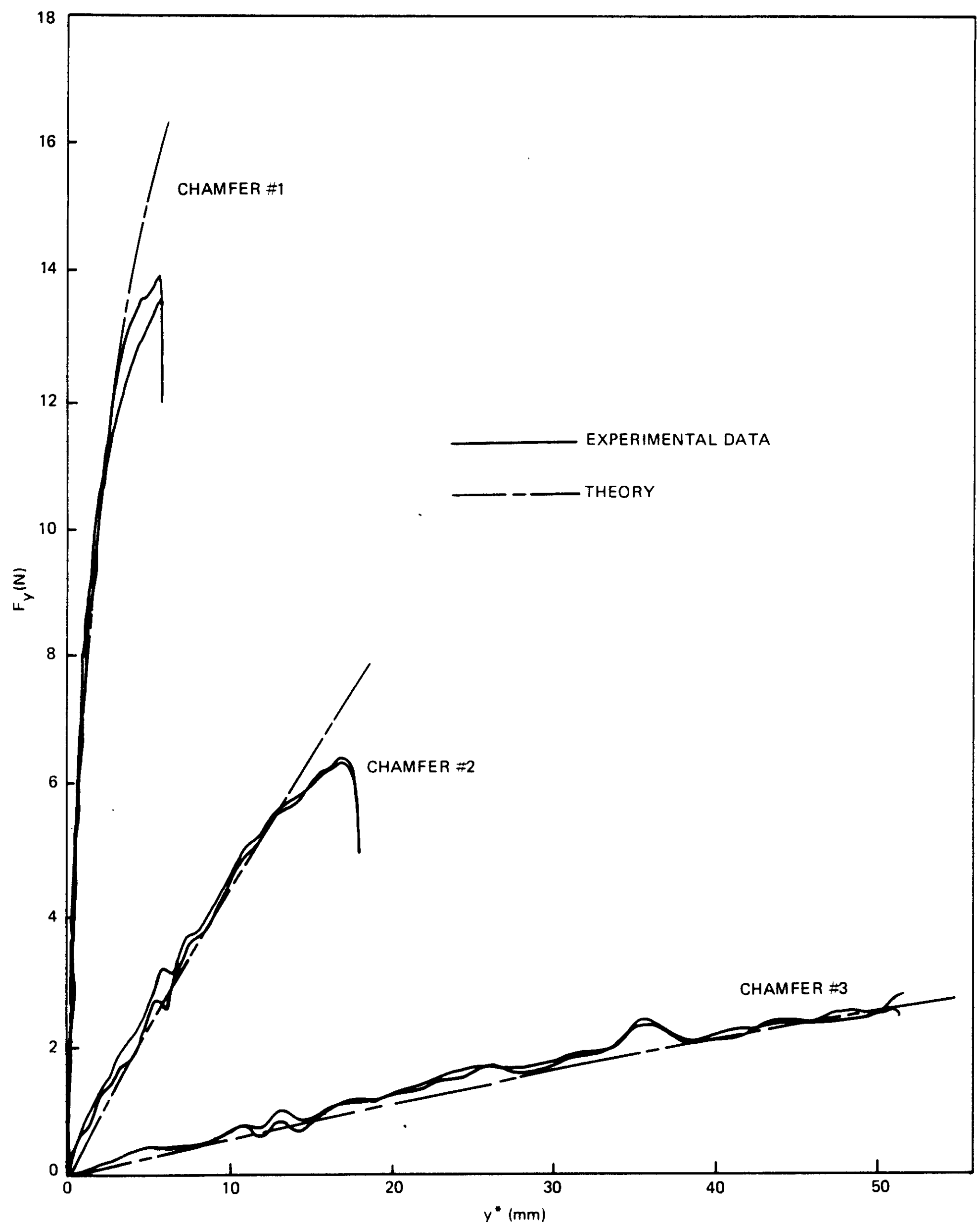

Figure 2.5.8. Insertion force versus depth—all chamfers.

2.5.5 Comparison with Theory

A. Friction Coefficient

As mentioned earlier the friction coefficient had to be estimated beforehand since the optimal slope chamfer's slope depended on it. A value of $\mu = 0.15$ was assumed in the design. The experimental value may be determined indirectly from the vertical force F_y, the lateral force F_x, and the slope of the chamfer $\bar{y}'$ by projecting the contact force into axes tangent and normal to the chamfer at the contact point. This yields the following expression for μ:

$$\mu = \frac{F_x/F_y + \bar{y}'}{\bar{y}'(F_x/F_y) - 1} \tag{2.5.3}$$

By evaluating Equation 2.5.3 at many points during the insertion an average coefficient of friction was established for each of the chamfers (see Table 2.5.2).

Table 2.5.2 Experimentally Determined Friction Coefficients

Chamfer	μ
1	0.135
2	0.221
3	0.169

B. Theoretical Plots of Insertion Force Versus Depth

Theoretical plots of insertion force versus depth were determined for each of the chamfers by using Equations 2.3.7 and 2.3.23 where appropriate substitutions have been made (e.g. for chamfer #1, $\mu = 0.135$, $\bar{y}' = -0.6$ etc.). Several computer programs were written to compute $F_y(y^*)$ (see Appendix A; FSTCH, FCHAM). In Figures 2.5.5-2.5.8 these theoretical plots are plotted along with the experimental plots for direct comparison. Note that the theoretical maximum insertion depth $y_t^*\text{max}$ tends to be greater than the experimentally determined maximum insertion depth $y_e^*\text{max}$. There are two reasons for this. First, as the spring deflects angularly it also bends, so the distance from the tip of the peg to the support point is slightly less than predicted. It then follows immediately from Equation 2.3.23 that $y_e^*\text{max} < y_t^*\text{max}$. Secondly, end effects make it impossible to start exactly at the top of the chamfer and end at the bottom of the chamfer. Also, the spring constant, K_θ, was not determined directly, but instead adjusted to fit the data (matching experimental energies) while not biasing any one particular chamfer (K_θ = 85.1 N/rad).

C. Insertion Force Characteristics

The experimental plots obtained (Figures 2.5.5-2.5.8) exhibit the general features of the corresponding theoretical ones. For example, in Figures 2.5.6 and 2.5.7 the experimental plots (use curve fit) are very linear; so are the theoretical plots. Also, in Figure 2.5.5 the theoretical plot is convex as is the experimental plot.

D. Insertion Energy

The insertion energy may be determined by evaluating the area under the force versus depth plot and comparison of the experimental energies with the theoretical energy predictions is the basis for the entire experiment. To eliminate end effects for each chamfer a smooth curve was run through the data and extrapolated to the theoretical maximum insertion depth. The experimental energy was then given by the area under this curve. Before comparing the experimental energies they must be multiplied by the theoretical ratio of the energy corresponding to μ = 0.15 (E(0.15)) to the energy corresponding to the actual μ (E(μ)) for that chamfer. These ratios were computed using numerical integration. This assures that the comparison will be fair since μ is artificially made the same for each chamfer (μ_o = 0.15). Only μ_o = 0.15 will do since the optimal slope chamfer was designed for μ = 0.15. Table 2.5.3 summarizes the results obtained.

Table 2.5.3 Comparison of Theoretical Energies with Experimental Energies

Chamfer	μ	Theoretical Energy (Nmm)	Experimental Energy (Nmm)	$\frac{E(0.15)}{E(\mu)}$
1	0.135	72.44	68.58	1.069
2	0.221	74.61	73.11	0.849
3	0.169	78.95	84.66	0.948

Chamfer	Theoretical Energy For μ = 0.15 (Nmm)	Experimental Energy for μ = 0.15 (Nmm)	Theoretical % Energy More Than Optimal	Experimental % Energy More Than Optimal
1	77.41	73.31	22.2	18.1
2	63.35	62.07	0	0
3	74.85	80.26	18.2	29.3

2.5.6 Conclusions and Recommendations

A. Conclusions

Good comparison between the experimental results and the results predicted by the theory was achieved. The experimental % energy more than optimal for chamfer #1 was very close to the theoretical value (18.1% versus 22.2%). For chamfer #3 there was more of a difference. However, despite experimental errors, the experimental results corroborate the theoretical predictions; namely that chamfers much flatter or steeper than the optimal slope chamfer give rise to larger insertion energies.

B. Recommendations

Although the optimal slope chamfer is the mathematically optimal solution, it is fairly complex and for many engineering applications a chamfer which is only close to optimal but not optimal may be good enough. Since the difference in insertion energy between a straight line chamfer with an aspect ratio slightly larger than optimal and the optimal chamfer is small when the friction is small (e.g. in experiment only a 29.3% increase from $S = 1.40$ to $S = 3.75$) and because the optimal slope chamfer is somewhat insensitive to L, a simple rule of thumb exists for designing approximately minimum energy chamfers (within a few %). Select appropriate materials for the peg and chamfer so the friction is small and construct a straight line chamfer with an aspect ratio of $S = \tan(\theta_o + \beta) + \sec(\theta_o + \beta)$. The larger L is the better this approximation will be.

SECTION 3

SUMMARY AND DIRECTION OF FURTHER RESEARCH

3.1 SUMMARY

A theoretical model of a compliantly supported rigid peg entering a compliant hole was used to understand the mechanics of an idealized assembly in terms of the assembly phases, the friction, geometry and compliance. This led to the classification of different assembly phases: chamfer crossing, one-point contact, two-point contact, resumption of one-point contact, and line contact. The effect of various insertion parameters on the "insertion force versus depth plot" was then determined and recommendations were made regarding the optimal location of the compliance centers of both the peg and the hole.

The sensitivity of the "insertion force versus depth plot" during chamfer crossing to the slope of the chamfer has led to the area of chamfer design. In this thesis different chamfers were designed subject to minimum energy criteria and in all cases an optimal slope chamfer was derived.

In general, if a chamfer is too flat when compared with the optimal slope chamfer very large forces will be present as well as large insertion energies. On the other hand, if a chamfer is too steep in comparison with the optimal slope chamfer the insertion energy will be large because the contact forces must act over a very large distance. This was verified experimentally.

3.2 DIRECTION OF FURTHER RESEARCH IN PART MATING

Thus far much research in part mating theory has centered on the study of insertion force characteristics (force versus depth) for quasi-static two-dimensional "peg-in-hole" models. Much has been learned but the need to extend the research in different directions can not be forgotten. Two related topics in particular which have been perhaps overlooked are (1) buckling and stability analysis and (2) extension to three-dimensional peg-in-hole models.

Buckling and stability analysis is very useful because it quantifies physical limitations of the parts involved. As a simple example, Equations 1.2.1 and 1.2.2 when properly interpreted may be used to compute the buckling load for the normal force during chamfer crossing: $K_\theta/d(\sin \phi - \mu \cos \phi)$ where the compliance center distance, a, has been optimally chosen.

Although three-dimensional models are inherently very complex, they can be used to better understand the characteristics of an actual assembly which can not be modelled using only two-dimensional models.

Other areas of research which could be investigated or extended are:

(1) Variations and extensions of minimum energy chamfer design:

* finite thickness peg
* both lateral and rotational support
* minimize energy subject to constraints (e.g. fixed amount of material - impossible?)
* design both contact surfaces subject to minimum energy criteria (impossible?)
* given one contact surface design the other contact surface

(2) Model a compliantly supported compliant peg entering a compliant hole

(3) Chamfer design in general:

* constant force chamfers (rotational support)
* buckling and stability
* minimum peak force chamfers (impossible?)

(4) Continuum elasticity models; finite element analysis

(5) Dynamic analysis (point out limitations of quasi-statis analysis)

(6) Design a mechanism which attempts to choose the compliance center distance, a, optimally (i.e. no angular errors) during each assembly phase. The RCC of course locates the compliance center distance, a, optimally (approximately) only during one-point contact.

(7) Multi-pin, multi-socket compliant part mating

(8) Energy propagation model of compliant part mating

APPENDIX A

COMPUTER PROGRAMS: "LINLAT"

"LINROT"

"LINLR"

"LATERAL"

"ROTATE"

"LATROT"

"CHAMFR"

"CHAMF"

"FSTCH"

"FCHAM"

This appendix contains a listing in BASIC of the computer programs described in Sections 1 and 2.

```
0010 REM PROGRAM NAME: LINLAT(LIN SOL FOR LAT COMP HOLE)
0020 CLOSE
0030 DIM A$[8]
0040 INPUT "DATA SET NAME: ",A$
0050 OPEN FILE[1,1],A$
0060 OPEN FILE[6,1],"$LPT"
0070 INPUT "CHAMFER ANGLE PHI(DEG)= ",P1
0080 INPUT "FRICTION COEFFICIENT MU= ",M
0090 INPUT "CLEARANCE RATIO C= ",C
0100 INPUT "INITIAL LATERAL ERROR DELTA/A= ",D2
0110 INPUT "HOLE DIAMETER D/A= ",D
0120 INPUT "STIFFNESS RATIO-KX*A^2/KTHETA= ",K9
0130 INPUT "STIFFNESS RATIO-K1/KX= ",H9
0140 INPUT "STIFFNESS RATIO-K2/KX= ",H0
0150 INPUT "NO. OF CHAMFER CROSSING SOLUTIONS-N1= ",N1
0160 PRINT FILE[6],"DATA SET NAME: ";A$
0170 PRINT FILE[6],USING "CHAMFER ANGLE PHI(DEG) ##.# ",P1
0180 PRINT FILE[6],USING "FRICTION COEFFICIENT MU #.## ",M
0190 PRINT FILE[6],USING "CLEARANCE RATIO C #.##### ",C
0200 PRINT FILE[6],USING "INITIAL LATERAL ERROR DELTA/A #.#### ",D2
0210 PRINT FILE[6],USING "HOLE DIAMETER D/A #.### ",D
0220 PRINT FILE[6],USING "STIFFNESS RATIO-KX*A^2/KTHETA ###.### ",K9
0230 PRINT FILE[6],USING "STIFFNESS RATIO-K1/KX ###.### ",H9
0240 PRINT FILE[6],USING "STIFFNESS RATIO-K2/KX ###.### ",H0
0250 PRINT FILE[6],USING "NO OF CHAMFER CROSSING SOLUTIONS-N1 ### ",N1
0260 LET O8=0
0270 LET P=3.1415926535*P1/180
0280 LET Z0=(D2-C*D/2)*TAN(P)
0290 LET Z9=Z0
0300 REM BEGIN CHAMFER CROSSING****************************************
0310 PRINT FILE[6],"CHAMFER CROSSING"
0320 FOR I=0 TO N1
0330   LET Z=Z0*I/N1
0340   LET X=Z/(TAN(P)*(K9+1+1/H9-(1-C)*D*K9/(2*TAN(P-ATN(M)))))
0350   LET T=Z/TAN(P)-X*(1+1/H9)
0360   LET Z5=Z-(1-C)*D*T/2
0370   LET F5=K9*X/(TAN(P-ATN(M)))
0380   PRINT "CHAMFER CROSSING"
0390   PRINT FILE[6],USING "-#####.#### ",F5,Z5,T*180/3.1415926535,X
0400   PRINT FILE[1,0],USING "-###.####, ",F5,Z5,T*180/3.1415926535,X
0410   LET O8=O8+1
0420 NEXT I
0430 REM BEGIN 1 POINT CONTACT*****************************************
0440 LET L0=0
0450 PRINT FILE[6],"1 POINT CONTACT"
0460 FOR K=0 TO 1000
0470   LET L=L0+K*Z9/N1
0480   LET X=(D2-C*D/2)/(1+1/H9+K9*(1-L)^2-M*(1-C)*D*K9*(1-L)/2)
0490   LET T=K9*X*(1-L-M*(1-C)*D/2)
0500   LET F5=K9*X*M
0510   LET Z5=Z0+L-(1-C)*D*T/2
0520   LET D4=D+X/H9
0530   LET D5=L*T+(1-C)*D
0540   PRINT "1 POINT CONTACT"
0550   PRINT USING "-###.#### ",D5,D4,L
0560   IF D5>D4 THEN LET K=1000
0570   IF D5>D4 THEN GOTO 0620
0580   IF T<0 THEN GOTO 0870
0590   PRINT FILE[6],USING "-#####.#### ",F5,Z5,T*180/3.1415926535,X
0600   PRINT FILE[1,0],USING "-###.####, ",F5,Z5,T*180/3.1415926535,X
```

```
0610    LET O8=O8+1
0620 NEXT K
0630 REM BEGIN 2 POINT CONTACT***************************************
0640 LET L2=L
0650 PRINT FILE[6],"2 POINT CONTACT"
0660 FOR K=0 TO 1000
0670    LET L=L2+K*Z0/N1
0680    LET C1=K9*H9+K9*H0+K9+K9*H9*K9*(1-L)^2+K9*H0*K9+K9*H9*K9*H0*L^2
0690    LET C2=K9*M*(1-C)*D*(K9*H9*(1-L)+K9*H0)/2
0700    LET C3=(K9*H9+K9*H0+K9*H9*K9*H0*L^2)*D2
0710    LET C4=K9*H0-K9*H9+K9*H9*K9*H0*L^2-2*K9*H9*K9*H0*L
0720    LET X=(C3+C4*C*D/2)/(C1-C2)
0730    LET X2=(K9*(L*K9*H9*(1-L-M*(1-C)*D/2)-1)*X-K9*H9*C*D)/(C3/D2)
0740    LET X8=L*K9*H9*(1-L-M*(1-C)*D/2)-1
0750    LET X1=((1+L*K9*H0*(1-M*(1-C)*D/2))*X2+C*D)/X8
0760    LET T=(X1+X2+C*D)/L
0770    LET F5=M*(K9*H9*X1+K9*H0*X2)
0780    LET Z5=Z0+L-(1-C)*D*T/2
0790    IF X2<0 THEN LET L0=L
0800    IF X2<0 THEN LET Z9=Z9/5
0810    IF X2<0 THEN GOTO 0450
0820    PRINT "2 POINT CONTACT"
0830    PRINT FILE[6],USING "-#####.#### ",F5,Z5,T*180/3.1415926535,X
0840    PRINT FILE[1,0],USING "-###.####, ",F5,Z5,T*180/3.1415926535,X
0850    LET O8=O8+1
0860 NEXT K
0870 PRINT FILE[6],USING "NO DATA POINTS ### ",O8
0880 PRINT USING "NO DATA POINTS ### ",O8
0890 CLOSE
0900 END
```

```
0010 REM PROGRAM NAME: LINROT(LIN SOL FOR ROT COMP HOLE)
0020 CLOSE
0030 DIM A$[8]
0040 INPUT "DATA SET NAME: ",A$
0050 OPEN FILE[1,1],A$
0060 OPEN FILE[6,1],"$LPT"
0070 INPUT "CHAMFER ANGLE PHI(DEG)= ",P1
0080 INPUT "FRICTION COEFFICIENT MU= ",M
0090 INPUT "CLEARANCE RATIO C= ",C
0100 INPUT "INITIAL LATERAL ERROR DELTA/A= ",D2
0110 INPUT "HOLE DIAMETER D/A= ",D
0120 INPUT "HOR. COMP. CEN. OF HOLE CH/A= ",G
0130 INPUT "VER. COMP. CEN. OF HOLE CV/A= ",G1
0140 INPUT "STIFFNESS RATIO-KX*A^2/KTHETA= ",K9
0150 INPUT "STIFFNESS RATIO-KTHETA1/KTHETA= ",R9
0160 INPUT "STIFFNESS RATIO-KTHETA2/KTHETA= ",R0
0170 INPUT "NO. OF CHAMFER CROSSING SOLUTIONS-N1= ",N1
0180 PRINT FILE[6],"DATA SET NAME: ";A$
0190 PRINT FILE[6],USING "CHAMFER ANGLE PHI(DEG) ##.# ",P1
0200 PRINT FILE[6],USING "FRICTION COEFFICIENT MU #.## ",M
0210 PRINT FILE[6],USING "CLEARANCE RATIO C #.##### ",C
0220 PRINT FILE[6],USING "INITIAL LATERAL ERROR DELTA/A #.#### ",D2
0230 PRINT FILE[6],USING "HOLE DIAMETER D/A #.### ",D
0240 PRINT FILE[6],USING "HOR COMP CEN OF HOLE CH/A #.## ",G
0250 PRINT FILE[6],USING "VER COMP CEN OF HOLE CV/A #.## ",G1
```

```
0260 PRINT FILE[6],USING "STIFFNESS RATIO-KX*A^2/KTHETA ###.### ",K9
0270 PRINT FILE[6],USING "STIFFNESS RATIO-KTHETA1/KTHETA ###.### ",R9
0280 PRINT FILE[6],USING "STIFFNESS RATIO-KTHETA2/KTHETA ###.### ",R0
0290 PRINT FILE[6],USING "NO OF CHAMFER CROSSING SOLS-N1 ### ",N1
0300 LET O8=0
0310 LET P=3.1415926535*P1/180
0320 LET Z0=(D2-C*D/2)*TAN(P)
0330 LET Z9=Z0
0340 REM BEGIN CHAMFER CROSSING**************************************
0350 PRINT FILE[6],"CHAMFER CROSSING"
0360 FOR I=0 TO N1
0370   LET Z=Z0*I/N1
0380   LET Z1=Z0-Z
0390   LET C1=TAN(P)*(K9+1)-(1-C)*D*K9*TAN(P)/(2*TAN(P-ATN(M)))
0400   LET C2=(G1+Z1)*TAN(P)*(G1+Z1-(G-Z1/(TAN(P)))/(TAN(P-ATN(M))))
0410   LET X=Z/(C1+C2*K9/R9)
0420   LET C3=(G1+Z1)*((G1+Z1)*TAN(P-ATN(M))-(G-Z1/(TAN(P))))
0430   LET C4=TAN(P)*(K9+1)+(1-C)*D*TAN(P)/(2*(TAN(P-ATN(M))-(1-C)*D/2))
0440   LET T=K9*Z/(C4+C3*K9*TAN(P)/(R9*(TAN(P-ATN(M))-(1-C)*D/2)))
0450   LET T1=(Z/(TAN(P))-T-X)/(G1+Z1)
0460   LET Z5=Z-(1-C)*D*T/2+(Z1/(TAN(P))-G)*T1
0470   LET F5=K9*X/(TAN(P-ATN(M)))
0480   PRINT "CHAMFER CROSSING"
0490   PRINT FILE[6],USING "-#####.#### ",F5,Z5,T*180/3.1415926535,X
0500   PRINT FILE[1,0],USING "-###.####, ",F5,Z5,T*180/3.1415926535,X
0510   LET O8=O8+1
0520 NEXT I
0530 REM BEGIN 1 POINT CONTACT*******************************************
0540 LET L0=0
0550 PRINT FILE[6],"1 POINT CONTACT"
0560 FOR K=0 TO 1000
0570   LET L=L0+K*Z9/N1
0580   LET C5=1+K9*(1-L)*(1-L-M*(1-C)*D/2)+G1*K9*(G1-M*G)/R9
0590   LET T=K9*(D2-C*D/2)*(1-L-M*(1-C)*D/2)/C5
0600   LET X=(D2-C*D/2)/C5
0610   LET F5=K9*X*M
0620   LET T1=T*(G1-M*G)/(R9*(1-L-M*(1-C)*D/2))
0630   LET Z5=Z0-(1-C)*D*T/2+L-G*T1
0640   LET D4=D+G1*T1
0650   LET D5=L*T+(1-C)*D
0660   PRINT "1 POINT CONTACT"
0670   PRINT USING "-###.#### ",D5,D4,L
0680   IF D5>D4 THEN LET K=1000
0690   IF D5>D4 THEN GOTO 0740
0700   IF T<0 THEN GOTO 1000
0710   PRINT FILE[6],USING "-#####.#### ",F5,Z5,T*180/3.1415926535,X
0720   PRINT FILE[1,0],USING "-###.####, ",F5,Z5,T*180/3.1415926535,X
0730   LET O8=O8+1
0740 NEXT K
0750 REM BEGIN 2 POINT CONTACT****************************************
0760 LET L2=L
0770 PRINT FILE[6],"2 POINT CONTACT"
0780 FOR K=0 TO 1000
0790   LET L=L2+K*Z0/N1
0800   LET C6=K9*G1*(G1-L)*(G1-M*G)*(G1-M*G-L)+R9*(G1-L)*(G1-M*G-L)
0810   LET C7=R0*G1*(G1-M*G)+R0*K9*G1*(1-M*(1-C)*D/2)*(G1-M*G)
0820   LET C8=R9*R0*L^2-K9*R9*(M*(1-C)*D/2-1+L)*(1-L)*(G1-L)*(G1-M*G-L)
0830   LET C9=-K9*R9*(D2-C*D/2)*(M*(1-C)*D/2-1+L)*(G1-L)*(G1-M*G-L)
0840   LET C0=K9*R0*G1*(1-M*(1-C)*D/2)*(D2+C*D/2)*(G1-M*G)
0850   LET T=(C9+C0+R9*R0*L*C*D)/(C6+C7+C8)
```

```
0860    LET O1=R9*R0*L*(D2*L-C*D*(1-L/2))+(D2+C*D/2)*G1*(G1-M*G)*R0
0870    LET X=(O1+(D2-C*D/2)*(G1-L)*(G1-M*G-L)*R9)/(C6+C7+C8)
0880    LET T1=(D2-C*D/2-(1-L)*T-X)/G1
0890    LET T2=(L*T-G1*T1-C*D)/(G1-L)
0900    LET F5=M*(R9*T1/(G1-M*G)+R0*T2/(G1-M*G-L))
0910    LET Z5=Z0-(1-C)*D*T/2+L-G*T1
0920    IF T2<0 THEN LET L0=L
0930    IF T2<0 THEN LET Z9=Z9/5
0940    IF T2<0 THEN GOTO 0550
0950    PRINT "2 POINT CONTACT"
0960    PRINT FILE[6],USING "-#####.#### ",F5,Z5,T*180/3.1415926535,X
0970    PRINT FILE[1,0],USING "-###.####, ",F5,Z5,T*180/3.1415926535,X
0980    LET O8=O8+1
0990 NEXT K
1000 PRINT FILE[6],USING "NO DATA POINTS ### ",O8
1010 PRINT USING "NO DATA POINTS ### ",O8
1020 CLOSE
1030 END
```

```
0010 REM PROGRAM NAME: LINLR(LIN SOL FOR LAT AND ROT COMP HOLE)
0020 CLOSE
0030 DIM A$[8]
0040 INPUT "DATA SET NAME: ",A$
0050 DIM B[3,3]
0060 DIM E[3,1]
0070 DIM J[3,1]
0080 DIM U[3,3]
0090 OPEN FILE[1,1],A$
0100 OPEN FILE[6,1],"$LPT"
0110 INPUT "CHAMFER ANGLE PHI(DEG)= ",P1
0120 INPUT "FRICTION COEFFICIENT MU= ",M
0130 INPUT "CLEARANCE RATIO C= ",C
0140 INPUT "INITIAL LATERAL ERROR DELTA/A= ",D2
0150 INPUT "HOLE DIAMETER D/A= ",D
0160 INPUT "HOR. COMP. CEN. OF HOLE CH/A= ",G
0170 INPUT "VER. COMP. CEN. OF HOLE CV/A= ",G1
0180 INPUT "STIFFNESS RATIO-KX*A^2/KTHETA= ",K9
0190 INPUT "STIFFNESS RATIO-K1/KX= ",H9
0200 INPUT "STIFFNESS RATIO-K2/KX= ",H0
0210 INPUT "STIFFNESS RATIO-KTHETA1/KTHETA= ",R9
0220 INPUT "STIFFNESS RATIO-KTHETA2/KTHETA= ",R0
0230 INPUT "NO. OF CHAMFER CROSSING SOLUTIONS-N1= ",N1
0240 PRINT FILE[6],"DATA SET NAME: ";A$
0250 PRINT FILE[6],USING "CHAMFER ANGLE PHI(DEG) ##.# ",P1
0260 PRINT FILE[6],USING "FRICTION COEFFICIENT MU #.## ",M
0270 PRINT FILE[6],USING "CLEARANCE RATIO C #.##### ",C
0280 PRINT FILE[6],USING "INITIAL LATERAL ERROR DELTA/A #.#### ",D2
0290 PRINT FILE[6],USING "HOLE DIAMETER D/A #.### ",D
0300 PRINT FILE[6],USING "HOR COMP CEN OF HOLE #.## ",G
0310 PRINT FILE[6],USING "VER COMP CEN OF HOLE #.## ",G1
0320 PRINT FILE[6],USING "STIFFNESS RATIO-KX*A^2/KTHETA ###.### ",K9
0330 PRINT FILE[6],USING "STIFFNESS RATIO-K1/KX ###.### ",H9
0340 PRINT FILE[6],USING "STIFFNESS RATIO-K2/KX ###.### ",H0
0350 PRINT FILE[6],USING "STIFFNESS RATIO-KTHETA1/KTHETA ###.### ",R9
0360 PRINT FILE[6],USING "STIFFNESS RATIO-KTHETA2/KTHETA ###.### ",R0
0370 PRINT FILE[6],USING "NO OF CHAMFER CROSSING SOLS-N1 ### ",N1
```

```
0380 LET O8=0
0390 LET P=3.1415926535*P1/180
0400 LET Z0=(D2-C*D/2)*TAN(P)
0410 LET Z9=Z0
0420 REM BEGIN CHAMFER CROSSING******************************
0430 PRINT FILE[6],"CHAMFER CROSSING"
0440 FOR I=0 TO N1
0450   LET Z=Z0*I/N1
0460   LET Z1=Z0-Z
0470   LET C1=TAN(P)*(K9+1)-(1-C)*D*K9*TAN(P)/(2*TAN(P-ATN(M)))
0480   LET C2=(G1+Z1)*TAN(P)*(G1+Z1-(G-Z1/(TAN(P)))/(TAN(P-ATN(M))))
0490   LET X=Z/(C1+C2*K9/R9+TAN(P)/H9)
0500   LET C3=(G1+Z1)*((G1+Z1)*TAN(P-ATN(M))-(G-Z1/(TAN(P))))
0510   LET C4=TAN(P)*(K9+1)+(1-C)*D*TAN(P)/(2*(TAN(P-ATN(M))-(1-C)*D/2))
0520   LET C5=C4+C3*K9*TAN(P)/(R9*(TAN(P-ATN(M))-(1-C)*D/2))
0530   LET T=K9*Z/(C5+TAN(P)*(1+(1-C)*D/(2*TAN(P-ATN(M))-(1-C)*D))/H9)
0540   LET T1=(Z/(TAN(P))-T-X*(1+1/H9))/(G1+Z1)
0550   LET Z5=Z-(1-C)*D*T/2+(Z1/(TAN(P))-G)*T1
0560   LET F5=K9*X/(TAN(P-ATN(M)))
0570   PRINT "CHAMFER CROSSING"
0580   PRINT FILE[6],USING "-#####.#### ",F5,Z5,T*180/3.1415926535,X
0590   PRINT FILE[1,0],USING "-###.####, ",F5,Z5,T*180/3.1415926535,X
0600   LET O8=O8+1
0610 NEXT I
0620 REM BEGIN 1 POINT CONTACT
0630 LET L0=0
0640 PRINT FILE[6],"1 POINT CONTACT"
0650 FOR K=0 TO 1000
0660   LET L=L0+K*Z9/N1
0670   LET C5=1+K9*(1-L)*(1-L-M*(1-C)*D/2)+G1*K9*(G1-M*G)/R9+1/H9
0680   LET T=K9*(D2-C*D/2)*(1-L-M*(1-C)*D/2)/C5
0690   LET X=(D2-C*D/2)/C5
0700   LET F5=K9*X*M
0710   LET T1=T*(G1-M*G)/(R9*(1-L-M*(1-C)*D/2))
0720   LET Z5=Z0-(1-C)*D*T/2+L-G*T1
0730   LET D4=D+G1*T1+X/H9
0740   LET D5=L*T+(1-C)*D
0750   PRINT "1 POINT CONTACT"
0760   PRINT USING "-###.#### ",D5,D4,L
0770   IF D5>D4 THEN LET K=1000
0780   IF D5>D4 THEN GOTO 0830
0790   IF T<0 THEN GOTO 1190
0800   PRINT FILE[6],USING "-#####.#### ",F5,Z5,T*180/3.1415926535,X
0810   PRINT FILE[1,0],USING "-###.####, ",F5,Z5,T*180/3.1415926535,X
0820   LET O8=O8+1
0830 NEXT K
0840 REM BEGIN 2 POINT CONTACT
0850 LET L2=L
0860 PRINT FILE[6],"2 POINT CONTACT"
0870 FOR K=0 TO 1000
0880   LET L=L2+K*Z0/N1
0890   LET B[1,1]=1
0900   LET B[1,2]=R9*((1-C)*D*M/2-1+L)/(G1-M*G)
0910   LET B[1,3]=R0*(1-(1-C)*D*M/2)/(G1-M*G-L)
0920   LET B[2,1]=1-L
0930   LET B[2,2]=(1/K9+1/(K9*H9))*R9/(G1-M*G)+G1
0940   LET B[2,3]=-R0/(K9*(G1-M*G-L))
0950   LET B[3,1]=L
0960   LET B[3,2]=-(R9/(K9*H9*(G1-M*G))+G1)
0970   LET B[3,3]=-(R0/(K9*H0*(G1-M*G-L))+G1-L)
```

```
0980    LET E[1,1]=0
0990    LET E[2,1]=D2-C*D/2
1000    LET E[3,1]=C*D
1010    MAT U=INV(B)
1020    MAT J=U*E
1030    LET X2=R0*J[3,1]/(K9*H0*(G1-M*G-L))
1040    LET X1=R9*J[2,1]/(K9*H9*(G1-M*G))
1050    LET F5=M*(K9*H9*X1+K9*H0*X2)
1060    LET Z5=Z0-(1-C)*D*J[1,1]/2+L-G*J[2,1]
1070    LET X=D2-C*D/2-X1-G1*J[2,1]-(1-L)*J[1,1]
1080    IF X2<0 THEN LET L0=L
1090    IF X2<0 THEN LET Z9=Z9/5
1100    IF X2<0 THEN GOTO 0640
1110    IF J[3,1]<0 THEN LET L0=L
1120    IF J[3,1]<0 THEN LET Z9=Z9/5
1130    IF J[3,1]<0 THEN GOTO 0640
1140    PRINT "2 POINT CONTACT"
1150    PRINT FILE[6],USING "-#####.#### ",F5,Z5,J[1,1]*180/3.141593,X
1160    PRINT FILE[1,0],USING "-###.####, ",F5,Z5,J[1,1]*180/3.141593,X
1170    LET O8=O8+1
1180 NEXT K
1190 PRINT FILE[6],USING "NO DATA POINTS ### ",O8
1200 PRINT USING "NO DATA POINTS ### ",O8
1210 CLOSE
1220 END


0010 REM PROGRAM NAME: LATERAL(GEN SOL FOR LAT COMP HOLE)
0020 CLOSE
0030 DIM A$[8]
0040 INPUT "DATA SET NAME: ",A$
0050 OPEN FILE[1,1],A$
0060 OPEN FILE[6,1],"$LPT"
0070 INPUT "CHAMFER ANGLE PHI (DEG)= ",P1
0080 INPUT "FRICTION COEFFICIENT MU= ",M
0090 INPUT "CLEARANCE RATIO C= ",C
0100 INPUT "INITIAL LATERAL ERROR DELTA/A= ",D2
0110 INPUT "HOLE DIAMETER D/A= ",D
0120 INPUT "STIFFNESS RATIO-KX*A^2/KTHETA= ",K9
0130 INPUT "STIFFNESS RATIO-K1/KX= ",H9
0140 INPUT "STIFFNESS RATIO-K2/KX= ",H0
0150 INPUT "NO. OF CHAMFER CROSSING SOLUTIONS-N1= ",N1
0160 PRINT FILE[6],"DATA SET NAME: ";A$
0170 PRINT FILE[6],USING "CHAMFER ANGLE PHI (DEG) ##.#",P1
0180 PRINT FILE[6],USING "FRICTION COEFFICIENT MU #.##",M
0190 PRINT FILE[6],USING "CLEARANCE RATIO C #.#####",C
0200 PRINT FILE[6],USING "INITIAL LATERAL ERROR DELTA/A #.#### ",D2
0210 PRINT FILE[6],USING "HOLE DIAMETER D/A #.### ",D
0220 PRINT FILE[6],USING "STIFFNESS RATIO-KX*A^2/KTHETA ###.###",K9
0230 PRINT FILE[6],USING "STIFFNESS RATIO-K1/KX ###.###",H9
0240 PRINT FILE[6],USING "STIFFNESS RATIO-K2/KX ###.###",H0
0250 PRINT FILE[6],USING "NO OF CHAMFER CROSSING SOLS-N1 ### ",N1
0260 LET O8=0
0270 LET P=3.1415926535*P1/180
0280 LET Z0=(D2-C*D/2)*TAN(P)
0290 LET Z9=Z0
0300 REM BEGIN CHAMFER CROSSING****************************************
```

```
0310 PRINT FILE[6],"CHAMFER CROSSING"
0320 FOR I=0 TO N1
0330   LET Z=Z0*I/N1
0340   LET T4=0
0350   LET T9=SQR(1+(D*(1-C))^2/4-(D2-D/2)^2)
0360   LET T3=ATN(D*(1-C)/2)+ATN((D2-D/2)/T9)
0370   FOR J=1 TO 4
0380     LET T5=T3*J/4+T4
0390     LET B=Z/(TAN(P))-SIN(T5)-D*(1-C)*(SIN(T5/2))^2
0400     LET B1=SIN(T5+P)-M*COS(T5+P)-(D*(1-C)/2)*(COS(T5+P)+M*SIN(T5+P))
0410     LET B2=(SIN(P)-M*COS(P))*(1/K9+1/(K9*H9))
0420     LET T=B*B1/B2
0430     PRINT USING "-###.#### ",I,J,T*180/3.141593,T5*180/3.141593
0440     IF ABS(T-T5)<.0000001 THEN GOTO 0510
0450     IF T<T5 THEN GOTO 0470
0460   NEXT J
0470   LET T4=T5-T3/4
0480   LET T3=T3/4
0490   GOTO 0370
0500   REM CHECK CHAMFER CROSSING SOLUTION**********************************
0510   LET B4=SIN(T+P)-M*COS(T+P)
0520   LET B5=(D*(1-C)/2)*(COS(T+P)+M*SIN(T+P))
0530   LET F5=T*(COS(P)+M*SIN(P))/(B4-B5)
0540   LET F2=F5/(COS(P)+M*SIN(P))
0550   LET F3=F2*(SIN(P)-M*COS(P))
0560   LET X=F3/K9
0570   LET X1=F3/(K9*H9)
0580   LET M1=T
0590   LET Z5=Z+1-COS(T)-D*(1-C)*SIN(T)/2
0600   LET E1=F3-F2*(SIN(P)-M*COS(P))
0610   LET E2=F5-F2*(M*SIN(P)+COS(P))
0620   LET E3=M1+F2*(M*COS(T+P)-SIN(T+P)+((1-C)/2)*D*(M*SIN(T+P)+COS(T+P)))
0630   LET E4=F3-K9*X
0640   LET E5=M1-T
0650   LET E6=K9*H9*X1-F2*(SIN(P)-M*COS(P))
0660   LET E7=Z/(TAN(P))-SIN(T)-X1-(1-C)*D*(SIN(T/2))^2-X
0670   LET E8=Z+1-Z5-(1-C)*D*SIN(T)/2-COS(T)
0680   PRINT USING "-#.####",E1,E2,E3,E4
0690   PRINT USING "-#.####",E5,E6,E7,E8
0700   PRINT "CHAMFER CROSSING"
0710   REM BACK TO MAIN PROGRAM*********************************************
0720   PRINT FILE[6],USING "-#####.#### ",F5,Z5,T*180/3.1415926535,X
0730   PRINT FILE[1,0],USING "-###.####, ",F5,Z5,T*180/3.1415926535,X
0740   LET O8=O8+1
0750 NEXT I
0760 REM BEGIN 1 POINT CONTACT*****************************************
0770 LET L0=0
0780 PRINT FILE[6],"1 POINT CONTACT"
0790 FOR K=0 TO 1000
0800   LET L=L0+K*Z9/N1
0810   LET T5=0
0820   LET P2=3.1415926535/2-P
0830   LET T8=P2
0840   FOR N=1 TO 4
0850     LET T7=T8*N/4+T5
0860     LET B6=D2-C*D/2-(1-L)*SIN(T7)-(1-C)*D*(SIN(T7/2))^2
0870     LET B7=1-L-M*(1-C)*D/2
0880     LET B8=(1+1/H9)*(COS(T7)-M*SIN(T7))
0890     LET T=K9*B6*B7/B8
0900     PRINT USING "-###.#### ",K,N,T*180/3.141593,T7*180/3.141593
```

```
0910     IF ABS(T-T7)<.0000001 THEN GOTO 0970
0920     IF T<T7 THEN GOTO 0940
0930   NEXT N
0940   LET T5=T7-T8/4
0950   LET T8=T8/4
0960   GOTO 0840
0970   REM CHECK 1 POINT CONTACT SOLUTION*****************************
0980   LET F2=T/(1-L-(1-C)*D*M/2)
0990   LET F3=F2*(COS(T)-M*SIN(T))
1000   LET X=F3/K9
1010   LET M1=T
1020   LET F5=F2*(SIN(T)+M*COS(T))
1030   LET Z5=Z0+1-COS(T)+L*COS(T)-(1-C)*D*SIN(T)/2
1040   LET X1=F2*(COS(T)-M*SIN(T))/(K9*H9)
1050   LET E1=F3-F2*(COS(T)-M*SIN(T))
1060   LET E2=F5-F2*(SIN(T)+M*COS(T))
1070   LET E3=M1-F2*(1-L-(1-C)*D*M/2)
1080   LET E4=F3-K9*X
1090   LET E5=M1-T
1100   LET E6=K9*H9*X1-F2*(COS(T)-M*SIN(T))
1110   LET E7=D2-X-X1-C*D/2-(1-L)*SIN(T)-(1-C)*D*(SIN(T/2))^2
1120   LET E8=Z0+1-Z5-(1-L)*COS(T)-(1-C)*D*SIN(T)/2
1130   PRINT USING "-#.#### ",E1,E2,E3,E4
1140   PRINT USING "-#.#### ",E5,E6,E7,E8
1150   PRINT "1 POINT CONTACT"
1160   REM BACK TO MAIN PROGRAM****************************************
1170   LET D4=X1+D
1180   LET D5=L*SIN(T)+(1-C)*D*COS(T)
1190   PRINT USING "-###.#### ",D5,D4,L
1200   IF D5>D4 THEN LET K=1000
1210   IF D5>D4 THEN GOTO 1250
1220   PRINT FILE[6],USING "-#####.#### ",F5,Z5,T*180/3.1415926535,X
1230   PRINT FILE[1,0],USING "-###.####, ",F5,Z5,T*180/3.1415926535,X
1240   LET O8=O8+1
1250 NEXT K
1260 REM BEGIN 2 POINT CONTACT****************************************
1270 LET L2=L
1280 PRINT FILE[6],"2 POINT CONTACT"
1290 FOR K=0 TO 1000
1300   LET L=L2+K*Z0/N1
1310   LET T5=0
1320   LET T8=P2
1330   FOR N=1 TO 4
1340     LET T7=T8*N/4+T5
1350     LET B1=D2-C*D/2-(1-L)*SIN(T7)-(1-C)*D*(SIN(T7/2))^2
1360     LET B2=(1-C)*D*COS(T7)-D+L*SIN(T7)
1370     LET B3=(1-L-(1-C)*D*M/2)/(COS(T7)-M*SIN(T7))
1380     LET F=M*(1-C)*D*COS(T7)/2+M*SIN(T7)+(1-C)*D*SIN(T7)/2-COS(T7)
1390     LET T0=(K9*H0*B2+K9*B1)*((K9*H9+K9)*F+K9*H9*B3)/(K9+K9*H9+K9*H0)
1400     LET T=T0-K9*F*B1
1410     PRINT USING "-###.#### ",K,N,T*180/3.141593,T7*180/3.141593
1420     IF ABS(T-T7)<.0000001 THEN GOTO 1480
1430     IF T<T7 THEN GOTO 1450
1440   NEXT N
1450   LET T5=T7-T8/4
1460   LET T8=T8/4
1470   GOTO 1330
1480   REM CHECK 2 POINT CONTACT SOLUTION*****************************
1490   LET X1=(T+K9*F*B1)/(F*(K9+K9*H9)+K9*H9*B3)
1500   LET F1=K9*H9*X1/(COS(T)-M*SIN(T))
```

```
1510    LET X2=D*(1-C)*COS(T)-D+L*SIN(T)-X1
1520    IF X2<0 THEN LET L0=L
1530    IF X2<0 THEN LET Z9=Z9/5
1540    IF X2<0 THEN GOTO 0780
1550    LET F2=K9*H0*X2
1560    LET F3=F1*(COS(T)-M*SIN(T))-F2
1570    LET X=F3/K9
1580    LET Z5=Z0+1-(1-L)*COS(T)-(1-C)*D*SIN(T)/2
1590    LET F5=F1*(SIN(T)+M*COS(T))+M*F2
1600    LET M1=T
1610    LET E1=F3-F1*(COS(T)-M*SIN(T))+F2
1620    LET E2=F5-F1*(SIN(T)+M*COS(T))-M*F2
1630    LET R3=M1+F1*((1-C)*D*M/2-1+L)
1640    LET R4=F2*(M*(1-C)*D*COS(T)/2+M*SIN(T)+(1-C)*D*SIN(T)/2-COS(T))
1650    LET E3=R3-R4
1660    LET E4=M1-T
1670    LET E5=F3-K9*X
1680    LET E6=F2-K9*H0*X2
1690    LET E7=F1*(COS(T)-M*SIN(T))-K9*H9*X1
1700    LET E8=D2-C*D/2-X-X1-(1-L)*SIN(T)-(1-C)*D*(SIN(T/2))^2
1710    LET E9=Z0+1-Z5-(1-L)*COS(T)-(1-C)*D*SIN(T)/2
1720    LET E0=(1-C)*D*COS(T)+L*SIN(T)-X1-X2-D
1730    PRINT USING "-#.#### ",E1,E2,E3,E4,E5
1740    PRINT USING "-#.#### ",E6,E7,E8,E9,E0
1750    PRINT "2 POINT CONTACT"
1760    REM BACK TO MAIN PROGRAM****************************************
1770    PRINT FILE[6],USING "-#####.#### ",F5,Z5,T*180/3.1415926535,X
1780    PRINT FILE[1,0],USING "-###.####, ",F5,Z5,T*180/3.1415926535,X
1790    PRINT USING "-###.#### ",X2,L
1800    LET O8=O8+1
1810 NEXT K
1820 PRINT FILE[6],USING "NO DATA POINTS ### ",O8
1830 PRINT USING "NO DATA POINTS ### ",O8
1840 CLOSE
1850 END
```

```
0010 REM PROGRAM NAME: ROTATE(GEN SOL FOR ROT COMP HOLE)
0020 CLOSE
0030 DIM A$[8]
0040 INPUT "DATA SET NAME: ",A$
0050 DIM J[2,2]
0060 DIM Y[2,1]
0070 DIM U[2,1]
0080 DIM H[2,1]
0090 DIM V[2,1]
0100 DIM W[2,2]
0110 DIM O[6,6]
0120 DIM A[6,1]
0130 DIM Q[6,1]
0140 DIM B[6,1]
0150 DIM R[6,1]
0160 DIM E[6,6]
0170 OPEN FILE[1,1],A$
0180 OPEN FILE[6,1],"$LPT"
0190 INPUT "CHAMFER ANGLE PHI(DEG)= ",P1
0200 INPUT "FRICTION COEFFICIENT MU= ",M
```

```
0210 INPUT "CLEARANCE RATIO C= ",C
0220 INPUT "INITIAL LATERAL ERROR DELTA/A= ",D2
0230 INPUT "HOLE DIAMETER D/A= ",D
0240 INPUT "HOR. COMP. CEN. OF HOLE CH/A= ",G
0250 INPUT "VER. COMP. CEN. OF HOLE CV/A= ",G1
0260 INPUT "STIFFNESS RATIO-KX*A^2/KTHETA= ",K9
0270 INPUT "STIFFNESS RATIO-KTHETA1/KTHETA= ",R9
0280 INPUT "STIFFNESS RATIO-KTHETA2/KTHETA= ",R0
0290 INPUT "SCALAR STEP SIZE S= ",S
0300 INPUT "NO. OF CHAMFER CROSSING SOLUTIONS-N1= ",N1
0310 PRINT FILE[6],"DATA SET NAME: ";A$
0320 PRINT FILE[6],USING "CHAMFER ANGLE PHI(DEG) ##.# ",P1
0330 PRINT FILE[6],USING "FRICTION COEFFICIENT MU #.## ",M
0340 PRINT FILE[6],USING "CLEARANCE RATIO C #.##### ",C
0350 PRINT FILE[6],USING "INITIAL LATERAL ERROR DELTA/A #.#### ",D2
0360 PRINT FILE[6],USING "HOLE DIAMETER D/A #.### ",D
0370 PRINT FILE[6],USING "HOR COMP CEN OF HOLE CH/A #.## ",G
0380 PRINT FILE[6],USING "VER COMP CEN OF HOLE CV/A #.## ",G1
0390 PRINT FILE[6],USING "STIFFNESS RATIO-KX*A^2/KTHETA ###.### ",K9
0400 PRINT FILE[6],USING "STIFFNESS RATIO-KTHETA1/KTHETA ###.### ",R9
0410 PRINT FILE[6],USING "STIFFNESS RATIO-KTHETA2/KTHETA ###.### ",R0
0420 PRINT FILE[6],USING "SCALAR STEP SIZE S #.## ",S
0430 PRINT FILE[6],USING "NO OF CHAMFER CROSSING SOLS-N1 ### ",N1
0440 LET D8=0
0450 LET P=3.1415926535*P1/180
0460 LET Z0=(D2-C*D/2)*TAN(P)
0470 REM BEGIN CHAMFER CROSSING********************************************
0480 PRINT FILE[6],"CHAMFER CROSSING"
0490 FOR I=0 TO N1
0500   LET Z=Z0*I/N1
0510   LET Z1=Z0-Z
0520   LET D1=(G1+Z1)*(SIN(P)-M*COS(P))+(Z1/(TAN(P))-G)*(COS(P)+M*SIN(P))
0530   LET Y[1,1]=0
0540   LET Y[2,1]=0
0550   LET H[1,1]=0
0560   LET H[2,1]=0
0570   LET U[1,1]=S*(Z/(TAN(P))-Y[1,1])
0580   LET U[2,1]=-S*Y[2,1]
0590   LET J[1,1]=COS(H[1,1])+(1-C)*D*SIN(H[1,1])/2
0600   LET C1=(G1+Z1)*COS(H[2,1])+(G-Z1/(TAN(P)))*SIN(H[2,1])
0610   LET C2=(1-M*H[2,1])*SIN(P-H[2,1])
0620   LET C3=-(M+H[2,1])*COS(P-H[2,1])
0630   LET J[1,2]=C1+(C2+C3)*R9/(D1*K9)
0640   LET C1=(1-M*(1-C)*D/2)*COS(P-H[2,1]+H[1,1])
0650   LET C2=(M+(1-C)*D/2)*SIN(P-H[2,1]+H[1,1])
0660   LET J[2,1]=1-R9*H[2,1]*(C1+C2)/D1
0670   LET C1=(M+(1-C)*D/2+H[2,1]*(1-(1-C)*D*M/2))*COS(P-H[2,1]+H[1,1])
0680   LET C2=(1-(1-C)*D*M/2-H[2,1]*(M+(1-C)*D/2))*SIN(P-H[2,1]+H[1,1])
0690   LET J[2,2]=R9*(C1-C2)/D1
0700   MAT W=INV(J)
0710   MAT V=W*U
0720   MAT H=H+V
0730   LET C1=SIN(H[1,1])+(1-C)*D*(SIN(H[1,1]/2))^2+G-Z1/(TAN(P))
0740   LET C2=(Z1/(TAN(P))-G)*COS(H[2,1])+(G1+Z1)*SIN(H[2,1])
0750   LET C3=SIN(P-H[2,1])-M*COS(P-H[2,1])
0760   LET C4=R9*H[2,1]*C3/(K9*D1)
0770   LET Y[1,1]=C1+C2+C4
0780   LET C1=SIN(P-H[2,1]+H[1,1])
0790   LET C2=COS(P-H[2,1]+H[1,1])
0800   LET C3=C1-M*C2-(1-C)*D*(C2+M*C1)/2
```

```
0810    LET Y[2,1]=H[1,1]-R9*H[2,1]*C3/D1
0820    PRINT USING "-###.#### ",I,V[1,1],V[2,1]
0830    LET F=0
0840    IF ABS(V[1,1])<.00000001 THEN LET F=1
0850    IF ABS(V[2,1])<.00000001 THEN LET F=F+1
0860    IF F=2 THEN GOTO 0880
0870    GOTO 0570
0880    REM CHECK CHAMFER CROSSING SOLUTION*************************
0890    REM CHECK 2 REDUCED EQUATIONS IN THETA,THETA1********
0900    LET C1=(1-C)*D*(SIN(H[1,1]/2))^2+SIN(H[1,1])
0910    LET C2=SIN(P-H[2,1])-M*COS(P-H[2,1])
0920    LET C3=(Z1/(TAN(P))-G)*COS(H[2,1])+(G1+Z1)*SIN(H[2,1])
0930    LET C4=G-Z1/(TAN(P))-Z/(TAN(P))
0940    LET E1=C1+C2*R9*H[2,1]/(K9*D1)+C3+C4
0950    LET C1=(M+(1-C)*D/2)*COS(P-H[2,1]+H[1,1])
0960    LET C2=((1-C)*D*M/2-1)*SIN(P-H[2,1]+H[1,1])
0970    LET E2=H[1,1]+R9*H[2,1]*(C1+C2)/D1
0980    PRINT USING "-#.####",E1,E2
0990    REM BACK TO CHECK ALL 8 CHAMFER EQUATIONS*************
1000    LET C1=SIN(P-H[2,1]+H[1,1])
1010    LET C2=COS(P-H[2,1]+H[1,1])
1020    LET F2=H[1,1]/(C1-M*C2-(1-C)*(C2+M*C1)*D/2)
1030    LET F5=F2*(COS(P-H[2,1])+M*SIN(P-H[2,1]))
1040    LET F3=F2*(SIN(P-H[2,1])-M*COS(P-H[2,1]))
1050    LET C1=(G1+Z1)*COS(H[2,1])-G1-Z1+(G-Z1/(TAN(P)))*SIN(H[2,1])
1060    LET Z5=1+Z-(1-C)*D*SIN(H[1,1])/2-COS(H[1,1])-C1
1070    LET M1=H[1,1]
1080    LET X=F3/K9
1090    LET E1=F3-F2*(SIN(P-H[2,1])-M*COS(P-H[2,1]))
1100    LET E2=F5-F2*(COS(P-H[2,1])+M*SIN(P-H[2,1]))
1110    LET C1=SIN(P-H[2,1]+H[1,1])
1120    LET E3=H[1,1]+F2*((1-C)*D*(M*C1+C2)/2+M*C2-C1)
1130    LET E4=F3-K9*X
1140    LET E5=M1-H[1,1]
1150    LET C1=(G1+Z1)*F2*(SIN(P)-M*COS(P))
1160    LET E6=R9*H[2,1]-C1+(G-Z1/(TAN(P)))*F2*(COS(P)+M*SIN(P))
1170    LET C1=(G1+Z1)*COS(H[2,1])-G1-Z1+(G-Z1/(TAN(P)))*SIN(H[2,1])
1180    LET E7=1+Z-Z5-(1-C)*D*SIN(H[1,1])/2-COS(H[1,1])-C1
1190    LET C1=(Z1/(TAN(P))-G)*COS(H[2,1])+(G1+Z1)*SIN(H[2,1])
1200    LET C2=G-Z1/(TAN(P))+SIN(H[1,1])+X-Z/(TAN(P))
1210    LET E8=C1+C2+(1-C)*D*(SIN(H[1,1]/2))^2
1220    PRINT USING "-#.####",E1,E2,E3,E4
1230    PRINT USING "-#.####",E5,E6,E7,E8
1240    PRINT "CHAMFER CROSSING"
1250    REM BACK TO MAIN PROGRAM*************************************
1260    PRINT FILE[6],USING "-#####.#### ",F5,Z5,H[1,1]*180/3.141593,X
1270    PRINT FILE[1,0],USING "-###.####, ",F5,Z5,H[1,1]*180/3.141593,X
1280    LET O8=O8+1
1290 NEXT I
1300 REM BEGIN 1 POINT CONTACT*****************************
1310 LET L0=0
1320 PRINT FILE[6],"1 POINT CONTACT"
1330 LET S1=N1
1340 LET O1=0
1350 FOR K=0 TO 1000
1360    LET L=L0+K*Z0/S1
1370    LET T8=3.1415926535/2
1380    LET T5=0
1390    FOR N=1 TO 10
1400      LET T7=T8*N/10+T5
```

```
1410      LET C1=T7*(COS(T7)-M*SIN(T7))/K9
1420      LET C2=D2-L*D/2-C1/(1-L-M*(1-C)*D/2)
1430      LET C3=C2-(1-L)*SIN(T7)-(1-C)*D*(SIN(T7/2))^2
1440      LET C4=(C3-G)/(SQR(G1^2+G^2))
1450      LET A1=3.1415926535-ATN(G1/G)
1460      IF C4<0 THEN GOTO 1490
1470      LET T1=A1-ATN((SQR(1-C4^2))/C4)
1480      GOTO 1520
1490      LET C1=ATN(-(SQR(1-C4^2))/C4)
1500      LET C2=3.1415926535-C1
1510      LET T1=A1-C2
1520      LET C1=(G1-M*G)*COS(T7-T1)-(G+M*G1)*SIN(T7-T1)
1530      LET C2=1-L-M*(1-C)*D/2
1540      LET T=R9*T1*C2/C1
1550      PRINT USING "-###.####",K,N,T*180/3.141593,T7*180/3.141593
1560      IF ABS(T-T7)<.00000001 THEN GOTO 1620
1570      IF T<T7 THEN GOTO 1590
1580    NEXT N
1590    LET T5=T7-T8/10
1600    LET T8=T8/10
1610    GOTO 1390
1620    REM CHECK 1 POINT CONTACT SOLUTION**************************
1630    LET F2=T/(1-L-(1-C)*D*M/2)
1640    LET F3=F2*(COS(T)-M*SIN(T))
1650    LET X=F3/K9
1660    LET M1=T
1670    LET F5=F2*(SIN(T)+M*COS(T))
1680    LET C1=G1*COS(T1)+G*SIN(T1)-G1
1690    LET C2=(D2-C*D/2)*TAN(P)+1
1700    LET Z5=C2-C1-(1-C)*D*SIN(T)/2-(1-L)*COS(T)
1710    LET E1=F3-F2*(COS(T)-M*SIN(T))
1720    LET E2=F5-F2*(SIN(T)+M*COS(T))
1730    LET E3=M1-F2*(1-L-(1-C)*D*M/2)
1740    LET E4=F3-K9*X
1750    LET E5=M1-T
1760    LET C1=F2*((G1-M*G)*COS(T-T1)-(G+M*G1)*SIN(T-T1))
1770    LET E6=R9*T1-C1
1780    LET C1=-G*COS(T1)+G1*SIN(T1)+G+(1-L)*SIN(T)
1790    LET E7=D2-C*D/2-X-C1-(1-C)*D*(SIN(T/2))^2
1800    LET C1=G1*COS(T1)+G*SIN(T1)-G1
1810    LET C2=(D2-C*D/2)*TAN(P)+1
1820    LET E8=Z5-C2+C1+(1-C)*D*SIN(T)/2+(1-L)*COS(T)
1830    PRINT USING "-#.####",E1,E2,E3,E4
1840    PRINT USING "-#.####",E5,E6,E7,E8
1850    PRINT "1 POINT CONTACT"
1860    REM BACK TO MAIN PROGRAM**********************************
1870    LET D4=D-G*COS(T1)+G1*SIN(T1)+G
1880    LET D5=L*SIN(T)+(1-C)*D*COS(T)
1890    PRINT USING "-###.####",D5,D4,L
1900    IF D5>D4 THEN LET O1=1
1910    IF O1=0 THEN GOTO 2000
1920    IF D5<D4 THEN GOTO 2030
1930    IF ABS(D4-D5)<.00000001 THEN LET K=1000
1940    IF ABS(D4-D5)<.00000001 THEN GOTO 2030
1950    LET L0=L-Z0/S1
1960    LET S1=N1*S1
1970    LET K=1000
1980 NEXT K
1990 GOTO 1350
2000 PRINT FILE[6],USING "-#####.#### ",F5,Z5,T*180/3.1415926535,X
```

```
2010 PRINT FILE[1,0],USING "-###.####, ",F5,Z5,T*180/3.1415926535,X
2020 LET O8=O8+1
2030 NEXT K
2040 REM BEGIN 2 POINT CONTACT****************************************
2050 LET L2=L
2060 PRINT FILE[6],"2 POINT CONTACT"
2070 FOR K=0 TO 1000
2080   LET L=L2+K*Z0/N1
2090   LET A[1,1]=0
2100   LET A[2,1]=0
2110   LET A[3,1]=0
2120   LET A[4,1]=0
2130   LET A[5,1]=0
2140   LET A[6,1]=0
2150   LET B[1,1]=F2
2160   LET B[2,1]=0
2170   LET B[3,1]=X
2180   LET B[4,1]=T
2190   LET B[5,1]=T1
2200   LET B[6,1]=0
2210   LET Q[1,1]=-S*A[1,1]
2220   LET Q[2,1]=-S*A[2,1]
2230   LET Q[3,1]=-S*A[3,1]
2240   LET Q[4,1]=-S*A[4,1]
2250   LET Q[5,1]=S*(D2-C*D/2-C-A[5,1])
2260   LET Q[6,1]=-S*A[6,1]
2270   LET O[1,1]=M*SIN(B[4,1])-COS(B[4,1])
2280   LET O[1,2]=COS(B[6,1])-M*SIN(B[6,1])
2290   LET O[1,3]=K9
2300   LET O[1,4]=B[1,1]*(SIN(B[4,1])+M*COS(B[4,1]))
2310   LET O[1,5]=0
2320   LET O[1,6]=-B[2,1]*(SIN(B[6,1])+M*COS(B[6,1]))
2330   LET O[2,1]=M*(1-C)*D/2-1+L
2340   LET C1=(1-M*(1-C)*D/2)*COS(B[4,1]+B[6,1])
2350   LET O[2,2]=C1-(M+(1-C)*D/2)*SIN(B[4,1]+B[6,1])
2360   LET O[2,3]=0
2370   LET C1=(1-M*(1-C)*D/2)*SIN(B[4,1]+B[6,1])
2380   LET C2=C1+(M+(1-C)*D/2)*COS(B[4,1]+B[6,1])
2390   LET O[2,4]=1-B[2,1]*C2
2400   LET O[2,5]=0
2410   LET O[2,6]=O[2,4]-1
2420   LET C1=(G+M*G1)*SIN(B[4,1]-B[5,1])
2430   LET O[3,1]=C1+(M*G-G1)*COS(B[4,1]-B[5,1])
2440   LET O[3,2]=0
2450   LET O[3,3]=0
2460   LET C1=(G+M*G1)*COS(B[4,1]-B[5,1])
2470   LET C2=C1+(G1-M*G)*SIN(B[4,1]-B[5,1])
2480   LET O[3,4]=B[1,1]*C2
2490   LET O[3,5]=-O[3,4]+R9
2500   LET O[3,6]=0
2510   LET O[4,1]=0
2520   LET C1=G*(SIN(B[5,1])-SIN(B[6,1]))
2530   LET C2=G1*COS(B[5,1])-L*COS(B[4,1])
2540   LET O[4,2]=-(C1+C2+(1-C)*D*SIN(B[4,1])-M*G*COS(B[6,1]))
2550   LET O[4,3]=0
2560   LET C1=L*SIN(B[4,1])+(1-C)*D*COS(B[4,1])
2570   LET O[4,4]=-B[2,1]*C1
2580   LET C1=G1*SIN(B[5,1])-G*COS(B[5,1])
2590   LET O[4,5]=B[2,1]*C1
2600   LET C1=-R0*SIN(B[6,1])
```

```
2610   LET C2=R0*COS(B[6,1])+C1*B[6,1]
2620   LET C3=COS(B[6,1])-M*SIN(B[6,1])
2630   LET O[4,6]=C2+B[2,1]*G*C3
2640   LET O[5,1]=0
2650   LET O[5,2]=0
2660   LET O[5,3]=1
2670   LET O[5,4]=(1-L)*COS(B[4,1])+(1-C)*D*SIN(B[4,1])/2
2680   LET O[5,5]=SQR(G^2+G1^2)*SIN(A1-B[5,1])
2690   LET O[5,6]=0
2700   LET O[6,1]=0
2710   LET O[6,2]=0
2720   LET O[6,3]=0
2730   LET C1=L*COS(B[4,1]+B[6,1])
2740   LET O[6,4]=C1-(1-C)*D*SIN(B[4,1]+B[6,1])
2750   LET O[6,5]=-SQR(G1^2+G^2)*SIN(A1-B[5,1]-B[6,1])
2760   LET C1=L*COS(B[4,1]+B[6,1])
2770   LET C2=-(1-C)*D*SIN(B[4,1]+B[6,1])
2780   LET C3=(D+2*G)*SIN(B[6,1])
2790   LET O[6,6]=C1+C2+C3-SQR(G1^2+G^2)*SIN(A1-B[5,1]-B[6,1])
2800   MAT E=INV(O)
2810   MAT R=E*Q
2820   MAT B=B+R
2830   LET C1=COS(B[6,1])-M*SIN(B[6,1])
2840   LET C2=COS(B[4,1])-M*SIN(B[4,1])
2850   LET C3=B[2,1]*C1-B[1,1]*C2
2860   LET A[1,1]=K9*B[3,1]+C3
2870   LET C1=(1-M*(1-C)*D/2)*COS(B[4,1]+B[6,1])
2880   LET C2=-(M+(1-C)*D/2)*SIN(B[4,1]+B[6,1])
2890   LET C3=-B[1,1]*(1-L-M*(1-C)*D/2)+B[2,1]*(C1+C2)
2900   LET A[2,1]=B[4,1]+C3
2910   LET C1=(G+M*G1)*SIN(B[4,1]-B[5,1])
2920   LET C2=(M*G-G1)*COS(B[4,1]-B[5,1])
2930   LET A[3,1]=K9*B[5,1]+B[1,1]*(C1+C2)
2940   LET C1=G*(SIN(B[5,1])-SIN(B[6,1]))
2950   LET C2=G1*COS(B[5,1])-L*COS(B[4,1])
2960   LET C3=(1-C)*D*SIN(B[4,1])-M*G*COS(B[6,1])
2970   LET C4=R0*B[6,1]*COS(B[6,1])
2980   LET A[4,1]=C4-B[2,1]*(C1+C2+C3)
2990   LET C1=B[3,1]+SQR(G1^2+G^2)*COS(A1-B[5,1])
3000   LET C2=(1-C)*D*(SIN(B[4,1]/2))^2
3010   LET A[5,1]=C1+C2+(1-L)*SIN(B[4,1])
3020   LET C2=-SQR(G1^2+G^2)*(COS(A1-B[5,1])-COS(A1))*COS(B[6,1])
3030   LET C3=-G*(1-COS(B[6,1]))*COS(B[6,1])
3040   LET C4=G*(SIN(B[5,1])-SIN(B[6,1]))
3050   LET C5=G1*COS(B[5,1])-L*COS(B[4,1])
3060   LET C6=(1-C)*D*SIN(B[4,1])
3070   LET C7=L*SIN(B[4,1])+(1-C)*D*COS(B[4,1])
3080   LET C8=C7*COS(B[6,1])+C2+C3
3090   LET A[6,1]=C8-(C4+C5+C6)*SIN(B[6,1])-D*COS(B[6,1])
3100   PRINT USING "-##.####",K,R[1,1],R[2,1],R[3,1],R[4,1],R[5,1],R[6,1]
3110   LET F=0
3120   FOR I1=1 TO 6
3130     IF ABS(R[I1,1])<.00000001 THEN LET F=F+1
3140   NEXT I1
3150   IF F=6 THEN GOTO 3170
3160   GOTO 2210
3170   LET C1=SIN(B[4,1])+M*COS(B[4,1])
3180   LET C2=SIN(B[6,1])+M*COS(B[6,1])
3190   LET F5=B[1,1]*C1+B[2,1]*C2
3200   LET C1=1+(D2-C*D/2)*TAN(P)-(1-C)*D*SIN(B[4,1])/2
```

```
3210   LET C2=C1-(1-L)*COS(B[4,1])
3220   LET Z5=C2-SQR(G1^2+G^2)*(SIN(A1-B[5,1])-SIN(A1))
3230   IF B[6,1]<0 THEN LET L0=L
3240   IF B[6,1]<0 THEN LET Z0=Z0/5
3250   IF B[6,1]<0 THEN GOTO 1320
3260   PRINT "2 POINT CONTACT"
3270   PRINT FILE[6],USING "-#####.#### ",F5,Z5,B[4,1]*180/3.141593,B[3,1]
3280   PRINT FILE[1,0],USING "-###.####, ",F5,Z5,B[4,1]*180/3.141593,B[3,1
3290   PRINT USING "-###.#### ",B[6,1],L
3300   LET O8=O8+1
3310 NEXT K
3320 PRINT FILE[6],USING "NO DATA POINTS ### ",O8
3330 PRINT USING "NO DATA POINTS ### ",O8
3340 CLOSE
3350 END
```

```
0010 REM PROGRAM NAME: LATROT(GEN SOL FOR LAT AND ROT COMP HOLE)
0020 CLOSE
0030 DIM A$[8]
0040 INPUT "DATA SET NAME: ",A$
0050 DIM J[2,2]
0060 DIM Y[2,1]
0070 DIM U[2,1]
0080 DIM H[2,1]
0090 DIM V[2,1]
0100 DIM W[2,2]
0110 DIM O[6,6]
0120 DIM A[6,1]
0130 DIM Q[6,1]
0140 DIM B[6,1]
0150 DIM R[6,1]
0160 DIM E[6,6]
0170 OPEN FILE[1,1],A$
0180 OPEN FILE[6,1],"$LPT"
0190 INPUT "CHAMFER ANGLE PHI(DEG)= ",P1
0200 INPUT "FRICTION COEFFICIENT MU= ",M
0210 INPUT "CLEARANCE RATIO C= ",C
0220 INPUT "INITIAL LATERAL ERROR DELTA/A= ",D2
0230 INPUT "HOLE DIAMETER D/A= ",D
0240 INPUT "HOR. COMP. CEN. OF HOLE CH/A= ",G
0250 INPUT "VER. COMP. CEN. OF HOLE CV/A= ",G1
0260 INPUT "STIFFNESS RATIO-KX*A^2/KTHETA= ",K9
0270 INPUT "STIFFNESS RATIO-K1/KX= ",H9
0280 INPUT "STIFFNESS RATIO-K2/KX= ",H0
0290 INPUT "STIFFNESS RATIO-KTHETA1/KTHETA= ",R9
0300 INPUT "STIFFNESS RATIO-KTHETA2/KTHETA= ",R0
0310 INPUT "SCALAR STEP SIZE S= ",S
0320 INPUT "NO. OF CHAMFER CROSSING SOLUTIONS-N1= ",N1
0330 PRINT FILE[6],"DATA SET NAME: ";A$
0340 PRINT FILE[6],USING "CHAMFER ANGLE PHI(DEG) ##.# ",P1
0350 PRINT FILE[6],USING "FRICTION COEFFICIENT MU #.## ",M
0360 PRINT FILE[6],USING "CLEARANCE RATIO C #.##### ",C
0370 PRINT FILE[6],USING "INITIAL LATERAL ERROR DELTA/A #.#### ",D2
0380 PRINT FILE[6],USING "HOLE DIAMETER D/A #.### ",D
0390 PRINT FILE[6],USING "HOR COMP CEN OF HOLE CH/A #.## ",G
0400 PRINT FILE[6],USING "VER COMP CEN OF HOLE CV/A #.## ",G1
```

```
0410 PRINT FILE[6],USING "STIFFNESS RATIO-KX*A^2/KTHETA ###.### ",K9
0420 PRINT FILE[6],USING "STIFFNESS RATIO-K1/KX ###.### ",H9
0430 PRINT FILE[6],USING "STIFFNESS RATIO-K2/KX ###.### ",H0
0440 PRINT FILE[6],USING "STIFFNESS RATIO-KTHETA1/KTHETA ###.### ",R9
0450 PRINT FILE[6],USING "STIFFNESS RATIO-KTHETA2/KTHETA ###.### ",R0
0460 PRINT FILE[6],USING "SCALAR STEP SIZE S #.## ",S
0470 PRINT FILE[6],USING "NO OF CHAMFER CROSSING SOLS-N1 ### ",N1
0480 LET O8=0
0490 LET P=3.1415926535*P1/180
0500 LET Z0=(D2-C*D/2)*TAN(P)
0510 REM BEGIN CHAMFER CROSSING****************************************
0520 PRINT FILE[6],"CHAMFER CROSSING"
0530 FOR I=0 TO N1
0540   LET Z=Z0*I/N1
0550   LET Z1=Z0-Z
0560   LET D1=(G1+Z1)*(SIN(P)-M*COS(P))+(Z1/(TAN(P))-G)*(COS(P)+M*SIN(P))
0570   LET Y[1,1]=0
0580   LET Y[2,1]=0
0590   LET H[1,1]=0
0600   LET H[2,1]=0
0610   LET U[1,1]=S*(Z/(TAN(P))-Y[1,1])
0620   LET U[2,1]=-S*Y[2,1]
0630   LET J[1,1]=COS(H[1,1])+(1-C)*D*SIN(H[1,1])/2
0640   LET C1=(G1+Z1)*COS(H[2,1])+(G-Z1/(TAN(P)))*SIN(H[2,1])
0650   LET C2=(1-M*H[2,1])*SIN(P-H[2,1])
0660   LET C3=-(M+H[2,1])*COS(P-H[2,1])
0670   LET J[1,2]=C1+(C2+C3)*R9*(1/K9+1/(K9*H9))/D1
0680   LET C1=(1-M*(1-C)*D/2)*COS(P-H[2,1]+H[1,1])
0690   LET C2=(M+(1-C)*D/2)*SIN(P-H[2,1]+H[1,1])
0700   LET J[2,1]=1-R9*H[2,1]*(C1+C2)/D1
0710   LET C1=(M+(1-C)*D/2+H[2,1]*(1-(1-C)*D*M/2))*COS(P-H[2,1]+H[1,1])
0720   LET C2=(1-(1-C)*D*M/2-H[2,1]*(M+(1-C)*D/2))*SIN(P-H[2,1]+H[1,1])
0730   LET J[2,2]=R9*(C1-C2)/D1
0740   MAT W=INV(J)
0750   MAT V=W*U
0760   MAT H=H+V
0770   LET C1=SIN(H[1,1])+(1-C)*D*(SIN(H[1,1]/2))^2+G-Z1/(TAN(P))
0780   LET C2=(Z1/(TAN(P))-G)*COS(H[2,1])+(G1+Z1)*SIN(H[2,1])
0790   LET C3=SIN(P-H[2,1])-M*COS(P-H[2,1])
0800   LET C4=R9*H[2,1]*C3*(1/K9+1/(K9*H9))/D1
0810   LET Y[1,1]=C1+C2+C4
0820   LET C1=SIN(P-H[2,1]+H[1,1])
0830   LET C2=COS(P-H[2,1]+H[1,1])
0840   LET C3=C1-M*C2-(1-C)*D*(C2+M*C1)/2
0850   LET Y[2,1]=H[1,1]-R9*H[2,1]*C3/D1
0860   PRINT USING "-###.#### ",I,V[1,1],V[2,1]
0870   LET F=0
0880   IF ABS(V[1,1])<.00000001 THEN LET F=1
0890   IF ABS(V[2,1])<.00000001 THEN LET F=F+1
0900   IF F=2 THEN GOTO 0920
0910   GOTO 0610
0920   REM CHECK CHAMFER CROSSING SOLUTION***************
0930   REM CHECK 2 REDUCED EQUATIONS IN THETA,THETA1*****************
0940   LET C1=(1-C)*D*(SIN(H[1,1]/2))^2+SIN(H[1,1])
0950   LET C2=SIN(P-H[2,1])-M*COS(P-H[2,1])
0960   LET C3=(Z1/(TAN(P))-G)*COS(H[2,1])+(G1+Z1)*SIN(H[2,1])
0970   LET C4=G-Z1/(TAN(P))-Z/(TAN(P))
0980   LET E1=C1+C2*R9*H[2,1]*(1/K9+1/(K9*H9))/D1+C3+C4
0990   LET C1=(M+(1-C)*D/2)*COS(P-H[2,1]+H[1,1])
1000   LET C2=((1-C)*D*M/2-1)*SIN(P-H[2,1]+H[1,1])
```

```
1010    LET E2=H[1,1]+R9*H[2,1]*(C1+C2)/D1
1020    PRINT USING "-#.####",E1,E2
1030    REM BACK TO CHECK ALL 9 CHAMFER EQUATIONS**********************
1040    LET C1=SIN(P-H[2,1]+H[1,1])
1050    LET C2=COS(P-H[2,1]+H[1,1])
1060    LET F2=H[1,1]/(C1-M*C2-(1-C)*(C2+M*C1)*D/2)
1070    LET F5=F2*(COS(P-H[2,1])+M*SIN(P-H[2,1]))
1080    LET F3=F2*(SIN(P-H[2,1])-M*COS(P-H[2,1]))
1090    LET C1=(G1+Z1)*COS(H[2,1])-G1-Z1+(G-Z1/(TAN(P)))*SIN(H[2,1])
1100    LET Z5=1+Z-(1-C)*D*SIN(H[1,1])/2-COS(H[1,1])-C1
1110    LET M1=H[1,1]
1120    LET X=F3/K9
1130    LET X1=X/H9
1140    LET E1=F3-F2*(SIN(P-H[2,1])-M*COS(P-H[2,1]))
1150    LET E2=F5-F2*(COS(P-H[2,1])+M*SIN(P-H[2,1]))
1160    LET C1=SIN(P-H[2,1]+H[1,1])
1170    LET E3=H[1,1]+F2*((1-C)*D*(M*C1+C2)/2+M*C2-C1)
1180    LET E4=F3-K9*X
1190    LET E5=M1-H[1,1]
1200    LET E6=X1-X/H9
1210    LET C1=(G1+Z1)*F2*(SIN(P)-M*COS(P))
1220    LET E7=R9*H[2,1]-C1+(G-Z1/(TAN(P)))*F2*(COS(P)+M*SIN(P))
1230    LET C1=(Z1/(TAN(P))-G)*COS(H[2,1])+(G1+Z1)*SIN(H[2,1])
1240    LET C2=G-Z1/(TAN(P))+X1+X+SIN(H[1,1])-Z/(TAN(P))
1250    LET E8=C1+C2+(1-C)*D*(SIN(H[1,1]/2))^2
1260    LET C1=(G1+Z1)*COS(H[2,1])-G1-Z1+(G-Z1/(TAN(P)))*SIN(H[2,1])
1270    LET E9=1+Z-Z5-(1-C)*D*SIN(H[1,1])/2-COS(H[1,1])-C1
1280    PRINT USING "-#.####",E1,E2,E3,E4
1290    PRINT USING "-#.####",E5,E6,E7,E8,E9
1300    PRINT "CHAMFER CROSSING"
1310    REM BACK TO MAIN PROGRAM***********************************
1320    PRINT FILE[6],USING "-#####.#### ",F5,Z5,H[1,1]*180/3.141593,X
1330    PRINT FILE[1,0],USING "-###.####, ",F5,Z5,H[1,1]*180/3.141593,X
1340    LET O8=O8+1
1350 NEXT I
1360 REM BEGIN 1 POINT CONTACT****************************************
1370 LET L0=0
1380 PRINT FILE[6],"1 POINT CONTACT"
1390 LET S1=N1
1400 LET O1=0
1410 FOR K=0 TO 1000
1420    LET L=L0+K*Z0/S1
1430    LET T8=3.1415926535/2
1440    LET T5=0
1450    FOR N=1 TO 10
1460      LET T7=T8*N/10+T5
1470      LET C1=T7*(COS(T7)-M*SIN(T7))*(1/K9+1/(K9*H9))
1480      LET C2=D2-L*D/2-C1/(1-L-M*(1-C)*D/2)
1490      LET C3=C2-(1-L)*SIN(T7)-(1-C)*D*(SIN(T7/2))^2
1500      LET C4=(C3-G)/(SQR(G1^2+G^2))
1510      LET A1=3.1415926535-ATN(G1/G)
1520      IF C4<0 THEN GOTO 1550
1530      LET T1=A1-ATN((SQR(1-C4^2))/C4)
1540      GOTO 1580
1550      LET C1=ATN(-(SQR(1-C4^2))/C4)
1560      LET C2=3.1415926535-C1
1570      LET T1=A1-C2
1580      LET C1=(G1-M*G)*COS(T7-T1)-(G+M*G1)*SIN(T7-T1)
1590      LET C2=1-L-M*(1-C)*D/2
1600      LET T=R9*T1*C2/C1
```

```
1610      PRINT USING "-###.####",K,N,T*180/3.141593,T7*180/3.141593
1620      IF ABS(T-T7)<.00000001 THEN GOTO 1680
1630      IF T<T7 THEN GOTO 1650
1640    NEXT N
1650    LET T5=T7-T8/10
1660    LET T8=T8/10
1670    GOTO 1450
1680    REM CHECK 1 POINT CONTACT SOLUTION*****************************
1690    LET F2=T/(1-L-(1-C)*D*M/2)
1700    LET F3=F2*(COS(T)-M*SIN(T))
1710    LET X=F3/K9
1720    LET M1=T
1730    LET F5=F2*(SIN(T)+M*COS(T))
1740    LET X1=X/H9
1750    LET C1=G1*COS(T1)+G*SIN(T1)-G1
1760    LET C2=(D2-C*D/2)*TAN(P)+1
1770    LET Z5=C2-C1-(1-C)*D*SIN(T)/2-(1-L)*COS(T)
1780    LET E1=F3-F2*(COS(T)-M*SIN(T))
1790    LET E2=F5-F2*(SIN(T)+M*COS(T))
1800    LET E3=M1-F2*(1-L-(1-C)*D*M/2)
1810    LET E4=F3-K9*X
1820    LET E5=M1-T
1830    LET E6=H9*X1-X
1840    LET C1=F2*((G1-M*G)*COS(T-T1)-(G+M*G1)*SIN(T-T1))
1850    LET E7=R9*T1-C1
1860    LET C1=-G*COS(T1)+G1*SIN(T1)+G+(1-L)*SIN(T)
1870    LET E8=D2-C*D/2-X-X1-C1-(1-C)*D*(SIN(T/2))^2
1880    LET C1=G1*COS(T1)+G*SIN(T1)-G1
1890    LET C2=(D2-C*D/2)*TAN(P)+1
1900    LET E9=Z5-C2+C1+(1-C)*D*SIN(T)/2+(1-L)*COS(T)
1910    PRINT USING "-#.####",E1,E2,E3,E4
1920    PRINT USING "-#.####",E5,E6,E7,E8,E9
1930    PRINT "1 POINT CONTACT"
1940    REM BACK TO MAIN PROGRAM********************************
1950    LET D4=D+X1-G*COS(T1)+G1*SIN(T1)+G
1960    LET D5=L*SIN(T)+(1-C)*D*COS(T)
1970    PRINT USING "-###.####",D5,D4,L
1980    IF D5>D4 THEN LET O1=1
1990    IF O1=0 THEN GOTO 2080
2000    IF D5<D4 THEN GOTO 2110
2010    IF ABS(D4-D5)<.00000001 THEN LET K=1000
2020    IF ABS(D4-D5)<.00000001 THEN GOTO 2110
2030    LET L0=L-Z0/S1
2040    LET S1=N1*S1
2050    LET K=1000
2060 NEXT K
2070 GOTO 1410
2080 PRINT FILE[6],USING "-#####.#### ",F5,Z5,T*180/3.1415926535,X
2090 PRINT FILE[1,0],USING "-###.####, ",F5,Z5,T*180/3.1415926535,X
2100 LET O8=O8+1
2110 NEXT K
2120 REM BEGIN 2 POINT CONTACT**************************************
2130 LET L2=L
2140 PRINT FILE[6],"2 POINT CONTACT"
2150 FOR K=0 TO 1000
2160    LET L=L2+K*Z0/N1
2170    LET A[1,1]=0
2180    LET A[2,1]=0
2190    LET A[3,1]=0
2200    LET A[4,1]=0
```

```
2210    LET A[5,1]=0
2220    LET A[6,1]=0
2230    LET B[1,1]=F2
2240    LET B[2,1]=0
2250    LET B[3,1]=X
2260    LET B[4,1]=T
2270    LET B[5,1]=T1
2280    LET B[6,1]=0
2290    LET Q[1,1]=-S*A[1,1]
2300    LET Q[2,1]=-S*A[2,1]
2310    LET Q[3,1]=-S*A[3,1]
2320    LET Q[4,1]=-S*A[4,1]
2330    LET Q[5,1]=S*(D2-C*D/2-G-A[5,1])
2340    LET Q[6,1]=-S*A[6,1]
2350    LET O[1,1]=M*SIN(B[4,1])-COS(B[4,1])
2360    LET O[1,2]=COS(B[6,1])-M*SIN(B[6,1])
2370    LET O[1,3]=K9
2380    LET O[1,4]=B[1,1]*(SIN(B[4,1])+M*COS(B[4,1]))
2390    LET O[1,5]=0
2400    LET O[1,6]=-B[2,1]*(SIN(B[6,1])+M*COS(B[6,1]))
2410    LET O[2,1]=M*(1-C)*D/2-1+L
2420    LET C1=(1-M*(1-C)*D/2)*COS(B[4,1]+B[6,1])
2430    LET O[2,2]=C1-(M+(1-C)*D/2)*SIN(B[4,1]+B[6,1])
2440    LET O[2,3]=0
2450    LET C1=(1-M*(1-C)*D/2)*SIN(B[4,1]+B[6,1])
2460    LET C2=C1+(M+(1-C)*D/2)*COS(B[4,1]+B[6,1])
2470    LET O[2,4]=1-B[2,1]*C2
2480    LET O[2,5]=0
2490    LET O[2,6]=O[2,4]-1
2500    LET C1=(G+M*G1)*SIN(B[4,1]-B[5,1])
2510    LET O[3,1]=C1+(M*G-G1)*COS(B[4,1]-B[5,1])
2520    LET O[3,2]=0
2530    LET O[3,3]=0
2540    LET C1=(G+M*G1)*COS(B[4,1]-B[5,1])
2550    LET C2=C1+(G1-M*G)*SIN(B[4,1]-B[5,1])
2560    LET O[3,4]=B[1,1]*C2
2570    LET O[3,5]=-O[3,4]+R9
2580    LET O[3,6]=0
2590    LET O[4,1]=0
2600    LET C1=G*(SIN(B[5,1])-SIN(B[6,1]))
2610    LET C2=G1*COS(B[5,1])-L*COS(B[4,1])
2620    LET O[4,2]=-(C1+C2+(1-C)*D*SIN(B[4,1])-M*G*COS(B[6,1]))
2630    LET O[4,3]=0
2640    LET C1=L*SIN(B[4,1])+(1-C)*D*COS(B[4,1])
2650    LET O[4,4]=-B[2,1]*C1
2660    LET C1=G1*SIN(B[5,1])-G*COS(B[5,1])
2670    LET O[4,5]=B[2,1]*C1
2680    LET C1=-R0*SIN(B[6,1])
2690    LET C2=R0*COS(B[6,1])+C1*B[6,1]
2700    LET C3=COS(B[6,1])-M*SIN(B[6,1])
2710    LET O[4,6]=C2+B[2,1]*G*C3
2720    LET O[5,1]=(COS(B[4,1])-M*SIN(B[4,1]))/(H9*K9)
2730    LET O[5,2]=0
2740    LET O[5,3]=1
2750    LET C1=(1-L)*COS(B[4,1])+(1-C)*D*SIN(B[4,1])/2
2760    LET C2=SIN(B[4,1])+M*COS(B[4,1])
2770    LET O[5,4]=C1-B[1,1]*C2/(H9*K9)
2780    LET O[5,5]=SQR(G^2+G1^2)*SIN(A1-B[5,1])
2790    LET O[5,6]=0
2800    LET O[6,1]=(M*SIN(B[4,1])-COS(B[4,1]))*COS(B[6,1])/(H9*K9)
```

```
2810   LET O[6,2]=(M*SIN(B[6,1])-COS(B[6,1]))*COS(B[6,1])/(H0*K9)
2820   LET O[6,3]=0
2830   LET C1=L*COS(B[4,1]+B[6,1])
2840   LET C2=-(1-C)*D*SIN(B[4,1]+B[6,1])
2850   LET C3=SIN(B[4,1])+M*COS(B[4,1])
2860   LET O[6,4]=C1+C2+C3*B[1,1]*COS(B[6,1])/(H9*K9)
2870   LET O[6,5]=-SQR(G1^2+G^2)*SIN(A1-B[5,1]-B[6,1])
2880   LET C1=L*COS(B[4,1]+B[6,1])
2890   LET C2=-(1-C)*D*SIN(B[4,1]+B[6,1])
2900   LET C2=C2+(2*G+D)*SIN(B[6,1])
2910   LET C3=-SQR(G1^2+G^2)*SIN(A1-B[5,1]-B[6,1])
2920   LET C4=COS(B[4,1])-M*SIN(B[4,1])
2930   LET C4=B[1,1]*C4/(H9*K9)
2940   LET C5=SIN(2*B[6,1])+M*COS(2*B[6,1])
2950   LET C5=B[2,1]*C5/(H0*K9)
2960   LET O[6,6]=C1+C2+C3+C4*SIN(B[6,1])+C5
2970   MAT E=INV(O)
2980   MAT R=E*Q
2990   MAT B=B+R
3000   LET C1=COS(B[6,1])-M*SIN(B[6,1])
3010   LET C2=COS(B[4,1])-M*SIN(B[4,1])
3020   LET C3=B[2,1]*C1-B[1,1]*C2
3030   LET A[1,1]=K9*B[3,1]+C3
3040   LET C1=(1-M*(1-C)*D/2)*COS(B[4,1]+B[6,1])
3050   LET C2=-(M+(1-C)*D/2)*SIN(B[4,1]+B[6,1])
3060   LET C3=-B[1,1]*(1-L-M*(1-C)*D/2)+B[2,1]*(C1+C2)
3070   LET A[2,1]=B[4,1]+C3
3080   LET C1=(G+M*G1)*SIN(B[4,1]-B[5,1])
3090   LET C2=(M*G-G1)*COS(B[4,1]-B[5,1])
3100   LET A[3,1]=R9*B[5,1]+B[1,1]*(C1+C2)
3110   LET C1=G*(SIN(B[5,1])-SIN(B[6,1]))
3120   LET C2=G1*COS(B[5,1])-L*COS(B[4,1])
3130   LET C3=(1-C)*D*SIN(B[4,1])-M*G*COS(B[6,1])
3140   LET C4=R0*B[6,1]*COS(B[6,1])
3150   LET A[4,1]=C4-B[2,1]*(C1+C2+C3)
3160   LET C1=B[3,1]+SQR(G1^2+G^2)*COS(A1-B[5,1])
3170   LET C2=(1-C)*D*(SIN(B[4,1]/2))^2+(1-L)*SIN(B[4,1])
3180   LET C3=COS(B[4,1])-M*SIN(B[4,1])
3190   LET A[5,1]=C1+C2+B[1,1]*C3/(H9*K9)
3200   LET C1=L*SIN(B[4,1])+(1-C)*D*COS(B[4,1])
3210   LET C1=C1*COS(B[6,1])
3220   LET C2=-SQR(G1^2+G^2)*(COS(A1-B[5,1])-COS(A1))*COS(B[6,1])
3230   LET C3=-G*(1-COS(B[6,1]))*COS(B[6,1])
3240   LET C4=G*(SIN(B[5,1])-SIN(B[6,1]))
3250   LET C5=G1*COS(B[5,1])-L*COS(B[4,1])
3260   LET C5=C5+(1-C)*D*SIN(B[4,1])
3270   LET C6=C1+C2+C3-(C4+C5)*SIN(B[6,1])-D*COS(B[6,1])
3280   LET C7=COS(B[4,1])-M*SIN(B[4,1])
3290   LET C7=-B[1,1]*C7*COS(B[6,1])/(H9*K9)
3300   LET C8=COS(B[6,1])-M*SIN(B[6,1])
3310   LET C8=-B[2,1]*C8*COS(B[6,1])/(H0*K9)
3320   LET A[6,1]=C6+C7+C8
3330   PRINT USING "-##.####",K,R[1,1],R[2,1],R[3,1],R[4,1],R[5,1],R[6,1]
3340   LET F=0
3350   FOR I1=1 TO 6
3360     IF ABS(R[I1,1])<1E-09 THEN LET F=F+1
3370   NEXT I1
3380   IF F=6 THEN GOTO 3400
3390   GOTO 2290
3400   LET C1=SIN(B[4,1])+M*COS(B[4,1])
```

```
3410   LET C1=B[1,1]*C1
3420   LET C2=SIN(B[6,1])+M*COS(B[6,1])
3430   LET F5=C1+B[2,1]*C2
3440   LET C1=1+(D2-C*D/2)*TAN(P)-(1-C)*D*SIN(B[4,1])/2
3450   LET C2=C1-(1-L)*COS(B[4,1])
3460   LET Z5=C2-SQR(G1^2+G^2)*(SIN(A1-B[5,1])-SIN(A1))
3470   IF B[6,1]<0 THEN LET L0=L
3480   IF B[6,1]<0 THEN LET Z0=Z0/5
3490   IF B[6,1]<0 THEN GOTO 1380
3500   LET C1=COS(B[6,1])-M*SIN(B[6,1])
3510   LET C1=B[2,1]*C1
3520   IF C1<0 THEN LET L0=L
3530   IF C1<0 THEN LET Z0=Z0/5
3540   IF C1<0 THEN GOTO 1380
3550   PRINT "2 POINT CONTACT"
3560   PRINT FILE[6],USING "-#####.#### ",F5,Z5,B[4,1]*180/3.141593,B[3,1]
3570   PRINT FILE[1,0],USING "-###.####, ",F5,Z5,B[4,1]*180/3.141593,B[3,1]
3580   PRINT USING "-###.#### ",B[6,1],C1/(H0*K9),L
3590   LET 08=08+1
3600 NEXT K
3610 PRINT FILE[6],USING "NO DATA POINTS ### ",08
3620 PRINT USING "NO DATA POINTS ### ",08
3630 CLOSE
3640 END
```

```
0010 REM PROGRAM NAME: CHAMFR (OPT WED ROT CHAMFER)
0020 CLOSE
0030 DIM A$[8]
0040 INPUT "DATA SET NAME: ",A$
0050 OPEN FILE[1,1],A$
0060 OPEN FILE[6,1],"$LPT"
0070 INPUT "FRICTION COEFFICIENT M= ",M
0080 PRINT USING "##.##",ATN(1/M)*180/3.1416
0090 INPUT "INITIAL OFFSET ANGLE T0(DEG)= ",T0
0100 LET T0=3.1415926535*T0/180
0110 PRINT USING "#####.##",1/SIN(T0)
0120 INPUT "LENGTH OF PEG L= ",L
0130 PRINT FILE[6],"DATA SET NAME: ";A$
0140 PRINT FILE[6],USING "FRICTION COEFFICIENT M ##.## ",M
0150 PRINT FILE[6],USING "INITIAL OFFSET ANGLE T0 ##.## ",T0
0160 PRINT FILE[6],USING "LENGTH OF PEG L #####.## ",L
0170 LET X1=1-L*SIN(T0)
0180 LET C1=SQR(L^2-X1^2)
0190 LET C2=SQR(1+M^2)
0200 FOR I=0 TO 74
0210   LET X=I/74
0220   LET X0=X-L*SIN(T0)
0230   LET F=SQR(L^2-X0^2)
0240   LET N1=(C2*F+M*L)*(L+C2*X1)
0250   LET D1=(C2*C1+M*L)*(L+C2*X0)
0260   LET Y9=C1-F+(M*L/C2)*LOG(N1/D1)
0270   LET N2=(F-M*X0)*(L^2-(C2*X1)^2)
0280   LET D2=(C1-M*X1)*(L^2-(C2*X0)^2)
0290   LET F1=(L/C2)*(ATN(X1/C1)-ATN(X0/F))
0300   LET Y0=Y9+F1+(M*L/C2)*LOG(N2/D2)
0310   LET Y5=Y0-Y9
```

```
0320    PRINT USING "-##.### ",Y0,X,Y9,Y5
0330    PRINT FILE[6],USING "-##.### ",Y0,X,Y9,Y5
0340    PRINT FILE[1,0],USING "-##.###, ",Y0,X,Y9,Y5
0350 NEXT I
0360 CLOSE
0370 END
```

```
0010 REM PROGRAM NAME: CHAMF(GEN SOL M1 AND M2)
0020 CLOSE
0030 DIM A$[8]
0040 INPUT "DATA SET NAME: ",A$
0050 OPEN FILE[1,1],A$
0060 OPEN FILE[6,1],"$LPT"
0070 INPUT "FRICTION COEFFICIENT M1= ",M1
0080 PRINT USING "###.# ",1/M1
0090 INPUT "FRICTION COEFFICIENT M2= ",M2
0100 LET S0=(M1+M2)/(1-M1*M2)
0110 LET S1=S0*(1+SQR((1+M1^2)/(M1*(M1+M2))))
0120 PRINT USING "##.## ",S0,S1
0130 INPUT "ASPECT RATIO S= ",S
0140 INPUT "INITIAL GUESS FOR C  G= ",G
0150 PRINT FILE[6],"DATA SET NAME: ";A$
0160 PRINT FILE[6],USING "FRICTION COEFFICIENT M1 #.## ",M1
0170 PRINT FILE[6],USING "FRICTION COEFFICIENT M2 #.## ",M2
0180 PRINT FILE[6],USING "ASPECT RATIO S ##.## ",S
0190 PRINT FILE[6],USING "INITIAL GUESS FOR C  G ####.#### ",G
0200 REM COMPUTE INTEGRATION CONSTANT C**********************
0210 LET C=G
0220 FOR I=1 TO 1000
0230   LET B=SQR((1+M1^2)*(M1+M2)/M1)/(1-M1*M2)
0240   LET B1=SQR(C)
0250   LET B2=SQR(1+C)
0260   LET B3=-1/(2*B2)+LOG((B2+1)/B1)
0270   LET B4=(B1/B2-(B2+1)/B1)/2
0280   LET F1=B*(B3+B4*B1/(B2+1))
0290   LET B3=B2-C*LOG((B2+1)/B1)
0300   LET F=S0+B*B3-S
0310   LET C=C+F/F1
0320   PRINT USING "-#####.##### ",C
0330   IF ABS(F/F1)<.00000001 THEN LET I=1000
0340 NEXT I
0350 PRINT USING "INTEGRATION CONSTANT C #####.##### ",C
0360 PRINT FILE[6],USING "INTEG CONST C #####.##### ",C
0370 REM COMPUTE CHAMFER SHAPE***************************
0380 FOR I=0 TO 74
0390   LET X=I/74
0400   LET B3=SQR(X+C)
0410   LET B4=SQR(X)
0420   LET B4=B3*B4-C*LOG((B3+B4)/B1)
0430   LET Y=S-S0*X-B*B4
0440   PRINT USING "##.## ",Y,X,S0*(1-X),S1*(1-X)
0450   PRINT FILE[6],USING "##.### ",Y,X,S0*(1-X),S1*(1-X)
0460   PRINT FILE[1,0],USING "##.###, ",Y,X,S0*(1-X),S1*(1-X)
0470 NEXT I
0480 CLOSE
0490 END
```

```
ØØ1Ø REM PROGRAM NAME: FSTCH (FORCE VS DEP STCH STCHR)
ØØ2Ø CLOSE
ØØ3Ø DIM A$[8]
ØØ4Ø INPUT "DATA SET NAME: ",A$
ØØ5Ø INPUT "SPRING STIFFNESS= ",K
ØØ6Ø INPUT "ASPECT RATIO= ",S
ØØ7Ø OPEN FILE[1,1],A$
ØØ8Ø OPEN FILE[6,1],"$LPT"
ØØ9Ø PRINT FILE[6],"DATA SET NAME: ";A$
Ø1ØØ PRINT FILE[6],USING "SPRING STIFFNESS K ####.### ",K
Ø11Ø PRINT FILE[6],USING "ASPECT RATIO S ##.##### ",S
Ø12Ø LET TØ=15*3.1415926535/180
Ø13Ø FOR I=Ø TO 74
Ø14Ø    LET X=.6*I/74
Ø15Ø    LET Y=S*(.6-X)
Ø16Ø    LET XØ=X-3*SIN(TØ)
Ø17Ø    LET T=ATN(-XØ/(SQR(3^2-XØ^2)))
Ø18Ø    LET C1=XØ-.15*(SQR(3^2-XØ^2))
Ø19Ø    LET C2=SQR(3^2-XØ^2)+.15*XØ
Ø2ØØ    LET Y2=3*COS(TØ)+.6*S-Y-3*COS(T)
Ø2Ø5    LET Y2=25.4*Y2
Ø21Ø    LET F=K*(TØ-T)*(1+.15*S)/(C1+S*C2)
Ø22Ø    PRINT USING "-###.#### ",Y2,F,X,Y
Ø23Ø    PRINT FILE[6],USING "-###.#### ",Y2,F,X,Y
Ø24Ø    PRINT FILE[1,Ø],USING "-###.####, ",Y2,F,X,Y
Ø25Ø NEXT I
Ø26Ø CLOSE
Ø27Ø END
```

```
ØØ1Ø REM PROGRAM NAME: FCHAM (FORCE VS DEP FOR CHAM)
ØØ2Ø CLOSE
ØØ3Ø DIM A$[8]
ØØ4Ø INPUT "DATA SET NAME: ",A$
ØØ5Ø INPUT "SPRING STIFFNESS= ",K
ØØ6Ø OPEN FILE[1,1],A$
ØØ7Ø OPEN FILE[6,1],"$LPT"
ØØ8Ø PRINT FILE[6],"DATA SET NAME: ";A$
ØØ9Ø PRINT FILE[6],USING "SPRING STIFFNESS K ####.### ",K
Ø1ØØ LET TØ=15*3.1415926535/180
Ø11Ø LET X1=.5-3*SIN(TØ)
Ø12Ø LET C1=SQR(3^2-X1^2)
Ø13Ø LET C2=SQR(1+.15^2)
Ø14Ø FOR I=Ø TO 74
Ø15Ø    LET X=.6*I/74
Ø16Ø    LET XØ=X-3*SIN(TØ)
Ø17Ø    LET F=SQR(3^2-XØ^2)
Ø18Ø    LET M1=(XØ-.15*F)/(F+.15*XØ)
Ø19Ø    LET Y1=M1-SQR(1+M1^2)
Ø2ØØ    LET N1=(C2*F+.15*3)*(3+C2*X1)
Ø21Ø    LET D1=(C2*C1+.15*3)*(3+C2*XØ)
Ø22Ø    LET Y9=C1-F+(.15*3/C2)*LOG(N1/D1)
Ø23Ø    LET N2=(F-.15*XØ)*(3^2-(C2*X1)^2)
Ø24Ø    LET D2=(C1-.15*X1)*(3^2-(C2*XØ)^2)
Ø25Ø    LET F1=(3/C2)*(ATN(X1/C1)-ATN(XØ/F))
Ø26Ø    LET Y=Y9+F1+(.15*3/C2)*LOG(N2/D2)
Ø27Ø    LET T=ATN(-XØ/(SQR(3^2-XØ^2)))
```

```
0280    LET Y2=3*COS(T0)+.6*1.3968-Y-3*COS(T)
0290    LET F1=K*(T0-T)*(1-.15*Y1)/(X0-.15*F-Y1*(F+.15*X0))
0300    PRINT USING "-###.#### ",Y2,F1,X,Y
0310    PRINT FILE[6],USING "-###.#### ",Y2,F1,X,Y
0320    PRINT FILE[1,0],USING "-###.####, ",Y2,F1,X,Y
0330 NEXT I
0340 CLOSE
0350 END
```

APPENDIX B

CALCULATION OF JACOBIAN MATRICES

Chamfer Crossing

The Jacobian matrix $\underline{J}$ is given by:

$$\underline{J} = \begin{bmatrix} \dfrac{\partial f_1}{\partial(\delta\theta)} & \dfrac{\partial f_1}{\partial(\delta\theta_1)} \\ \\ \dfrac{\partial f_2}{\partial(\delta\theta)} & \dfrac{\partial f_2}{\partial(\delta\theta_1)} \end{bmatrix} \tag{B.1}$$

where

$$\frac{\partial f_1}{\partial(\delta\theta)} = a \cos \delta\theta + \frac{d}{2} \sin \delta\theta$$

$$\frac{\partial f_1}{\partial(\delta\theta_1)} = \frac{(1/K_x + 1/K_{x_1})K_{\theta_1}}{D_1} \left[(1-\mu\delta\theta_1)\sin(\phi-\delta\theta_1)-(\mu+\delta\theta_1)\cos(\phi-\delta\theta_1)\right]$$

$$+ r_c \sin(\gamma_c-\delta\theta_1) \tag{B.2}$$

$$\frac{\partial f_2}{\partial(\delta\theta)} = K_\theta - \frac{K_{\theta_1}\delta\theta_1}{D_1} \left[(a-\frac{\mu d}{2})\cos(\phi+\delta\theta-\delta\theta_1)+(a\mu + \frac{d}{2})\sin(\phi+\delta\theta-\delta\theta_1)\right]$$

$$\frac{\partial f_2}{\partial(\delta\theta_1)} = \frac{K_{\theta_1}}{D_1} \left\{ \left[(a-\frac{\mu d}{2})\delta\theta_1 + (a\mu + \frac{d}{2})\right] \cos(\phi + \delta\theta - \delta\theta_1)\right.$$

$$\left. - \left[(a-\frac{\mu d}{2}) - (a\mu + \frac{d}{2})\delta\theta_1\right] \sin(\phi + \delta\theta - \delta\theta_1)\right\}$$

Two-Point Contact

The Jacobian matrix $\underline{J}$ is given by:

$$\underline{J} = \begin{bmatrix} \frac{\partial f_1}{\partial F_{n_1}} & \frac{\partial f_1}{\partial F_{n_2}} & \frac{\partial f_1}{\partial(\delta x)} & \frac{\partial f_1}{\partial(\delta\theta)} & \frac{\partial f_1}{\partial(\delta\theta_1)} & \frac{\partial f_1}{\partial(\delta\theta_2)} \\ \frac{\partial f_2}{\partial F_{n_1}} & \cdot & & & & \\ \frac{\partial f_3}{\partial F_{n_1}} & & \cdot & & & \\ \frac{\partial f_4}{\partial F_{n_1}} & & & \cdot & & \\ \frac{\partial f_5}{\partial F_{n_1}} & & & & \cdot & \\ \frac{\partial f_6}{\partial F_{n_1}} & & & & & \cdot \end{bmatrix} \qquad (B.3)$$

or

$$\underline{J} = \begin{bmatrix} \underline{J}_{11} & \underline{J}_{12} & \underline{J}_{13} \\ \underline{J}_{21} & \underline{J}_{22} & \underline{J}_{23} \\ \underline{J}_{31} & \underline{J}_{32} & \underline{J}_{33} \end{bmatrix} \qquad (B.4)$$

where

$$
\underline{J}_{11} = \left[\begin{array}{c|c}
\mu\sin\delta\theta - \cos\delta\theta & \cos\delta\theta_2 - \mu\sin\delta\theta_2 \\
\hline
-\left[(a-\ell) - \frac{\mu d}{2}\right] & \begin{array}{l}(a-\frac{\mu d}{2})\ \cos(\delta\theta+\delta\theta_2) \\ \\ -(a\mu+\frac{d}{2})\ \sin(\delta\theta+\delta\theta_2)\end{array}
\end{array}\right]
$$

$$
\underline{J}_{12} = \left[\begin{array}{c|l}
K_x & F_{n_1}(\sin\delta\theta+\mu\cos\delta\theta) \\
\hline
0 & \begin{array}{l}K_\theta - F_{n_2}\left[(a-\frac{\mu d}{2})\sin(\delta\theta+\delta\theta_2)\right. \\ \\ \left.+(a\mu+\frac{d}{2})\ \cos(\delta\theta+\delta\theta_2)\right]\end{array}
\end{array}\right] \qquad \text{(B.5)}
$$

$$
\underline{J}_{13} = \left[\begin{array}{c|l}
0 & -F_{n_2}(\sin\delta\theta_2+\mu\cos\delta\theta_2) \\
\hline
0 & \begin{array}{l}-F_{n_2}\left[(a-\frac{\mu d}{2})\sin(\delta\theta+\delta\theta_2)\right. \\ \\ \left.+(a\mu+\frac{d}{2})\ \cos(\delta\theta+\delta\theta_2)\right]\end{array}
\end{array}\right]
$$

$$\underline{J}_{21} = \left[\begin{array}{c|c} -r\sqrt{1+\mu^2}\,\sin(\gamma+\delta\theta-\delta\theta_1-\beta) & 0 \\ \hline 0 & \begin{array}{l} \ell\cos\delta\theta-d\sin\delta\theta \\ -C_h(\sin\delta\theta_1-\sin\delta\theta_2) \\ -C_v\cos\delta\theta_1+\mu C_h\cos\delta\theta_2 \end{array} \end{array}\right]$$

$$\underline{J}_{22} = \left[\begin{array}{c|c} 0 & -r\sqrt{1+\mu^2}F_{n_1}\cos(\gamma+\delta\theta-\delta\theta_1+\beta) \\ \hline 0 & -F_{n_2}(\ell\sin\delta\theta+d\cos\delta\theta) \end{array}\right] \qquad \text{(B.6)}$$

$$\underline{J}_{23} = \left[\begin{array}{c|c} \begin{array}{l} K_{\theta_1} \\ +r\sqrt{1+\mu^2}F_{n_1}\cos(\gamma+\delta\theta-\delta\theta_1+\beta) \end{array} & 0 \\ \hline rF_{n_2}\cos(\gamma-\delta\theta_1) & \begin{array}{l} K_{\theta_2}(\cos\delta\theta_2-\delta\theta_2\sin\delta\theta_2) \\ +C_hF_{n_2}(\cos\delta\theta_2-\mu\sin\delta\theta_2) \end{array} \end{array}\right]$$

$$\underline{J}_{31} = \left[\begin{array}{c|c} 0 & 0 \\ \hline 0 & 0 \end{array}\right]$$

$$\underline{J}_{32} = \left[\begin{array}{c|l} 1 & (a-\ell)\cos\delta\theta + \frac{d}{2}\sin\delta\theta \\ \hline 0 & \begin{array}{l} \ell\cos(\delta\theta+\delta\theta_2) \\ -d\sin(\delta\theta+\delta\theta_2) \end{array} \end{array}\right] \tag{B.7}$$

$$\underline{J}_{33} = \left[\begin{array}{c|l} r\sin(\gamma-\delta\theta_1) & 0 \\ \hline -r\sin(\gamma-\delta\theta_1-\delta\theta_2) & \begin{array}{l} \ell\cos(\delta\theta+\delta\theta_2)-d\sin(\delta\theta+\delta\theta_2) \\ +(D+2C_h)\sin\delta\theta_2 \\ -r\sin(\gamma-\delta\theta_1-\delta\theta_2) \end{array} \end{array}\right]$$

LIST OF REFERENCES

1. Whitney, D.E., Rigid Part Mating, C.S. Draper Laboratory Report No. P-1447, Session No. 8, November 1981, presented at the 2nd Annual Seminar on Advanced Assembly Research, Cambridge, MA, November 1981.

2. Whitney, D.E., et al., Part Mating Theory for Compliant Parts, First Report, C.S. Draper Laboratory Report No. R-1407, September 1, 1979 to August 31, 1980.

3. Arai, T. and Kinoshita, N., The Part Mating Forces that Arise when using a Worktable with Compliance, Assembly Automation, August 1981, pp. 204-210.

4. Gustavson, R.E. and Hennessey, M.P., Compliant Part Mating, C.S. Draper Laboratory Report No. P-1447, Session No. 9, November 1981, presented at the 2nd Annual Seminar on Advanced Assembly Research, Cambridge, MA 1981.

5. Nevins, J.L., et al., Exploratory Research in Industrial Modular Assembly, C.S. Draper Laboratory Report No. R-1218, September 1, 1977 to August 30, 1978.

6. Whitney, D.E., et al., Part Mating Theory for Compliant Parts, C.S. Draper Laboratory Report No. P-1390, November 1981, presented at the 9th Conference on Production Research and Technology, Ann Arbor, MI, November 1981.

7. Crandall, Stephen H., Dahl, Norman C., and Lardner, Thomas J., An Introduction to the Mechanics of Solids, second edition, Chapter 2, McGraw-Hill, New York, 1972.

8. Whitney, D.E., Optimum Step Size Control for Newton-Raphson Solution of Nonlinear Vector Equations, IEEE Trans. Auto. Control, Vol. AC-14, No. 5, October 1969.

9. Sokolnikoff, I.S. and Redheffer, R.M., Mathematics of Physics and Modern Engineering, second edition, Chapter 5, Section 15, McGraw-Hill, New York, 1966.

10. Courant and Hilbert: Methods of Mathematical Physics, Vol. 1, pp. 214-216, Interscience Publishers, Inc., New York, 1953.

11. Dwight, Herbert B., Tables of Integrals and Other Mathematical Data, fourth edition, p. 49, MacMillian, New York, 1961.

12. Gradshteyn, I.S., and Ryzhik, I.M., Table of Integrals, Series, and Products-Corrected and Enlarged Edition, pp. 157, 160, Academic Press, New York, 1980.